

**INFLATION, BOUNCES, AND
PRIMORDIAL CORRELATIONS**

*A THESIS
submitted by*

DEBIKA CHOWDHURY

*for the award of the degree
of*

DOCTOR OF PHILOSOPHY



**DEPARTMENT OF PHYSICS
INDIAN INSTITUTE OF TECHNOLOGY MADRAS
SEPTEMBER 2018**

*Dedicated to
my parents*

THESIS CERTIFICATE

This is to certify that the thesis titled **Inflation, bounces, and primordial correlations**, submitted by **Ms. Debika Chowdhury**, to the Indian Institute of Technology, Madras, for the award of the degree of **Doctor of Philosophy**, is a bona fide record of the research work done by her under our supervision. The contents of this thesis, in full or in parts, have not been submitted to any other Institute or University for the award of the degree.

Prof. L. Sriramkumar
Research Guide
Professor
Department of Physics
Indian Institute of Technology Madras
Chennai 600 036

Dr. Dawood Kothawala
Co-Guide
Assistant Professor
Department of Physics
Indian Institute of Technology Madras
Chennai 600 036

Place: Chennai
Date: September 7, 2018

ACKNOWLEDGEMENTS

I am particularly beholden to my thesis supervisor, Prof. L. Sriramkumar, for the unwavering patience and kindness with which he treated me throughout the duration of my time as a doctoral student. I thank him for relentlessly inspiring me to further my abilities. I have learned a lot through my conversations with him regarding matters pertaining to research, as well as about other topics of mutual interest. I am grateful to him for his persistent support and encouragement.

I am thankful to my co-guide, Dr. Dawood Kothawala, for his invaluable help and guidance. I would like to thank the other members of my doctoral committee – Dr. Prasanta Kumar Tripathy, Prof. Suresh Govindarajan, Prof. T. R. Govindarajan, and the committee chairperson Prof. S. Lakshmi Bala – for their support.

I would like to express my gratitude towards my research collaborators – Prof. Marc Kamionkowski and Prof. Jérôme Martin – for endowing me with the priceless opportunity of working with them. I have benefited greatly from my interactions with them. I would also like to thank Dr. Christophe Ringeval and Dr. Vincent Vennin for insightful discussions.

I am grateful to Dr. Rajeev Kumar Jain – my research collaborator – for his assistance and counsel.

I am thankful to Sreenath – my collaborator and erstwhile office mate – for his indispensable help, especially during the initial stages of my research career. I am indebted to him for being exceedingly supportive and helpful at all times.

I would like to thank my colleagues – Jaffino, Rathul, Ragavendra, Sagarika, Debotam, and Rahul – for always being considerate and cooperative. I have immensely enjoyed the time spent in their company and shall cherish these memories forever.

I am tremendously grateful to my friends – Arpita, Sutapa, Ushasi di, Anupama, Moulika, and Sreetama – for their companionship and unfaltering support. I would especially like to thank Arpita and Sutapa for being a constant source of comfort to me.

I thank the Indo-U.S. Science and Technology Forum (IUSSTF), for providing me with the opportunity to visit and collaborate with Prof. Marc Kamionkowski at the Johns Hopkins University, Baltimore, U.S.A.. I would also like to thank the Centre Franco-Indien

pour la Promotion de la Recherche Avancée (CEFIPRA), and the Centre for Cosmological Studies (University of Oxford, United Kingdom), for providing me with opportunities to visit and work with Prof. Jérôme Martin at the Institut d'Astrophysique de Paris, Paris, France.

I consider myself fortunate to have been introduced to the highly versatile and beneficial practice of yoga. I sincerely thank our yoga teacher, Mrs. Katyayini Reddy, for being extremely patient and helpful. I also thank the Dean of Students for organizing the yoga classes at IIT Madras.

I thank my parents, for their belief in me and for their unhindered support. I owe them a debt of gratitude for being a perpetual source of inspiration for me. I would also like to thank my uncle, Mr. Pradip Kumar Kanjilal, for being extremely supportive and encouraging.

I feel blessed to have met and interacted with a myriad of people during my time as a Ph.D. student, all of whom have contributed richly toward my development. I shall reminisce about the time spent at IIT Madras with utmost fondness, always.

ABSTRACT

KEYWORDS: Inflation, Bouncing scenarios, Non-Gaussianities, Primordial magnetic fields

Inflation refers to a period of exponentially rapid expansion of the universe in the very early stages of the radiation dominated era. In this paradigm, we can overcome the various difficulties associated with the conventional hot big bang model of the universe, such as the horizon and the flatness problems. In addition to this, the inflationary scenario also provides us with a simple mechanism to generate the primordial perturbations, which are expected to have acted as seeds for the formation of the Large Scale Structure (LSS). The imprints of the primordial fluctuations can be observed in the form of small anisotropies in the Cosmic Microwave Background (CMB). The predictions of the plethora of inflationary models can be tested against the increasingly accurate cosmological measurements. However, the profusion of inflationary models that are consistent with the data at the level of two-point functions raises the question as to whether a unique model of inflation is attainable. It is expected that with the aid of future high precision experiments, it may be possible to arrive at tighter constraints at the level of three-point functions, importantly those involving tensors, which can then lead to a smaller class of viable inflationary models.

Bouncing scenarios correspond to situations wherein the universe undergoes a phase of contraction followed by an expanding era, with a bounce connecting the two epochs. At the bounce, the scale factor describing the universe attains a minimum value. Such scenarios have been introduced as possible alternatives to the inflationary paradigm as they can help in overcoming the horizon problem in ways similar to inflation. Certain bouncing models have been known to generate scale invariant primordial perturbation spectra, and also lead to a viable tensor-to-scalar ratio. Nevertheless, the characteristics of the two-point functions alone do not seem sufficient to distinguish between the predictions of the inflationary and the bouncing scenarios. The behavior of the three-point functions in these models can be expected to act as a possible discriminator between these two scenarios.

The advancement in obtaining increasingly precise cosmological data has allowed for rigorous assessment of models of the early universe. Observational bounds at the level of two-point functions alone do not appear to be adequate to constrain these models or to efficiently distinguish between alternative scenarios of the early universe, such as

inflation and bounces. With the aim to arrive at strongly discriminating observables, the signatures of which can demarcate between inflationary and bouncing scenarios, in this thesis, we have investigated three-point functions involving scalar and tensor modes, as well as cross-correlations between scalar perturbations and primordial magnetic fields. In what follows, we shall provide a brief outline of the various issues that we have studied in this thesis.

- **The scalar-scalar-tensor three-point function in the axion monodromy model:** The axion monodromy model involves a canonical scalar field that is governed by a linear potential with superimposed modulations. The modulations in the potential are responsible for a resonant behavior which gives rise to persisting oscillations in the scalar and, to a smaller extent, in the tensor power spectra. Interestingly, such spectra have been shown to lead to an improved fit to the cosmological data than the more conventional, nearly scale invariant, primordial power spectra. The scalar bispectrum in the model too exhibits continued modulations and the resonance is known to boost the amplitude of the scalar non-Gaussianity parameter to rather large values. An analytical expression for the scalar bispectrum had been arrived at earlier which, in fact, has been used to compare the model with the cosmic microwave background anisotropies at the level of three-point functions involving scalars. In this work, with future applications in mind, we arrive at a similar analytical template for the scalar-scalar-tensor cross-correlation. We also analytically establish the consistency relation (in the squeezed limit) for this three-point function. We conclude with a summary of the main results obtained.

- **The tensor bispectrum in a matter bounce:** Matter bounces are bouncing scenarios wherein the universe contracts as in a matter dominated phase at early times. Such scenarios are known to lead to a scale invariant spectrum of tensor perturbations, just as de Sitter inflation does. In this work, we examine if the tensor bispectrum can discriminate between the inflationary and the bouncing scenarios. Using the Maldacena formalism, we analytically evaluate the tensor bispectrum in a matter bounce for an arbitrary triangular configuration of the wavevectors. We show that, over scales of cosmological interest, the non-Gaussianity parameter h_{NL} that characterizes the amplitude of the tensor bispectrum is quite small when compared to the corresponding values in de Sitter inflation. During inflation, the amplitude of the tensor perturbations freeze on super-Hubble scales, a behavior that leads to the so-called consistency condition relating the tensor bispectrum and the power spectrum in the squeezed limit. In contrast, in the bouncing scenarios, the amplitude of the tensor perturbations grow strongly as one approaches the bounce, which suggests that the consistency condition will not be valid in such situations. We explicitly show that the consistency relation is indeed violated in the matter bounce. We discuss the implications of the results.

- **Scale invariant magnetic fields in bouncing scenarios:** Recently, it has been numerically shown that, for a non-minimal coupling that is a simple power of the scale factor, scale invariant magnetic fields arise in a class of bouncing universes. In this work, we *analytically* evaluate the spectrum of magnetic and electric fields generated in a sub-class of

such models. We illustrate that, for cosmological scales which have wavenumbers much smaller than the wavenumber associated with the bounce, the shape of the spectrum is preserved across the bounce. Using the analytical solutions obtained, we also illustrate that the problem of backreaction is severe at the bounce. Finally, we show that the power spectrum of the magnetic field remains invariant under a two parameter family of transformations of the non-minimal coupling function.

• **Cross-correlations between scalar perturbations and magnetic fields in bouncing universes:** As we have already mentioned, bouncing scenarios offer an alternative to the inflationary paradigm for the generation of perturbations in the early universe. Recently, there has been a surge in interest in examining the issue of primordial magnetogenesis in the context of bouncing universes. As in the case of inflation, the conformal invariance of the electromagnetic action needs to be broken in bouncing scenarios in order to generate primordial magnetic fields which correspond to observed strengths today. The non-minimal coupling, which typically depends on a scalar field that possibly drives the homogeneous background, leads to a cross-correlation at the level of the three-point function between the perturbation in the scalar field and the magnetic fields. This has been studied in some detail in the context of inflation and, specifically, it has been established that the three-point function satisfies the consistency relation in the squeezed limit. In this work, we study the cross-correlation between the magnetic fields and the perturbation in an auxiliary scalar field in a certain class of bouncing scenarios. We consider couplings that lead to scale invariant spectra of the magnetic field and evaluate the corresponding cross-correlation between the magnetic field and the perturbation in the scalar field. We find that, when compared to de Sitter inflation, the dimensionless non-Gaussianity parameter that characterizes the amplitude of the cross-correlations proves to be considerably larger in bouncing scenarios. We also show that the aforementioned consistency condition governing the cross-correlation is violated in the bouncing models. We discuss the implications of our results.

• **Enhancing the cross-correlations between magnetic fields and scalar perturbations through parity violation:** One often resorts to a non-minimal coupling of the electromagnetic field in order to generate magnetic fields during inflation. The coupling is expected to depend on a scalar field, possibly the same as the one driving inflation. At the level of three-point functions, such a coupling leads to a non-trivial cross-correlation between the perturbation in the scalar field and the magnetic field. This cross-correlation has been evaluated analytically earlier for the case of non-helical electromagnetic fields. In this work, we *numerically* compute the cross-correlation for helical magnetic fields. Non-Gaussianities are often generated as modes leave the Hubble radius. The helical electromagnetic modes evolve strongly (when compared to the non-helical case) around Hubble exit and one type of polarization is strongly amplified immediately after Hubble exit. We find that helicity considerably boosts the amplitude of the dimensionless non-Gaussianity parameter that characterizes the amplitude and shape of the cross-correlation between the perturbations in the scalar field and the magnetic field. We discuss the implications of the enhancement in the non-Gaussianity parameter due to parity violation.

Contents

ACKNOWLEDGEMENTS	i
ABSTRACT	iii
SUMMARY OF NOTATIONS	xi
LIST OF FIGURES	xix
1 Introduction	1
1.1 The standard model of cosmology	3
1.2 The inflationary paradigm	6
1.2.1 Drawbacks of the hot big bang model	7
1.2.2 Overcoming the horizon problem with inflation	8
1.2.3 Driving inflation with scalar fields	10
1.3 Classical bouncing scenarios	12
1.3.1 A brief review of bouncing scenarios	13
1.3.2 Issues associated with bouncing models	13
1.3.3 Characteristics of a matter bounce	14
1.4 Generation of primordial perturbations and power spectra	18
1.4.1 Classification of the perturbations	18
1.4.2 Quantization of the perturbations and the power spectra	20
1.4.3 Power spectra in slow roll inflation	24
1.4.4 Duality invariance of the power spectra	25
1.4.5 Observational constraints on the power spectra	26
1.5 Beyond power spectra: three-point correlation functions	27
1.5.1 The Maldacena formalism	27
1.5.2 Definitions of the three-point functions	29
1.5.3 Non-Gaussianity parameters	33
1.5.4 The three-point functions in slow roll inflation	34
1.5.5 The three-point functions in the squeezed limit	37
1.5.6 Observational constraints on the three-point functions	39
1.6 Generation of magnetic fields in the early universe	40

CONTENTS

1.6.1	Observational constraints on magnetic fields	41
1.6.2	Origin of primordial magnetic fields during inflation	41
1.6.3	The backreaction and strong coupling problems	45
1.7	Organization of the thesis	45
2	Three-point functions in the axion monodromy model	47
2.1	Introduction	47
2.2	The axion monodromy model	49
2.2.1	The evolution of the background and the slow roll parameters	49
2.2.2	The evolution of the perturbations and the power spectra	51
2.3	The scalar bispectrum in the Maldacena formalism	56
2.4	Analytical template for the cross-correlation	58
2.4.1	Analytical evaluation of the three-point function	58
2.4.2	Comparison with the numerical results	62
2.5	The squeezed limit and the consistency relation	62
2.6	Discussion	65
3	The tensor bispectrum in a matter bounce	67
3.1	Introduction	67
3.2	The tensor modes and the power spectrum	69
3.3	Evaluating the tensor bispectrum	75
3.4	Amplitude and shape of the non-Gaussianity parameter	79
3.5	Discussion	82
4	Scale invariant magnetic fields in bouncing scenarios	85
4.1	Introduction	85
4.2	Non-minimal coupling in bounces	86
4.3	Analytical evaluation of the modes and the power spectra	87
4.4	The issue of backreaction	92
4.5	Duality invariance	94
4.6	Discussion	97
5	Cross-correlations with magnetic fields	99
5.1	Introduction	99
5.2	Evaluating cross-correlations with magnetic fields	100
5.2.1	The three-point function in de Sitter inflation	103
5.2.2	The three-point function in a matter bounce	106
5.3	Amplitude and shape of the non-Gaussianity parameter	113
5.4	The three-point function in the squeezed limit	118
5.5	Discussion	120
6	Enhancing the cross-correlations through parity violation	121

6.1	Introduction	121
6.2	Non-minimally coupled helical electromagnetic fields	122
6.3	Power spectra of the helical magnetic fields	124
6.4	Formal structure of the three-point function	125
6.5	Numerical evaluation of the three-point function	127
6.5.1	Evolution of the modes	127
6.5.2	Evaluation of the three-point function	129
6.6	Amplitude and shape of the non-Gaussianity parameter	133
6.7	Discussion	135
7	Conclusions	137
7.1	Summary of work done	137
7.2	Outlook	140

CONTENTS

SUMMARY OF NOTATIONS

The notations used in this thesis have been listed below in the order of their appearance in the thesis.

Notation	Description
t	Cosmic time
\boldsymbol{x}	Position three-vector
η	Conformal time
N	E-folds
\mathcal{N}	E-N-folds
a	Scale factor describing the universe
\hbar	Reduced Planck's constant, 1.054×10^{-34} J s
c	Speed of light, 299792458 m s $^{-1}$
M_{Pl}	Reduced Planck mass, 2.435×10^{18} GeV/c 2
G	Universal gravitational constant, 6.674×10^{-11} N kg $^{-2}$ m 2
k	Wavenumber of perturbations
H	Hubble parameter
H_0	Hubble constant: value of the Hubble parameter today
h	Parameter describing the Hubble constant as: $H_0 = 100 h$ km s $^{-1}$ Mpc $^{-1}$
K	Spatial curvature
ρ	Energy density
w	Equation of state parameter
p	Pressure
Ω	Density parameter
ρ_{cr}	Critical energy density
z	Redshift
t_0	Present time
Ω_{R}^0	Density parameter due to radiation at present
Ω_{NR}^0	Density parameter due to non-relativistic matter at present
Ω_{Λ}^0	Density parameter due to dark energy at present

SUMMARY OF NOTATIONS

Notation	Description
Ω_K^0	Density parameter due to spatial curvature at present
Ω_i^0	Density parameter due to species ‘i’ at present
Ω_b^0	Density parameter due to baryonic matter in the universe at present
Ω_c^0	Density parameter due to cold dark matter in the universe at present
τ	Reionization optical depth
A_s	Amplitude of primordial scalar power spectrum
n_s	Spectral index of primordial scalar power spectrum
t_{dec}	Time of decoupling
λ_P	Physical wavelength
d_H	Hubble radius
t_i	Time at the beginning of inflation
t_f	Time at the end of inflation
H_i	Value of the Hubble parameter during inflation
ϕ	Scalar field
$V(\phi)$	Potential for the scalar field ϕ
$S[\phi]$	Action for the scalar field ϕ
g	Determinant of the metric $g_{\mu\nu}$
∂_μ	Partial derivative with respect to x^μ
V_ϕ	Derivative of the potential V with respect to the scalar field ϕ
T_ν^μ	Stress-energy tensor
δ_ν^μ	Kronecker delta in four dimensions
ϵ_i	i -th slow roll parameter
a_0	Value of the scale factor at the bounce
$\eta_0, 1/k_0$	Time scale associated with the bounce
r	Primordial tensor-to-scalar ratio
Φ	Bardeen potential
δT_ν^μ	Perturbation in stress-energy tensor
∇_μ	Covariant derivative with respect to x^μ
$\delta\rho$	Perturbation in energy density
$\delta\sigma$	Perturbation in momentum flux
δp	Perturbation in pressure
δG_ν^μ	Perturbation in Einstein tensor
∇^2	Laplacian operator

Notation	Description
\mathcal{H}	Conformal Hubble parameter
c_A	Speed of adiabatic perturbations
δp^{NA}	Non-adiabatic component of the pressure perturbation
\mathcal{R}	Curvature perturbation
γ_{ij}	Tensor perturbation
$\delta\phi$	Perturbation in the scalar field ϕ
f_k	Fourier mode of the scalar perturbations corresponding to the wavenumber k
v_k	Fourier mode of the Mukhanov-Sasaki variable for the scalar perturbations, corresponding to the wavenumber k
$\langle A B \rangle$	Two-point function involving perturbations of type AB , where $(A, B) = (\mathcal{R}, \gamma_{ij})$
$\mathcal{P}_s(k)$	Power spectrum of the scalar perturbations
h_k	Fourier mode of the tensor perturbations corresponding to the wavenumber k
$\varepsilon_{ij}^s(\mathbf{k})$	Polarization tensor of the gravitational waves, with the indices $s = (1, 2)$ denoting the two states of polarization
u_k	Fourier mode of the Mukhanov-Sasaki variable for the tensor perturbations, corresponding to the wavenumber k
$\mathcal{P}_T(k)$	Power spectrum of the tensor perturbations
$\Pi_{ij,mn}^{\mathbf{k}}$	Sum of products of the polarization tensor of the gravitational waves, given by $\sum_s \varepsilon_{ij}^s(\mathbf{k}) \varepsilon_{mn}^{s*}(\mathbf{k})$
n_T	Spectral index of primordial tensor power spectrum
k_*	Pivot scale
S_{ABD}^3	Third order action involving perturbations of type ABD , where $(A, B, D) = (\mathcal{R}, \gamma_{ij})$
\mathcal{L}_{AB}^2	Second order Lagrangian density involving perturbations of type AB , where $(A, B) = (\mathcal{R}, \gamma_{ij})$
S_{AB}^2	Second order action involving perturbations of type AB , where $(A, B) = (\mathcal{R}, \gamma_{ij})$
$\langle A B D \rangle$	Three-point function involving perturbations of type ABD , where $(A, B, D) = (\mathcal{R}, \gamma_{ij})$

SUMMARY OF NOTATIONS

Notation	Description
G_{ABD}	Three-point function in Fourier space involving perturbations of type ABD , where $(A, B, D) = (\mathcal{R}, \gamma_{ij})$
$\hat{H}_{ABD}^{\text{int}}$	Interaction Hamiltonian involving perturbations of type ABD , where $(A, B, D) = (\mathcal{R}, \gamma_{ij})$
$\hat{L}_{ABD}^{\text{int}}$	Interaction Lagrangian involving perturbations of type ABD , where $(A, B, D) = (\mathcal{R}, \gamma_{ij})$
\mathcal{G}_{ABD}^C	The C -th integral contained in the three-point function G_{ABD} involving perturbations of type ABD , where $(A, B, D) = (\mathcal{R}, \gamma_{ij})$
η_{i}	Suitably early conformal time when the modes are inside the Hubble radius
η_{e}	Conformal time at the end of inflation
\hat{n}_{ij}	Component of the unit vector $\hat{n}_i = \mathbf{k}_i/k_i$ along the j -spatial direction
k_{ij}	Component of the wavevector \mathbf{k}_i along the j -spatial direction
f_{NL}	Non-Gaussianity parameter corresponding to the scalar bispectrum
$C_{\text{NL}}^{\mathcal{R}}$	Non-Gaussianity parameter corresponding to the scalar-scalar-tensor three-point function
C_{NL}^{γ}	Non-Gaussianity parameter corresponding to the scalar-tensor-tensor three-point function
h_{NL}	Non-Gaussianity parameter corresponding to the tensor bispectrum
$A^{(\text{G})}$	Gaussian component of the perturbation A , where $A = (\mathcal{R}, \gamma_{ij})$
k_{T}	$k_1 + k_2 + k_3$
\mathcal{R}^{B}	Constant amplitude of the long wavelength scalar mode in the squeezed limit
γ_{ij}^{B}	Constant amplitude of the long wavelength tensor mode in the squeezed limit
$\langle A B \rangle_k$	Two-point function involving perturbations of type AB , where $(A, B) = (\mathcal{R}, \gamma_{ij})$, in the presence of a long wavelength mode \mathbf{k}
$\langle A B D \rangle_k$	Three-point function involving perturbations of type ABD , where $(A, B, D) = (\mathcal{R}, \gamma_{ij})$, in the presence of a long wavelength mode \mathbf{k}
$S_{\text{em}}[A^\mu, \phi]$	Electromagnetic action with non-minimal coupling
A_μ	Electromagnetic four-vector potential
$F_{\mu\nu}$	Electromagnetic field tensor

Notation	Description
$J(\phi)$	Non-minimal coupling function in the electromagnetic action
A_i	Electromagnetic three-vector potential
$\varepsilon_{\lambda i}^{\mathbf{k}}$	Polarization vector of the electromagnetic vector potential, where $\lambda = (1, 2)$, corresponding to the mode \mathbf{k} , along the i -spatial direction
\bar{A}_k	Fourier mode of the electromagnetic vector potential corresponding to the wavenumber k
\mathcal{A}_k	Redefined Fourier mode of the electromagnetic vector potential corresponding to the wavenumber k
$\hat{\rho}_B$	Operator corresponding to the energy density associated with the magnetic field
$\hat{\rho}_E$	Operator corresponding to the energy density associated with the electric field
$\mathcal{P}_B(k)$	Power spectrum of the magnetic field
$\mathcal{P}_E(k)$	Power spectrum of the electric field
μ, b, f	Parameters describing the axion monodromy model
ϕ_0	<i>Slowly rolling</i> part of the inflaton in the axion monodromy model
ϕ_1	Part of the inflaton describing the modulations in the axion monodromy model
t_*	Time when the pivot scale k_* leaves the Hubble radius
ϕ_*	Value of the inflaton at the time when the pivot scale k_* leaves the Hubble radius
ϵ_1^0	Contribution to the first slow roll parameter due to the <i>slowly rolling</i> part of the inflaton in the axion monodromy model
ϵ_1^c	Contribution to the first slow roll parameter due to the modulations in the axion monodromy model
ϵ_1^*	Value of the first slow roll parameter at the time when the pivot scale k_* leaves the Hubble radius
δ	Redefined slow roll parameter
δ_0	Contribution to the redefined slow roll parameter δ due to the <i>slowly rolling</i> part of the inflaton in the axion monodromy model
δ_1	Contribution to the redefined slow roll parameter δ due to the modulations in the axion monodromy model

SUMMARY OF NOTATIONS

Notation	Description
ϵ_2^*	Value of the second slow roll parameter at the time when the pivot scale k_* leaves the Hubble radius
f_k^\pm	Positive and negative frequency scalar de Sitter modes
$c_k(x)$	Function describing the non-trivial evolution of the scalar modes in the axion monodromy model
ϕ_k	Value of the inflaton at the time when the scale corresponding to the wavenumber k leaves the Hubble radius
\mathcal{P}_s^0	Amplitude of the scalar power spectrum which arises in the slow roll scenario when the oscillations in the potential are absent
n_s^0	Scalar spectral index in the slow roll approximation when the oscillations in the potential are absent
n_s^c	First order correction to scalar spectral index in the axion monodromy model
h_k^\pm	Positive and negative frequency tensor de Sitter modes
$d_k(x)$	Function describing the non-trivial evolution of the tensor modes in the axion monodromy model
\mathcal{P}_T^0	Amplitude of the tensor power spectrum which arises in the slow roll scenario when the oscillations in the potential are absent
n_T^0	Tensor spectral index in the slow roll approximation when the oscillations in the potential are absent
n_T^c	First order correction to tensor spectral index in the axion monodromy model
H_{int}	Interaction Hamiltonian obtained from the third order action involving the perturbation in the scalar field and the electromagnetic field
$G_{\delta\phi BB}$	Three-point function in Fourier space involving perturbations in a scalar field and the primordial magnetic field
$\mathcal{G}_{\delta\phi BB}^C$	The C -th integral contained in the three-point function $G_{\delta\phi BB}$ involving the perturbations in a scalar field and the non-helical magnetic field

Notation	Description
b_{NL}	Non-Gaussianity parameter that characterizes the cross-correlation between the magnetic field and the perturbation in a scalar field
$\mathcal{P}_{\delta\phi}(k)$	Power spectrum of the perturbations in the scalar field ϕ
$n_{\text{B}}(k)$	Spectral index of the power spectrum of the magnetic field
$\tilde{F}^{\mu\nu}$	Dual of the electromagnetic tensor $F^{\mu\nu}$
$I(\phi)$	Non-minimal coupling function leading to parity violation
σ	Polarization of the helical electromagnetic mode, where $\sigma = (+, -)$
$\varepsilon_{\sigma i}^{\mathbf{k}}$	Polarization vector of the electromagnetic vector potential in the helicity basis, corresponding to the mode \mathbf{k} , along the i -spatial direction
\bar{A}_k^σ	Fourier mode of the helical electromagnetic vector potential corresponding to the wavenumber k
\mathcal{A}_k^σ	Redefined Fourier mode of the helical electromagnetic vector potential corresponding to the wavenumber k
$\mathcal{G}_C^{\sigma\sigma'}$	The C -th integral contained in the three-point function $G_{\delta\phi BB}$ involving the perturbations in a scalar field and the helical magnetic field

List of Figures

1.1	Evolution of Hubble radius and physical wavelength during inflation . . .	9
1.2	Evolution of Hubble radius and physical wavelength in a matter bounce . .	15
1.3	Behavior of the background energy density during a matter bounce	16
1.4	Evolution of \dot{H}/M_{Pl}^2 during a matter bounce	17
2.1	$C_{\text{NL}}^{\mathcal{R}}(\mathbf{k}_1, \mathbf{k}_2, \mathbf{k}_3)$ in the axion monodromy model	63
3.1	Evolution of tensor mode in a matter bounce	73
3.2	Behavior of the tensor power spectrum in a matter bounce	74
3.3	$h_{\text{NL}}(\mathbf{k}_1, \mathbf{k}_2, \mathbf{k}_3)$ in the equilateral limit in a matter bounce	80
3.4	$h_{\text{NL}}(\mathbf{k}_1, \mathbf{k}_2, \mathbf{k}_3)$ in the squeezed limit in a matter bounce	81
3.5	$h_{\text{NL}}(\mathbf{k}_1, \mathbf{k}_2, \mathbf{k}_3)$ in a matter bounce	82
4.1	Electromagnetic power spectra evaluated before the bounce	90
4.2	Behavior of J''/J in a bouncing scenario	91
4.3	Electromagnetic power spectra evaluated after the bounce	93
4.4	Evolution of the ratio of background and electromagnetic energy densities .	94
4.5	Behavior of the coupling function and its dual	97
5.1	Evolution of scalar and electromagnetic modes in a bouncing scenario . . .	112
5.2	$b_{\text{NL}}(\mathbf{k}_1, \mathbf{k}_2, \mathbf{k}_3)$ in de Sitter inflation	116
5.3	$b_{\text{NL}}(\mathbf{k}_1, \mathbf{k}_2, \mathbf{k}_3)$ in a bouncing scenario	117
6.1	Evolution of the non-helical and helical electromagnetic modes	130
6.2	Behavior of $G_{\delta\phi BB}(\mathbf{k}_1, \mathbf{k}_2, \mathbf{k}_3)$ with different sub-Hubble cut-off parameters .	132
6.3	Behavior of $G_{\delta\phi BB}(\mathbf{k}_1, \mathbf{k}_2, \mathbf{k}_3)$ with different N_s	134
6.4	$b_{\text{NL}}(\mathbf{k}_1, \mathbf{k}_2, \mathbf{k}_3)$ for the non-helical and helical magnetic fields	135

Chapter 1

Introduction

Mankind has been fascinated by questions related to the origin and evolution of the universe since time immemorial. Observations of celestial bodies, in particular, spawned a multitude of propositions about how the universe came into existence. However, for a long time, such ruminations were merely of philosophical interest, for lack of observational evidence and a well developed scientific framework. It has only been over the last century that we have gained access to precise observational data that could lend credence to one scientific theory over the other contending hypotheses. Cosmology has thereby gained ground as a precision science.

The Newtonian theory of gravitation is inadequate to describe gravity on the largest scales and at the greatest strengths [1]. One needs to resort to a relativistic theory of gravity, such as Einstein's general relativity, to satisfactorily explain gravitational effects over these domains. When coupled with observational data, general relativity provides the most comprehensive framework to study cosmology. The emergence of cosmology as a scientific discipline can be said to have been heralded by the discovery of the expansion of the universe (for the original paper, see Ref. [2]), about a century ago. These findings were initially encoded in the form of an empirical linear relation between the so-called luminosity distance and redshift, referred to as Hubble's law (for detailed discussions, see the standard textbooks [1]). Following the advent of this law, the discovery of the nearly perfectly thermal Cosmic Microwave Background (CMB) around half a century back (for more recent observational efforts, see Refs. [3–9]), and the formulation of the theory of big bang nucleosynthesis (see, for instance, [10]), which explains the formation of light elements in the early universe, lent further support to the advancement of cosmology.

Theoretically, in order to study our universe, it is convenient to assume that it is homogeneous and isotropic on large scales. This presumption of the large scale homogeneity and isotropy of the universe has been corroborated by observations of the Large Scale Structure (LSS) (for discussions on observations of the last decade, see Refs. [11, 12]), as well as the CMB [3–9]. The LSS suggests that the universe is homogeneous on scales

of the order of 100 Mpc [13]. Additionally, the CMB, which carries signatures of the early universe, has been observed to be exceedingly isotropic, with the amplitude of the anisotropies being only of the order of 10^{-5} [3–9]. The early universe can therefore be well described by a smooth and homogeneous background, with tiny perturbations leading to deviations from homogeneity, in concordance with the observations. The origin of such anisotropies can be attributed to quantum fluctuations in the early universe. The generation of primordial perturbations will be discussed in due course.

This thesis will be aimed at investigating various aspects of primordial physics. We shall compare and contrast between two alternative scenarios of the early universe, namely the inflationary and bouncing scenarios, both of which provide mechanisms for the generation of primordial scalar and tensor perturbations. By examining results at the level of two and three-point functions involving the scalar and tensor perturbations, we shall make efforts towards arriving at observables that can, in principle, be made use of to discriminate between these alternative scenarios. Furthermore, we shall also study the generation of primordial magnetic fields, which could act as seed fields for the large scale magnetic fields observed in the universe today (see, for instance, the reviews [14]). In addition to examining the origin and evolution of the primordial magnetic fields, we shall also study their cross-correlations with scalar perturbations.

In this introductory chapter, we shall outline some of the crucial concepts and gather the essential results that we shall make use of in the rest of the thesis. In Sec. 1.1, we shall briefly describe the standard model of cosmology and the observational constraints on the primary parameters describing the model. In Sec. 1.2, after explaining the horizon problem associated with the hot big bang model, we shall introduce the concept of inflation and present a brief review of the paradigm. In Sec. 1.3, we shall move on to discuss the key features of an alternative to inflation, the so-called bouncing scenarios. We shall then describe the mechanism of generation of primordial perturbations in Sec. 1.4, which shall apply to both inflation and bounces. We shall also evaluate the resultant power spectra associated with them, and discuss the constraints on the spectra from cosmological data. Further, in Sec. 1.5, we shall discuss the evaluation of three-point functions involving the scalar and tensor perturbations, and the possible non-Gaussian signatures therein. Sec. 1.6 will be devoted to elucidating the generation of primordial magnetic fields, particularly in the inflationary scenario. We shall conclude this chapter with Sec. 1.7, wherein we shall outline the organization of the thesis.

At this stage, let us summarize the notations and conventions that will be followed in this thesis. We shall consider general relativity as the theory describing gravity and, unless otherwise stated, we shall work with the spatially flat (3+1)-dimensional Friedmann-Lemaître-Robertson-Walker (FLRW) background metric with the signature $(-, +, +, +)$, given by

$$ds^2 = -dt^2 + a^2(t) d\mathbf{x}^2 = a^2(\eta) (-d\eta^2 + d\mathbf{x}^2), \quad (1.1)$$

where the function a denotes the scale factor, t refers to cosmic time, whereas $\eta = \int dt/a(t)$

denotes the conformal time coordinate. Additionally, we shall also use two other time variables, *viz.* the number of e-folds N and the number of e-N-folds \mathcal{N} , the latter of which will be specifically used to describe bouncing universes. We shall switch between the different time variables according to our convenience. We shall work with units such that $\hbar = c = 1$ and assume the Planck mass to be $M_{\text{Pl}} = (8\pi G)^{-1/2}$. Greek indices will denote the spacetime coordinates, while Latin indices will represent the spatial coordinates (except for the index k which will be reserved for representing the wavenumber of the perturbations). An overdot and an overprime will denote differentiation with respect to the cosmic and the conformal time coordinates, respectively.

1.1 The standard model of cosmology

The knowledge about the characteristics of and the interplay between three of the four fundamental forces, *viz.* the electromagnetic, weak, and strong interactions, as well as the classification of the elementary particles is encapsulated in the standard model of particle physics (for instance, see the standard textbooks [15]). One of the salient features of the standard model is the unification of the three fundamental forces alluded to above. This model was brought about as a result of path-breaking investigations in particle physics over the latter half of the twentieth century. In a similar manner, over the last two decades, there has been an unprecedented headway in obtaining precise cosmological data. This has facilitated the conception of a standard model of cosmology, that encompasses our present knowledge about the origin and evolution of the universe, while being compatible with the burgeoning wealth of accurate cosmological data [1].

Let us begin our description of the standard model of cosmology, popularly referred to as the hot big bang model, by introducing various quantities that are used to characterize the background evolution of the universe. As we have already mentioned before, the universe has been observed to be expanding. If we envision spacetime as a grid of points, and consider that the coordinates of each point remain the same with the passage of time, then it is clear that the distance between the coordinates of any two points, namely the comoving distance, remains constant in time. However, the physical distance between two points would increase with the expansion of spacetime. The scale factor, commonly denoted by $a(t)$ [as introduced in the line element (1.1)], is a monotonically increasing function of time in an expanding universe. In terms of this quantity, the physical distance can be expressed as a product of the comoving distance and the scale factor.

A quantity known as the Hubble parameter is defined to describe the rate of change in the scale factor as follows:

$$H(t) = \frac{\dot{a}}{a}. \quad (1.2)$$

The value of the Hubble parameter today, denoted by H_0 , is known as the Hubble con-

stant. H_0 is also often parameterized using a quantity h as: $H_0 = 100 h \text{ km s}^{-1} \text{ Mpc}^{-1}$. (It should be noted that this quantity h is distinct from Planck's constant \hbar .)

For a generic spatial curvature K , the Einstein's equations corresponding to the FLRW background can be written as:

$$H^2 + \frac{K}{a^2} = \frac{8\pi G}{3} \rho, \quad (1.3a)$$

$$H^2 + 2\frac{\ddot{a}}{a} + \frac{K}{a^2} = -8\pi G p, \quad (1.3b)$$

where H is the Hubble parameter [cf. Eq. (1.2)], ρ denotes the background energy density, and p denotes the total pressure. These equations are known as the Friedmann equations. In addition to Eqs. (1.3), we also have another equation arising from the conservation of the stress-energy tensor, which is given by

$$\dot{\rho} + 3H(\rho + p) = 0. \quad (1.4)$$

It is useful to note that Eqs. (1.3) and (1.4) are not independent. Therefore, if we introduce a simplifying assumption, *viz.* an equation of state of the form: $p = w\rho$, from Eq. (1.4), we can obtain the energy density to be: $\rho \propto a^{-3(1+w)}$. It is well known that besides matter, there is also radiation present (such as the CMB, which comprises the most dominant form of radiation [16]) in the universe. Radiation has the equation of state parameter $w = 1/3$, while for pressureless matter, $w = 0$. Hence, the energy density of radiation scales as a^{-4} , while that of non-relativistic matter scales as a^{-3} . Using these expressions and the observational evidence for the expansion of the universe, it is easy to infer that at very early times, the universe was radiation dominated. The era of radiation domination was succeeded by a matter dominated epoch. Interestingly, the energy content of the present universe has been determined to be dominated by an as yet obscure form of energy, referred to as dark energy, which is driving its current expansion. Using the observations of the standard candles, *viz.* astronomical objects having the same intrinsic brightness, such as distant Type Ia supernovae, it has been well established that our universe is in fact presently undergoing an accelerated expansion [17, 18]. The simplest model of dark energy, referred to as the cosmological constant, is consistent with the observations of the supernovae, as well as those of the CMB [19].

Let us now briefly describe the dynamics of the Friedmann universe. We can rewrite Eq. (1.3a) as

$$\Omega - 1 = \frac{K}{a^2 H^2}, \quad (1.5)$$

where Ω is a quantity known as the density parameter, which is defined as

$$\Omega = \frac{8\pi G}{3H^2} \rho. \quad (1.6)$$

Further, we can define a quantity known as the critical density (ρ_{cr}) via the relation: $\rho_{\text{cr}} = 3H^2/(8\pi G)$. In terms of this quantity, the density parameter can be expressed as: $\Omega = \rho/\rho_{\text{cr}}$. Using the above definitions and Eq. (1.5), it is easy to classify the spatial geometry of the universe as flat, closed or open, which corresponds to $K = 0, +1$ and -1 , respectively. The energy density in a flat universe can be shown to be equal to the critical energy density. A closed geometry is characterized by an energy density larger than ρ_{cr} , whereas, in an open geometry, the total energy density is lower than ρ_{cr} .

Let us now introduce a quantity known as the redshift, denoted by z , which is a convenient observational variable for characterizing the different epochs of the universe. It is defined as: $1 + z = a(t_0)/a(t)$, with $a(t_0)$ denoting the scale factor today (*i.e.* at t_0). In terms of the redshift, the Hubble parameter can be related to the total energy density of the universe via Eq. (1.3a) as follows:

$$H^2(z) = H_0^2 [\Omega_{\text{R}}^0 (1+z)^4 + \Omega_{\text{NR}}^0 (1+z)^3 + \Omega_{\Lambda}^0 - \Omega_{\text{K}}^0 (1+z)^2]. \quad (1.7)$$

As we have mentioned before, H_0 represents the value of the Hubble parameter at the present time, while $\Omega_{\text{R}}^0, \Omega_{\text{NR}}^0, \Omega_{\Lambda}^0$ and Ω_{K}^0 are the density parameters corresponding to the relativistic matter, the non-relativistic matter, the dark energy and the spatial curvature, respectively. These parameters are defined as: $\Omega_{\text{i}}^0 = \rho_{\text{i}}^0/\rho_{\text{cr}}^0$. The superscripts '0' on all these quantities denote their value today. The density parameter Ω_{NR}^0 is constituted of both the baryons as well as the cold dark matter, while Ω_{K}^0 is related to the spatial curvature as: $\Omega_{\text{K}}^0 = \Omega^0 - 1 = (K/a_0^2 H_0^2)$ [cf. Eq. (1.5)]. The quantity Ω_{K}^0 is also referred to as the spatial flatness parameter. The values of these parameters are constrained by a wide variety of data from sources including the CMB, LSS, as well as supernovae. From Eq. (1.7), it is clear that we would require to know the temporal evolution of the energy densities in order to comprehend the behavior of the scale factor over time. For instance, it is useful to note that, for a spatially flat universe (*i.e.* when $K = 0$), the scale factor during a radiation dominated era can be written as $a(t) \propto t^{1/2}$ or, equivalently, as $a(\eta) \propto \eta$. During a matter dominated epoch, the scale factor is given by $a(t) \propto t^{2/3}$, which also implies that $a(\eta) \propto \eta^2$. The behavior of the scale factor suggests that at $t = 0$ (or, at $\eta = 0$), the energy densities were infinitely high. This domain in time is often referred to as the big bang, wherein general relativity is expected to fail and quantum gravitational effects are supposed to take over.

As the CMB is thermal and the energy density of radiation falls as a^{-4} , it is easy to infer that the temperature of radiation scales as a^{-1} . Since all the relativistic particles are in thermal equilibrium with the photons at early times, their energy decreases as the temperature falls in an expanding universe. As the rates of interaction of these relativistic species drop below the expansion rate, they cannot stay in thermal equilibrium with the photons and decouple. The CMB that we observe today is constituted of photons that decoupled from the electrons about 380,000 years after the big bang, and have traveled freely through space and time ever since.

The standard model of cosmology, also popularly known as the hot big bang model, can be described by the following six parameters: the energy density of baryons $\Omega_b h^2$, the energy density of cold dark matter $\Omega_c h^2$, the Hubble parameter H_0 , the reionization optical depth τ , the amplitude of scalar fluctuations A_s and the scalar spectral index n_s . These parameters have been constrained by the most recent Planck data to be [8, 9]:

$$\Omega_b^0 h^2 = 0.02237 \pm 0.00015, \quad (1.8a)$$

$$\Omega_c^0 h^2 = 0.1200 \pm 0.0012, \quad (1.8b)$$

$$H_0 = 67.36 \pm 0.54 \text{ km s}^{-1} \text{ Mpc}^{-1}, \quad (1.8c)$$

$$\tau = 0.0544 \pm 0.0073, \quad (1.8d)$$

$$\ln(10^{10} A_s) = 3.044 \pm 0.014, \quad (1.8e)$$

$$n_s = 0.9649 \pm 0.0042. \quad (1.8f)$$

In the above list of parameters, the quantity $\Omega_b^0 h^2$ represents the total energy density of baryonic matter in the universe, which comprises all the known visible matter, including the large scale structure. $\Omega_c^0 h^2$, on the other hand, refers to the energy density of cold dark matter, which indisputably dominates the matter content of the universe. The quantity τ is the Thomson scattering optical depth of reionized intergalactic medium. The parameters A_s and n_s are related to the amplitude of the primordial inhomogeneities, albeit tiny, whose imprints are observed in the CMB. The quantities A_s and n_s and their significance will be discussed in detail in a later section. It is useful to note that, using the value of the Hubble constant today as arrived at by the Planck collaboration [8, 9], the critical energy density can be obtained to be $\rho_{\text{cr}} \sim 10^{-29} \text{ g cm}^{-3}$, and the age of the universe can be obtained to be approximately 13.7 billion years. Also, upon using the Planck and the Baryon Acoustic Oscillations (BAO) data, the flatness parameter characterizing the geometry of the universe is constrained to be $|\Omega_k^0| = 0.0007 \pm 0.0019$ [8], so that the universe we live in can be considered to be essentially flat. Accordingly, in this thesis, we shall work with the spatially flat FLRW metric [cf. Eq. (1.1)].

1.2 The inflationary paradigm

Inflation has so far been the most successful paradigm to describe the early universe. In this section, we shall discuss the motivations for introducing the concept of inflation. We shall show that inflation can provide an efficient mechanism to circumvent some of the issues associated with the standard model of cosmology. We shall also discuss how inflation can be easily achieved using scalar fields.

1.2.1 Drawbacks of the hot big bang model

The hot big bang model, in spite of its various triumphs, has been mired in certain complications, such as the horizon and flatness problems (see the following texts [1] and reviews [20–22]). The horizon problem, which can be said to be the most severe issue afflicting the hot big bang theory, refers to the conundrum that the CMB is observed to have a nearly uniform temperature all over the sky. However, within the hot big bang scenario, two points separated by more than a few degrees in the sky could not have been causally connected at the era of decoupling and, hence, the fact that they exhibit the same temperature at present cannot be explained by any causal mechanism.

The horizon problem can be comprehended easily if we consider the ratio of the dimensions of the forward light cone from the big bang to decoupling to that of the backward light cone from the present to the decoupling era. Let us assume that the universe was dominated by non-relativistic matter from the time of decoupling (say, t_{dec}) till today (say, t_0). Then the size of the backward light cone at the time of last scattering of the CMB photons can be obtained to be

$$l_{\text{B}}(t_0, t_{\text{dec}}) = a(t_{\text{dec}}) \int_{t_{\text{dec}}}^{t_0} \frac{d\tilde{t}}{a(\tilde{t})} \simeq 3 (t_{\text{dec}}^2 t_0)^{1/3}, \quad (1.9)$$

where we have assumed that $t_0 \gg t_{\text{dec}}$. Now, if we consider the universe to have been radiation dominated from big bang till decoupling, the dimension of the forward light cone at decoupling can be evaluated to be

$$l_{\text{F}}(t_{\text{dec}}, 0) = a(t_{\text{dec}}) \int_0^{t_{\text{dec}}} \frac{d\tilde{t}}{a(\tilde{t})} = 2 t_{\text{dec}}. \quad (1.10)$$

Therefore, the ratio of the sizes of the backward and forward light cones can be estimated to be

$$\frac{l_{\text{B}}}{l_{\text{F}}} = \left(\frac{3}{2}\right) \left(\frac{t_0}{t_{\text{dec}}}\right)^{1/3} \simeq 70. \quad (1.11)$$

Note that we have used the fact that $t_0 \simeq 10^{10}$ years and $t_{\text{dec}} \simeq 10^5$ years to arrive at the final value in the previous equation. Since the backward light cone is about 70 times larger than the forward light cone, widely separated points in the sky could not have been in causal contact at decoupling. Therefore, the observation that the temperature is uniform throughout the CMB sky is irreconcilable with the hot big bang model.

In the preceding section, we had mentioned that according to the most recent bounds arrived at by Planck, the flatness parameter today has been constrained to be $|\Omega_{\text{K}}^0| = 0.0007 \pm 0.0019$ [8], which implies that the universe can essentially be considered to be spatially flat at the present time. If we make use of Eq. (1.5) within the standard model, we find that in order for the flatness parameter to be nearly close to zero today, $|\Omega_{\text{K}}^0|$ must

have been of the order of 10^{-50} at the very early stages of the radiation dominated epoch (for instance, when the temperature was around 10^{14} GeV). This seems to necessitate a tremendous extent of fine tuning of the flatness parameter. Therefore, the flatness problem too seems to call for a revision or an extension of the standard hot big bang model of cosmology to conform with the gradually proliferating amount of precise cosmological data.

1.2.2 Overcoming the horizon problem with inflation

It is evident that the physical wavelength always grows linearly with the scale factor, *i.e.* $\lambda_p \propto a$. However, the horizon size and, consequently, the Hubble radius ($d_H = H^{-1}$), in a power law expansion characterized by the scale factor $a(t) \propto t^q$, with $q < 1$, scales as $a^{1/q}$. Therefore, we have that $\lambda_p/d_H \propto a^{(q-1)/q}$. In radiation dominated and matter dominated scenarios, $q < 1$. Hence the physical wavelength grows faster than the Hubble radius as we go back in time and, accordingly, the primordial perturbations have to be correlated on scales larger than the horizon size in order to account for the observations of the CMB. This behavior has been illustrated in Fig. 1.1. This is essentially a restatement of the horizon problem that we had discussed above.

In order to avoid invoking an acausal mechanism, it is imperative to have an epoch in the early universe wherein the physical wavelength would decrease faster than the Hubble radius as we go back in time, *i.e.*

$$-\frac{d}{dt} \left(\frac{\lambda_p}{d_H} \right) < 0. \quad (1.12)$$

This directly leads to the condition that $\ddot{a} > 0$. Therefore, it is necessary for the universe to have undergone a period of accelerated expansion at very early times. Such an epoch of accelerated expansion is referred to as inflation. In order to surmount the horizon problem, the inflationary phase should last at least long enough so that the sizes of the backward and the forward light cones at the time of last scattering of the CMB photons are equal. Let us assume that inflation lasts from t_i to t_f in the early stages of the radiation dominated epoch. The size of the horizon at decoupling, incremented during inflation, is given by

$$l_I(t_0, t_{\text{dec}}) = a(t_{\text{dec}}) \int_{t_{\text{dec}}}^{t_0} \frac{d\tilde{t}}{a(\tilde{t})} \simeq \left[\frac{a(t_{\text{dec}})}{H_I} \right] \left(\frac{t_{\text{dec}}}{t_f} \right)^{1/2} R, \quad (1.13)$$

where H_I is the constant value of the Hubble parameter during exponential inflation, R quantifies the amount by which the scale factor increases during inflation and, for simplicity, we have set $t_i = H_I^{-1}$. In this case the ratio of the backward and forward light cones at decoupling is given by

$$\frac{l_B}{l_I} \simeq \frac{10^{26}}{R}, \quad (1.14)$$

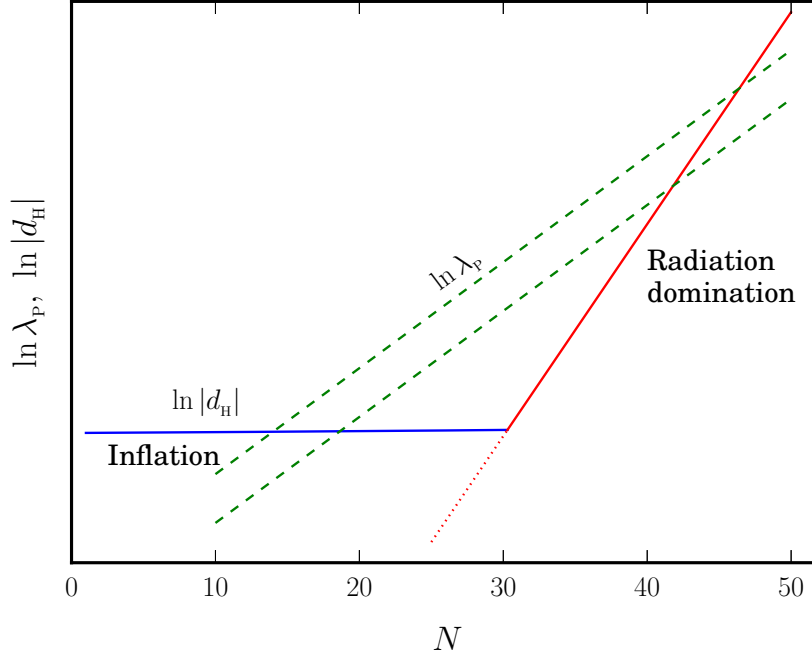


Figure 1.1: This figure illustrates the behavior of the Hubble radius and the physical wavelengths in the early universe. The blue solid line denotes the behavior of the Hubble radius during inflation, wherein it is nearly constant. The red solid line represents the Hubble radius during the radiation dominated era, when $d_H \propto a^2$, while the red dotted line shows the behavior of the Hubble radius in non-inflationary cosmology. The two green dashed lines denote the behavior of the physical wavelengths, *i.e.* $\lambda_p \propto a$, corresponding to two different wavenumbers. The quantity N plotted on the abscissa is known as the e-folds, and is defined as $N = \ln[a/a(t_i)]$. It is evident from the figure that, without an epoch of inflation, it is not possible to bring the modes inside the Hubble radius at early times.

where, for illustrative purposes, we have chosen $H_i = 10^{13}$ GeV. Evidently, for the two light cones to be equal in size, we must have $R \simeq 10^{26}$.

Let us introduce another temporal variable known as e-folds N (in this context, also see the caption of Fig. 1.1), defined as

$$N = \int_{t_i}^t dt H = \ln \left[\frac{a(t)}{a(t_i)} \right]. \quad (1.15)$$

Therefore, in order to obtain $R \simeq 10^{26}$, we must have $N \simeq 60$, *i.e.* allowing for at least 60 e-folds of inflation resolves the horizon problem [20–22]. It should be noted that, achieving 60 e-folds of inflation ensures that the largest observable scale today was inside the Hubble radius during the early stages of inflation [23]. Furthermore, as should be evident from Eq. (1.5), if one assumes H to be nearly constant, such an extended phase of inflation also alleviates the flatness problem, because even a very large value of the flatness

parameter at the beginning of the inflationary era can be exponentially reduced by means of a sufficient duration of expansion so as to result in the nearly flat spatial geometry that is observed today.

1.2.3 Driving inflation with scalar fields

Let ρ and p denote the energy density and the pressure of the matter field driving inflation. Recall that, hereafter, we shall be working with a *spatially flat* FLRW metric. In a spatially flat, homogeneous and isotropic background, the Friedmann equations can be written as

$$H^2 = \frac{8\pi G}{3} \rho, \quad (1.16a)$$

$$\frac{\ddot{a}}{a} = -\frac{4\pi G}{3} (\rho + 3p). \quad (1.16b)$$

Note that Eq. (1.16b) has been obtained by combining Eqs. (1.3). Further, the two Friedmann equations (1.16) can be combined to arrive at

$$\dot{H} = -4\pi G (\rho + p). \quad (1.17)$$

From Eq. (1.16b), it is evident that in order to obtain inflation (*i.e.* $\ddot{a} > 0$), we must have $(\rho + 3p) < 0$. The energy density and pressure associated with ordinary matter or radiation cannot satisfy this relation. Therefore, one resorts to using scalar fields to achieve this condition.

Let us consider a canonical scalar field ϕ described by the potential $V(\phi)$. The action governing this field is given by

$$S[\phi] = - \int d^4x \sqrt{-g} \left[\frac{1}{2} \partial_\mu \phi \partial^\mu \phi + V(\phi) \right]. \quad (1.18)$$

Varying the action for the scalar field results in the following equation of motion:

$$\ddot{\phi} + 3H\dot{\phi} + V_\phi = 0, \quad (1.19)$$

where $V_\phi = dV/d\phi$. The stress-energy tensor associated with this field can be obtained to be

$$T^\mu_\nu = \partial^\mu \phi \partial_\nu \phi - \delta^\mu_\nu \left[\frac{1}{2} \partial_\mu \phi \partial^\mu \phi + V(\phi) \right], \quad (1.20)$$

and the components of this tensor are given by

$$T^0_0 = -\rho = -\frac{\dot{\phi}^2}{2} - V(\phi), \quad (1.21a)$$

$$T^i_j = p \delta^i_j = \left[\frac{\dot{\phi}^2}{2} - V(\phi) \right] \delta^i_j, \quad (1.21b)$$

where ρ and p now denote the energy density and the pressure associated with the scalar field ϕ . From these two expressions, it is evident that the condition for inflation, *viz.* $(\rho + 3p) < 0$, can be rewritten as

$$\dot{\phi}^2 < V(\phi), \quad (1.22)$$

i.e. the potential energy of the scalar field must dominate over the kinetic energy in order to lead to a phase of inflation.

The Friedmann equations (1.16a) and (1.17) for the scalar field can now be written as

$$H^2 = \frac{1}{3 M_{\text{Pl}}^2} \left[\frac{\dot{\phi}^2}{2} + V(\phi) \right], \quad (1.23a)$$

$$\dot{H} = -\frac{\dot{\phi}^2}{2 M_{\text{Pl}}^2}. \quad (1.23b)$$

Combining these two equations, we obtain

$$\phi(t) = \sqrt{2} M_{\text{Pl}} \int dt \sqrt{-\dot{H}}, \quad (1.24a)$$

$$V(t) = M_{\text{Pl}}^2 \left(3 H^2 + \dot{H} \right). \quad (1.24b)$$

Knowing the form of the scale factor, these two equations can be used to obtain the corresponding inflationary potential. For example, it can be shown that a scale factor corresponding to power law expansion, *viz.* $a(t) \propto t^q$, with $q > 1$, can be obtained from an exponential potential of the form [1, 20–22]

$$V(\phi) = V_0 \exp \left[-\sqrt{\frac{2}{q}} \frac{\phi}{M_{\text{Pl}}} \right], \quad (1.25)$$

where V_0 is a constant of integration.

The scalar field that drives inflation is commonly referred to as the inflaton. As mentioned before, for obtaining inflation, the potential energy of the inflaton must dominate over its kinetic energy. In order to achieve the requisite 60 or so e-folds of inflation, we must have the field *slowly rolling* down the potential such that

$$\dot{\phi}^2 \ll V(\phi) \quad (1.26)$$

and

$$\ddot{\phi} \ll 3 H \dot{\phi}. \quad (1.27)$$

A hierarchy of the so-called dimensionless slow roll parameters are often introduced to quantify this behavior. The first of these parameters is defined as [24]

$$\epsilon_1 = -\frac{\dot{H}}{H^2}. \quad (1.28)$$

The subsequent slow roll parameters are defined as

$$\epsilon_{i+1} = \frac{d \ln \epsilon_i}{dN}, \quad (1.29)$$

where $i \geq 1$. It is evident from the definition that the condition for inflation corresponds to $\epsilon_1 < 1$ while the condition for slow roll inflation is given by $\epsilon_1 \ll 1$. Under the slow roll approximation, the first Friedmann equation (1.23a) and the scalar field equation (1.19) reduce to

$$H^2 \simeq \frac{V}{3 M_{\text{Pl}}^2}, \quad (1.30a)$$

$$3 H \dot{\phi} \simeq -V_{\phi}. \quad (1.30b)$$

Upon using these equations, the number of e-folds of inflation can be expressed as

$$N = \int_{t_i}^t dt H \simeq -\frac{1}{M_{\text{Pl}}^2} \int_{\phi_i}^{\phi} d\phi \left(\frac{V}{V_{\phi}} \right), \quad (1.31)$$

where ϕ_i and ϕ are the values of the inflation at t_i and t respectively.

As an example, let us consider the case of large field inflation, wherein the potential is given by: $V(\phi) = V_0 \phi^n$, where V_0 is a constant and $n > 0$. Using Eq. (1.31), the value of the scalar field and the Hubble parameter at any e-fold N can be obtained to be

$$\phi^2(N) \simeq \phi_i^2 - 2 n M_{\text{Pl}}^2 N, \quad (1.32a)$$

$$H^2(N) \simeq \frac{V_0 M_{\text{Pl}}^{n-2}}{3} \left[\left(\frac{\phi_i}{M_{\text{Pl}}} \right)^2 - 2 n N \right]^{n/2}. \quad (1.32b)$$

These analytical expressions, when compared with the exact numerical solutions of Eq. (1.19) for the large field potential, are found to be an excellent approximation.

1.3 Classical bouncing scenarios as an alternative to inflation

Bouncing scenarios, wherein the big bang is replaced by a bounce, are a promising alternative to the inflationary framework. One of the primary aims for studying these scenarios in this thesis is to arrive at discriminating observables that can help us distinguish them from inflationary models. In this section, we shall briefly introduce the key features of bouncing scenarios. We shall restrict our attention to *classical* bouncing scenarios, wherein the background energy density remains much smaller than the Planckian energy density at all times, particularly around the bounce, thereby averting the necessity to consider quantum gravitational effects. We shall also consider the specific case of a matter bounce scenario, and describe its characteristics as an illustrative example.

1.3.1 A brief review of bouncing scenarios

Notwithstanding the prodigious success of the inflationary paradigm [20–22], alternative frameworks to describe the early universe have been propounded. Such efforts have been prompted by the dearth of a means to arrive at a unique model of inflation, as well as apprehensions with regard to its falsifiability (in this context, see Ref. [25]; for a recent popular account, see Ref. [26]). Among these possibilities, the bouncing scenarios seem to have garnered substantial attention [27–45]. Broadly speaking, in bouncing models, the universe undergoes a period of contraction which culminates at a point in time, known as the bounce, where the scale factor attains a minimum value. Thereafter, the universe transits to a phase of expansion. As is the case with inflation, these models too provide a way to overcome the horizon problem, by permitting the imposition of well-motivated causal initial conditions on the primordial perturbations early on in the contracting phase (see, for instance, Refs. [30, 32, 33, 37, 38, 42, 46–50]; for reviews, see Refs. [51, 52]). Additionally, in certain bouncing scenarios, it has also been possible to achieve nearly scale invariant primordial perturbation spectra consistent with observations (see, for example, Refs. [37, 49, 50]), which further affirms their footing as an alternative to inflation. As we have mentioned before, in this thesis, we shall confine our attention to the so-called classical bounces, wherein the background energy density always remains smaller than the Planckian energy density, thereby precluding the need to account for possible Planck scale effects.

1.3.2 Issues associated with bouncing models

The construction of a viable bouncing scenario which leads to predictions in conformity with CMB observations, while being free of pathologies, has proved to be an intricate task. Since a bouncing model necessarily involves a contracting phase, perturbations initially present in the sub-Hubble regime, instead of decaying as in an inflationary expansion, can grow during contraction. This could conceivably interfere with the requirement of an initial homogeneous background. Further, such a behavior could cast doubt on the validity of linear perturbation theory close to the bounce [36, 52, 53]. The contracting epoch may also expedite the growth of anisotropies, leading to the Belinsky-Khalatnikov-Lifshitz instability [54]. These issues can be ameliorated to a certain extent in ekpyrotic scenarios [29, 35, 37] or by a finely tuned choice of initial conditions [31]. Owing to the behavior of the Hubble parameter, which changes sign from negative during the contracting phase to positive during the expanding phase, the quantity \dot{H} becomes positive for a narrow range of time around the bounce. In order to obtain such a behavior of \dot{H} , it is evident from Eq. (1.17) that, for a spatially flat case, we must have $(\rho + p) < 0$ during the period when $\dot{H} > 0$. Therefore, the null energy condition ought to be violated in the vicinity of the bounce. This can precipitate in the divergence of certain gauge invariant quantities and hinder the smooth evolution of perturbations across the bounce. One may need to

adopt a suitable gauge to sidestep these issues [32]. The possible complications due to the amplification of vector perturbations can be thwarted by assuming the absence of vector sources in the early universe [36]. There have been intense efforts to construct efficient bouncing models. In this thesis, we shall mostly restrict our attention to the simpler and symmetric matter bounce models.

1.3.3 Characteristics of a matter bounce

A matter bounce is a specific class of bouncing scenarios characterized by a scale factor which, in the early phase of contraction, behaves as in a matter dominated universe. Let us consider a scale factor of the form:

$$a(\eta) = a_0 \left(1 + \eta^2/\eta_0^2\right) = a_0 \left(1 + k_0^2 \eta^2\right), \quad (1.33)$$

where a_0 is the value of the scale factor at the bounce, *i.e.* at $\eta = 0$, while η_0 or, equivalently, $1/k_0$, denotes the time scale associated with the bounce¹. As we have asserted previously, matter bounces resolve the horizon problem by bringing the modes inside the Hubble radius at early times during the phase of contraction. This property has been illustrated in Fig. 1.2.

Let us now turn to a brief appraisal of the matter bounce scenarios that have been studied so far. It has been repeatedly asserted that symmetric matter bounces lead to a large tensor-to-scalar ratio (r) that cannot be reconciled with the constraint of $r < 0.064$ from the Planck mission [9] (the tensor-to-scalar ratio and related constraints will be discussed in Subsec. 1.4.2). However, in a recent piece of work, it has been illustrated that a symmetric matter bounce modeled using two scalar fields can lead to a feasible value of r [56]. Further, by means of tweaking the initial conditions suitably, it is possible to obtain a realistic value of the tensor-to-scalar ratio even in asymmetric bounces [32]. It is straightforward to establish that, in a spatially flat matter bounce, the Hubble parameter and, consequently, the background energy density vanishes at the bounce. This behavior has been depicted in Fig. 1.3. Since the universe transits from an initially contracting epoch to an expanding era, the Hubble parameter changes sign from negative to positive at the bounce. In order to facilitate such behavior, as we have discussed before, the quantity \dot{H} must become positive for a short period of time around the bounce. As a result, from Eq. (1.17), it is clear that within the context of Einsteinian gravity, it is imperative to violate the null energy condition in order to obtain a matter bounce. This point has also been illustrated in Fig. 1.4. Evidently, investigating the generation of perturbations and their evolution in a matter bounce entails meticulous modeling of the background. Several methods have been suggested to achieve this purpose, such as introduction of a ghost

¹Previously, we have used the subscript ‘0’ to denote the values of various quantities at the present time. For instance, t_0 denotes the time today and $a(t_0)$ has been used to refer to the scale factor today. We should emphasize here that while discussing bounces, a_0 will describe the value of the scale factor *at* the bounce.

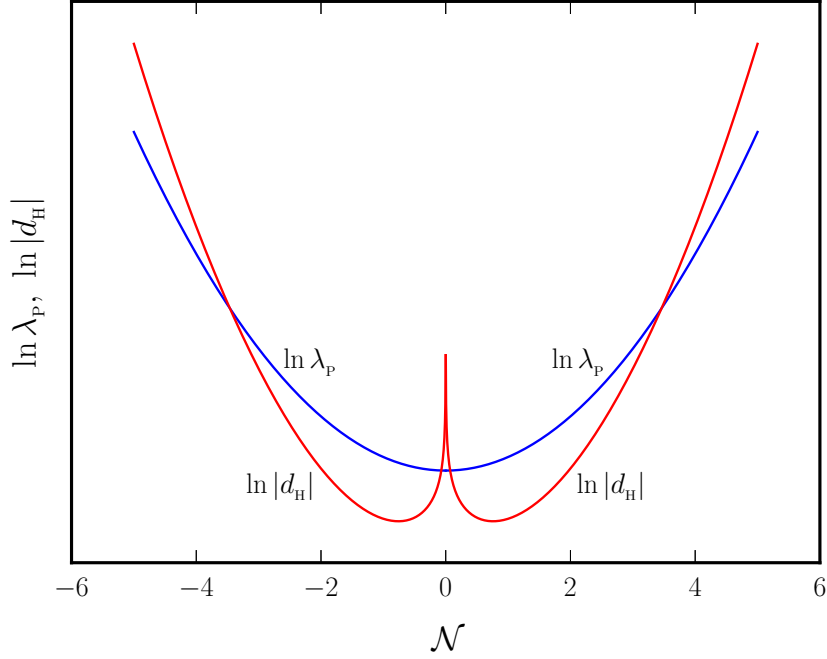


Figure 1.2: This figure illustrates the behavior of the Hubble radius d_H and the physical wavelength λ_p in a symmetric matter bounce. The blue solid line denotes the physical wavelength, *i.e.* $\lambda_p \propto a$, and the red solid line represents the Hubble radius during the matter bounce scenario of our interest. The quantity along the abscissa is known as e-N-folds and is a convenient time variable for describing bouncing scenarios [55]. In terms of this variable, the scale factor is defined as: $a(\mathcal{N}) = a_0 e^{\mathcal{N}^2/2}$, wherein a_0 is the minimum value of the scale factor at the bounce, which corresponds to the time when $\mathcal{N} = 0$. Note that, in order to plot this figure, we only need the value of the parameter $k_0/(a_0 M_{\text{Pl}})$, which we have set to be $k_0/(a_0 M_{\text{Pl}}) = 3.3 \times 10^{-8}$ [56]. It is evident from the figure that the modes are well inside the Hubble radius at very early times during the contracting phase. The red spike at $\mathcal{N} = 0$ indicates that the Hubble radius diverges at the bounce. We had mentioned that $1/k_0$ is the time scale associated with the bounce. Note that, in terms of cosmic time t , the duration of the bounce is of the order of a_0/k_0 .

field with negative energy density [32–34], the ghost-condensate mechanism [39, 40], the matter bounce curvaton scenario [41] and the Galileon Lagrangian [42–44].

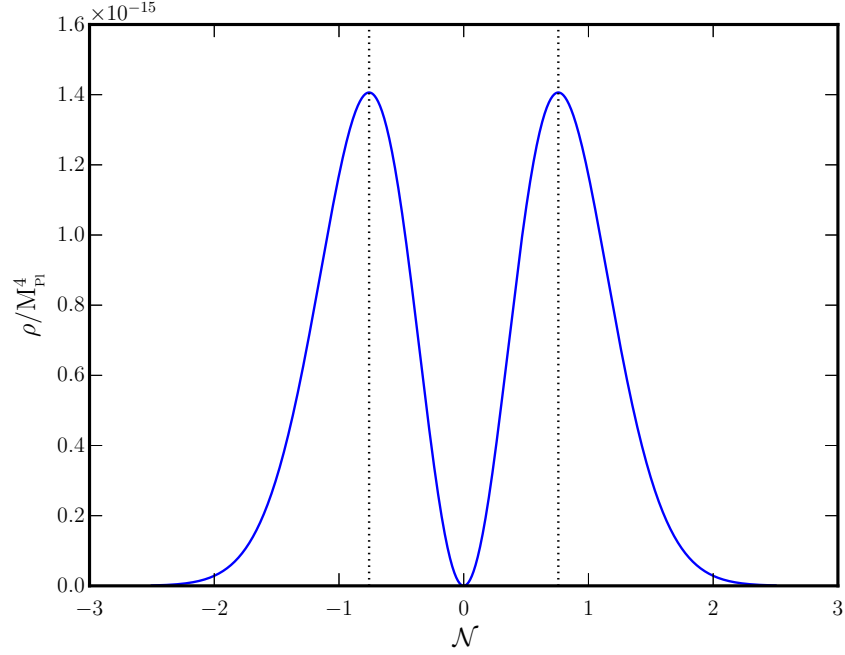


Figure 1.3: The background energy density ρ/M_{Pl}^4 during the matter bounce has been plotted. This figure has also been plotted for $k_0/(a_0 M_{\text{Pl}}) = 3.3 \times 10^{-8}$, as in Fig. 1.2. The value of the background energy density depends only on this parameter. It is clear from the plot that ρ vanishes at the bounce, a behavior that arises due to the vanishing of the Hubble parameter at the bounce. Further, the energy density reaches its maximum value at two points symmetrically prior to and after the bounce, at times $\eta = \pm 1/(\sqrt{3} k_0)$, which corresponds to $\mathcal{N} = \pm 0.758$. The vertical black dotted lines denote the time on either side of the bounce when the energy density attains maximum value. Beyond this point in time, the energy density decreases on either side of the bounce. Further, it is important to note that the background energy density remains much smaller than the Planckian energy density at all times, as should be the case for a classical bouncing scenario.

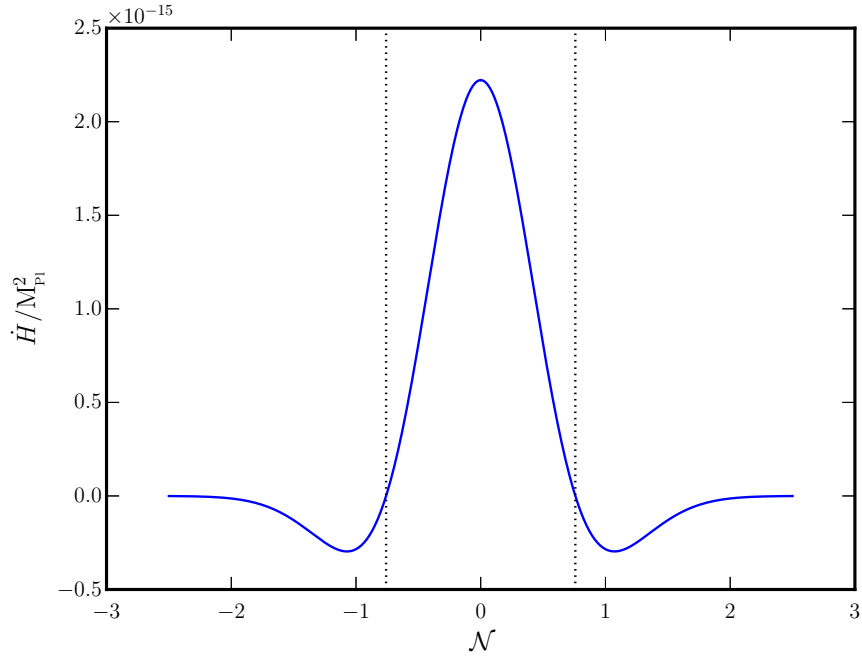


Figure 1.4: The behavior of \dot{H} has been plotted for the case of the matter bounce, for the same values of the parameters as in the previous figures. In the domain wherein the energy decreases as one approaches the bounce, one finds that $\dot{H} > 0$. The range of time during which $\dot{H} > 0$ has been bounded by the vertical black dotted lines. As in Fig. 1.3, the vertical black dotted lines also represent the time on either side of the bounce when the background energy density attains maximum value. Using Eq. (1.17), we obtain that $(\rho + p) < 0$ during the period when $\dot{H} > 0$, which suggests that the null energy condition is violated over this domain.

1.4 Generation of primordial perturbations and power spectra

Inflation provides a natural mechanism for the generation of primordial perturbations that can, in the course of time, evolve and amplify to form the large scale structures observed today [1, 20–22]. As noted before, from the CMB observations, it has been deduced that the amplitude of anisotropies in the CMB are only about one part in 10^5 . Owing to the tiny amplitude of these perturbations, we can study them using linear perturbation theory. In this section, we shall briefly describe the generation of primordial perturbations. After arriving at the equations of motion governing their evolution, we shall discuss the quantization of these perturbations and the resultant power spectra, which can be constrained by observations. We shall also describe an interesting property of the power spectra, known as duality invariance. We should emphasize here that the methods we shall use to describe the origin and evolution of primordial perturbations in this section shall apply to inflationary scenarios. The generation of primordial perturbations in bouncing scenarios often need to be dealt with on a case-by-case basis. We shall discuss the relevant details of such investigations in due course.

1.4.1 Classification of the perturbations

In the Friedmann background, the metric perturbations can be decomposed into scalar, vector and tensor perturbations. In the $(3 + 1)$ spacetime dimensions of our interest, one can show that there are two independent degrees of freedom for each of the scalar, vector and tensor components of the metric perturbations. The perturbed stress-energy tensor can also be classified into its scalar, vector and tensor components. At the linear order in perturbation theory, these components evolve independently.

Let us first consider the case of the scalar perturbations. For convenience, we shall work in the longitudinal gauge. The Friedmann line element in this gauge is given by [20–22]

$$ds^2 = -(1 + 2\Phi) dt^2 + a^2(t) (1 - 2\Psi) d\mathbf{x}^2, \quad (1.34)$$

where Φ and Ψ are functions of space and time that denote the two independent scalar degrees of freedom describing the inhomogeneities. Neglecting anisotropic stresses (as we shall be considering scalar field sources which do not possess them), the components of the perturbed stress-energy tensor are given by

$$\delta T_0^0 = -\delta\rho, \quad (1.35a)$$

$$\delta T_i^0 = -\nabla_i \delta\sigma, \quad (1.35b)$$

$$\delta T_j^i = \delta p \delta_j^i, \quad (1.35c)$$

where $\delta\rho$, $\delta\sigma$ and δp denote the perturbations in the energy density, momentum flux, and pressure, respectively, and ∇_i denotes the covariant derivative. Using the above expressions in the perturbed first order Einstein's equations, *viz.* $\delta G^\mu_\nu = 8\pi G \delta T^\mu_\nu$, we obtain

$$\delta G^0_0 = 6H \left(\dot{\Phi} + H\Phi \right) - \frac{2}{a^2} \nabla^2 \Phi = -8\pi G \delta\rho, \quad (1.36a)$$

$$\delta G^0_i = -2\nabla_i \left(\dot{\Phi} + H\Phi \right) = -8\pi G (\nabla_i \delta\sigma), \quad (1.36b)$$

$$\delta G^i_j = 2 \left[\ddot{\Phi} + 4H\dot{\Phi} + \left(2\dot{H} + 3H^2 \right) \Phi \right] \delta^i_j = 8\pi G \delta p \delta^i_j, \quad (1.36c)$$

where we have made use of the fact that, in the absence of anisotropic stresses, $\Phi = \Psi$. The first and the third of the above equations can be combined to obtain the following equation governing the evolution of the scalar perturbation Φ , also known as the Bardeen potential:

$$\Phi'' + 3\mathcal{H}(1 + c_A^2)\Phi' - c_A^2 \nabla^2 \Phi + [2\mathcal{H}' + (1 + 3c_A^2)\mathcal{H}^2]\Phi = (4\pi G a^2) \delta p^{\text{NA}}, \quad (1.37)$$

where $\mathcal{H} = a'/a$ is the conformal Hubble parameter, $c_A = \sqrt{p'/\rho'}$ is the adiabatic speed of perturbations, and δp^{NA} is the non-adiabatic component of the pressure perturbation, defined as

$$\delta p^{\text{NA}} = \delta p - c_A^2 \delta\rho. \quad (1.38)$$

Let us now define a quantity known as the curvature perturbation as follows:

$$\mathcal{R} = \Phi + \frac{2\rho}{3\mathcal{H}} \left(\frac{\Phi' + \mathcal{H}\Phi}{\rho + p} \right). \quad (1.39)$$

Using the above definition in Eq. (1.37), in Fourier space, we obtain

$$\mathcal{R}'_k = \left(\frac{\mathcal{H}}{\mathcal{H}^2 - \mathcal{H}'} \right) [(4\pi G a^2) \delta p^{\text{NA}}_k - c_A^2 k^2 \Phi_k], \quad (1.40)$$

where the subscript k denotes the Fourier modes of the perturbations. Now, on super-Hubble scales, *i.e.* when $k/aH = k/\mathcal{H} \ll 1$, the term $c_A^2 k^2 \Phi_k$ in the above equation can be neglected. Further, if the non-adiabatic component of the pressure perturbation δp^{NA} vanishes, we obtain that $\mathcal{R}'_k \simeq 0$ on super-Hubble scales. Therefore, in such cases, the curvature perturbation is conserved when the modes are well outside the Hubble radius [20–22].

We shall now consider the case of the vector perturbations. In such a case, the Friedmann metric can be written as

$$ds^2 = -dt^2 + a^2(t) [\delta_{ij} + (\nabla_i F_j + \nabla_j F_i)] dx^i dx^j, \quad (1.41)$$

where F_i is a divergence free vector that depends on space and time. Using this metric, the components of the Einstein tensor can be obtained to be

$$\delta G_0^0 = 0, \quad (1.42a)$$

$$\delta G_i^0 = -\frac{1}{2} \nabla^2 \dot{F}_i, \quad (1.42b)$$

$$\delta G_j^i = \frac{1}{2} \left[3H \left(\nabla_i \dot{F}_j + \nabla_j \dot{F}_i \right) + \left(\nabla_i \ddot{F}_j + \nabla_j \ddot{F}_i \right) \right]. \quad (1.42c)$$

In the absence of vector sources (as in the context of inflation driven by scalar fields), we must have that $\delta G_i^0 = 0$ and $\delta G_j^i = 0$. Then the above equations indicate that F_i also vanishes. Hence, no vector perturbations are generated in the absence of sources with vorticity.

Lastly, let us consider the tensor perturbations. The Friedmann metric, in this case, can be written as

$$ds^2 = -dt^2 + a^2(t) (\delta_{ij} + \gamma_{ij}) dx^i dx^j, \quad (1.43)$$

where γ_{ij} is a symmetric, transverse and traceless tensor having two degrees of freedom which correspond to the two types of polarization of the gravitational waves. The components of the perturbed Einstein tensor can be obtained to be

$$\delta G_0^0 = 0, \quad (1.44a)$$

$$\delta G_i^0 = 0, \quad (1.44b)$$

$$\delta G_j^i = \frac{1}{2} \left(\ddot{\gamma}_{ij} + 3H \dot{\gamma}_{ij} - \frac{1}{a^2} \nabla^2 \gamma_{ij} \right). \quad (1.44c)$$

Using the above expressions in the perturbed Einstein's equations at the first order, we obtain the following equation:

$$\gamma''_{ij} + 2\mathcal{H} \gamma'_{ij} - \nabla^2 \gamma_{ij} = 0. \quad (1.45)$$

This differential equation admits non-trivial solutions even in the absence of a source term. This implies that, on quantization, tensor perturbations can be generated even in the absence of sources.

1.4.2 Quantization of the perturbations and the power spectra

The perturbations in the homogeneous scalar field ϕ driving inflation and described by the action (1.18), *viz.* the inflaton, are denoted by $\delta\phi$. The components of the perturbed stress-energy tensor can then be written as

$$\delta T_0^0 = -\dot{\phi} \delta\dot{\phi} + \dot{\phi}^2 \Phi - V_\phi \delta\phi = -\delta\rho, \quad (1.46a)$$

$$\delta T_i^0 = -\nabla_i \left(\dot{\phi} \delta\phi \right) = -\nabla_i (\delta\sigma), \quad (1.46b)$$

$$\delta T_j^i = \left(\dot{\phi} \delta\dot{\phi} - \dot{\phi}^2 \Phi - V_\phi \delta\phi \right) \delta_j^i = \delta p \delta_j^i. \quad (1.46c)$$

Evidently the scalar field does not possess any anisotropic stress. Using the above expressions, the equation governing the Bardeen potential can be written as

$$\Phi'' + 3\mathcal{H}(1 + c_A^2)\Phi' - c_A^2 \nabla^2 \Phi + [2\mathcal{H}' + (1 + 3c_A^2)\mathcal{H}^2]\Phi = (1 - c_A^2)\nabla^2 \Phi. \quad (1.47)$$

Comparing this equation with Eq (1.37), we can infer that the non-adiabatic pressure perturbation associated with the inflaton is given by

$$\delta p^{\text{NA}} = \left(\frac{1 - c_A^2}{4\pi G a^2} \right) \nabla^2 \Phi. \quad (1.48)$$

Using this expression in Eq. (1.40), we obtain that

$$\mathcal{R}' = \left(\frac{\mathcal{H}}{\mathcal{H}^2 - \mathcal{H}'} \right) \nabla^2 \Phi. \quad (1.49)$$

Differentiating this equation once and using the background equations and the Bardeen equation (1.47), we obtain the equation of motion governing the evolution of the curvature perturbation to be

$$\mathcal{R}'' + 2\frac{z'}{z}\mathcal{R}' - \nabla^2 \mathcal{R} = 0, \quad (1.50)$$

where we have defined $z = a\dot{\phi}/H = a\phi'/\mathcal{H}$.

The primordial perturbations are expected to originate from quantum fluctuations in the early universe. Therefore, we elevate the classical quantity \mathcal{R} to a quantum operator $\hat{\mathcal{R}}$ and express it in the homogeneous Friedmann background as follows:

$$\hat{\mathcal{R}}(\eta, \mathbf{x}) = \int \frac{d^3 \mathbf{k}}{(2\pi)^{3/2}} \hat{\mathcal{R}}_{\mathbf{k}}(\eta) e^{i\mathbf{k}\cdot\mathbf{x}}, \quad (1.51)$$

where

$$\hat{\mathcal{R}}_{\mathbf{k}}(\eta) = \hat{a}_{\mathbf{k}} f_{\mathbf{k}}(\eta) + \hat{a}_{\mathbf{k}}^\dagger f_{\mathbf{k}}^*(\eta). \quad (1.52)$$

In this equation, the creation and annihilation operators $\hat{a}_{\mathbf{k}}^\dagger$ and $\hat{a}_{\mathbf{k}}$ satisfy the standard commutation relations given by

$$[\hat{a}_{\mathbf{k}}, \hat{a}_{\mathbf{k}'}] = [\hat{a}_{\mathbf{k}}^\dagger, \hat{a}_{\mathbf{k}'}^\dagger] = 0, \quad [\hat{a}_{\mathbf{k}}, \hat{a}_{\mathbf{k}'}^\dagger] = \delta^{(3)}(\mathbf{k} - \mathbf{k}'). \quad (1.53)$$

Also, using Eq. (1.50), it can be obtained that the mode $f_{\mathbf{k}}$ and its complex conjugate $f_{\mathbf{k}}^*$ satisfy the following equation:

$$f_{\mathbf{k}}'' + 2\frac{z'}{z}f_{\mathbf{k}}' + k^2 f_{\mathbf{k}} = 0. \quad (1.54)$$

Let us now introduce a quantity known as the Mukhanov-Sasaki variable $v_{\mathbf{k}} = \mathcal{R}_{\mathbf{k}} z$, so that the Fourier modes of this variable satisfy the equation

$$v_{\mathbf{k}}'' + \left(k^2 - \frac{z''}{z} \right) v_{\mathbf{k}} = 0. \quad (1.55)$$

The power spectrum of the curvature perturbation, denoted by $\mathcal{P}_s(k)$, can be expressed via the following two-point function:

$$\langle 0 | \hat{\mathcal{R}}_{\mathbf{k}}(\eta) \hat{\mathcal{R}}_{\mathbf{k}'}(\eta) | 0 \rangle = \frac{(2\pi)^2}{2k^3} \mathcal{P}_s(k) \delta^{(3)}(\mathbf{k} + \mathbf{k}'), \quad (1.56)$$

where $|0\rangle$ is the vacuum state corresponding to the annihilation operator $\hat{a}_{\mathbf{k}}$, *i.e.* $\hat{a}_{\mathbf{k}} |0\rangle = 0 \forall \mathbf{k}$. Using Eq. (1.51), we obtain

$$\mathcal{P}_s(k) = \frac{k^3}{2\pi^2} |f_k|^2 = \frac{k^3}{2\pi^2} \left(\frac{|v_k|}{z} \right)^2, \quad (1.57)$$

where the quantities on the right hand side are to be evaluated on super-Hubble scales during inflation. For the case of bouncing universes, the power spectra are typically estimated at a suitable time after the bounce, roughly corresponding to the epoch of reheating. The details of the evaluation of the power spectra of perturbations in a scalar field will be explained in Chap. 5.

In a similar manner, the tensor perturbations can be quantized as follows:

$$\hat{\gamma}_{ij}(\eta, \mathbf{x}) = \int \frac{d^3 \mathbf{k}}{(2\pi)^{3/2}} \hat{\gamma}_{ij}^{\mathbf{k}}(\eta) e^{i\mathbf{k} \cdot \mathbf{x}}, \quad (1.58)$$

where

$$\hat{\gamma}_{ij}^{\mathbf{k}}(\eta) = \sum_{s=1}^2 \left[\hat{b}_{\mathbf{k}}^s \varepsilon_{ij}^s(\mathbf{k}) h_k(\eta) + \hat{b}_{\mathbf{k}}^{s\dagger} \varepsilon_{ij}^{s*}(\mathbf{k}) h_k^*(\eta) \right]. \quad (1.59)$$

In this equation, the creation and annihilation operators $\hat{b}_{\mathbf{k}}^{s\dagger}$ and $\hat{b}_{\mathbf{k}}^s$ satisfy the standard commutation relations given by

$$[\hat{b}_{\mathbf{k}}^s, \hat{b}_{\mathbf{k}'}^{s'}] = [\hat{b}_{\mathbf{k}}^{s\dagger}, \hat{b}_{\mathbf{k}'}^{s'\dagger}] = 0, \quad [\hat{b}_{\mathbf{k}}^s, \hat{b}_{\mathbf{k}'}^{s'\dagger}] = \delta_{ss'} \delta^{(3)}(\mathbf{k} - \mathbf{k}'). \quad (1.60)$$

The quantity $\varepsilon_{ij}^s(\mathbf{k})$ represents the polarization tensor of the gravitational waves, with the indices $s = (1, 2)$ denoting the two states of polarization. The transverse and traceless nature of the gravitational waves implies that the polarization tensor obeys the relations: $\varepsilon_{ii}^s(\mathbf{k}) = k_i \varepsilon_{ij}^s(\mathbf{k}) = 0$. We shall choose to work with the normalization $\varepsilon_{ij}^r(\mathbf{k}) \varepsilon_{ij}^s(\mathbf{k}) = 2\delta^{rs}$. Also, using Eq. (1.45), the mode h_k and its complex conjugate h_k^* can be found to satisfy the following equation:

$$h_k'' + 2 \frac{a'}{a} h_k' + k^2 h_k = 0. \quad (1.61)$$

Let us define the Mukhanov-Sasaki variable for the tensor perturbations to be $u_k = a h_k M_{\text{Pl}} / \sqrt{2}$. In terms of this variable, in Fourier space, Eq. (1.61) can be rewritten as

$$u_k'' + \left(k^2 - \frac{a''}{a} \right) u_k = 0. \quad (1.62)$$

The power spectrum of the tensor perturbation, denoted by $\mathcal{P}_T(k)$, can be expressed via the following two-point function:

$$\langle 0 | \hat{\gamma}_{ij}^{\mathbf{k}}(\eta) \hat{\gamma}_{mn}^{\mathbf{k}'}(\eta) | 0 \rangle = \frac{(2\pi)^2}{2k^3} \frac{\Pi_{ij,mn}^{\mathbf{k}}}{4} \mathcal{P}_T(k) \delta^{(3)}(\mathbf{k} + \mathbf{k}'), \quad (1.63)$$

where $|0\rangle$ is the vacuum state corresponding to the annihilation operator $\hat{b}_{\mathbf{k}}^s$, i.e. $\hat{b}_{\mathbf{k}}^s |0\rangle = 0 \forall \mathbf{k}$ and s , and

$$\Pi_{ij,mn}^{\mathbf{k}} = \sum_s \varepsilon_{ij}^s(\mathbf{k}) \varepsilon_{mn}^{s*}(\mathbf{k}). \quad (1.64)$$

Using Eq. (1.58), we obtain

$$\mathcal{P}_T(k) = 4 \frac{k^3}{2\pi^2} |h_k|^2 = 4 \frac{k^3}{2\pi^2} \left(\frac{|u_k|}{a} \right)^2, \quad (1.65)$$

where the quantities on the right hand side are to be evaluated on super-Hubble scales for the case of inflation. The details of the evaluation of the tensor power spectra in bounces will be explained in Chap. 3. The factor of four in the definition of the power spectrum arises due to the two states of polarization of the gravitational waves.

During inflation as well as in bounces, the initial conditions for the modes are imposed when they are well inside the Hubble radius, i.e. when $k/aH = k/\mathcal{H} \gg 1$. In the sub-Hubble regime, the modes are not affected by the curvature of spacetime and behave as in Minkowski spacetime. The asymptotic forms of the positive frequency modes on sub-Hubble scales are given by

$$\lim_{(k/\mathcal{H} \rightarrow \infty)} (v_k(\eta), u_k(\eta)) \rightarrow \frac{1}{\sqrt{2k}} e^{-ik\eta}. \quad (1.66)$$

The vacuum state $|0\rangle$ associated with such modes is known as the Bunch-Davies vacuum. The modes are allowed to evolve from this initial condition and, as already mentioned, the power spectra are evaluated in the super-Hubble domain during inflation. We shall comment on the estimation of power spectra in bounces in Chaps. 3 and 5. As we have already mentioned before, the power spectra are typically evaluated after the bounce, at a time roughly corresponding to the epoch of reheating. We can also define spectral indices for the scalar and tensor power spectra as follows:

$$n_s = 1 + \frac{d \ln \mathcal{P}_s}{d \ln k}, \quad (1.67a)$$

$$n_T = \frac{d \ln \mathcal{P}_T}{d \ln k}. \quad (1.67b)$$

For scale invariant scalar and tensor spectra, it is evident from the above definitions that $n_s = 1$ and $n_T = 0$, respectively. Another quantity that is often used to characterize the

relative amplitude of the scalar and tensor power spectra is known as the tensor-to-scalar ratio. It is defined as

$$r(k) = \frac{\mathcal{P}_T(k)}{\mathcal{P}_S(k)}. \quad (1.68)$$

It follows from the above definition that the tensor-to-scalar ratio is a scale dependent quantity. However, as we shall describe in the following section, for the case of slow roll inflation, the scale dependence of $r(k)$ is often ignored (as a first approximation) for the sake of convenience while comparing with data.

1.4.3 Power spectra in slow roll inflation

Let us evaluate the scalar and tensor power spectra in slow roll inflation. Using the definitions of the slow roll parameter and the Mukhanov-Sasaki variable, we can write

$$z = a M_{\text{Pl}} \sqrt{2\epsilon_1}. \quad (1.69)$$

At the leading order in slow roll, the conformal Hubble parameter \mathcal{H} (which is defined as $\mathcal{H} = a'/a$) can be obtained to be

$$\mathcal{H} \simeq -\frac{1}{(1 - \epsilon_1) \eta}. \quad (1.70)$$

Using the above two expressions, at the leading order in slow roll, the quantities z''/z and a''/a in the Mukhanov-Sasaki equation can be written in terms of the slow roll parameters as [21,57]

$$\frac{z''}{z} \simeq \frac{1}{\eta^2} \left(2 + 3\epsilon_1 + \frac{3\epsilon_2}{2} \right), \quad (1.71a)$$

$$\frac{a''}{a} \simeq \frac{1}{\eta^2} (2 + 3\epsilon_1), \quad (1.71b)$$

where the slow roll parameters ϵ_1 and ϵ_2 have been defined in Eqs. (1.28) and (1.29). Then the solutions to the equations governing the evolution of the Mukhanov-Sasaki variables v_k and u_k can be expressed in terms of Hankel functions $H_\nu(x)$ as follows:

$$v_k(\eta) = \sqrt{-\frac{\pi \eta}{4}} e^{i(\nu_S + 1/2)\pi/2} H_{\nu_S}^{(1)}(-k\eta), \quad (1.72a)$$

$$u_k(\eta) = \sqrt{-\frac{\pi \eta}{4}} e^{i(\nu_T + 1/2)\pi/2} H_{\nu_T}^{(1)}(-k\eta), \quad (1.72b)$$

with the quantities ν_S and ν_T given by

$$\nu_S \simeq \frac{3}{2} + \epsilon_1 + \frac{\epsilon_2}{2}, \quad (1.73a)$$

$$\nu_T \simeq \frac{3}{2} + \epsilon_1, \quad (1.73b)$$

where the subscripts S and T refer to the scalar and tensor perturbations, respectively. In order to evaluate the power spectra, we expand the Hankel functions in the limit $(-k\eta) \rightarrow 0$ to obtain [57]

$$\mathcal{P}_S(k) = \frac{H_I^2}{8\pi^2 M_{\text{Pl}}^2 \epsilon_1} \left[1 - 2\epsilon_1 - (2\epsilon_1 + \epsilon_2) \ln\left(\frac{k}{k_*}\right) - (2\epsilon_1 + \epsilon_2)(\gamma_E + \ln 2 - 2) \right], \quad (1.74a)$$

$$\mathcal{P}_T(k) = \frac{2H_I^2}{\pi^2 M_{\text{Pl}}^2} \left[1 - 2\epsilon_1 \ln\left(\frac{k}{k_*}\right) - 2\epsilon_1(\gamma_E + \ln 2 - 1) \right], \quad (1.74b)$$

where γ_E is the Euler-Mascheroni constant [58], k_* is the pivot scale at which the amplitudes of the power spectra are quoted, and H_I is the value of the Hubble parameter during inflation. Using the above expressions for the power spectra, we can evaluate the spectral indices to be

$$n_S \simeq 1 - 2\epsilon_1 - \epsilon_2, \quad (1.75a)$$

$$n_T \simeq -2\epsilon_1. \quad (1.75b)$$

Therefore, it is evident that the power spectra in slow roll inflation are nearly scale invariant. Further, ignoring the scale dependence in the power spectra, the tensor-to-scalar ratio can be obtained to be

$$r \simeq 16\epsilon_1 = -8n_T. \quad (1.76)$$

This expression is known as the inflationary consistency relation.

1.4.4 Duality invariance of the power spectra

It is clear from Eqs. (1.55) and (1.62) that the Mukhanov-Sasaki equation for the scalar and tensor modes can be generally written as

$$y_k'' + (k^2 - \xi^2) y_k = 0, \quad (1.77)$$

where $y_k = v_k$ or u_k , and $\xi^2 = (z''/z)$ or (a''/a) for the scalar and tensor cases respectively. Further, from this equation, it is straightforward to establish that identical power spectra are produced by a two parameter family of solutions for z and a , given by

$$z(\eta) \rightarrow \tilde{z}(\eta) = C_1 z(\eta) \int_{\eta_*}^{\eta} \frac{d\eta'}{z^2(\eta')}, \quad (1.78)$$

or

$$a(\eta) \rightarrow \tilde{a}(\eta) = C_2 a(\eta) \int_{\eta_*}^{\eta} \frac{d\eta'}{a^2(\eta')}, \quad (1.79)$$

for the scalar and tensor cases respectively, where C_1 and C_2 are constants of integration. Both the quantity z and its dual \tilde{z} result in identical ξ^2 and hence lead to the same

form of power spectra. This property is known as duality invariance [48]. While this phenomenon has been studied for the case of the scalar and tensor power spectra, in this thesis, we shall establish that it also holds true for the case of the power spectra of primordial magnetic fields. The duality invariance exhibited in such cases and its implications will be explored in detail in a later chapter.

For instructive purposes, let us consider a power law expansion or contraction characterized by the scale factor $a(t) \propto t^q$, or, equivalently, $a(\eta) = a_0 (\eta/\eta_0)^{(1-2\nu)/2}$, where

$$\nu = \frac{3}{2} + \frac{1}{q-1}. \quad (1.80)$$

In such cases, the solution to Eq. (1.77) can be expressed in terms of Hankel functions as

$$y_k(\eta) = \sqrt{-k\eta} \left[y_+ H_\nu^{(1)}(-k\eta) + y_- H_\nu^{(2)}(-k\eta) \right], \quad (1.81)$$

where y_+ and y_- are constants that can be fixed from the initial conditions. The corresponding power spectrum can be obtained to be

$$\mathcal{P}_y(k) = \frac{C_3^2(\nu) k^2 (-k\eta)^{1-2\nu}}{(2\pi)^2}, \quad (1.82)$$

where $C_3(\nu)$ is a constant given by

$$C_3(\nu) = \frac{2^\nu \Gamma(\nu)}{2^{3/2} \Gamma(3/2)}. \quad (1.83)$$

Evidently, the power spectrum obtained above is invariant under the transformation $\nu \rightarrow \tilde{\nu} = -\nu$ or, equivalently [48],

$$q \rightarrow \tilde{q} = \frac{1-2q}{2-3q}. \quad (1.84)$$

Consequently, inflationary expansion described by a scale factor of power law form would be indistinguishable from, say, a power law contraction, so long as they are related by the above expression. Note that the dual to de Sitter inflation (corresponding to $q \rightarrow \infty$) is the matter bounce ($\tilde{q} = 2/3$). As we shall see, it is for this reason that matter bounces lead to scale invariant power spectra, similar to de Sitter inflation.

1.4.5 Observational constraints on the power spectra

We had earlier arrived at the power spectra in slow roll inflation [cf. Eqs. (1.74)]. At the leading order in slow roll, the scalar and tensor power spectra can be reduced to the following simple forms:

$$\mathcal{P}_S(k) = A_S \left(\frac{k}{k_*} \right)^{n_S-1}, \quad (1.85a)$$

$$\mathcal{P}_T(k) = A_T \left(\frac{k}{k_*} \right)^{n_T}, \quad (1.85b)$$

where A_s and A_T denote the amplitudes of the scalar and tensor power spectra, n_s and n_T are the corresponding spectral indices [cf. Eqs. (1.75)], and k_* is known as the pivot scale. In order to compare the scalar and tensor power spectra with inflationary models, the above expressions are often considered as templates. According to the most recent constraints from CMB measurements by Planck, which we have mentioned earlier [cf. Eqs. (1.8e) and (1.8f)], but nonetheless repeat here for completeness, the amplitude A_s is given by [8, 9, 59]

$$\ln(10^{10} A_s) = 3.044 \pm 0.014. \quad (1.86)$$

Further, joint constraints have been arrived at on the scalar spectral index n_s and the tensor-to-scalar ratio r . The Planck collaboration has obtained the value $n_s = 0.9649 \pm 0.0042$ and the upper limit $r_{0.002} < 0.064$, where the subscript 0.002 refers to the conveniently chosen value of the pivot scale, *i.e.* $k_* = 0.002 \text{ Mpc}^{-1}$.

1.5 Beyond power spectra: three-point correlation functions

There have been extensive efforts to constrain models of inflation using the bounds arrived at on the parameters at the level of the power spectra. As delineated previously, the emergence of a proliferating quantity of precise cosmological data has allowed for stringent tests of the inflationary models with unprecedented accuracy. However, at the level of the two-point correlation functions, an almost scale invariant power spectrum of the scalar perturbations, which conforms to observations, can be achieved in most scenarios of inflation (for instance, see Refs. [7, 9, 60–62]). As a result, even with the latest results from Planck, an inordinately large number of inflationary models remain in agreement with the data at the level of the two-point functions. Therefore, constraining the varied assortment of inflationary models into a smaller, viable class still remains a formidable target, particularly in the absence of a direct detection of primordial gravitational waves on cosmological scales. It has been increasingly realized that one of the most efficacious ways to decisively break the degeneracy among the models would be to look for constraints on the three-point functions involving the primordial perturbations. This could, in principle, lead to more stringent tests for feasibility, thereby ruling out a wider class of models [63, 64]. In this section, we shall introduce the various three-point functions involving the scalar and tensor perturbations and illustrate their characteristics by evaluating them in slow roll inflation.

1.5.1 The Maldacena formalism

In the preceding section, we have described the origin and evolution of primordial perturbations, and the evaluation of the two-point functions, *viz.* the power spectra, generated

therein. The non-Gaussian signatures, if any, would be encoded in the higher point functions beyond the power spectra. The existence of non-vanishing three-point functions would therefore be the first hint of non-Gaussianities. The Maldacena formalism is the most comprehensive approach to study the non-Gaussianities generated during inflation. In order to evaluate the three-point functions, this formalism entails arriving at the cubic order action governing the evolution of the scalar and tensor perturbations, using the Arnowitt-Deser-Misner formalism [65]. With this action in hand, the standard rules of perturbative quantum field theory can be implemented to arrive at the three-point functions.

At the linear order in perturbation theory, the scalar and tensor perturbations are known to evolve independently and therefore do not give rise to cross-correlations in the two-point functions. In contrast, at the level of the third-order action, the scalar and tensor perturbations affect each other and lead to cross-correlations. As a result, four different three-point functions arise, governed by the following four third-order actions (in the comoving gauge) [66–76]:

$$\begin{aligned}
 S_{\mathcal{R}\mathcal{R}\mathcal{R}}^3[\mathcal{R}] &= M_{\text{Pl}}^2 \int d\eta \int d^3\mathbf{x} \left[a^2 \epsilon_1^2 \mathcal{R} \mathcal{R}'^2 + a^2 \epsilon_1^2 \mathcal{R} (\partial\mathcal{R})^2 - 2a \epsilon_1 \mathcal{R}' \partial_i \mathcal{R} \partial_i \chi \right. \\
 &\quad + \frac{a^2}{2} \epsilon_1 \epsilon_2' \mathcal{R}^2 \mathcal{R}' + \frac{\epsilon_1}{2} \partial_i \mathcal{R} \partial_i \chi \partial^2 \chi + \frac{\epsilon_1}{4} \partial^2 \mathcal{R} (\partial\chi)^2 \\
 &\quad \left. + a \mathcal{F}^1(\mathcal{R}) \frac{\delta \mathcal{L}_{\mathcal{R}\mathcal{R}}^2}{\delta \mathcal{R}} \right], \tag{1.87a}
 \end{aligned}$$

$$\begin{aligned}
 S_{\mathcal{R}\mathcal{R}\gamma}^3[\mathcal{R}, \gamma_{ij}] &= M_{\text{Pl}}^2 \int d\eta \int d^3\mathbf{x} \left[a^2 \epsilon_1 \gamma_{ij} \partial_i \mathcal{R} \partial_j \mathcal{R} + \frac{1}{4} \partial^2 \gamma_{ij} \partial_i \chi \partial_j \chi \right. \\
 &\quad \left. + \frac{a \epsilon_1}{2} \gamma_{ij}' \partial_i \mathcal{R} \partial_j \chi + \mathcal{F}_{ij}^2(\mathcal{R}) \frac{\delta \mathcal{L}_{\gamma\gamma}^2}{\delta \gamma_{ij}} + \mathcal{F}^3(\mathcal{R}, \gamma_{ij}) \frac{\delta \mathcal{L}_{\mathcal{R}\mathcal{R}}^2}{\delta \mathcal{R}} \right], \tag{1.87b}
 \end{aligned}$$

$$\begin{aligned}
 S_{\mathcal{R}\gamma\gamma}^3[\mathcal{R}, \gamma_{ij}] &= \frac{M_{\text{Pl}}^2}{4} \int d\eta \int d^3\mathbf{x} \left[\frac{a^2 \epsilon_1}{2} \mathcal{R} \gamma_{ij}' \gamma_{ij}' + \frac{a^2 \epsilon_1}{2} \mathcal{R} \partial_l \gamma_{ij} \partial_l \gamma_{ij} \right. \\
 &\quad \left. - a \gamma_{ij}' \partial_l \gamma_{ij} \partial_l \chi + \mathcal{F}_{ij}^4(\mathcal{R}, \gamma_{mn}) \frac{\delta \mathcal{L}_{\gamma\gamma}^2}{\delta \gamma_{ij}} \right], \tag{1.87c}
 \end{aligned}$$

$$S_{\gamma\gamma\gamma}^3[\gamma_{ij}] = \frac{M_{\text{Pl}}^2}{2} \int d\eta \int d^3\mathbf{x} \left[\frac{a^2}{2} \gamma_{lj} \gamma_{im} \partial_l \partial_m \gamma_{ij} - \frac{a^2}{4} \gamma_{ij} \gamma_{lm} \partial_l \partial_m \gamma_{ij} \right], \tag{1.87d}$$

where the quantities $\mathcal{F}^1(\mathcal{R})$, $\mathcal{F}_{ij}^2(\mathcal{R})$, $\mathcal{F}^3(\mathcal{R}, \gamma_{ij})$ and $\mathcal{F}_{ij}^4(\mathcal{R}, \gamma_{mn})$ are given by

$$\begin{aligned}
 \mathcal{F}^1(\mathcal{R}) &= \frac{1}{2aH} \left\{ \left[a^2 H \epsilon_2 \mathcal{R}^2 + 4a H \mathcal{R} \mathcal{R}' + \partial_i \mathcal{R} \partial_i \chi - \frac{1}{H} (\partial\mathcal{R})^2 \right] \frac{\delta \mathcal{L}_{\mathcal{R}\mathcal{R}}^2}{\delta \mathcal{R}} \right. \\
 &\quad + [\partial_i \mathcal{R} \partial^2 \chi + \partial^2 \mathcal{R} \partial_i \chi] \delta_{ij} \partial_j \left[\partial^{-2} \left(\frac{\delta \mathcal{L}_{\mathcal{R}\mathcal{R}}^2}{\delta \mathcal{R}} \right) \right] \\
 &\quad \left. + \frac{1}{H} \delta_{im} \delta_{jn} \partial_i \mathcal{R} \partial_j \mathcal{R} \partial_m \partial_n \left[\partial^{-2} \left(\frac{\delta \mathcal{L}_{\mathcal{R}\mathcal{R}}^2}{\delta \mathcal{R}} \right) \right] \right\}, \tag{1.88a}
 \end{aligned}$$

$$\mathcal{F}_{ij}^2(\mathcal{R}) = -\frac{1}{a^2 H^2} \partial_i \mathcal{R} \partial_j \mathcal{R} + \frac{1}{a^2 H} (\partial_i \chi \partial_j \mathcal{R} + \partial_j \chi \partial_i \mathcal{R}), \quad (1.88b)$$

$$\mathcal{F}^3(\mathcal{R}, \gamma_{ij}) = -\frac{1}{4aH} \gamma'_{ij} \partial^{-2} \partial_i \partial_j \mathcal{R}, \quad (1.88c)$$

$$\mathcal{F}_{ij}^4(\mathcal{R}, \gamma_{mn}) = \frac{1}{aH} \gamma'_{ij} \mathcal{R}. \quad (1.88d)$$

The quantity χ is given by $\partial^2 \chi = a \epsilon_1 \mathcal{R}'$. Also, $\mathcal{L}_{\mathcal{R}\mathcal{R}}^2$ and $\mathcal{L}_{\gamma\gamma}^2$ are the second order Lagrangian densities corresponding to the following quadratic order actions:

$$\mathcal{S}_{\mathcal{R}\mathcal{R}}^2[\mathcal{R}] = \frac{1}{2} \int d\eta \int d^3 \mathbf{x} \, z^2 \left[\mathcal{R}'^2 - (\partial \mathcal{R})^2 \right], \quad (1.89a)$$

$$\mathcal{S}_{\gamma\gamma}^2[\gamma_{ij}] = \frac{M_{\text{Pl}}^2}{8} \int d\eta \int d^3 \mathbf{x} \, a^2 \left[\gamma_{ij}'^2 - (\partial \gamma_{ij})^2 \right], \quad (1.89b)$$

respectively, where, recall that, $z = \sqrt{2 \epsilon_1} M_{\text{Pl}} a$, with ϵ_1 being the first slow roll parameter. These second order actions lead to the equations of motion (1.50) and (1.45) that we had considered earlier. It can be shown that the terms involving $\delta \mathcal{L}_{\mathcal{R}\mathcal{R}}^2 / \delta \mathcal{R}$, $\delta \mathcal{L}_{\gamma\gamma}^2 / \delta \gamma_{ij}$, $\mathcal{F}^1(\mathcal{R})$, $\mathcal{F}_{ij}^2(\mathcal{R})$, $\mathcal{F}^3(\mathcal{R}, \gamma_{ij})$, and $\mathcal{F}_{ij}^4(\mathcal{R}, \gamma_{mn})$ can be removed by the following field redefinitions [66, 68–70]:

$$\mathcal{R} \rightarrow \mathcal{R} + \mathcal{F}^1(\mathcal{R}) + \mathcal{F}^3(\mathcal{R}, \gamma_{ij}), \quad (1.90a)$$

$$\gamma_{ij} \rightarrow \gamma_{ij} + \mathcal{F}_{ij}^2(\mathcal{R}) + \mathcal{F}_{ij}^4(\mathcal{R}, \gamma_{mn}). \quad (1.90b)$$

As we shall discuss later, these field redefinitions lead to an additional term in the three-point function involving the scalar perturbations.

1.5.2 Definitions of the three-point functions

In Fourier space, the scalar bispectrum, the scalar-scalar-tensor three-point function, the scalar-tensor-tensor three-point function, and the tensor bispectrum, *viz.* $G_{\mathcal{R}\mathcal{R}\mathcal{R}}(\mathbf{k}_1, \mathbf{k}_2, \mathbf{k}_3)$, $G_{\mathcal{R}\mathcal{R}\gamma}^{m_3 n_3}(\mathbf{k}_1, \mathbf{k}_2, \mathbf{k}_3)$, $G_{\mathcal{R}\gamma\gamma}^{m_2 n_2 m_3 n_3}(\mathbf{k}_1, \mathbf{k}_2, \mathbf{k}_3)$, and $G_{\gamma\gamma\gamma}^{m_1 n_1 m_2 n_2 m_3 n_3}(\mathbf{k}_1, \mathbf{k}_2, \mathbf{k}_3)$, evaluated towards the end of inflation at the conformal time, say, η_e , are defined as [66–75]

$$\langle \hat{\mathcal{R}}_{\mathbf{k}_1}(\eta_e) \hat{\mathcal{R}}_{\mathbf{k}_2}(\eta_e) \hat{\mathcal{R}}_{\mathbf{k}_3}(\eta_e) \rangle \equiv (2\pi)^{-3/2} G_{\mathcal{R}\mathcal{R}\mathcal{R}}(\mathbf{k}_1, \mathbf{k}_2, \mathbf{k}_3) \delta^{(3)}(\mathbf{k}_1 + \mathbf{k}_2 + \mathbf{k}_3), \quad (1.91a)$$

$$\langle \hat{\mathcal{R}}_{\mathbf{k}_1}(\eta_e) \hat{\mathcal{R}}_{\mathbf{k}_2}(\eta_e) \hat{\gamma}_{m_3 n_3}^{\mathbf{k}_3}(\eta_e) \rangle \equiv (2\pi)^{-3/2} G_{\mathcal{R}\mathcal{R}\gamma}^{m_3 n_3}(\mathbf{k}_1, \mathbf{k}_2, \mathbf{k}_3) \delta^{(3)}(\mathbf{k}_1 + \mathbf{k}_2 + \mathbf{k}_3), \quad (1.91b)$$

$$\langle \hat{\mathcal{R}}_{\mathbf{k}_1}(\eta_e) \hat{\gamma}_{m_2 n_2}^{\mathbf{k}_2}(\eta_e) \hat{\gamma}_{m_3 n_3}^{\mathbf{k}_3}(\eta_e) \rangle \equiv (2\pi)^{-3/2} G_{\mathcal{R}\gamma\gamma}^{m_2 n_2 m_3 n_3}(\mathbf{k}_1, \mathbf{k}_2, \mathbf{k}_3) \delta^{(3)}(\mathbf{k}_1 + \mathbf{k}_2 + \mathbf{k}_3), \quad (1.91c)$$

$$\langle \hat{\gamma}_{m_1 n_1}^{\mathbf{k}_1}(\eta_e) \hat{\gamma}_{m_2 n_2}^{\mathbf{k}_2}(\eta_e) \hat{\gamma}_{m_3 n_3}^{\mathbf{k}_3}(\eta_e) \rangle \equiv (2\pi)^{-3/2} G_{\gamma\gamma\gamma}^{m_1 n_1 m_2 n_2 m_3 n_3}(\mathbf{k}_1, \mathbf{k}_2, \mathbf{k}_3) \delta^{(3)}(\mathbf{k}_1 + \mathbf{k}_2 + \mathbf{k}_3). \quad (1.91d)$$

In the preceding section, we had discussed the evaluation of scalar and tensor power spectra in slow roll inflation, which involves only the scalar and tensor modes respectively. However, for the calculation of the different three-point functions, in addition to the scalar and tensor modes, we would also be required to integrate over the modes and various background quantities. Here, we shall only provide the essential equations for the evaluation of these three-point functions. In a later subsection, as an illustrative example, we shall discuss the three-point functions generated in slow roll inflation. Further, we shall evaluate the scalar-scalar-tensor three-point function explicitly for the case of a particular inflationary model, known as the axion monodromy model, in Chap. 2. We shall also discuss the tensor bispectrum generated in a matter bounce scenario in Chap. 3. Nevertheless, it is instructive to study the cases of the scalar bispectrum and the scalar-tensor-tensor three-point functions as well.

Let us first consider the case of the scalar bispectrum. It can be expressed in terms of the corresponding interaction Hamiltonian as follows [66]:

$$\langle \hat{\mathcal{R}}_{\mathbf{k}_1}(\eta_e) \hat{\mathcal{R}}_{\mathbf{k}_2}(\eta_e) \hat{\mathcal{R}}_{\mathbf{k}_3}(\eta_e) \rangle = -i \int_{\eta_i}^{\eta_e} d\eta \langle [\hat{\mathcal{R}}_{\mathbf{k}_1}(\eta_e) \hat{\mathcal{R}}_{\mathbf{k}_2}(\eta_e) \hat{\mathcal{R}}_{\mathbf{k}_3}(\eta_e), \hat{H}_{\mathcal{R}\mathcal{R}\mathcal{R}}^{\text{int}}(\eta)] \rangle, \quad (1.92)$$

where the expectation value has to be calculated in the perturbative vacuum. For a third order action, it can be shown that $\hat{H}_{\mathcal{R}\mathcal{R}\mathcal{R}}^{\text{int}} = -\hat{L}_{\mathcal{R}\mathcal{R}\mathcal{R}}^{\text{int}}$ [66] [cf. Eq. (1.87a)]. Upon using the above expression and Wick's theorem, it can be shown that the scalar bispectrum can be written as [75,77,78]

$$\begin{aligned} G_{\mathcal{R}\mathcal{R}\mathcal{R}}(\mathbf{k}_1, \mathbf{k}_2, \mathbf{k}_3) &\equiv \sum_{C=1}^7 G_C(\mathbf{k}_1, \mathbf{k}_2, \mathbf{k}_3) \\ &\equiv M_{\text{Pl}}^2 \sum_{C=1}^6 \left\{ [f_{k_1}(\eta_e) f_{k_2}(\eta_e) f_{k_3}(\eta_e)] \mathcal{G}_{\mathcal{R}\mathcal{R}\mathcal{R}}^C(\mathbf{k}_1, \mathbf{k}_2, \mathbf{k}_3) \right. \\ &\quad \left. + \text{complex conjugate} \right\} + G_7(\mathbf{k}_1, \mathbf{k}_2, \mathbf{k}_3), \end{aligned} \quad (1.93)$$

where f_k are the Fourier modes, which satisfy Eq. (1.54). The above expression involves the following six integrals:

$$\mathcal{G}_{\mathcal{R}\mathcal{R}\mathcal{R}}^1(\mathbf{k}_1, \mathbf{k}_2, \mathbf{k}_3) = 2i \int_{\eta_i}^{\eta_e} d\eta a^2 \epsilon_1^2 (f_{k_1}^* f_{k_2}' f_{k_3}' + \text{two permutations}), \quad (1.94a)$$

$$\mathcal{G}_{\mathcal{R}\mathcal{R}\mathcal{R}}^2(\mathbf{k}_1, \mathbf{k}_2, \mathbf{k}_3) = -2i (\mathbf{k}_1 \cdot \mathbf{k}_2 + \text{two permutations}) \int_{\eta_i}^{\eta_e} d\eta a^2 \epsilon_1^2 f_{k_1}^* f_{k_2}' f_{k_3}', \quad (1.94b)$$

$$\mathcal{G}_{\mathcal{R}\mathcal{R}\mathcal{R}}^3(\mathbf{k}_1, \mathbf{k}_2, \mathbf{k}_3) = -2i \int_{\eta_i}^{\eta_e} d\eta a^2 \epsilon_1^2 \left[\left(\frac{\mathbf{k}_1 \cdot \mathbf{k}_2}{k_2^2} \right) f_{k_1}^* f_{k_2}' f_{k_3}' + \text{five permutations} \right], \quad (1.94c)$$

$$\mathcal{G}_{\mathcal{RRR}}^4(\mathbf{k}_1, \mathbf{k}_2, \mathbf{k}_3) = i \int_{\eta_i}^{\eta_e} d\eta a^2 \epsilon_1 \epsilon_2' (f_{k_1}^* f_{k_2}^* f_{k_3}' + \text{two permutations}), \quad (1.94d)$$

$$\mathcal{G}_{\mathcal{RRR}}^5(\mathbf{k}_1, \mathbf{k}_2, \mathbf{k}_3) = \frac{i}{2} \int_{\eta_i}^{\eta_e} d\eta a^2 \epsilon_1^3 \left[\left(\frac{\mathbf{k}_1 \cdot \mathbf{k}_2}{k_2^2} \right) f_{k_1}^* f_{k_2}' f_{k_3}' + \text{five permutations} \right], \quad (1.94e)$$

$$\mathcal{G}_{\mathcal{RRR}}^6(\mathbf{k}_1, \mathbf{k}_2, \mathbf{k}_3) = \frac{i}{2} \int_{\eta_i}^{\eta_e} d\eta a^2 \epsilon_1^3 \left\{ \left[\frac{k_1^2 (\mathbf{k}_2 \cdot \mathbf{k}_3)}{k_2^2 k_3^2} \right] f_{k_1}^* f_{k_2}' f_{k_3}' + \text{two permutations} \right\}. \quad (1.94f)$$

These integrals are to be evaluated from a sufficiently early time (η_i), when the modes are inside the Hubble radius, until very late times, which can be conveniently chosen to be a time close to the end of inflation (η_e). The seventh term $G_7(\mathbf{k}_1, \mathbf{k}_2, \mathbf{k}_3)$ in the expression for the three-point functions essentially arises due to the field redefinitions (1.90) and is given by

$$G_7(\mathbf{k}_1, \mathbf{k}_2, \mathbf{k}_3) = \frac{\epsilon_2(\eta_e)}{2} (|f_{k_1}(\eta_e)|^2 |f_{k_2}(\eta_e)|^2 + \text{two permutations}). \quad (1.95)$$

We shall now consider the scalar-tensor cross-correlations. The scalar-scalar-tensor three-point function can be expressed in terms of the corresponding interaction Hamiltonian as follows [66, 76]:

$$\langle \hat{\mathcal{R}}_{\mathbf{k}_1}(\eta_e) \hat{\mathcal{R}}_{\mathbf{k}_2}(\eta_e) \hat{\gamma}_{m_3 n_3}^{\mathbf{k}_3}(\eta_e) \rangle = -i \int_{\eta_i}^{\eta_e} d\eta \langle [\hat{\mathcal{R}}_{\mathbf{k}_1}(\eta_e) \hat{\mathcal{R}}_{\mathbf{k}_2}(\eta_e) \hat{\gamma}_{m_3 n_3}^{\mathbf{k}_3}(\eta_e), \hat{H}_{\mathcal{RR}\gamma}^{\text{int}}(\eta)] \rangle. \quad (1.96)$$

Again, for a third order action, it can be shown that $\hat{H}_{\mathcal{RR}\gamma}^{\text{int}} = -\hat{L}_{\mathcal{RR}\gamma}^{\text{int}}$ [66] [cf. Eq. (1.87b)]. The three-point function $G_{\mathcal{RR}\gamma}^{m_3 n_3}(\mathbf{k}_1, \mathbf{k}_2, \mathbf{k}_3)$, when evaluated in the perturbative vacuum, can be written as (see, for example, Ref. [76])

$$\begin{aligned} G_{\mathcal{RR}\gamma}^{m_3 n_3}(\mathbf{k}_1, \mathbf{k}_2, \mathbf{k}_3) &= \sum_{C=1}^3 G_{\mathcal{RR}\gamma(C)}^{m_3 n_3}(\mathbf{k}_1, \mathbf{k}_2, \mathbf{k}_3) \\ &= M_{\text{Pl}}^2 \Pi_{m_3 n_3, ij}^{\mathbf{k}_3} \hat{n}_{1i} \hat{n}_{2j} \sum_{C=1}^3 [f_{k_1}(\eta_e) f_{k_2}(\eta_e) h_{k_3}(\eta_e) \\ &\quad \times \mathcal{G}_{\mathcal{RR}\gamma}^C(\mathbf{k}_1, \mathbf{k}_2, \mathbf{k}_3) + \text{complex conjugate}], \end{aligned} \quad (1.97)$$

where h_k are the Fourier modes which satisfy Eq. (1.61), the quantity $\Pi_{m_3 n_3, ij}^{\mathbf{k}_3}$ is given by Eq. (1.64), and the quantities $\mathcal{G}_{\mathcal{RR}\gamma}^C(\mathbf{k}_1, \mathbf{k}_2, \mathbf{k}_3)$ are described by the integrals

$$\mathcal{G}_{\mathcal{RR}\gamma}^1(\mathbf{k}_1, \mathbf{k}_2, \mathbf{k}_3) = -2i k_1 k_2 \int_{\eta_i}^{\eta_e} d\eta a^2 \epsilon_1 f_{k_1}' f_{k_2}' h_{k_3}^*, \quad (1.98a)$$

$$\mathcal{G}_{\mathcal{RR}\gamma}^2(\mathbf{k}_1, \mathbf{k}_2, \mathbf{k}_3) = \frac{i}{2} \frac{k_3^2}{k_1 k_2} \int_{\eta_i}^{\eta_e} d\eta a^2 \epsilon_1^2 f_{k_1}' f_{k_2}' h_{k_3}^*, \quad (1.98b)$$

$$\mathcal{G}_{\mathcal{R}\mathcal{R}\gamma}^3(\mathbf{k}_1, \mathbf{k}_2, \mathbf{k}_3) = \frac{i}{2} \frac{1}{k_1 k_2} \int_{\eta_i}^{\eta_e} d\eta a^2 \epsilon_1^2 [k_1^2 f_{k_1}^* f_{k_2}' + k_2^2 f_{k_1}' f_{k_2}^*] h_{k_3}'^*. \quad (1.98c)$$

Note that for a given wavevector \mathbf{k} , $\hat{\mathbf{n}}$ denotes the unit vector $\hat{\mathbf{n}} = \mathbf{k}/k$. Hence, the quantities \hat{n}_{1i} and \hat{n}_{2i} represent the components of the unit vectors $\hat{\mathbf{n}}_1 = \mathbf{k}_1/k_1$ and $\hat{\mathbf{n}}_2 = \mathbf{k}_2/k_2$ along the i -spatial direction.

Similarly, the scalar-tensor-tensor three-point function can be expressed in terms of the corresponding interaction Hamiltonian as follows [66, 76]:

$$\langle \hat{\mathcal{R}}_{\mathbf{k}_1}(\eta_e) \hat{\gamma}_{m_2 n_2}^{\mathbf{k}_2}(\eta_e) \hat{\gamma}_{m_3 n_3}^{\mathbf{k}_3}(\eta_e) \rangle = -i \int_{\eta_i}^{\eta_e} d\eta \langle [\hat{\mathcal{R}}_{\mathbf{k}_1}(\eta_e) \hat{\gamma}_{m_2 n_2}^{\mathbf{k}_2}(\eta_e) \hat{\gamma}_{m_3 n_3}^{\mathbf{k}_3}(\eta_e), \hat{H}_{\mathcal{R}\gamma\gamma}^{\text{int}}(\eta)] \rangle. \quad (1.99)$$

As before, for a third order action, it can be shown that $\hat{H}_{\mathcal{R}\gamma\gamma}^{\text{int}} = -\hat{L}_{\mathcal{R}\gamma\gamma}^{\text{int}}$ [66] [cf. Eq. (1.87c)]. The scalar-tensor-tensor cross-correlation $G_{\mathcal{R}\gamma\gamma}^{m_2 n_2 m_3 n_3}(\mathbf{k}_1, \mathbf{k}_2, \mathbf{k}_3)$, evaluated in the perturbative vacuum, can be expressed as [67–70, 76]

$$\begin{aligned} G_{\mathcal{R}\gamma\gamma}^{m_2 n_2 m_3 n_3}(\mathbf{k}_1, \mathbf{k}_2, \mathbf{k}_3) &= \sum_{C=1}^3 G_{\mathcal{R}\gamma\gamma(C)}^{m_2 n_2 m_3 n_3}(\mathbf{k}_1, \mathbf{k}_2, \mathbf{k}_3) \\ &= M_{\text{Pl}}^2 \Pi_{m_2 n_2, ij}^{\mathbf{k}_2} \Pi_{m_3 n_3, ij}^{\mathbf{k}_3} \sum_{C=1}^3 [f_{k_1}(\eta_e) h_{k_2}(\eta_e) h_{k_3}(\eta_e) \\ &\quad \times \mathcal{G}_{\mathcal{R}\gamma\gamma}^C(\mathbf{k}_1, \mathbf{k}_2, \mathbf{k}_3) + \text{complex conjugate}], \end{aligned} \quad (1.100)$$

with the quantities $\mathcal{G}_{\mathcal{R}\gamma\gamma}^C(\mathbf{k}_1, \mathbf{k}_2, \mathbf{k}_3)$ being given by

$$\mathcal{G}_{\mathcal{R}\gamma\gamma}^1(\mathbf{k}_1, \mathbf{k}_2, \mathbf{k}_3) = \frac{i}{4} \int_{\eta_i}^{\eta_e} d\eta a^2 \epsilon_1 f_{k_1}^* h_{k_2}' h_{k_3}'^*, \quad (1.101a)$$

$$\mathcal{G}_{\mathcal{R}\gamma\gamma}^2(\mathbf{k}_1, \mathbf{k}_2, \mathbf{k}_3) = -\frac{i}{4} (\mathbf{k}_2 \cdot \mathbf{k}_3) \int_{\eta_i}^{\eta_e} d\eta a^2 \epsilon_1 f_{k_1}^* h_{k_2}' h_{k_3}'^*, \quad (1.101b)$$

$$\mathcal{G}_{\mathcal{R}\gamma\gamma}^3(\mathbf{k}_1, \mathbf{k}_2, \mathbf{k}_3) = -\frac{i}{4} \int_{\eta_i}^{\eta_e} d\eta a^2 \epsilon_1 f_{k_1}^* \left[\frac{\mathbf{k}_1 \cdot \mathbf{k}_2}{k_1^2} h_{k_2}' h_{k_3}'^* + \frac{\mathbf{k}_1 \cdot \mathbf{k}_3}{k_1^2} h_{k_2}'^* h_{k_3}' \right]. \quad (1.101c)$$

We finally consider the case of the tensor bispectrum. In terms of the interaction Hamiltonian, it can be expressed as [70, 71, 76]

$$\langle \hat{\gamma}_{m_1 n_1}^{\mathbf{k}_1}(\eta_e) \hat{\gamma}_{m_2 n_2}^{\mathbf{k}_2}(\eta_e) \hat{\gamma}_{m_3 n_3}^{\mathbf{k}_3}(\eta_e) \rangle = -i \int_{\eta_i}^{\eta_e} d\eta \langle [\hat{\gamma}_{m_1 n_1}^{\mathbf{k}_1}(\eta_e) \hat{\gamma}_{m_2 n_2}^{\mathbf{k}_2}(\eta_e) \hat{\gamma}_{m_3 n_3}^{\mathbf{k}_3}(\eta_e), \hat{H}_{\gamma\gamma\gamma}^{\text{int}}(\eta)] \rangle. \quad (1.102)$$

Again, for a third order action, it is found that $\hat{H}_{\gamma\gamma\gamma}^{\text{int}} = -\hat{L}_{\gamma\gamma\gamma}^{\text{int}}$ [66] [cf. Eq. (1.87d)]. The corresponding three-point function can be obtained to be [66, 70, 71, 76]

$$\begin{aligned} G_{\gamma\gamma\gamma}^{m_1 n_1 m_2 n_2 m_3 n_3}(\mathbf{k}_1, \mathbf{k}_2, \mathbf{k}_3) &= M_{\text{Pl}}^2 \left[\left(\Pi_{m_1 n_1, ij}^{\mathbf{k}_1} \Pi_{m_2 n_2, im}^{\mathbf{k}_2} \Pi_{m_3 n_3, lj}^{\mathbf{k}_3} \right. \right. \\ &\quad \left. \left. - \frac{1}{2} \Pi_{m_1 n_1, ij}^{\mathbf{k}_1} \Pi_{m_2 n_2, ml}^{\mathbf{k}_2} \Pi_{m_3 n_3, ij}^{\mathbf{k}_3} \right) k_{1m} k_{1l} + \text{five permutations} \right] \\ &\quad \times [h_{k_1}(\eta_e) h_{k_2}(\eta_e) h_{k_3}(\eta_e) \mathcal{G}_{\gamma\gamma\gamma}(\mathbf{k}_1, \mathbf{k}_2, \mathbf{k}_3) \\ &\quad + \text{complex conjugate}], \end{aligned} \quad (1.103)$$

where

$$\mathcal{G}_{\gamma\gamma\gamma}(\mathbf{k}_1, \mathbf{k}_2, \mathbf{k}_3) = -\frac{i}{4} \int_{\eta_i}^{\eta_e} d\eta a^2 h_{k_1}^* h_{k_2}^* h_{k_3}^*, \quad (1.104)$$

and (k_{1i}, k_{2i}, k_{3i}) denote the components of the three wavevectors $(\mathbf{k}_1, \mathbf{k}_2, \mathbf{k}_3)$ along the i -spatial direction.

1.5.3 Non-Gaussianity parameters

Recall that the scalar and tensor power spectra are parameterized in terms of A_s and A_t , which characterize their respective amplitudes, and n_s and n_t , which refer to the scalar and tensor spectral indices. Similarly, it is often convenient to describe the three-point functions in terms of non-Gaussianity parameters. With one such parameter defined for each of the three-point functions, we can define four dimensionless non-Gaussianity parameters, *viz.* f_{NL} , $C_{\text{NL}}^{\mathcal{R}}$, C_{NL}^{γ} , and h_{NL} , which characterize the amplitude of the various three-point functions. All these parameters can, in principle, be used to distinguish between disparate models of inflation, as well as between inflationary and alternative scenarios. In terms of these four parameters, the perturbations can be written as

$$\begin{aligned} \mathcal{R}(\eta, \mathbf{x}) &= \mathcal{R}^{(\text{G})}(\eta, \mathbf{x}) - \frac{3f_{\text{NL}}}{5} [\mathcal{R}^{(\text{G})2}(\eta, \mathbf{x}) - \langle \mathcal{R}^{(\text{G})2}(\eta, \mathbf{x}) \rangle] \\ &\quad - C_{\text{NL}}^{\mathcal{R}} \mathcal{R}^{(\text{G})}(\eta, \mathbf{x}) \gamma_{\bar{m}\bar{n}}^{(\text{G})}(\eta, \mathbf{x}), \end{aligned} \quad (1.105a)$$

$$\begin{aligned} \gamma_{ij}(\eta, \mathbf{x}) &= \gamma_{ij}^{(\text{G})}(\eta, \mathbf{x}) - h_{\text{NL}} [\gamma_{ij}^{(\text{G})}(\eta, \mathbf{x}) \gamma_{\bar{m}\bar{n}}^{(\text{G})}(\eta, \mathbf{x}) - \langle \gamma_{ij}^{(\text{G})}(\eta, \mathbf{x}) \gamma_{\bar{m}\bar{n}}^{(\text{G})}(\eta, \mathbf{x}) \rangle] \\ &\quad - C_{\text{NL}}^{\gamma} \gamma_{ij}^{(\text{G})}(\eta, \mathbf{x}) \mathcal{R}^{(\text{G})}(\eta, \mathbf{x}), \end{aligned} \quad (1.105b)$$

where $\mathcal{R}^{(\text{G})}$ and $\gamma_{ij}^{(\text{G})}$ denote the Gaussian quantities, and the overbars on the indices imply that they need to be summed over all allowed values. Note that, in these equations, the non-Gaussianity parameters have been assumed to be constants. We can introduce a more general form of these parameters wherein they are essentially expressed as the three-point functions scaled by products of the power spectra. By making use of these

definitions along with Wick's theorem to evaluate the three-point functions, the non-Gaussianity parameters can be evaluated to be [76,79]:

$$f_{\text{NL}}(\mathbf{k}_1, \mathbf{k}_2, \mathbf{k}_3) = -\frac{10}{3} \frac{1}{(2\pi)^4} [k_1^3 k_2^3 k_3^3 G_{\mathcal{R}\mathcal{R}\mathcal{R}}(\mathbf{k}_1, \mathbf{k}_2, \mathbf{k}_3)] \\ \times \left[k_1^3 \mathcal{P}_s(k_2) \mathcal{P}_s(k_3) + \text{two permutations} \right]^{-1}, \quad (1.106a)$$

$$C_{\text{NL}}^{\mathcal{R}}(\mathbf{k}_1, \mathbf{k}_2, \mathbf{k}_3) = -\frac{4}{(2\pi^2)^2} [k_1^3 k_2^3 k_3^3 G_{\mathcal{R}\mathcal{R}\gamma}^{m_3 n_3}(\mathbf{k}_1, \mathbf{k}_2, \mathbf{k}_3)] \\ \times (\Pi_{m_3 n_3, \bar{m} \bar{n}}^{k_3})^{-1} \left\{ [k_1^3 \mathcal{P}_s(k_2) + k_2^3 \mathcal{P}_s(k_1)] \mathcal{P}_T(k_3) \right\}^{-1}, \quad (1.106b)$$

$$C_{\text{NL}}^{\gamma}(\mathbf{k}_1, \mathbf{k}_2, \mathbf{k}_3) = -\frac{4}{(2\pi^2)^2} [k_1^3 k_2^3 k_3^3 G_{\mathcal{R}\gamma\gamma}^{m_2 n_2 m_3 n_3}(\mathbf{k}_1, \mathbf{k}_2, \mathbf{k}_3)] \\ \times \left\{ \mathcal{P}_s(k_1) [\Pi_{m_2 n_2, m_3 n_3}^{k_2} k_3^3 \mathcal{P}_T(k_2) + \Pi_{m_3 n_3, m_2 n_2}^{k_3} k_2^3 \mathcal{P}_T(k_3)] \right\}^{-1}, \quad (1.106c)$$

$$h_{\text{NL}}(\mathbf{k}_1, \mathbf{k}_2, \mathbf{k}_3) = -\left(\frac{4}{2\pi^2}\right)^2 [k_1^3 k_2^3 k_3^3 G_{\gamma\gamma\gamma}^{m_1 n_1 m_2 n_2 m_3 n_3}(\mathbf{k}_1, \mathbf{k}_2, \mathbf{k}_3)] \\ \times \left[\Pi_{m_1 n_1, m_3 n_3}^{k_1} \Pi_{m_2 n_2, \bar{m} \bar{n}}^{k_2} k_3^3 \mathcal{P}_T(k_1) \mathcal{P}_T(k_2) + \text{five permutations} \right]^{-1}. \quad (1.106d)$$

There are two important aspects to be considered in the behavior of the non-Gaussianity parameters. While their amplitude evidently points to the extent of non-Gaussianity generated in the model under study, it is also important to understand their shape [80]. The shape of the non-Gaussianity parameters alludes to their scale dependence, specifically with regard to where their amplitude peaks, *i.e.* where they have the maximum value. The shape of the non-Gaussianity parameters is used to classify them, as will be described in a subsequent subsection.

1.5.4 The three-point functions in slow roll inflation

In order to have a grasp on the evaluation of three-point functions generated in inflationary scenarios and their characteristics, it is instructive to examine the three-point functions in slow roll inflation. At the leading order in slow roll approximation, the slow roll parameters ϵ_1 and ϵ_2 are assumed to be much smaller than unity and they can be considered to be effectively constant. Further, the scale factor as well as the scalar and tensor modes f_k and h_k can be approximated by their de Sitter forms [66,74]. These are given by

the following expressions:

$$a(\eta) = -\frac{1}{H_I \eta}, \quad (1.107a)$$

$$f_k(\eta) = \frac{i H_I}{2 M_{\text{Pl}} \sqrt{k^3} \epsilon_1} (1 + i k \eta) e^{-i k \eta}, \quad (1.107b)$$

$$h_k(\eta) = \frac{i H_I}{M_{\text{Pl}} \sqrt{k^3}} (1 + i k \eta) e^{-i k \eta}, \quad (1.107c)$$

where H_I is the value of the Hubble parameter during inflation.

Let us first attend to the case of the scalar bispectrum. Up to the leading order in the slow roll parameters, we find that the dominant contribution to the three-point function arises from the first three integrals [cf. Eqs. (1.94a), (1.94b), and (1.94c)] and the seventh term which appears due to field redefinition [cf. Eq. (1.95)]. These terms can be obtained to be

$$G_{\mathcal{RRR}(1)}(\mathbf{k}_1, \mathbf{k}_2, \mathbf{k}_3) = \frac{H_I^4}{16 M_{\text{Pl}}^4 \epsilon_1} \frac{1}{(k_1 k_2 k_3)^3} \times \left[k_2^2 k_3^2 \left(\frac{1}{k_T} + \frac{k_1}{k_T^2} \right) + \text{two permutations} \right], \quad (1.108a)$$

$$G_{\mathcal{RRR}(2)}(\mathbf{k}_1, \mathbf{k}_2, \mathbf{k}_3) = \frac{H_I^4}{16 M_{\text{Pl}}^4 \epsilon_1} \frac{\mathbf{k}_1 \cdot \mathbf{k}_2 + \mathbf{k}_2 \cdot \mathbf{k}_3 + \mathbf{k}_3 \cdot \mathbf{k}_1}{(k_1 k_2 k_3)^3} \times \left[-k_T + \frac{(k_1 k_2 + k_2 k_3 + k_3 k_1)}{k_T} + \frac{k_1 k_2 k_3}{k_T^2} \right], \quad (1.108b)$$

$$G_{\mathcal{RRR}(3)}(\mathbf{k}_1, \mathbf{k}_2, \mathbf{k}_3) = \frac{-H_I^4}{16 M_{\text{Pl}}^4 \epsilon_1} \frac{1}{(k_1 k_2 k_3)^3} \times \left\{ \left[(\mathbf{k}_1 \cdot \mathbf{k}_2) k_3^2 + (\mathbf{k}_1 \cdot \mathbf{k}_3) k_2^2 \right] \left(\frac{1}{k_T} + \frac{k_1}{k_T^2} \right) + \text{two permutations} \right\}, \quad (1.108c)$$

$$G_{\mathcal{RRR}(7)}(\mathbf{k}_1, \mathbf{k}_2, \mathbf{k}_3) = \frac{H_I^4}{32 M_{\text{Pl}}^4 \epsilon_1^2} \left[\frac{1}{k_1^3 k_2^3} + \frac{1}{k_2^3 k_3^3} + \frac{1}{k_3^3 k_1^3} \right], \quad (1.108d)$$

where $k_T = k_1 + k_2 + k_3$. Upon adding the above expressions, we obtain the total contribution to the scalar bispectrum $G_{\mathcal{RRR}}(\mathbf{k}_1, \mathbf{k}_2, \mathbf{k}_3)$ during slow roll inflation. It should be noted that in arriving at the above equations, we have introduced a small cut-off of the form $e^{\kappa k \eta}$ at very early times (*i.e.* as $k \eta \rightarrow -\infty$), so as to regulate the highly oscillatory behavior of the integrands in the extreme sub-Hubble domain. Theoretically, this allows us to make the right choice of the perturbative vacuum [72].

For the case of the scalar-scalar-tensor three-point function, the major contribution in the leading order in slow roll parameters arises due to the first integral [cf. Eq. (1.98a)].

This quantity can be obtained to be

$$G_{\mathcal{RR}\gamma(1)}^{m_3 n_3}(\mathbf{k}_1, \mathbf{k}_2, \mathbf{k}_3) = \frac{H_I^4}{4 M_{\text{Pl}}^4 \epsilon_1} \frac{k_1 k_2}{(k_1 k_2 k_3)^3} \Pi_{m_3 n_3, ij}^{\mathbf{k}_3} \hat{n}_{1i} \hat{n}_{2j} \times \left[-k_T + \frac{k_1 k_2 + k_2 k_3 + k_3 k_1}{k_T} + \frac{k_1 k_2 k_3}{k_T^2} \right]. \quad (1.109)$$

On the other hand, for the case of the scalar-tensor-tensor three-point function, all the three integrals [cf. Eqs. (1.101a), (1.101b), and (1.101c)] contribute at the same order under the slow roll approximation. These quantities can be evaluated to be

$$G_{\mathcal{R}\gamma\gamma(1)}^{m_2 n_2 m_3 n_3}(\mathbf{k}_1, \mathbf{k}_2, \mathbf{k}_3) = \frac{H_I^4}{8 M_{\text{Pl}}^4} \frac{k_2^2 k_3^2}{(k_1 k_2 k_3)^3} \Pi_{m_2 n_2, ij}^{\mathbf{k}_2} \Pi_{m_3 n_3, ij}^{\mathbf{k}_3} \left[\frac{1}{k_T} + \frac{k_1}{k_T^2} \right], \quad (1.110a)$$

$$G_{\mathcal{R}\gamma\gamma(2)}^{m_2 n_2 m_3 n_3}(\mathbf{k}_1, \mathbf{k}_2, \mathbf{k}_3) = \frac{H_I^4}{8 M_{\text{Pl}}^4} \frac{\mathbf{k}_2 \cdot \mathbf{k}_3}{(k_1 k_2 k_3)^3} \Pi_{m_2 n_2, ij}^{\mathbf{k}_2} \Pi_{m_3 n_3, ij}^{\mathbf{k}_3} \times \left[-k_T + \frac{k_1 k_2 + k_2 k_3 + k_3 k_1}{k_T} + \frac{k_1 k_2 k_3}{k_T^2} \right], \quad (1.110b)$$

$$G_{\mathcal{R}\gamma\gamma(3)}^{m_2 n_2 m_3 n_3}(\mathbf{k}_1, \mathbf{k}_2, \mathbf{k}_3) = -\frac{H_I^4}{8 M_{\text{Pl}}^4} \frac{1}{(k_1 k_2 k_3)^3} \Pi_{m_2 n_2, ij}^{\mathbf{k}_2} \Pi_{m_3 n_3, ij}^{\mathbf{k}_3} \times \left[(\mathbf{k}_1 \cdot \mathbf{k}_2) k_3^2 \left(\frac{1}{k_T} + \frac{k_2}{k_T^2} \right) + (\mathbf{k}_1 \cdot \mathbf{k}_3) k_2^2 \left(\frac{1}{k_T} + \frac{k_3}{k_T^2} \right) \right]. \quad (1.110c)$$

As in the case of the scalar bispectrum, the above three expressions can be added to obtain the total contribution to the scalar-tensor-tensor three-point function $G_{\mathcal{R}\gamma\gamma}^{m_2 n_2 m_3 n_3}(\mathbf{k}_1, \mathbf{k}_2, \mathbf{k}_3)$.

Let us finally evaluate the tensor bispectrum. It involves only one integral [cf. Eq. (1.104)], which can be integrated at the leading order in slow roll to arrive at

$$G_{\gamma\gamma\gamma}^{m_1 n_1 m_2 n_2 m_3 n_3}(\mathbf{k}_1, \mathbf{k}_2, \mathbf{k}_3) = \frac{H_I^4}{2 M_{\text{Pl}}^4} \frac{1}{(k_1 k_2 k_3)^3} \left[(\Pi_{m_1 n_1, ij}^{\mathbf{k}_1} \Pi_{m_2 n_2, im}^{\mathbf{k}_2} \Pi_{m_3 n_3, lj}^{\mathbf{k}_3} - \frac{1}{2} \Pi_{m_1 n_1, ij}^{\mathbf{k}_1} \Pi_{m_2 n_2, ml}^{\mathbf{k}_2} \Pi_{m_3 n_3, ij}^{\mathbf{k}_3}) k_{1m} k_{1l} + \text{five permutations} \right] \times \left[-k_T + \frac{k_1 k_2 + k_2 k_3 + k_3 k_1}{k_T} + \frac{k_1 k_2 k_3}{k_T^2} \right]. \quad (1.111)$$

It is interesting to observe that all the non-Gaussianity parameters, *viz.* f_{NL} , $C_{\text{NL}}^{\mathcal{R}}$, C_{NL}^{γ} , and h_{NL} , can be obtained to be scale invariant in both the equilateral and squeezed limits of the wavenumbers for the case of de Sitter inflation.

1.5.5 The three-point functions in the squeezed limit and the consistency relations

An important property of the three-point functions is their behavior in the so-called squeezed limit [66, 81–84]. The squeezed limit corresponds to the situation wherein one of the three wavenumbers is much smaller than the other two. In such a limit, under certain conditions, it is known that all the three-point functions involving the scalars and tensors generated during inflation can be expressed entirely in terms of the two-point functions [68–70, 79]. In the context of inflation, these consistency conditions arise essentially because of the fact that the amplitude of the long wavelength scalar and tensor modes freeze on super-Hubble scales. In this subsection, we shall outline the proof of the consistency conditions satisfied by the three-point functions during inflation.

Since the amplitude of a long wavelength mode freezes on super-Hubble scales during inflation, such modes can be treated as a background as far as the smaller wavelength modes are concerned. Let us denote the constant amplitude of the long wavelength scalar and tensor modes as \mathcal{R}^B and γ_{ij}^B . In the presence of such a long wavelength mode, the background FLRW metric can be written as

$$ds^2 = -dt^2 + a^2(t) e^{2\mathcal{R}^B} [e^{\gamma^B}]_{ij} d\mathbf{x}^i d\mathbf{x}^j, \quad (1.112)$$

i.e. the spatial coordinates are modified according to a spatial transformation of the form $\mathbf{x}' = \Lambda \mathbf{x}$, where the components of the matrix Λ are given by $\Lambda_{ij} = e^{\mathcal{R}^B} [e^{\gamma^B/2}]_{ij}$. Under such a spatial transformation, the small wavelength scalar and tensor perturbations transform as [70, 79]

$$\mathcal{R}_{\mathbf{k}} \rightarrow \det(\Lambda^{-1}) \mathcal{R}_{\Lambda^{-1} \mathbf{k}}, \quad (1.113a)$$

$$\gamma_{ij}^{\mathbf{k}} \rightarrow \det(\Lambda^{-1}) \gamma_{ij}^{\Lambda^{-1} \mathbf{k}}, \quad (1.113b)$$

where $\det(\Lambda^{-1}) = 1$. Under these conditions, we also obtain that

$$|\Lambda^{-1} \mathbf{k}| = [1 - \mathcal{R}^B - \gamma_{ij}^B k_i k_j / (2 k^2)] k, \quad (1.114)$$

where k_i is the component of the wavevector \mathbf{k} along the i -spatial direction and we have restricted ourselves to the leading order in \mathcal{R}^B and γ_{ij}^B . Moreover, one can show that

$$\delta^{(3)}(\Lambda^{-1} \mathbf{k}_1 + \Lambda^{-1} \mathbf{k}_2) = \det(\Lambda) \delta^{(3)}(\mathbf{k}_1 + \mathbf{k}_2) = \delta^{(3)}(\mathbf{k}_1 + \mathbf{k}_2), \quad (1.115)$$

since $\det(\Lambda) = 1$.

Upon using the above results, we find that the scalar and tensor two-point functions

in the presence of a long wavelength mode can be written as

$$\begin{aligned} \langle \hat{\mathcal{R}}_{\mathbf{k}_1} \hat{\mathcal{R}}_{\mathbf{k}_2} \rangle_k &= \frac{(2\pi)^2}{2k_1^3} \mathcal{P}_s(k_1) \delta^{(3)}(\mathbf{k}_1 + \mathbf{k}_2) \\ &\times \left[1 - (n_s - 1) \mathcal{R}^B - \left(\frac{n_s - 4}{2} \right) \gamma_{ij}^B \hat{n}_{1i} \hat{n}_{1j} \right], \end{aligned} \quad (1.116a)$$

$$\begin{aligned} \langle \hat{\gamma}_{m_1 n_1}^{\mathbf{k}_1} \hat{\gamma}_{m_2 n_2}^{\mathbf{k}_2} \rangle_k &= \frac{(2\pi)^2}{2k_1^3} \frac{\Pi_{m_1 n_1, m_2 n_2}^{\mathbf{k}_1}}{4} \mathcal{P}_T(k_1) \delta^{(3)}(\mathbf{k}_1 + \mathbf{k}_2) \\ &\times \left[1 - n_T \mathcal{R}^B - \left(\frac{n_T - 3}{2} \right) \gamma_{ij}^B \hat{n}_{1i} \hat{n}_{1j} \right], \end{aligned} \quad (1.116b)$$

where $\hat{n}_{1i} = \mathbf{k}_{1i}/k_1$ and the long wavelength mode is denoted by the wavenumber k , while n_s and n_T represent the scalar and tensor spectral indices. The corresponding expressions for the three-point functions can be obtained from the above results to be

$$\begin{aligned} \langle \hat{\mathcal{R}}_{\mathbf{k}_1} \hat{\mathcal{R}}_{\mathbf{k}_2} \hat{\mathcal{R}}_{\mathbf{k}_3} \rangle_{k_3} &\equiv \langle \langle \hat{\mathcal{R}}_{\mathbf{k}_1} \hat{\mathcal{R}}_{\mathbf{k}_2} \rangle_{k_3} \hat{\mathcal{R}}_{\mathbf{k}_3} \rangle \\ &= -\frac{(2\pi)^{5/2}}{4k_1^3 k_3^3} (n_s - 1) \mathcal{P}_s(k_1) \mathcal{P}_s(k_3) \delta^3(\mathbf{k}_1 + \mathbf{k}_2), \end{aligned} \quad (1.117a)$$

$$\begin{aligned} \langle \hat{\mathcal{R}}_{\mathbf{k}_1} \hat{\mathcal{R}}_{\mathbf{k}_2} \hat{\gamma}_{m_3 n_3}^{\mathbf{k}_3} \rangle_{k_3} &\equiv \langle \langle \hat{\mathcal{R}}_{\mathbf{k}_1} \hat{\mathcal{R}}_{\mathbf{k}_2} \rangle_{k_3} \hat{\gamma}_{m_3 n_3}^{\mathbf{k}_3} \rangle \\ &= -\frac{(2\pi)^{5/2}}{4k_1^3 k_3^3} \left(\frac{n_s - 4}{8} \right) \mathcal{P}_s(k_1) \mathcal{P}_T(k_3) \\ &\times \Pi_{m_3 n_3, ij}^{\mathbf{k}_3} \hat{n}_{1i} \hat{n}_{1j} \delta^3(\mathbf{k}_1 + \mathbf{k}_2), \end{aligned} \quad (1.117b)$$

$$\begin{aligned} \langle \hat{\mathcal{R}}_{\mathbf{k}_1} \hat{\gamma}_{m_2 n_2}^{\mathbf{k}_2} \hat{\gamma}_{m_3 n_3}^{\mathbf{k}_3} \rangle_{k_1} &\equiv \langle \hat{\mathcal{R}}_{\mathbf{k}_1} \langle \hat{\gamma}_{m_2 n_2}^{\mathbf{k}_2} \hat{\gamma}_{m_3 n_3}^{\mathbf{k}_3} \rangle_{k_1} \rangle \\ &= -\frac{(2\pi)^{5/2}}{4k_1^3 k_2^3} \frac{n_T}{4} \mathcal{P}_s(k_1) \mathcal{P}_T(k_2) \Pi_{m_2 n_2, m_3 n_3}^{\mathbf{k}_2} \delta^3(\mathbf{k}_2 + \mathbf{k}_3), \end{aligned} \quad (1.117c)$$

$$\begin{aligned} \langle \hat{\gamma}_{m_1 n_1}^{\mathbf{k}_1} \hat{\gamma}_{m_2 n_2}^{\mathbf{k}_2} \hat{\gamma}_{m_3 n_3}^{\mathbf{k}_3} \rangle_{k_3} &\equiv \langle \langle \hat{\gamma}_{m_1 n_1}^{\mathbf{k}_1} \hat{\gamma}_{m_2 n_2}^{\mathbf{k}_2} \rangle_{k_3} \hat{\gamma}_{m_3 n_3}^{\mathbf{k}_3} \rangle \\ &= -\frac{(2\pi)^{5/2}}{4k_1^3 k_3^3} \left(\frac{n_T - 3}{32} \right) \mathcal{P}_T(k_1) \mathcal{P}_T(k_3) \\ &\times \Pi_{m_1 n_1, m_2 n_2}^{\mathbf{k}_1} \Pi_{m_3 n_3, ij}^{\mathbf{k}_3} \hat{n}_{1i} \hat{n}_{1j} \delta^3(\mathbf{k}_1 + \mathbf{k}_2), \end{aligned} \quad (1.117d)$$

where \mathbf{k}_3 has been considered to be the squeezed mode for the case of the scalar bispectrum, the scalar-scalar-tensor three-point function and the tensor bispectrum, while \mathbf{k}_1 has been considered to be the squeezed mode for the case of the scalar-tensor-tensor three-point function. The above relations wherein the three-point functions have been expressed completely in terms of the power spectra are known as the consistency conditions [70, 79]. Upon substituting these expressions in the definitions for the non-Gaussianity parameters [cf. Eq. (1.106)], we find that we can express the consistency rela-

tions in the squeezed limit as follows:

$$\lim_{k_3 \rightarrow 0} f_{\text{NL}}(\mathbf{k}, -\mathbf{k}, \mathbf{k}_3) = \frac{5}{12} [n_s(k) - 1], \quad (1.118a)$$

$$\lim_{k_3 \rightarrow 0} C_{\text{NL}}^{\mathcal{R}}(\mathbf{k}, -\mathbf{k}, \mathbf{k}_3) = \left[\frac{n_s(k) - 4}{4} \right] (\Pi_{m_3 n_3, \bar{m} \bar{n}}^{k_3})^{-1} \Pi_{m_3 n_3, ij}^{k_3} \hat{n}_i \hat{n}_j, \quad (1.118b)$$

$$\lim_{k_1 \rightarrow 0} C_{\text{NL}}^{\gamma}(\mathbf{k}_1, \mathbf{k}, -\mathbf{k}) = \frac{n_T(k)}{2} (\Pi_{m_2 n_2, m_3 n_3}^k)^{-1} \Pi_{m_2 n_2, m_3 n_3}^k, \quad (1.118c)$$

$$\begin{aligned} \lim_{k_3 \rightarrow 0} h_{\text{NL}}(\mathbf{k}, -\mathbf{k}, \mathbf{k}_3) &= \left[\frac{n_T(k) - 3}{2} \right] \left(2 \Pi_{m_1 n_1, m_2 n_2}^k \Pi_{m_3 n_3, \bar{m} \bar{n}}^{k_3} + \Pi_{m_1 n_1, \bar{m} \bar{n}}^k \Pi_{m_3 n_3, m_2 n_2}^{k_3} \right. \\ &\quad \left. + \Pi_{\bar{m} \bar{n}, m_2 n_2}^k \Pi_{m_3 n_3, m_1 n_1}^{k_3} \right)^{-1} \Pi_{m_1 n_1, m_2 n_2}^k \Pi_{m_3 n_3, ij}^{k_3} \hat{n}_i \hat{n}_j. \end{aligned} \quad (1.118d)$$

The above expression for h_{NL} in the squeezed limit is an important result, as its evaluation and validity will be discussed in the context of a matter bounce in Chap. 3.

1.5.6 Observational constraints on the three-point functions

In order to compare the amplitude of the three-point functions generated in inflationary scenarios, it is convenient to assume specific analytical templates for these functions so as to facilitate their comparison with data. For the case of the scalar bispectrum, the following templates are often considered [74, 80]:

$$G_{\mathcal{R}\mathcal{R}\mathcal{R}}^{\text{local}}(\mathbf{k}_1, \mathbf{k}_2, \mathbf{k}_3) = f_{\text{NL}}^{\text{local}} \frac{6}{5} \left[\frac{(2\pi^2)^2}{k_1^3 k_2^3 k_3^3} \right] [k_1^3 \mathcal{P}_s(k_2) \mathcal{P}_s(k_3) + \text{two permutations}], \quad (1.119a)$$

$$\begin{aligned} G_{\mathcal{R}\mathcal{R}\mathcal{R}}^{\text{equil}}(\mathbf{k}_1, \mathbf{k}_2, \mathbf{k}_3) &= f_{\text{NL}}^{\text{equil}} \frac{3}{5} \left[\frac{(2\pi^2)^2}{k_1^3 k_2^3 k_3^3} \right] \left[6 k_2 k_3^2 \mathcal{P}_s(k_1) \mathcal{P}_s^{2/3}(k_2) \mathcal{P}_s^{1/3}(k_3) \right. \\ &\quad - 3 k_3^3 \mathcal{P}_s(k_1) \mathcal{P}_s(k_2) - 2 k_1 k_2 k_3 \mathcal{P}_s^{2/3}(k_1) \mathcal{P}_s^{2/3}(k_2) \mathcal{P}_s^{2/3}(k_3) \\ &\quad \left. + \text{five permutations} \right], \end{aligned} \quad (1.119b)$$

$$\begin{aligned} G_{\mathcal{R}\mathcal{R}\mathcal{R}}^{\text{ortho}}(\mathbf{k}_1, \mathbf{k}_2, \mathbf{k}_3) &= f_{\text{NL}}^{\text{ortho}} \frac{3}{5} \left[\frac{(2\pi^2)^2}{k_1^3 k_2^3 k_3^3} \right] \left[18 k_2 k_3^2 \mathcal{P}_s(k_1) \mathcal{P}_s^{2/3}(k_2) \mathcal{P}_s^{1/3}(k_3) \right. \\ &\quad - 9 k_3^3 \mathcal{P}_s(k_1) \mathcal{P}_s(k_2) - 8 k_1 k_2 k_3 \mathcal{P}_s^{2/3}(k_1) \mathcal{P}_s^{2/3}(k_2) \mathcal{P}_s^{2/3}(k_3) \\ &\quad \left. + \text{five permutations} \right], \end{aligned} \quad (1.119c)$$

where the superscripts (local, equil, ortho) refer to the local, equilateral, and orthogonal shapes respectively. The local form of the bispectrum refers to the case wherein the bispectrum is largely independent of the wavenumbers, while for the case of the equilateral

form, the bispectrum peaks in the equilateral limit. The orthogonal shape refers to the case which cannot be represented by either the local or equilateral forms. The local shape is generated in multi-field models of inflation [85] as well as in certain post-inflationary scenarios. The equilateral shape can be generated in both canonical and non-canonical models of inflation [74], and they are considerably enhanced in non-canonical models. For generating the orthogonal shape, one needs to consider a special class of models involving higher derivatives of the field [86]. The quantities $(f_{\text{NL}}^{\text{local}}, f_{\text{NL}}^{\text{equil}}, f_{\text{NL}}^{\text{ortho}})$ are the non-Gaussianity parameters corresponding to the scalar bispectrum generated in each of these cases. These parameters are constrained by Planck to be [64]

$$f_{\text{NL}}^{\text{local}} = 0.8 \pm 5.0, \quad (1.120a)$$

$$f_{\text{NL}}^{\text{equil}} = -4 \pm 43, \quad (1.120b)$$

$$f_{\text{NL}}^{\text{ortho}} = -26 \pm 21. \quad (1.120c)$$

It should be noted here that these constraints are applicable for the particular templates used to arrive at them, and their values are only suggestive for other cases. The non-Gaussianity parameters generated in conventional slow roll models of inflation, wherein f_{NL} is of the order of the first slow roll parameter ϵ_1 , are consistent with the above constraints. The amplitude and shapes of the non-Gaussianity parameters are likely to differ considerably when there are deviations from slow roll behavior, such as for the inflationary scenarios which lead to features in the power spectra (see, for instance, Ref. [78]). In these cases, the non-Gaussianity parameters have to be constrained directly from the observational data, with the corresponding shapes taken into account.

1.6 Generation of magnetic fields in the early universe

Magnetic fields have been reported to have been observed in the universe across a large range of scales and varying strengths. It has been ascertained that such magnetic fields could not have originated from astrophysical processes alone. Moreover, even the generation of magnetic fields in stars and galaxies calls for some seed fields that can be amplified via astrophysical processes. Therefore, it seems indispensable to have some progenitor fields, conceivably originating in the early universe, that can source the magnetic fields of the strengths observed today on cosmological scales (for instance, see the recent reviews [14, 87]). In this section, we shall briefly discuss the generation of these primordial magnetic fields, a process referred to as magnetogenesis, and illustrate the evaluation of the power spectra of these magnetic fields in a typical inflationary scenario.

1.6.1 Observational constraints on magnetic fields

Magnetic fields are ubiquitous in the universe. Coherent magnetic fields have been observed over a wide variety of scales, ranging from astrophysical systems such as stars and galaxies, to cosmological systems such as the large scale structures (in this context, see Refs. [88]). More recently, magnetic fields have been observed even in the intergalactic medium [89]. While the strength of magnetic fields observed in galaxies and clusters of galaxies are typically about a few micro Gauss, in the intergalactic medium, the lower bounds on their strengths have been inferred to be of the order of 10^{-17} Gauss at 1 Mpc from the Fermi/LAT and HESS observations of TeV blazars (see Refs. [89,90]). This should be contrasted with the upper bound of a few nano Gauss which has been arrived at from the CMB observations (for current constraints from the Planck and POLARBEAR data, see Refs. [91,92] and references therein). Similar upper limits have also been obtained independently using the rotation measures from the NRAO VLA Sky Survey [93]. These bounds are broadly in agreement with the limits arrived at from the LSS data, either alone or when combined with the CMB data (in this context, see Refs. [91,92,94]; for improved limits from LSS and reionization, see Refs. [95]. Though astrophysical processes such as the dynamo mechanism can, in principle, boost the amplitude of magnetic fields in galaxies, a seed field is nevertheless required for such mechanisms to work. Therefore, a primordial origin for the magnetic fields seems inevitable to explain their prevalence, particularly on the largest scales.

1.6.2 Origin of primordial magnetic fields during inflation

The generation of primordial scalar and tensor perturbations and the subsequent evaluation of the power spectra associated with them have already been discussed in the previous sections. It is well known that the standard electromagnetic action leads to the generation of magnetic fields whose amplitude scales as a^{-2} , with a being the scale factor. For instance, for the case of an inflationary phase lasting for sixty e-folds, the amplitude of the magnetic fields would be suppressed by a factor of about e^{-120} . As a result, in an expanding universe, it would not be possible to produce magnetic fields of the requisite strength over large scales, so as to be in concordance with observations. Therefore, it seems imperative to break the conformal invariance of the standard electromagnetic action [96]. In this section, we shall describe the generation of primordial magnetic fields via a non-minimal coupling function, which can depend on, say, the scalar field driving inflation, thereby leading to a different evolution of the magnetic fields. We shall introduce the form of the electromagnetic action and, after choosing to work in a specific gauge, we shall quantize the electromagnetic vector potential and obtain the equations of motion governing the same. We shall also define the power spectra corresponding to the energy densities associated with the magnetic and electric fields. Thereafter, we shall consider a certain form of the coupling function wherein it can be expressed as a power of the scale

factor, and analytically evaluate the magnetic power spectra in de Sitter inflation and in a specific class of bouncing scenarios.

Let us consider the action

$$S_{\text{em}}[A^\mu, \phi] = -\frac{1}{16\pi} \int d^4x \sqrt{-g} J^2(\phi) F_{\mu\nu} F^{\mu\nu}, \quad (1.121)$$

where ϕ denotes a scalar field which, say, drives the background evolution and $J(\phi)$ is the non-minimal coupling function. The electromagnetic field tensor is given by

$$F_{\mu\nu} = \nabla_\mu A_\nu - \nabla_\nu A_\mu = \partial_\mu A_\nu - \partial_\nu A_\mu. \quad (1.122)$$

In the above expression, ∇_μ denotes the covariant derivative. We shall assume that there is no homogeneous component to the electromagnetic field. We shall choose to work in the Coulomb gauge wherein $A_0 = 0$ and $\partial_i A^i = 0$. In such a gauge, at the quadratic order in the inhomogeneous modes, the action describing the electromagnetic field is found to be

$$S_{\text{em}}[A_i, \phi] = \frac{1}{4\pi} \int d\eta \int d^3\mathbf{x} \left\{ J^2(\phi) \left[\frac{1}{2} A_i'^2 - \frac{1}{4} (\partial_i A_j - \partial_j A_i)^2 \right] \right\}. \quad (1.123)$$

We can vary this action to arrive at the following equation of motion for the electromagnetic vector potential:

$$A_i'' + 2 \frac{J'}{J} A_i' - \nabla^2 A_i = 0. \quad (1.124)$$

Note that it is the time dependence of J which leads to a non-trivial evolution of the electromagnetic vector potential A_i .

For each comoving wave vector \mathbf{k} , we can define the right-handed orthonormal basis $(\varepsilon_1^{\mathbf{k}}, \varepsilon_2^{\mathbf{k}}, \hat{\mathbf{k}})$, where

$$|\varepsilon_i^{\mathbf{k}}|^2 = 1, \quad \varepsilon_1^{\mathbf{k}} \times \varepsilon_2^{\mathbf{k}} = \hat{\mathbf{k}}, \quad \text{and} \quad \varepsilon_1^{\mathbf{k}} \cdot \varepsilon_2^{\mathbf{k}} = \hat{\mathbf{k}} \cdot \varepsilon_1^{\mathbf{k}} = \hat{\mathbf{k}} \cdot \varepsilon_2^{\mathbf{k}} = 0. \quad (1.125)$$

On quantization, the vector potential \hat{A}_i can be Fourier decomposed as follows²:

$$\hat{A}_i(\eta, \mathbf{x}) = \sqrt{4\pi} \int \frac{d^3\mathbf{k}}{(2\pi)^{3/2}} \sum_{\lambda=1}^2 \varepsilon_{\lambda i}^{\mathbf{k}} \left[\hat{b}_{\mathbf{k}}^\lambda \bar{A}_k(\eta) e^{i\mathbf{k} \cdot \mathbf{x}} + \hat{b}_{\mathbf{k}}^{\lambda\dagger} \bar{A}_k^*(\eta) e^{-i\mathbf{k} \cdot \mathbf{x}} \right], \quad (1.126)$$

where the quantities $\varepsilon_{\lambda i}^{\mathbf{k}}$ represent polarization vectors and the summation corresponds to the two orthonormal transverse polarizations. The Fourier modes \bar{A}_k satisfy the differential equation

$$\bar{A}_k'' + 2 \frac{J'}{J} \bar{A}_k' + k^2 \bar{A}_k = 0. \quad (1.127)$$

²It should be noted that in the expression for the quantization of the vector potential \hat{A}_i , we have introduced an overbar on the Fourier modes \bar{A}_k , so as to distinguish them from the vector potential A_i . Also, the subscript k denotes the wavenumber of the mode under consideration. The quantity $\varepsilon_{\lambda i}^{\mathbf{k}}$ is the polarization vector corresponding to the electromagnetic modes. Recall that we had used $\varepsilon_{ij}^s(\mathbf{k})$ to denote the polarization tensor of the gravitational waves [cf. Eq. (1.59)].

The operators $\hat{b}_{\mathbf{k}}^\lambda$ and $\hat{b}_{\mathbf{k}}^{\lambda\dagger}$ are the annihilation and creation operators satisfying the following standard commutation relations³:

$$[\hat{b}_{\mathbf{k}}^\lambda, \hat{b}_{\mathbf{k}'}^{\lambda'}] = [\hat{b}_{\mathbf{k}}^{\lambda\dagger}, \hat{b}_{\mathbf{k}'}^{\lambda'\dagger}] = 0, \quad [\hat{b}_{\mathbf{k}}^\lambda, \hat{b}_{\mathbf{k}'}^{\lambda'\dagger}] = \delta_{\lambda\lambda'} \delta^{(3)}(\mathbf{k} - \mathbf{k}'). \quad (1.128)$$

Let us now define a new variable $\mathcal{A}_k = J \bar{A}_k$ which, as we shall see, proves to be convenient to deal with. In terms of the new variable, Eq. (1.127) for \bar{A}_k simplifies to

$$\mathcal{A}_k'' + \left(k^2 - \frac{J''}{J} \right) \mathcal{A}_k = 0. \quad (1.129)$$

Note that \mathcal{A}_k is similar to the Mukhanov-Sasaki variables v_k and u_k for the scalar and tensor perturbations, whose evolution is governed by Eqs. (1.55) and (1.62), respectively. Therefore, the property of duality invariance [48] exhibited by the scalar and tensor perturbations, which was discussed in Subsec. 1.4.4, can be expected to hold true for the case of the magnetic fields as well. This issue will be discussed in further detail in Chap. 4.

Let us now turn to evaluation of the power spectra of the electromagnetic fields generated in this scenario. Let $\hat{\rho}_B$ and $\hat{\rho}_E$ denote the operators corresponding to the energy densities associated with the magnetic and electric fields, respectively. Upon using the decomposition (1.126) of the vector potential, the expectation values of the energy densities $\hat{\rho}_B$ and $\hat{\rho}_E$ can be evaluated in the vacuum state, say, $|0\rangle$, that is annihilated by the operator $\hat{b}_{\mathbf{k}}^\lambda$, *i.e.* $\hat{b}_{\mathbf{k}}^\lambda |0\rangle = 0 \forall (\mathbf{k}, \lambda)$. It can be shown that the spectral energy densities of the magnetic field and the electric field can be expressed in terms of the modes \bar{A}_k and \mathcal{A}_k and the coupling function J as follows [97, 98]

$$\begin{aligned} \mathcal{P}_B(k) &= \frac{d\langle 0 | \hat{\rho}_B | 0 \rangle}{d \ln k} \\ &= \frac{J^2(\eta)}{2\pi^2} \frac{k^5}{a^4(\eta)} |\bar{A}_k(\eta)|^2 = \frac{1}{2\pi^2} \frac{k^5}{a^4(\eta)} |\mathcal{A}_k(\eta)|^2, \end{aligned} \quad (1.130a)$$

$$\begin{aligned} \mathcal{P}_E(k) &= \frac{d\langle 0 | \hat{\rho}_E | 0 \rangle}{d \ln k} \\ &= \frac{J^2(\eta)}{2\pi^2} \frac{k^3}{a^4(\eta)} |\bar{A}_k(\eta)|^2 = \frac{1}{2\pi^2} \frac{k^3}{a^4(\eta)} \left| \mathcal{A}_k'(\eta) - \frac{J'(\eta)}{J(\eta)} \mathcal{A}_k(\eta) \right|^2. \end{aligned} \quad (1.130b)$$

The spectral energy densities $\mathcal{P}_B(k)$ and $\mathcal{P}_E(k)$ are often referred to as the power spectra for the generated magnetic and electric fields, respectively. A flat or scale invariant magnetic field spectrum corresponds to a constant, *i.e.* k -independent, $\mathcal{P}_B(k)$.

We shall now illustrate the generation of primordial magnetic fields using the simple case of de Sitter inflation, wherein the scale factor is given by Eq. (1.107a). In order to solve for the electromagnetic modes, we need to choose a form of the coupling function.

³Recall that we had used $\hat{b}_{\mathbf{k}}^s$ and $\hat{b}_{\mathbf{k}}^{s\dagger}$ to denote the annihilation and creation operators in the quantization of the tensor perturbations [cf. Eq. (1.59)].

In keeping with the expressions for the coupling functions that have been adopted previously [99–101], we select a coupling function that can be written as a simple power of the scale factor as follows:

$$J(\eta) = \left[\frac{a(\eta)}{a(\eta_e)} \right]^n = \left(\frac{\eta}{\eta_e} \right)^{-n}, \quad (1.131)$$

where η_e denotes the end of inflation, and n is a constant that can be both positive and negative. It should also be noted that we have chosen $J(\eta)$ to be such that at the end of inflation, *i.e.* when $\eta = \eta_e$, we obtain $J(\eta) = 1$, and thereby recover the standard electromagnetic action.

The solutions to Eq. (1.129) can then be expressed as [87,97]:

$$\mathcal{A}_k(\eta) = \sqrt{-k\eta} \left[C_1(k) J_{n+1/2}(-k\eta) + C_2(k) J_{-n-1/2}(-k\eta) \right], \quad (1.132)$$

where $J_\nu(x)$ is the Bessel function and the coefficients $C_1(k)$ and $C_2(k)$ can be fixed from the Bunch-Davies initial conditions to be

$$C_1(k) = \sqrt{\frac{\pi}{4k}} \frac{e^{-i(n-1)\pi/2}}{\cos(n\pi)}, \quad C_2(k) = \sqrt{\frac{\pi}{4k}} \frac{e^{i n \pi/2}}{\cos(n\pi)}. \quad (1.133)$$

It is often convenient to write the expression for the mode \mathcal{A}_k in terms of Hankel functions as follows:

$$\mathcal{A}_k(\eta) = \sqrt{-\frac{\pi\eta}{4}} e^{i(n+1)\pi/2} H_{n+1/2}^{(1)}(-k\eta). \quad (1.134)$$

Using the behavior of the Bessel functions at late times, *i.e.* as $(-k\eta) \rightarrow 0$, and the expression (1.130a), we obtain the magnetic field power spectrum to be

$$\mathcal{P}_B(k) = \frac{H_1^4}{8\pi} \mathcal{F}_1(m) (-k\eta)^{2m+6}, \quad (1.135)$$

where

$$\mathcal{F}_1(m) = \frac{1}{2^{2m+1} \cos^2(m\pi) \Gamma^2(m+3/2)}, \quad (1.136)$$

with

$$m = \begin{cases} n, & \text{if } n < -\frac{1}{2}, \\ -n-1, & \text{if } n > -\frac{1}{2}. \end{cases} \quad (1.137)$$

Note that the spectral index of the magnetic field n_B can be written as

$$n_B = \begin{cases} 2n+6, & \text{if } n < -\frac{1}{2}, \\ 4-2n, & \text{if } n > -\frac{1}{2}. \end{cases} \quad (1.138)$$

Evidently, in order to obtain a scale invariant power spectrum, we must have either $n = 2$ or $n = -3$.

Similarly, the electric field power spectrum can be evaluated to be

$$\mathcal{P}_E(k) = \frac{H_1^4}{8\pi} \mathcal{G}_1(m) (-k\eta)^{2m+4}, \quad (1.139)$$

where

$$\mathcal{G}_1(m) = \frac{1}{2^{2m-1} \cos^2(m\pi) \Gamma^2(m+1/2)}, \quad (1.140)$$

with

$$m = \begin{cases} n, & \text{if } n < \frac{1}{2}, \\ 1 - n, & \text{if } n > \frac{1}{2}. \end{cases} \quad (1.141)$$

The cases $n = 2$ or $n = -3$, which lead to scale invariant magnetic power spectra, also result in electric field power spectra which scale as k^2 and k^{-2} , respectively.

1.6.3 The backreaction and strong coupling problems

Since the electromagnetic fields are test fields, their total energy density should always remain sub-dominant compared to the background energy density ρ_1 that drives inflation, *viz.* $(\rho_B + \rho_E) \lesssim \rho_1$ at all times during inflation. If the electromagnetic energy density becomes larger than the background energy density, inflation cannot proceed. This is known as the backreaction problem [87,97]. If we evaluate the energy density contained in the electric and magnetic fields at any time $\eta_f = (a_f H)^{-1}$, using the expressions for the electromagnetic spectra obtained before, we find that the case $n = 2$, which results in a scale invariant magnetic power spectrum, does not contribute to any backreaction. However, for the other case which leads to scale invariant magnetic field, *viz.* $n = -3$, it can be shown that it is only possible to achieve about ten e-folds of inflation before it is interrupted by backreaction [99–101]. Therefore, only the coupling function with $n = 2$ is consistent with inflation.

We have considered the case wherein $J(\eta) \propto a^n(\eta)$. Also, as mentioned before, we must have $J(\eta_e) \rightarrow 1$, in order to recover the standard electromagnetic action at the end of inflation. This implies that at the onset of inflation, $J(\eta_i) \sim [a(\eta_i)/a(\eta_e)]^n = e^{-nN_i}$, where N_i denotes the number of e-folds of inflation. In the scale invariant case of $n = 2$, for 60 e-folds of inflation, we must have $J(\eta_i) \sim e^{-120}$. This implies that the model is in a strongly coupled regime at the beginning of inflation. This is referred to as the strong coupling problem [99,102–104]. Therefore, it is desirable to have $J(\eta) \gtrsim 1$ during inflation.

1.7 Organization of the thesis

The remainder of this thesis will be organized as follows. In the following chapter, we shall arrive at an analytical template for the scalar-scalar-tensor three-point function

[cf. Eq. (1.97)] arising in the axion monodromy model. This model is interesting to study because it leads to persistent oscillations in the scalar and tensor power spectra, which, in turn, result in an improvement in fit to the CMB data when compared with the conventional, nearly scale invariant power spectrum. In Chap. 3, we shall consider a specific matter bounce scenario, and evaluate the tensor bispectrum [cf. Eq. (1.103)] generated therein. Further, we shall compare and contrast between the characteristics of the corresponding non-Gaussianity parameter h_{NL} [cf. Eq. (1.106d)] generated in the matter bounce scenario under consideration with the h_{NL} evaluated in de Sitter inflation. In Chap. 4, we shall examine the generation of primordial magnetic fields in a specific matter bounce, and their subsequent evolution across the bounce. We shall also explicitly illustrate the phenomenon of duality invariance of the magnetic field power spectrum. In Chap. 5, we shall evaluate the cross-correlation between perturbations in a scalar field and the primordial magnetic fields in a matter bounce scenario. We shall also calculate the associated non-Gaussianity parameter and compare its characteristics with the corresponding parameter evaluated in de Sitter inflation. In Chap. 6, we shall add a non-minimally coupled parity violating term to the electromagnetic action and numerically study the subsequent origin and evolution of helical magnetic fields in de Sitter inflation, as well as their cross-correlations with the perturbations in a scalar field. We shall also examine how helicity affects the non-Gaussian signatures generated due to such cross-correlations. We shall conclude in Chap. 7 with a summary of the work done in the thesis and the scope of future work.

Chapter 2

The scalar-scalar-tensor three-point function in the axion monodromy model

2.1 Introduction

Until very recently, inflationary models were compared with the data at the level of two-point functions, *i.e.* the inflationary scalar and tensor power spectra were compared with the angular power spectra of the CMB and the matter power spectrum associated with the LSS [7, 9, 60, 61, 63, 105]. Over the last decade and a half, it has been realized that non-Gaussianities in general and the three-point functions in particular can provide strong constraints on the physics of the early universe. On one hand, there has been tremendous progress in understanding the generation of non-Gaussianities during inflation [22, 66, 72–74, 106] and the corresponding signatures on the CMB and the LSS [80, 107]. On the other hand, the expectation alluded to above has been largely corroborated by the strong constraints that have been arrived at from the Planck CMB data on the scalar non-Gaussianity parameter f_{NL} [64]. The recent observations seem to suggest that the primordial perturbations are consistent with a Gaussian distribution.

A nearly scale invariant primordial scalar power spectrum is remarkably consistent with the observations of the CMB [7, 9, 60, 61, 63, 105]. However, it has been repeatedly noticed that certain features in the inflationary power spectrum can improve the fit to the data (for instance, see Refs. [108, 109]). One such type of feature is continued oscillations in the scalar power spectrum that extends over a wide range of scales [110–113]. Such a power spectrum is known to be generated by the so-called axion monodromy model, motivated by string theory [114–116]. The model is described by a linear potential with superimposed oscillations. The oscillations in the potential give rise to a resonant behav-

ior which leads to continued modulations in the scalar and tensor power spectra. At the cost of two or three extra parameters, the resulting power spectra are known to improve the fit to the CMB data from the Wilkinson Microwave Anisotropy Probe (WMAP) and Planck by as much as $\Delta\chi^2 \simeq 10\text{--}20$ [110, 111, 115]. Ideally, one would like to carry out a similar analysis of comparing the model with the CMB data at the level of the three-point functions as well. But, it proves to be numerically taxing to evaluate the three-point functions in these models (see, for instance, Ref. [78]). In such a situation, clearly, it will be convenient if there exist analytical templates for the inflationary three-point functions. Such a template for the scalar bispectrum has been arrived at earlier [114, 117], which has been utilized towards comparing models leading to oscillatory features with the CMB data [113].

As we have discussed before, apart from the scalar bispectrum, there exist three other three-point functions which involve the tensor perturbations [66]. Amongst these three-point functions, the scalar-scalar-tensor cross-correlation has the largest amplitude after the scalar bispectrum (in this context, see Refs. [66–68, 70, 71, 76, 118, 119]). In this chapter, motivated by the efforts towards arriving at an analytical template for the scalar bispectrum in the axion monodromy model, we obtain a similar template for the scalar-scalar-tensor three-point function for an arbitrary triangular configuration of the wavevectors. In the case of the scalar bispectrum, in order to determine the dominant contribution due to the oscillations in the potential, it was sufficient to take into account the effects due to the changes in the behavior of the slow roll parameters, and one could work with the simple de Sitter modes for the curvature perturbation. In contrast, to evaluate the scalar-scalar-tensor cross correlation, we find that apart from the changes in the behavior of the slow roll parameters, we also need to take into account the modifications to the de Sitter modes. As in the purely scalar case [81, 120], the other three-point functions involving the tensors are also known to satisfy the so-called consistency relation in the squeezed limit [68, 70, 79, 84, 118]. We shall analytically establish the consistency condition for the scalar-scalar-tensor three-point function in the axion monodromy model.

The remainder of this chapter is organized as follows. In the next section, we shall introduce the important aspects of the axion monodromy model and arrive at the scalar and tensor power spectra in the model. In Sec. 2.3, we shall briefly discuss the evaluation of the scalar bispectrum in the axion monodromy model. In Sec. 2.4, we shall arrive at an analytical expression for the scalar-scalar-tensor cross-correlation under certain approximations. To illustrate the extent of accuracy of the approximations, we shall also compare the analytical result with the corresponding numerical result. Further, in Sec. 2.5, we shall analytically verify the consistency relation for the three-point function in the squeezed limit. We shall conclude in Sec. 2.6 with a brief summary of the results obtained.

2.2 The axion monodromy model

In this section, we shall summarize the essential aspects of the axion monodromy model. We shall discuss the evolution of the background as well as the evolution of the scalar and tensor perturbations and also arrive at the corresponding power spectra.

2.2.1 The evolution of the background and the slow roll parameters

The axion monodromy model is described by a linear potential with superimposed oscillations [114,115]. The potential is given by

$$V(\phi) = \mu^3 \phi + \mu^3 b f \cos \left(\frac{\phi}{f} \right), \quad (2.1)$$

where b is a dimensionless quantity and we have ignored a possible phase factor in the trigonometric function. Throughout this chapter, we shall assume that b is small and attempt to derive all the results at the linear order in b (as we shall discuss in due course, the constraint from the Planck data suggests that b is indeed small, of the order of 10^{-2} [111]). Evidently, this assumption is equivalent to considering the trigonometric modulations as small departures from the linear potential. We shall also assume that the linear potential admits slow roll and that the modulations lead to deviations from the monotonic slow roll behavior [114].

The equation of motion governing the scalar field described by the potential (2.1) above is given by [cf. Eq. (1.19)]

$$\ddot{\phi} + 3H\dot{\phi} + \mu^3 - \mu^3 b \sin \left(\frac{\phi}{f} \right) = 0, \quad (2.2)$$

with the Hubble parameter $H = \dot{a}/a$ being determined by the first Friedmann equation (1.23a). Since we shall assume that b is small, we can write the background inflaton as a slowly rolling part plus a part which describes the modulations as

$$\phi = \phi_0 + b \phi_1 + \dots \quad (2.3)$$

As we mentioned, we shall limit ourselves to terms which are linear in b . At the leading order, under the slow roll approximation, the equations (1.23a) and (2.2) simplify to

$$3H\dot{\phi}_0 \simeq -\mu^3, \quad (2.4a)$$

$$3H^2 M_{\text{Pl}}^2 \simeq \mu^3 \phi_0. \quad (2.4b)$$

These equations can be easily integrated to yield the leading order term in the inflaton to be

$$\phi_0(t) = \left[\phi_*^{3/2} - \frac{\sqrt{3}\mu^3}{2} M_{\text{Pl}} (t - t_*) \right]^{2/3}, \quad (2.5)$$

where $\phi_0(t_*) = \phi_*$, with t_* denoting the time when the pivot scale, say, k_* , leaves the Hubble radius. It should be noted that, in order to achieve about 60–70 e-folds of inflation, we shall require that $\phi_* \simeq 10 M_{\text{Pl}}$.

Let us now consider the behavior of ϕ_1 . The differential equation satisfied by the component ϕ_1 can be obtained to be

$$\ddot{\phi}_1 + \frac{\sqrt{3\mu^3\phi_0}}{M_{\text{Pl}}} \dot{\phi}_1 - \frac{\mu^3}{2\phi_0} \phi_1 = \mu^3 \sin\left(\frac{\phi_0}{f}\right), \quad (2.6)$$

where we have made use of the fact that, until the first order in b , under the slow roll approximation, we can write

$$H^2 \simeq \frac{\mu^3}{3M_{\text{Pl}}^2} (\phi_0 + b\phi_1). \quad (2.7)$$

If we make use of the solution (2.5) for ϕ_0 , the above equation governing ϕ_1 can be expressed as

$$\frac{d^2\phi_1}{d\phi_0^2} - \frac{3\phi_0}{M_{\text{Pl}}^2} \frac{d\phi_1}{d\phi_0} - \frac{3\phi_1}{2M_{\text{Pl}}^2} = \frac{3\phi_0}{M_{\text{Pl}}^2} \sin\left(\frac{\phi_0}{f}\right). \quad (2.8)$$

This equation can be integrated to arrive at the following solution for ϕ_1 :

$$\phi_1(\phi_0) = \frac{3f^2\phi_*/M_{\text{Pl}}^2}{1 + (3f\phi_*/M_{\text{Pl}}^2)^2} \left[-\sin\left(\frac{\phi_0}{f}\right) + \frac{3f\phi_*}{M_{\text{Pl}}^2} \cos\left(\frac{\phi_0}{f}\right) \right], \quad (2.9)$$

which can be written as

$$\phi_1(\phi_0) = -\frac{3f^2\phi_*/M_{\text{Pl}}^2}{[1 + (3f\phi_*/M_{\text{Pl}}^2)^2]^{1/2}} \sin\left(\frac{\phi_0}{f} - \psi_1\right), \quad (2.10)$$

where

$$\sin\psi_1 = \frac{3f\phi_*/M_{\text{Pl}}^2}{[1 + (3f\phi_*/M_{\text{Pl}}^2)^2]^{1/2}}. \quad (2.11)$$

Note that, when $f\phi_*/M_{\text{Pl}}^2$ is assumed to be small (as we shall discuss later, the constraints from the recent CMB observations suggest that $f\phi_*/M_{\text{Pl}}^2 \simeq 7.6346 \times 10^{-2}$ [111]), we can write

$$\phi_1(\phi_0) = -\frac{3f^2\phi_*}{M_{\text{Pl}}^2} \sin\left(\frac{\phi_0}{f}\right). \quad (2.12)$$

Having understood the behavior of the background inflaton, let us now evaluate the first and the second slow roll parameters. Recall that the first slow roll parameter is given by Eq. (1.28). Let us write the first slow roll parameter as $\epsilon_1 = \epsilon_1^0 + \epsilon_1^c$, where ϵ_1^0 is the contribution due to ϕ_0 , while ϵ_1^c is the correction at the first order in b . As one would expect, ϵ_1^0 will roughly be constant and will be of the order of $\epsilon_1^0 = \epsilon_1^* \simeq M_{\text{Pl}}^2/(2\phi_*^2)$,

determined by the linear term in the potential. Upon making use of the solutions we have obtained above, we can show that, the quantity ϵ_1^c is given by

$$\epsilon_1^c = -\frac{3bf}{\phi_*} \cos\left(\frac{\phi_0}{f}\right). \quad (2.13)$$

In arriving at this expression, we have again made the assumption that $f\phi_*/M_{\text{Pl}}^2 \ll 1$. The second slow roll parameter can be expressed as $\epsilon_2 = \dot{\epsilon}_1/(H\epsilon_1)$ [cf. Eq. (1.29)]. One can show that $\epsilon_2 = 2(\delta + \epsilon_1)$, where $\delta = \ddot{H}/(H\dot{H}) = \ddot{\phi}/(H\dot{\phi})$. If we write $\delta = \delta_0 + \delta_1$, where δ_0 corresponds to the case wherein b vanishes, then we can show that $\delta_0 = \epsilon_1^*$ and $\epsilon_2^* = 4\epsilon_1^*$. Also, for small $f\phi_*/M_{\text{Pl}}^2$, we find that δ_1 can be expressed as

$$\delta_1 = -3b \sin\left(\frac{\phi_0}{f}\right). \quad (2.14)$$

2.2.2 The evolution of the perturbations and the power spectra

The assumptions and approximations that we have made in the previous subsection enable us to analytically explore the evolution of perturbations and calculation of the power spectra [114]. Let us begin by summarizing a few basic points concerning the scalar power spectrum. Recall that, upon quantization, the curvature perturbation \mathcal{R} can be decomposed in terms of the corresponding Fourier modes f_k [in this context, see Eqs. (1.51) and (1.52)]. The modes f_k satisfy the differential equation (1.54).

Let us analytically evaluate the scalar power spectrum in the axion monodromy model [114]. If we choose to work in terms of a new variable $x = -k\eta$ and use the exact relation

$$\frac{z'}{z} = aH(1 + \epsilon_1 + \delta), \quad (2.15)$$

we can rewrite the differential equation (1.54) governing the mode f_k as

$$\frac{d^2 f_k}{dx^2} + 2(1 + \epsilon_1 + \delta) \left(\frac{aH}{-k}\right) \frac{df_k}{dx} + f_k = 0. \quad (2.16)$$

At the leading order in slow roll, we have [cf. Eq. (1.70)]

$$aH \simeq -\frac{1 + \epsilon_1}{\eta}. \quad (2.17)$$

We shall work in the de Sitter approximation when $b = 0$, which corresponds to ignoring the contributions due to the ϵ_1^* term. The effects due to the δ_1 term dominates the effects due to the ϵ_1^c term. Under these conditions, we can write the above differential equation describing f_k as follows:

$$\frac{d^2 f_k}{dx^2} - \frac{2(1 + \delta_1)}{x} \frac{df_k}{dx} + f_k = 0. \quad (2.18)$$

In the slow roll limit determined by the linear potential wherein δ_1 can be ignored, the positive frequency modes satisfying the above differential equation can be written in the de Sitter form as

$$f_k^+(x) = i f_k^0 (1 - i x) e^{i x}, \quad (2.19)$$

where $f_k^0 = H_1/(2 M_{\text{Pl}} \sqrt{k^3 \epsilon_1^*})$, with H_1 being given by $H_1^2 = \mu^3 \phi_*/(3 M_{\text{Pl}}^2)$. Hence, in the presence of a non-zero δ_1 , let us write the modes describing the curvature perturbation as [114]

$$f_k(x) = f_k^+(x) + c_k(x) f_k^-(x), \quad (2.20)$$

where $f_k^-(x)$ are the negative frequency modes that are related to the positive frequency modes by the relation $f_k^-(x) = f_k^{+*}(x)$. Note that the non-vanishing δ_1 modifies the standard de Sitter modes $f_k^+(x)$. The non-trivial evolution of the modes is captured by the function $c_k(x)$.

The de Sitter modes f_k^\pm satisfy the differential equation

$$\frac{d^2 f_k^\pm}{dx^2} - \frac{2}{x} \frac{df_k^\pm}{dx} + f_k^\pm = 0. \quad (2.21)$$

Therefore, upon substituting the expression (2.20) in the differential equation (2.18), we obtain the following equation governing c_k :

$$\frac{d}{dx} \left[\left(1 - \frac{i}{x} \right) e^{-2 i x} \frac{dc_k}{dx} \right] + \frac{i}{x^2} e^{-2 i x} \frac{dc_k}{dx} = \frac{2 i \delta_1}{x}. \quad (2.22)$$

As is well known, the perturbations oscillate when they are well inside the Hubble radius. In this sub-Hubble regime, the oscillations in the perturbations resonate with the oscillations in the background quantities. This resonance occurs when $x \simeq M_{\text{Pl}}^2/(2 f \phi_*)$, which proves to be a large quantity for the parameter ranges of our interest (recall that, we had assumed $f \phi_*/M_{\text{Pl}}^2$ to be small). Therefore, the terms involving inverse powers of x on the left hand side of the above differential equation can be ignored in the sub-Hubble regime and, under these conditions, the equation can be easily integrated. We find that the resulting $c_k(x)$ can be expressed as

$$\begin{aligned} c_k(x) = & -\frac{3 b f \phi_*}{2 M_{\text{Pl}}^2} \left[e^{i(\alpha_1 + \phi_k/f)} e^{-\pi M_{\text{Pl}}^2/(2 f \phi_*)} \Gamma \left(1 + \frac{i M_{\text{Pl}}^2}{f \phi_*}, -2 i x \right) \right. \\ & \left. + e^{-i(\alpha_1 + \phi_k/f)} e^{\pi M_{\text{Pl}}^2/(2 f \phi_*)} \Gamma \left(1 - \frac{i M_{\text{Pl}}^2}{f \phi_*}, -2 i x \right) \right], \end{aligned} \quad (2.23)$$

where $\Gamma(a, x)$ is the incomplete Gamma function [58] and $\alpha_1 = -X_{\text{res}} \ln 2$, with $X_{\text{res}} = M_{\text{Pl}}^2/(f \phi_*)$. Note that X_{res} is a large quantity since we have assumed $f \phi_*/M_{\text{Pl}}^2$ to be small. In arriving at the above expression, we have expressed ϕ_0 in terms of x as

$$\phi_0 = \phi_k + \sqrt{2 \epsilon_1^*} M_{\text{Pl}} \ln x, \quad (2.24)$$

where the quantity ϕ_k is given by

$$\phi_k = \phi_* - \sqrt{2\epsilon_1^*} M_{\text{Pl}} \ln \left(\frac{k}{k_*} \right), \quad (2.25)$$

with k_* denoting the pivot scale. Since we have assumed that $f\phi_*/M_{\text{Pl}}^2 \ll 1$, the first term in Eq. (2.23) is exponentially suppressed and hence can be ignored. Thus, we can express c_k as

$$c_k(x) = -\frac{3b f \phi_*}{2 M_{\text{Pl}}^2} e^{-i(\phi_k/f + \alpha_1)} e^{\pi M_{\text{Pl}}^2/2 f \phi_*} \Gamma \left(1 - \frac{i M_{\text{Pl}}^2}{f \phi_*}, -2i x \right). \quad (2.26)$$

Note that, in deriving the above solution for $c_k(x)$, we had ignored inverse powers of x on the left hand side of Eq. (2.22). We should emphasize here that this approximation is strictly valid only at sub-Hubble scales. However, since the complete mode approaches a constant value at late times, one finds that the largest contribution to the three-point functions arises from the sub-Hubble domain [114]. Hence, the above solution for $c_k(x)$ proves to be sufficient for evaluating the three-point function of our interest analytically. As we shall see, these arguments are corroborated by the numerical results we obtain.

The scalar power spectrum can now be obtained from the late time limit (*i.e.* as $x \rightarrow 0$) of the modes f_k . We find that

$$c_k(0) = \frac{3ib\sqrt{\pi}}{\sqrt{2} X_{\text{res}}} e^{-i(\phi_k/f + \beta_1)}, \quad (2.27)$$

where the phase $\beta_1 = X_{\text{res}} \ln X_{\text{res}} - X_{\text{res}} - X_{\text{res}} \ln 2 - \pi/4$. Upon using this result and the expression (1.57) for the scalar power spectrum, at the order b , we can express the power spectrum involving the scalar perturbations as [114]

$$\mathcal{P}_s(k) = \mathcal{P}_s^0 [1 - c_k(0) - c_k^*(0)] = \mathcal{P}_s^0 \left[1 - \delta n_s \sin \left(\frac{\phi_k}{f} + \beta_1 \right) \right], \quad (2.28)$$

where \mathcal{P}_s^0 represents the amplitude of the scalar power spectrum which arises in the slow roll scenario when the oscillations in the potential are absent and the quantity ϕ_k depends on the wavenumber through the relation (2.25). The quantity \mathcal{P}_s^0 is given by

$$\mathcal{P}_s^0 = \frac{H_1^2}{8\pi^2 M_{\text{Pl}}^2 \epsilon_1^*}, \quad (2.29)$$

and, for small $f\phi_*/M_{\text{Pl}}^2$, the quantity δn_s can be expressed as

$$\delta n_s = \frac{3b\sqrt{2\pi}}{\sqrt{X_{\text{res}}}}. \quad (2.30)$$

The sinusoidal term in the power spectrum leads to oscillations that extend over a wide range of scales. These oscillations result in continued modulations in the scalar spectral

index n_s [cf. Eq. (1.67a)], which can be obtained from the expression (2.28) for the scalar power spectrum. In order to separate the contributions at the zeroth and first order in b , it is convenient to write the scalar spectral index in the form $n_s = n_s^0 + n_s^c$, where n_s^0 is the scalar spectral index in the slow roll approximation when the oscillations are ignored and n_s^c is the correction at order b . One can show that [cf. Eq. (1.75a)] $n_s^0 = 1 - 2\epsilon_1^* - \epsilon_2^* = 1 - 6\epsilon_1^*$. The first order correction to the scalar spectral index can be evaluated from Eqs. (1.67a) and (2.28) to be

$$n_s^c(k) = 3b \sqrt{2\pi X_{\text{res}}} \cos\left(\frac{\phi_k}{f} + \beta_1\right). \quad (2.31)$$

The power spectrum (2.28) that we have arrived at above has been compared with the WMAP and Planck data [110, 111, 115]. As we have discussed earlier, the persistent oscillations in the power spectrum lead to a better fit to the data than the more conventional nearly scale invariant primordial spectrum. The values of the parameters describing the axion monodromy model that are found to lead to the best fit to the Planck data are as follows: $(\mu/M_{\text{Pl}})^3 = 2.512 \times 10^{-10}$, $b = 1.063 \times 10^{-2}$, and $f/M_{\text{Pl}} = 7.6346 \times 10^{-3}$ [111]. Note that these values lead to $f\phi_*/M_{\text{Pl}}^2 = 7.6346 \times 10^{-2}$, which in turn corresponds to $X_{\text{res}} \simeq 13$. It should be mentioned that earlier CMB data had suggested values for f that was smaller by an order of magnitude or more and hence a suitably larger value of X_{res} (of the order of 250 or so). While $X_{\text{res}} \simeq 13$ is not very large, we find that our analytical results match the numerical results fairly well over a range of f and b .

Let us now turn to the case of the tensor power spectrum. On quantization, the tensor perturbation γ_{ij} can be decomposed in terms of the corresponding Fourier modes h_k [in this context, see Eqs. (1.58) and (1.59)]. The modes h_k satisfy the differential equation (1.61). In the axion monodromy model, the tensor modes and the tensor power spectrum can be determined in a manner very similar to the scalar case. On substituting the expression (2.17) in the equation (1.61) governing the evolution of the tensor modes, we obtain that

$$\frac{d^2 h_k}{dx^2} - \frac{2(1 + \epsilon_1)}{x} \frac{dh_k}{dx} + h_k = 0. \quad (2.32)$$

When the modulations in the potential are ignored, the positive frequency tensor modes in the slow roll limit are given by

$$h_k^+(x) = i h_k^0 (1 - ix) e^{ix}, \quad (2.33)$$

where $h_k^0 = H_I/(M_{\text{Pl}} \sqrt{k^3})$. In the presence of the modulations, let us write the modes describing the tensor perturbation as

$$h_k(x) = h_k^+(x) + d_k(x) h_k^-(x), \quad (2.34)$$

where $h_k^-(x) = h_k^{+*}(x)$. The de Sitter modes h_k^\pm satisfy the differential equation (2.21). On substituting the expression (2.34) for the tensor modes in Eq. (1.61), we find that the

quantity d_k satisfies the differential equation

$$\frac{d}{dx} \left[\left(1 - \frac{i}{x} \right) e^{-2ix} \frac{dd_k}{dx} \right] + \frac{i}{x^2} e^{-2ix} \frac{dd_k}{dx} = \frac{2i\epsilon_1}{x}. \quad (2.35)$$

As in the scalar case, due to the resonance that arises in the sub-Hubble regime (*i.e.* when x is large), we can ignore the terms involving the inverse powers of x on the left hand side of the above differential equation. Upon integrating the above equation under these conditions, we obtain d_k to be

$$\begin{aligned} d_k(x) = & -\frac{3ibf^2}{2M_{\text{Pl}}^2} \left[e^{i(\phi_k/f+\alpha_1)} e^{-\pi M_{\text{Pl}}^2/(2f\phi_*)} \Gamma \left(1 + \frac{iM_{\text{Pl}}^2}{f\phi_*}, -2ix \right) \right. \\ & \left. - e^{-i(\phi_k/f+\alpha_1)} e^{\pi M_{\text{Pl}}^2/(2f\phi_*)} \Gamma \left(1 - \frac{iM_{\text{Pl}}^2}{f\phi_*}, -2ix \right) \right]. \end{aligned} \quad (2.36)$$

In the domain $f\phi_*/M_{\text{Pl}}^2 \ll 1$, the first term in the above expression is exponentially suppressed and hence d_k simplifies to be

$$d_k(x) = \frac{3ibf^2}{2M_{\text{Pl}}^2} e^{-i(\phi_k/f+\alpha_1)} e^{\pi M_{\text{Pl}}^2/(2f\phi_*)} \Gamma \left(1 - \frac{iM_{\text{Pl}}^2}{f\phi_*}, -2ix \right). \quad (2.37)$$

This expression for d_k allows us to evaluate the tensor power spectrum and, we find that in the limit $x \rightarrow 0$, it can be expressed as [cf. Eq. (1.65)]

$$\mathcal{P}_{\text{T}}(k) = \mathcal{P}_{\text{T}}^0 [1 - d_k(0) - d_k^*(0)] = \mathcal{P}_{\text{T}}^0 \left[1 - \frac{f}{\phi_*} \delta n_{\text{s}} \cos \left(\frac{\phi_k}{f} + \beta_1 \right) \right], \quad (2.38)$$

where \mathcal{P}_{T}^0 represents the amplitude of the tensor power spectrum which arises in the slow roll scenario when the oscillations are absent in the potential and is given by

$$\mathcal{P}_{\text{T}}^0 = \frac{2H_{\text{I}}^2}{\pi^2 M_{\text{Pl}}^2}. \quad (2.39)$$

The amplitude of the oscillations in the tensor power spectrum prove to be about f/ϕ_* (which is nearly 10^{-3} , for the best fit values) times smaller than the magnitude of the oscillations in the case of scalars. As in the case of the scalar spectral index, it is convenient to split the contribution to the tensor spectral index into a slow roll part and a part which is first order in b as $n_{\text{T}} = n_{\text{T}}^0 + n_{\text{T}}^{\text{c}}$. The contribution at the zeroth order in b to the tensor spectral index is given by $n_{\text{T}}^0 = -2\epsilon_1^*$, which is the standard slow roll result [cf. Eq. (1.75b)]. The first order correction to the tensor spectral index can be arrived at using the tensor power spectrum (2.38) and is found to be [116]

$$n_{\text{T}}^{\text{c}} = -3b \sqrt{\frac{2\pi f}{M_{\text{Pl}}}} (2\epsilon_1^*)^{3/4} \sin \left(\frac{\phi_k}{f} + \beta_1 \right), \quad (2.40)$$

which reflects the continued oscillations in the tensor power spectrum.

2.3 The scalar bispectrum in the Maldacena formalism

Our aim in this chapter is to evaluate the scalar-scalar-tensor three-point function generated in the axion monodromy model. However, for the sake of completeness, we shall first discuss the behavior of the scalar bispectrum evaluated in this model, especially to illustrate how the oscillations in the potential boost the scalar non-Gaussianity parameter f_{NL} [117]. As we had discussed previously in Subsec. 1.5.4, up to the leading order in the slow roll parameters, the dominant contribution to the three-point function arises from the first three integrals and the seventh term [cf. Eqs. (1.108)], which are combined together to obtain the total contribution to the scalar bispectrum in slow roll inflation. In contrast, since the axion monodromy model involves deviation from slow roll, the major contribution to the scalar bispectrum arises from the fourth term [cf. Eq. (1.94d)]. In the fourth term, it is the presence of the time derivative of ϵ_2 which makes this contribution dominant.

As discussed before, at the linear order in b , we can replace ϵ_2 by $2\delta_1$ and ϵ_1 by ϵ_1^0 and use Eq. (2.14) to write

$$\begin{aligned} \mathcal{G}_{\mathcal{RRR}}^4(\mathbf{k}_1, \mathbf{k}_2, \mathbf{k}_3) &= \frac{3bH_I}{4M_{\text{Pl}}^2 f} \left(\frac{2}{k_1^3 k_2^3 k_3^3} \right)^{1/2} \int_0^\infty dx \left[-k_1 k_2 k_3 + i \sum_{i \neq j} \frac{k_i^2 k_j}{x} \right. \\ &\quad \left. + \frac{k_T(k_1^2 + k_2^2 + k_3^2)}{x^2} \right] \cos\left(\frac{\phi_0}{f}\right) e^{-ix}. \end{aligned} \quad (2.41)$$

Now, upon substituting (2.24) in the above equation, we get

$$\begin{aligned} \mathcal{G}_{\mathcal{RRR}}^4(\mathbf{k}_1, \mathbf{k}_2, \mathbf{k}_3) &= \frac{3bH_I}{8M_{\text{Pl}}^2 f} \left(\frac{2}{k_1^3 k_2^3 k_3^3} \right)^{1/2} \int_0^\infty dx \left[-k_1 k_2 k_3 + i \sum_{i \neq j} \frac{k_i^2 k_j}{x} \right. \\ &\quad \left. + \frac{k_T(k_1^2 + k_2^2 + k_3^2)}{x^2} \right] \left\{ \exp\left(\frac{i\phi_{k_T}}{f} + \frac{i\sqrt{2}\epsilon_1^*}{f} M_{\text{Pl}} \ln x - ix\right) \right. \\ &\quad \left. + \exp\left(-\frac{i\phi_{k_T}}{f} - \frac{i\sqrt{2}\epsilon_1^*}{f} M_{\text{Pl}} \ln x - ix\right) \right\}. \end{aligned} \quad (2.42)$$

For small $f\phi_*/M_{\text{Pl}}^2$, the second term in the curly brackets in the above integrand is exponentially suppressed. Also, the first term in the curly brackets in the integrand becomes stationary at $x = X_{\text{res}} = \sqrt{2\epsilon_1^*} M_{\text{Pl}}/f$, so that the major contribution to the integral is from this value of x . Hence, on replacing the x 's in the polynomial expressions in the integrand by X_{res} 's, up to the leading order in b and a k -independent phase, we can arrive at

the scalar bispectrum to be [cf. Eq. (1.93)]

$$\begin{aligned}
 G_{\mathcal{R}\mathcal{R}\mathcal{R}}(\mathbf{k}_1, \mathbf{k}_2, \mathbf{k}_3) = & \frac{H_I^4}{32 M_{\text{Pl}}^4} \frac{1}{(k_1 k_2 k_3)^3} \frac{3 b \sqrt{2} \pi}{\epsilon_1^{*2}} \left(\frac{\sqrt{2} \epsilon_1^* M_{\text{Pl}}}{f} \right)^{3/2} \\
 & \times \left\{ \left[-k_1 k_2 k_3 + \frac{k_T (k_1^2 + k_2^2 + k_3^2)}{X_{\text{res}}^2} \right] \sin \left(\frac{\phi_k}{f} \right) \right. \\
 & \left. + \left[\frac{k_1^2 (k_2 + k_3) + k_2^2 (k_3 + k_1) + k_3^2 (k_1 + k_2)}{X_{\text{res}}} \right] \cos \left(\frac{\phi_k}{f} \right) \right\}. \quad (2.43)
 \end{aligned}$$

This expression for the bispectrum, when combined with the contribution to the scalar bispectrum during slow roll inflation [cf. Eqs. (1.108)], gives the complete expression for the scalar bispectrum in the axion monodromy model. Subsequently, when the non-Gaussianity parameter f_{NL} is evaluated for this model, its amplitude is found to be rather large [83], which is incompatible with the Planck constraints [cf. Eqs. (1.120)] [64]. However, it should be noted that, as discussed in Subsec. 1.5.6, the constraints from Planck on the non-Gaussianity parameters have been arrived at by considering certain particular shapes for the non-Gaussianities. Since the shape of f_{NL} obtained from the axion monodromy model is quite different from the templates considered by Planck, the earlier constraints do not apply to this case and the specific shape of f_{NL} obtained in this model has to be compared separately with the data.

Let us now discuss the behavior of the scalar bispectrum in the squeezed limit. In this limit, where $\mathbf{k}_1 = -\mathbf{k}_2 = \mathbf{k}$ and $k_3 \rightarrow 0$, up to a k -independent phase, we obtain,

$$k^3 k_3^3 G_{\mathcal{R}\mathcal{R}\mathcal{R}}(\mathbf{k}, -\mathbf{k}, \mathbf{k}_3) = \frac{H_I^4}{16 M_{\text{Pl}}^4} \frac{3 b \sqrt{2} \pi}{\epsilon_1^{*2}} \left(\frac{\sqrt{2} \epsilon_1^* M_{\text{Pl}}}{f} \right)^{1/2} \cos \left(\frac{\phi_k}{f} \right). \quad (2.44)$$

Let us now verify the consistency relation for the scalar bispectrum. The relation (1.117a) can be rewritten as

$$k^3 k_3^3 G_{\mathcal{R}\mathcal{R}\mathcal{R}}(\mathbf{k}, -\mathbf{k}, \mathbf{k}_3) = -\frac{(2\pi)^4}{4} (n_s - 1) \mathcal{P}_s(k) \mathcal{P}_s(k_3). \quad (2.45)$$

At the linear order in b , the right hand side of this equation can be obtained to be

$$-\frac{(2\pi)^4}{4} (n_s - 1) \mathcal{P}_s(k) \mathcal{P}_s(k_3) \simeq -\frac{(2\pi)^4}{4} n_s^c \mathcal{P}_s^0(k) \mathcal{P}_s^0(k_3). \quad (2.46)$$

Using Eqs. (2.31) and (2.29) to evaluate this expression and comparing with Eq. (2.44), we find that, up to a k -independent phase factor, the consistency relation for the scalar bispectrum holds true.

2.4 Analytical template for the scalar-scalar-tensor cross-correlation

In this section, we shall first arrive at an analytical expression for the scalar-scalar-tensor three-point function. Then, in order to illustrate the accuracy of the analytical results, we shall compare them with the exact numerical results.

2.4.1 Analytical evaluation of the three-point function

Among the three different contributions to the scalar-scalar-tensor three-point function, the term $\mathcal{G}_{\mathcal{RR}\gamma}^1(\mathbf{k}_1, \mathbf{k}_2, \mathbf{k}_3)$ [cf. Eq. (1.98a)] is linear in the first slow roll parameter ϵ_1 and hence it dominates over the other two terms [cf. Eqs. (1.98b) and (1.98c)], both of which are quadratic in ϵ_1 . The term $\mathcal{G}_{\mathcal{RR}\gamma}^1(\mathbf{k}_1, \mathbf{k}_2, \mathbf{k}_3)$ can be decomposed into a slow roll part, which is zeroth order in b , and terms involving b . The contribution when $b = 0$ corresponds to the standard slow roll result [cf. Eq. (1.109)] and it can be easily evaluated using the de Sitter modes [79].

Let us now turn to the contributions involving b . As we have discussed, we shall ignore terms which are of higher order in b and focus only on the contributions that are linear in b . Even amongst the various terms which are linear in b , we shall further restrict ourselves to terms which are of the leading order in $f\phi_*/M_{\text{Pl}}^2$. In the case of the scalar bispectrum, as we have discussed, the dominant contribution arises due to a term dependent on ϵ_2 , which grows to be quite large in the axion monodromy model. This in turn boosts the scalar bispectrum and the corresponding non-Gaussianity parameter to rather significant values [117]. Moreover, since ϵ_2 becomes large, it proves to be sufficient to work with the de Sitter modes to evaluate the dominant contribution. In contrast, in the case of the scalar-scalar-tensor cross-correlation, apart from the correction to the slow roll parameter ϵ_1^* (*viz.* ϵ_1^c), we have to take into account the modification to the de Sitter modes, which are quantified by c_k and d_k . It should be clear that, at the linear order in b , there arise four contributions due to c_k and d_k , two from the $c_k(x)$ and $d_k(x)$ inside the integral [cf. Eq. (1.98a)] and two others due to the terms $c_k(0)$ and $d_k(0)$ outside [cf. Eq. (1.97)]. One finds that $d_k/c_k \sim f/\phi_*$, which is a small quantity. Therefore, one can actually ignore the terms involving d_k and retain only those containing c_k . Under these conditions, at the first order in b , we can write the expression for the scalar-scalar-tensor three-point

function as

$$\begin{aligned}
 G_{\mathcal{RR}\gamma}^{1(1)}(\mathbf{k}_1, \mathbf{k}_2, \mathbf{k}_3) = & M_{\text{Pl}}^2 \Pi_{m_3 n_3, ij}^{\mathbf{k}_3} \hat{n}_{1i} \hat{n}_{2j} \left\{ -2 i k_1 k_2 \left[f_{k_1}^+(0) f_{k_2}^+(0) h_{k_3}^+(0) \int_{-\infty}^0 d\eta a^2 \right. \right. \\
 & \times (\epsilon_1^* c_{k_1}^* f_{k_1}^+ f_{k_2}^{++} h_{k_3}^{++} + \epsilon_1^* c_{k_2}^* f_{k_1}^{++} f_{k_2}^+ h_{k_3}^{++} + \epsilon_1^c f_{k_1}^{++} f_{k_2}^{++} h_{k_3}^{++}) \\
 & + (c_{k_1}(0) f_{k_1}^{++}(0) f_{k_2}^+(0) h_{k_3}^+(0) + c_{k_2}(0) f_{k_1}^+(0) f_{k_2}^{++}(0) h_{k_3}^+(0)) \\
 & \left. \left. \times \int_{-\infty}^0 d\eta a^2 \epsilon_1^* f_{k_1}^{++} f_{k_2}^{++} h_{k_3}^{++} \right] + \text{complex conjugate} \right\}. \quad (2.47)
 \end{aligned}$$

Let us first consider the term containing ϵ_1^c in the above expression. At the linear order in b and $f \phi_*/M_{\text{Pl}}^2$, we have

$$\begin{aligned}
 G_{\mathcal{RR}\gamma}^{1(1a)}(\mathbf{k}_1, \mathbf{k}_2, \mathbf{k}_3) = & \Pi_{m_3 n_3, ij}^{\mathbf{k}_3} \hat{n}_{1i} \hat{n}_{2j} \left[\frac{H_{\text{I}}^4}{8 M_{\text{Pl}}^4 \epsilon_1^{*2}} \frac{-i k_1 k_2}{(k_1 k_2 k_3)^3} \int_{-\infty}^0 \frac{d\eta}{\eta^2} \epsilon_1^c \left(1 - i k_{\text{T}} \eta \right. \right. \\
 & \left. \left. - (k_1 k_2 + k_2 k_3 + k_3 k_1) \eta^2 + i k_1 k_2 k_3 \eta^3 \right) e^{i k_{\text{T}} \eta} \right. \\
 & \left. + \text{complex conjugate} \right], \quad (2.48)
 \end{aligned}$$

where we have used the expressions (2.20) and (2.34) for the modes f_k and h_k in Eqs. (1.97) and (1.98a). We can use the expressions (2.13) and (2.24) and substitute $x = -k_{\text{T}} \eta$ for performing the above integrals. Each of these integrals are found to be of the following form:

$$I_1(k_1, k_2, k_3, X_{\text{res}}, f) = \int_0^\infty dx q(x) e^{-ix} \left\{ e^{i[(\phi_{k_{\text{T}}}/f) + X_{\text{res}} \ln x]} + e^{-i[(\phi_{k_{\text{T}}}/f) + X_{\text{res}} \ln x]} \right\}, \quad (2.49)$$

where $q(x)$ is some polynomial function of x . The two terms in the above integral can be expressed in terms of the Gamma functions. However, we find that, for small $f \phi_*/M_{\text{Pl}}^2$, the contribution due to the second term is exponentially suppressed when compared to the first term and hence can be ignored. Under this assumption, we can evaluate the integrals in Eq. (2.48) to obtain

$$\begin{aligned}
 G_{\mathcal{RR}\gamma}^{1(1a)}(\mathbf{k}_1, \mathbf{k}_2, \mathbf{k}_3) = & \Pi_{m_3 n_3, ij}^{\mathbf{k}_3} \hat{n}_{1i} \hat{n}_{2j} \frac{H_{\text{I}}^4}{4 M_{\text{Pl}}^4 \epsilon_1^*} \frac{3 b \sqrt{2} \pi}{\sqrt{X_{\text{res}}}} \frac{k_1 k_2}{(k_1 k_2 k_3)^3} \\
 & \times \left\{ \frac{k_{\text{T}}}{1 + X_{\text{res}}^2} \left[-\sin \left(\frac{\phi_{k_{\text{T}}}}{f} + \beta_2 \right) + \frac{1}{X_{\text{res}}} \cos \left(\frac{\phi_{k_{\text{T}}}}{f} + \beta_2 \right) \right] \right. \\
 & - \frac{k_{\text{T}}}{X_{\text{res}}} \cos \left(\frac{\phi_{k_{\text{T}}}}{f} + \beta_2 \right) + \frac{k_1 k_2 + k_2 k_3 + k_3 k_1}{k_{\text{T}}} \sin \left(\frac{\phi_{k_{\text{T}}}}{f} + \beta_2 \right) \\
 & \left. + \frac{k_1 k_2 k_3}{k_{\text{T}}^2} \left[X_{\text{res}} \cos \left(\frac{\phi_{k_{\text{T}}}}{f} + \beta_2 \right) + \sin \left(\frac{\phi_{k_{\text{T}}}}{f} + \beta_2 \right) \right] \right\}, \quad (2.50)
 \end{aligned}$$

where the phase factor β_2 is given by $\beta_2 = X_{\text{res}} \ln X_{\text{res}} - X_{\text{res}} - \pi/4$.

Let us now consider the terms containing c_k in Eq. (2.47). We shall consider terms involving both $c_k(0)$ as well as $c_k(\eta)$. We can substitute the expressions for the modes f_k^+ and h_k^+ [cf. Eqs. (2.19) and (2.33)] to obtain the contributions due to these terms to be

$$\begin{aligned}
 G_{\mathcal{RR}\gamma}^{1(b)}(\mathbf{k}_1, \mathbf{k}_2, \mathbf{k}_3) &= \Pi_{m_3 n_3, ij}^{k_3} \hat{n}_{1i} \hat{n}_{2j} \left\{ \frac{i H_I^4}{8 M_{\text{Pl}}^4 \epsilon_1^*} \frac{k_1 k_2}{(k_1 k_2 k_3)^3} \left[\int_{-\infty}^0 \frac{d\eta}{\eta^2} c_{k_1}^*(\eta) \right. \right. \\
 &\quad \times \underbrace{\left(1 - i k_{T1} \eta \right)}_{\text{I}} + \underbrace{\left((k_1 k_2 - k_2 k_3 + k_3 k_1) \eta^2 - i k_1 k_2 k_3 \eta^3 \right)}_{\text{II}} \left. \right] e^{i k_{T1} \eta} \\
 &\quad + c_{k_1}(0) \int_{-\infty}^0 \frac{d\eta}{\eta^2} \left(\underbrace{1 - i k_T \eta}_{\text{I}} - \underbrace{(k_1 k_2 + k_2 k_3 + k_3 k_1) \eta^2}_{\text{II}} \right. \\
 &\quad \left. \left. + \underbrace{i k_1 k_2 k_3 \eta^3}_{\text{II}} \right) e^{i k_T \eta} \right] + \text{complex conjugate} \Big\} \\
 &\quad + \text{a similar term with } k_1 \text{ and } k_2 \text{ exchanged,}
 \end{aligned} \tag{2.51}$$

where $k_{T1} = k_T - 2 k_1$. Let us first consider the integrals which have been highlighted as (I) in the above equation. The integrals involving $c_{k_1}^*(\eta)$ are found to diverge as $\eta \rightarrow 0$ [note that $c_k(\eta)$ is given by Eq. (2.26)]. However, as we shall soon see, their complete contribution to the three-point function proves to be finite in the limit. Therefore, we initially set the upper limit of the integrals to be, say, η_e (which denotes the conformal time at the end of inflation), and eventually consider the $\eta_e \rightarrow 0$ limit. We also evaluate the integrals containing $c_{k_1}(0)$ in the same fashion. Thereafter, we combine all the integrals marked as (I), add the resultant expressions to their complex conjugates, and take the $\eta_e \rightarrow 0$ limit to finally arrive at the corresponding contribution to the scalar-scalar-tensor cross-correlation. We find that the contributions due to the terms marked as (I) can be written as

$$\begin{aligned}
 G_{\mathcal{RR}\gamma}^{1(bI)}(\mathbf{k}_1, \mathbf{k}_2, \mathbf{k}_3) &= \Pi_{m_3 n_3, ij}^{k_3} \hat{n}_{1i} \hat{n}_{2j} \left\{ \frac{i H_I^4}{8 M_{\text{Pl}}^4 \epsilon_1^*} \frac{k_1 k_2}{(k_1 k_2 k_3)^3} \right. \\
 &\quad \times \left[\int_{-\infty}^0 \frac{d\eta}{\eta^2} c_{k_1}^*(\eta) (1 - i k_{T1} \eta) e^{i k_{T1} \eta} \right. \\
 &\quad \left. \left. + c_{k_1}(0) \int_{-\infty}^0 \frac{d\eta}{\eta^2} (1 - i k_T \eta) e^{i k_T \eta} \right] + \text{complex conjugate} \right\} \\
 &= \frac{H_I^4}{4 M_{\text{Pl}}^4 \epsilon_1^*} \frac{3 b \sqrt{2 \pi}}{\sqrt{X_{\text{res}}}} \frac{k_1 k_2}{(k_1 k_2 k_3)^3} (k_2 + k_3) \sin \left(\frac{\phi_{k_1}}{f} + \beta_1 \right), \tag{2.52}
 \end{aligned}$$

where, to obtain the final result, we have made use of the expression (2.27) for $c_{k_1}(0)$.

We can now consider the integrals which have been indicated as (II) in Eq (2.51). We switch to the variable $x = -k_1 \eta$ and substitute for $c_{k_1}(\eta)$ from Eq. (2.26). Note that the expression for $c_{k_1}(\eta)$ involves the incomplete Gamma function [cf. Eq. (2.26)]. These terms contain integrals of the following form:

$$I_2(k_1, k_2, k_3, X_{\text{res}}) = \int_0^\infty dx u(x) e^{v(x)} \Gamma(1 + i X_{\text{res}}, 2 i x), \quad (2.53)$$

where $u(x)$ and $v(x)$ are some polynomial functions of x and $\Gamma(1 + i X_{\text{res}}, 2 i x)$ is the incomplete Gamma function [58]. We find that these integrals can be evaluated if we make use of the integral representations for the incomplete Gamma function and interchange the order of the integrals as follows:

$$\int_0^\infty dx u(x) e^{v(x)} \int_{2 i x}^\infty dy y^{i X_{\text{res}}} e^{-y} = \int_0^\infty dy y^{i X_{\text{res}}} e^{-y} \int_0^y \frac{dp}{2 i} u\left(\frac{p}{2 i}\right) e^{v(p/2 i)}, \quad (2.54)$$

where we have set $p = 2 i x$. The complete contribution due to the terms marked as (II) is found to be

$$\begin{aligned} G_{\mathcal{R}\mathcal{R}\gamma}^{1(1b\text{II})}(\mathbf{k}_1, \mathbf{k}_2, \mathbf{k}_3) = & -\Pi_{m_3 n_3, ij}^{k_3} \hat{n}_{1i} \hat{n}_{2j} \frac{H_1^4}{4 M_{\text{Pl}}^4 \epsilon_1^*} \frac{3 b \sqrt{2 \pi}}{\sqrt{X_{\text{res}}}} \frac{k_1 k_2}{(k_1 k_2 k_3)^3} \\ & \times \left(\frac{k_1 k_2 + k_2 k_3 + k_3 k_1}{2 k_T} \sin\left(\frac{\phi_{k_1}}{f} + \beta_1\right) + \frac{k_1 k_2 k_3}{2 k_T^2} \sin\left(\frac{\phi_{k_1}}{f} + \beta_1\right) \right. \\ & + \frac{k_1 k_2 - k_2 k_3 + k_3 k_1}{2 k_{T1}} \left\{ \frac{1}{1 + (k_{T1}/2 k_1)} \right. \\ & \times \sin\left[\frac{\phi_{k_1}}{f} + \beta_1 - X_{\text{res}} \ln\left(1 + \frac{k_{T1}}{2 k_1}\right)\right] - \sin\left(\frac{\phi_{k_1}}{f} + \beta_1\right) \Big\} \\ & + \frac{k_2 k_3}{4 k_{T1}} \left(1 + \frac{k_{T1}}{2 k_1}\right)^{-2} \left\{ \sin\left[\frac{\phi_{k_1}}{f} + \beta_1 - X_{\text{res}} \ln\left(1 + \frac{k_{T1}}{2 k_1}\right)\right] \right. \\ & + X_{\text{res}} \cos\left[\frac{\phi_{k_1}}{f} + \beta_1 - X_{\text{res}} \ln\left(1 + \frac{k_{T1}}{2 k_1}\right)\right] \Big\} \\ & + \frac{k_1 k_2 k_3}{2 k_{T1}^2} \left\{ \frac{1}{1 + (k_{T1}/2 k_1)} \sin\left[\frac{\phi_{k_1}}{f} + \beta_1 - X_{\text{res}} \ln\left(1 + \frac{k_{T1}}{2 k_1}\right)\right] \right. \\ & \left. \left. - \sin\left(\frac{\phi_{k_1}}{f} + \beta_1\right) \right\} \right) \\ & + \text{a similar term with } k_1 \text{ and } k_2 \text{ exchanged.} \end{aligned} \quad (2.55)$$

The sum of the contributions (2.50), (2.52) and (2.55) together with the contribution (1.109) gives the complete contribution to the scalar-scalar-tensor cross-correlation under the approximations we have worked with [121].

2.4.2 Comparison with the numerical results

In order to illustrate the accuracy of our analytical calculations, we shall now compare our analytical results that have been arrived at under certain approximations with the exact results obtained numerically. We have obtained the numerical results using a code developed earlier (for details about the code, see Ref. [76]). In fact, we shall compare the results for the corresponding non-Gaussianity parameter $C_{\text{NL}}^{\mathcal{R}}$ [cf. Eq. (1.106b)]. In Fig. 2.1, we have plotted the analytical and the exact numerical results for two sets of values of the parameters involved. We have chosen values for the parameters such that the approximations we have worked with are valid.

In these plots, the x -axis corresponds to the ratio of the amplitudes of \mathbf{k}_3 and \mathbf{k}_1 , while the y -axis corresponds to the ratio of the amplitudes of \mathbf{k}_2 and \mathbf{k}_1 . For the case of three-point functions involving perturbations of similar nature, such as the scalar and tensor bispectra, due to the symmetrical nature of these three-point functions, it is sufficient to construct these density plots over the domain $0.0 < k_3/k_1 < 1.0$ and $0.5 < k_2/k_1 < 1.0$. However, for the cases of three-point functions involving one mode of a nature dissimilar from the other two, such as in the case of the three-point function with two scalar modes and one tensor mode that we are studying here, we find that the above ranges of ratios of the wavenumbers do not adequately represent all the various combinations of wavenumbers that can arise in such a context. Therefore, in Fig. 2.1, we have plotted the $C_{\text{NL}}^{\mathcal{R}}$ parameter over the ranges $0.0 < k_3/k_1 < 2.0$ and $0.0 < k_2/k_1 < 1.0$. These values of the ratios of wavenumbers can satisfactorily represent the entire range of triangular configuration of wavevectors of our interest. It is evident from the figures that the analytical results match the numerical ones quite well.

2.5 The squeezed limit and the consistency relation

In this section, we shall discuss the behavior of the scalar-scalar-tensor three-point function in the so-called squeezed limit. In the case of the scalar-scalar-tensor three-point function, when the wavenumber of the tensor mode is considered to be much smaller than the two scalar modes, it is found that the three-point function can be completely expressed in terms of the scalar and tensor power spectra through the relation (1.117b). This condition can essentially be expressed as

$$k^3 k_3^3 G_{\mathcal{R}\mathcal{R}\gamma}^{m_3 n_3}(\mathbf{k}, -\mathbf{k}, \mathbf{k}_3) = -\Pi_{m_3 n_3, ij}^{k_3} \hat{n}_i \hat{n}_j \frac{(2\pi)^4}{4} \left(\frac{n_s - 4}{8} \right) \mathcal{P}_s(k) \mathcal{P}_T(k_3), \quad (2.56)$$

with the limit $k_3 \rightarrow 0$ kept in mind. In what follows, using the analytical results we have obtained for the power spectra and the scalar-scalar-tensor cross-correlation, we shall explicitly show that such a consistency relation is indeed satisfied in the axion monodromy model.

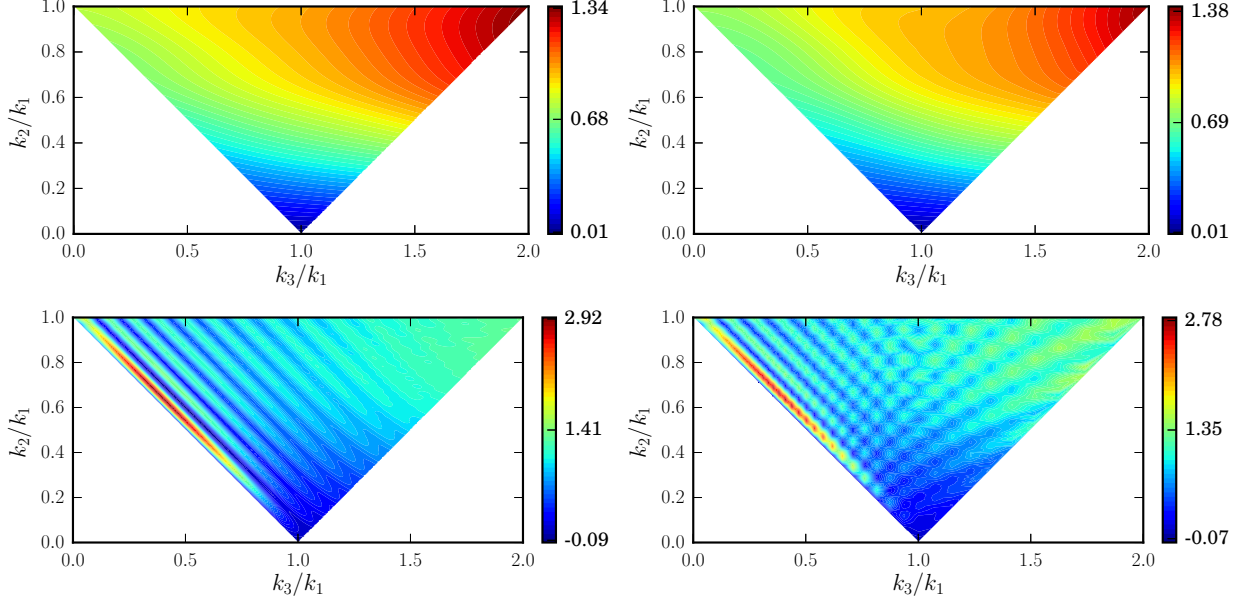


Figure 2.1: A comparison of the analytical results (on the left) with the numerical results (on the right) for the non-Gaussianity parameter $C_{\text{NL}}^{\mathcal{R}}(\mathbf{k}_1, \mathbf{k}_2, \mathbf{k}_3)$ characterizing the scalar-scalar-tensor three-point function. We have plotted the results for two sets of values of the parameters involved. We have chosen $(\mu/M_{\text{Pl}})^3 = 2.512 \times 10^{-10}$ in arriving at all these figures. The results in the top row correspond to $b = 1.063 \times 10^{-2}$ and $f/M_{\text{Pl}} = 7.6346 \times 10^{-3}$, which are values that lead to the best fit to the Planck 2015 data [111]. The results in the bottom row correspond to $b = 5.0 \times 10^{-2}$ and $f/M_{\text{Pl}} = 7.6346 \times 10^{-4}$. We find that the analytical results match the numerical results very well for both these sets of values. In fact, we find that the match is about 5% over the range of wavenumbers that we have considered. Note that, as expected, the non-Gaussianity parameter $C_{\text{NL}}^{\mathcal{R}}(\mathbf{k}_1, \mathbf{k}_2, \mathbf{k}_3)$ exhibits more oscillations for smaller values of f , as is illustrated by the figures in the bottom row. Also, the strength of these oscillations is more for larger values of b .

Let us now consider the squeezed limit of the three-point function we have arrived at analytically. In the limit $\mathbf{k}_1 = -\mathbf{k}_2 = \mathbf{k}$ and $k_3 \rightarrow 0$, at the leading order in X_{res} , we find that the three-point function at the order b [*i.e.* the sum of the contributions (2.50), (2.52) and (2.55)] reduces to

$$\begin{aligned}
 k^3 k_3^3 G_{\mathcal{R}\mathcal{R}\gamma}^{1(1)}(\mathbf{k}, -\mathbf{k}, \mathbf{k}_3) &= \Pi_{m_3 n_3, ij}^{\mathbf{k}_3} \hat{n}_i \hat{n}_j \frac{H_1^4}{8 i M_{\text{Pl}}^4 \epsilon_1^*} \frac{3 b \sqrt{2 \pi}}{\sqrt{X_{\text{res}}}} \frac{k}{k_{\text{T1}}} \\
 &\times \left(e^{i \phi_k / f} \left\{ \frac{[1 + (k_{\text{T1}}/2 k)]^{-i X_{\text{res}}}}{1 + (k_{\text{T1}}/2 k)} - 1 \right\} \right. \\
 &\left. - e^{-i \phi_k / f} \left\{ \frac{[1 + (k_{\text{T1}}/2 k)]^{i X_{\text{res}}}}{1 + (k_{\text{T1}}/2 k)} - 1 \right\} \right), \quad (2.57)
 \end{aligned}$$

where, recall that, $k_{\text{T1}} = k_{\text{T}} - 2 k_1$. Hence, in the squeezed limit, $k_{\text{T1}} \rightarrow 0$. Therefore, we can expand the terms $(1 + k_{\text{T1}}/2 k)^{\pm i X_{\text{res}}}$ in the above equation up to the first order in k_{T1} to obtain the following expression for the three-point function:

$$k^3 k_3^3 G_{\mathcal{R}\mathcal{R}\gamma}^{1(1)}(\mathbf{k}, -\mathbf{k}, \mathbf{k}_3) = -\Pi_{m_3 n_3, ij}^{k_3} \hat{n}_i \hat{n}_j \frac{3 b H_1^4 \sqrt{2\pi}}{8 M_{\text{Pl}}^4 \epsilon_1^*} X_{\text{res}}^{1/2} \cos\left(\frac{\phi_k}{f}\right). \quad (2.58)$$

We should mention that, in arriving at this expression, we have ignored a k -independent phase.

Let us now turn to the right hand side of the relation (2.56). Up to the linear order in b , we can have four combinations of the various terms, given by

$$\begin{aligned} \left(\frac{n_s - 4}{8}\right) \mathcal{P}_s(k) \mathcal{P}_T(k_3) &\simeq \left(\frac{n_s^0 - 4}{8}\right) \mathcal{P}_s^0(k) \mathcal{P}_T^0(k_3) + \left(\frac{n_s^0 - 4}{8}\right) \mathcal{P}_s^c(k) \mathcal{P}_T^0(k_3) \\ &+ \left(\frac{n_s^0 - 4}{8}\right) \mathcal{P}_s^0(k) \mathcal{P}_T^c(k_3) + \left(\frac{n_s^c}{8}\right) \mathcal{P}_s^0(k) \mathcal{P}_T^0(k_3), \end{aligned} \quad (2.59)$$

where $\mathcal{P}_s^0(k)$ and $\mathcal{P}_T^0(k)$ and n_s^0 are the scalar and the tensor power spectra and the scalar spectral index, respectively, which arise in the absence of oscillations in the axion monodromy model. Note that $\mathcal{P}_T^c(k)$ involves terms of order d_k and, as we have discussed before, these terms are of lower order when compared to the other terms involving c_k . Hence, for consistency, we can ignore the contribution due to $\mathcal{P}_T^c(k)$ in the above equation. Therefore, we finally obtain that

$$\begin{aligned} \left(\frac{n_s - 4}{8}\right) \mathcal{P}_s(k) \mathcal{P}_T(k_3) &\simeq \left(\frac{n_s^0 - 4}{8}\right) \mathcal{P}_s^0(k) \mathcal{P}_T^0(k_3) + \left(\frac{n_s^0 - 4}{8}\right) \mathcal{P}_s^c(k) \mathcal{P}_T^0(k_3) \\ &+ \left(\frac{n_s^c}{8}\right) \mathcal{P}_s^0(k) \mathcal{P}_T^0(k_3). \end{aligned} \quad (2.60)$$

The first term in the above expression is the slow roll term for which the consistency relation involving the $b = 0$ contribution to the scalar-scalar-tensor cross correlation [cf. Eq. (1.109)] can be verified easily [70, 79]. On evaluating the remaining two terms, we find that the one involving n_s^c is of leading order, as the other term is suppressed relative to this by a factor of X_{res} . Hence, at the leading order in b , we can replace $[(n_s - 4)/8] \mathcal{P}_s(k) \mathcal{P}_T(k_3)$ by $(n_s^c/8) \mathcal{P}_s^0(k) \mathcal{P}_T^0(k_3)$ in Eq. (2.56). Upon making this replacement, the consistency relation at the linear order in b can be written as

$$k^3 k_3^3 G_{\mathcal{R}\mathcal{R}\gamma}^{1(1)}(\mathbf{k}, -\mathbf{k}, \mathbf{k}_3) = -\Pi_{m_3 n_3, ij}^{k_3} \hat{n}_{1i} \hat{n}_{1j} \frac{(2\pi)^4}{4} \left(\frac{n_s^c}{8}\right) \mathcal{P}_s^0 \mathcal{P}_T^0. \quad (2.61)$$

Now, on substituting the expression for n_s^c [cf. Eqs. (2.31)] and the slow roll amplitudes for the scalar and tensor power spectra [cf. Eqs. (2.29) and (2.39)] in the above expression,

we find that the resultant expression is the same as that obtained in Eq. (2.58), up to a k -independent phase. This implies that the consistency relation is valid in the axion monodromy model even in the presence of persistent oscillations in the two as well as the three-point functions [79].

2.6 Discussion

The axion monodromy model is described by a linear potential with small periodic modulations. The modulations in the potential lead to oscillations in the slow roll parameters. These oscillations associated with the background resonate with the oscillations of the scalar and tensor perturbations at sub-Hubble scales for suitable values of the parameters of the model. This resonance leads to persistent oscillations in the two and three-point functions. The scalar and tensor power spectra as well as the scalar bispectrum have been analytically evaluated earlier in the axion monodromy model under certain approximations.

In terms of their hierarchy, after the scalar bispectrum, the scalar-scalar-tensor cross-correlation proves to be the most important of the three-point functions. In this chapter, we have analytically calculated the scalar-scalar-tensor three-point function in the axion monodromy model in the same approximation under which the scalar and tensor power spectra and the scalar bispectrum have been evaluated earlier. We find that the analytical results we have obtained match the corresponding numerical results very well for a range of the parameters involved. Subsequently, using the analytical results, we have also been able to explicitly verify the consistency relation governing the three-point function.

The template that we have obtained here can be used to compare the inflationary models with the CMB data at the level of three-point functions involving the tensor perturbations (in this context, see the recent work, Ref. [122]). Clearly, it will be interesting to extend our analysis to the scalar-tensor-tensor three-point function as well as the tensor bispectrum. We find that the tensor bispectrum can be easily evaluated using the methods adopted here. However, comparison with the corresponding numerical results suggest that these methods do not prove to be adequate to evaluate the scalar-tensor-tensor three-point function to the same level of accuracy. Also, for instance, the consistency relation for the scalar-tensor-tensor three-point function does not seem to hold under the approximations adopted here. These approximations need to be extended in order to evaluate the scalar-tensor-tensor cross-correlation analytically to a good level of accuracy. We are currently investigating this issue.

Chapter 3

The tensor bispectrum in a matter bounce

3.1 Introduction

As we have already discussed in the introductory chapter, bouncing models correspond to situations wherein the universe initially goes through a period of contraction until the scale factor reaches a certain minimum value before transiting to the expanding phase. They offer an alternative to inflation to overcome the horizon problem, as they permit well motivated, Minkowski-like initial conditions to be imposed on the perturbations at early times during the contracting phase (see, for instance, Refs. [30, 32, 33, 37, 38, 42, 46–50]; for reviews, see Refs. [51, 52]). Interestingly, certain bouncing scenarios can lead to nearly scale invariant perturbation spectra (see, for example, Refs. [37, 49, 50]), as is required by observations [6–9]. For instance, a bouncing model wherein the universe goes through a contracting phase as driven by matter – referred to as a matter bounce – is known to lead to an exactly scale invariant spectrum of tensor perturbations as in de Sitter inflation [47–49]. Clearly, it will be worthwhile to examine if non-Gaussianities can help us discriminate between such scenarios [45, 123, 124].

The most dominant of the non-Gaussian signatures are the non-vanishing three-point functions involving the scalars as well as the tensors [66–69, 71, 76]. In order to drive a bounce, it is well known that one requires matter fields that violate the null energy condition. Therefore, analyzing the evolution of the scalar perturbations requires suitable modeling of the matter fields [51, 52]. In contrast, the tensor perturbations depend only on the scale factor and hence are simpler to study. For this reason, we shall focus on the tensor bispectrum in this chapter. Further, we shall assume a specific functional form for the scale factor and we shall not attempt to construct sources that can give rise to such a behavior.

An interesting aspect of the three-point functions is their property in the so-called squeezed limit wherein the wavelength of one of the three modes involved is much larger

than the other two [66,81–84]. In this limit, under fairly general conditions, it is known that the three-point functions can be expressed completely in terms of the two-point functions via a relation that is referred to as the consistency condition, as we have discussed earlier. We should mention that, while the scalar consistency relation has drawn most of the attention, it has been established that all the four three-point functions involving scalars and tensors satisfy similar relations under certain conditions [68–70,79]. It is interesting to examine if the three-point functions generated in the bouncing scenarios satisfy the consistency condition. In the context of inflation, it is well known that the consistency relations arise due to the fact that the amplitude of the long wavelength mode freezes on super-Hubble scales. In contrast, in a bouncing universe, it can be readily shown that the amplitude of the long wavelength mode grows sharply as one approaches the bounce during the contracting phase. This behavior suggests that the consistency relation may not hold in bouncing models [123]. The primordial consistency conditions lead to corresponding imprints on the anisotropies in the cosmic microwave background (see, for instance, Refs. [125]; in particular, see Ref. [126] for the signatures of the tensor modes) and the large scale structure (see, for example, Refs. [127]). It is clear that the consistency condition, if confirmed by observations, can help us discriminate between models of the early universe.

The most comprehensive formalism to study the generation of non-Gaussianities in the early universe is the approach due to Maldacena [66], as we discussed in Sec. 1.5. In this chapter, we analytically evaluate the tensor bispectrum in a matter bounce using the Maldacena formalism. To arrive at the tensor bispectrum analytically, apart from the behavior of the tensor modes, one also needs to be able to evaluate a certain integral involving the scale factor and the tensor modes. We conveniently divide the evolution into two domains and use the analytical solutions available in these domains to carry out the integrals and obtain the tensor bispectrum.

This chapter is organized as follows. In the following section, considering a specific form for the scale factor, we shall divide the time period of our interest into two domains, the first corresponding to early times during the contracting phase and the other close to and across the bounce. We shall describe the analytical solutions for the tensor modes during these two domains, both before and after the bounce, to arrive at the corresponding tensor power spectrum over wavenumbers much smaller than the wavenumber associated with the bounce. We shall also compare the analytical solutions for the tensor modes with the corresponding results obtained numerically. In Sec. 3.3, we shall evaluate the tensor bispectrum using the analytical solutions to the modes and the behavior of the scale factor in the two domains. We shall calculate the bispectrum for an arbitrary triangular configuration of the wavevectors. In Sec. 3.4, we shall illustrate the results in the equilateral and the squeezed limits. We shall also plot the non-Gaussianity parameter h_{NL} that characterizes the tensor bispectrum for an arbitrary triangular configuration of the wavevectors. We shall show that h_{NL} is very small for cosmological scales and that

the consistency relation is violated in the squeezed limit. We shall conclude with a brief discussion in Sec. 3.5.

3.2 The tensor modes and the power spectrum

As discussed previously in Chap. 1, we shall assume that the scale factor describing the bouncing scenario is given in terms of the conformal time coordinate η by the relation

$$a(\eta) = a_0 \left(1 + \eta^2/\eta_0^2\right) = a_0 \left(1 + k_0^2 \eta^2\right), \quad (3.1)$$

where a_0 is the minimum value of the scale factor at the bounce (*i.e.* when $\eta = 0$) and $\eta_0 = k_0^{-1}$ denotes the time scale that determines the duration of the bounce. Note that, at very early times, *viz.* when $\eta \ll -\eta_0$, the scale factor behaves as in a matter dominated universe (*i.e.* as $a \propto \eta^2$) and, for this reason, such a bouncing model is often referred to as a matter bounce. It should be mentioned that the wavenumbers of cosmological interest are expected to be 25–30 orders of magnitude smaller than the wavenumber k_0 .

The tensor modes h_k satisfy the differential equation (1.61). If we write $h_k = u_k/a$, then the modes u_k satisfy the equation (1.62). The quantity a''/a corresponding to the scale factor (3.1) is given by

$$\frac{a''}{a} = \frac{2 k_0^2}{1 + k_0^2 \eta^2}, \quad (3.2)$$

which has essentially a Lorentzian profile. Note that the quantity a''/a exhibits a maximum at the bounce, with the maximum value being of the order of k_0^2 . Also, it goes to zero as $\eta \rightarrow \pm\infty$. For modes of cosmological interest, one finds that $k^2 \gg a''/a$ at suitably early times (*i.e.* as $\eta \rightarrow -\infty$). In this domain, the quantity u_k oscillates and we can impose the standard initial conditions on these modes and study their evolution thereafter.

Let us divide the time period of our interest into two domains, a domain corresponding to early times and another closer to and across the bounce. Let the first domain be determined by the condition $-\infty < \eta < -\alpha \eta_0$, where α is a relatively large number, which we shall set to be, say, 10^5 . The second domain corresponds to $-\alpha \eta_0 < \eta < \beta \eta_0$, where $\beta = 10^2$ (the reason for this choice will be explained later). In the first domain, we can assume that the scale factor behaves as

$$a(\eta) \simeq a_0 k_0^2 \eta^2, \quad (3.3)$$

so that $a''/a = 2/\eta^2$. Since the condition $k^2 = a''/a$ corresponds to, say, $\eta_k = -\sqrt{2}/k$, the initial conditions can be imposed when $\eta \ll \eta_k$. The modes h_k can be easily obtained in such a case and the positive frequency modes that correspond to the vacuum state at early times are given by [47–49]

$$h_k(\eta) = \frac{\sqrt{2}}{M_{\text{Pl}}} \frac{1}{\sqrt{2k}} \frac{1}{a_0 k_0^2 \eta^2} \left(1 - \frac{i}{k\eta}\right) e^{-ik\eta}. \quad (3.4)$$

Let us now consider the behavior of the modes in the second domain, *i.e.* when $-\alpha \eta_0 < \eta < \beta \eta_0$. Since we are interested in scales much smaller than k_0 , we shall assume that $\eta_k \ll -\alpha \eta_0$, which corresponds to the condition $k \ll k_0/\alpha$. Therefore, in this domain, for scales of cosmological interest, the equation governing the tensor mode h_k reduces to

$$h_k'' + \frac{2a'}{a} h_k' \simeq 0. \quad (3.5)$$

This equation can be immediately integrated to yield

$$h_k'(\eta) \simeq h_k'(\eta_*) \frac{a^2(\eta_*)}{a^2(\eta)}, \quad (3.6)$$

where η_* is a suitably chosen time and the scale factor $a(\eta)$ is given by the complete expression (3.1). On further integration, we obtain that

$$h_k(\eta) = h_k(\eta_*) + h_k'(\eta_*) a^2(\eta_*) \int_{\eta_*}^{\eta} \frac{d\tilde{\eta}}{a^2(\tilde{\eta})}, \quad (3.7)$$

where we have chosen the constant of integration to be $h_k(\eta_*)$. If we choose $\eta_* = -\alpha \eta_0$, we can make use of the solution (3.4) to determine $h_k(\eta_*)$ and $h_k'(\eta_*)$. Note that, in the domain of interest, the first term in the above expression is, evidently, a constant, while the second term grows rapidly as one approaches the bounce. Upon using the form (3.1) of the scale factor, we find that we can express the behavior of the mode h_k in the second domain as

$$h_k = \mathcal{T}_{1k} + \mathcal{T}_{2k} g_1(k_0 \eta), \quad (3.8)$$

where the function $g_1(x)$ is defined as

$$g_1(x) = \frac{x}{1+x^2} + \tan^{-1} x, \quad (3.9)$$

while the quantities \mathcal{T}_{1k} and \mathcal{T}_{2k} are given by

$$\mathcal{T}_{1k} = \frac{\sqrt{2}}{M_{\text{Pl}}} \frac{1}{\sqrt{2}k} \frac{1}{a_0 \alpha^2} \left(1 + \frac{i k_0}{\alpha k} \right) e^{i \alpha k/k_0} + \mathcal{T}_{2k} g(\alpha), \quad (3.10)$$

$$\mathcal{T}_{2k} = \frac{\sqrt{2}}{M_{\text{Pl}}} \frac{1}{\sqrt{2}k} \frac{1}{2 a_0 \alpha^2} (1 + \alpha^2)^2 \left(\frac{3 i k_0}{\alpha^2 k} + \frac{3}{\alpha} - \frac{i k}{k_0} \right) e^{i \alpha k/k_0}. \quad (3.11)$$

We should highlight the fact that, whereas the bounce (3.1) is a symmetric one, the solution (3.8) is asymmetric in η . Moreover, one may have naively expected the amplitude of the long wavelength modes to freeze once the universe starts expanding. This is largely true, though not completely so, and the behavior can possibly be attributed to the specific form of the scale factor (3.1). Note that, after the bounce, while the first term in $g_1(k_0 \eta)$ decays, the second term actually grows, albeit extremely mildly. We shall assume that,

after the bounce, the universe transits to the conventional radiation domination epoch at, say, $\eta = \beta \eta_0$, where we shall set $\beta \simeq 10^2$. We should mention that this choice is somewhat arbitrary and we shall discuss the dependence of the tensor power spectrum and the bispectrum on β in due course.

In order to understand the extent of accuracy of the approximations involved, it would be worthwhile to compare the above analytical results for the mode h_k with the corresponding numerical results. Clearly, given the scale factor (3.1), it is a matter of integrating the differential equation (1.61), along with the standard Bunch-Davies initial conditions, to arrive at the behavior of h_k . The conformal time coordinate does not prove to be an efficient time variable for numerical integration, particularly when a large range in the scale factor needs to be covered. In the context of inflation, it is often the e-fold N , defined as $a(N) = a_0 \exp N$, where $N = 0$ is a suitable time at which the scale factor takes the value a_0 , that is utilized to integrate the equations of motion (see, for instance, Refs. [78,108,128]). Due to the exponential factor involved, a small range in e-folds covers a large range in time and scale factor. However, since e^N is a monotonically increasing function, while it is useful to describe expanding universes, e-folds are not helpful in characterizing bouncing scenarios. In order to characterize a bounce, it would be convenient to choose a variable that is negative during the contracting phase of the universe, zero at the bounce and positive during the expanding phase. We shall choose to perform the integration using a new variable \mathcal{N} , which we call the e-N-fold, in terms of which the scale factor is defined as $a(\mathcal{N}) = a_0 \exp(\mathcal{N}^2/2)$ [55]. We shall assume that \mathcal{N} is zero at the bounce, with negative values representing the phase prior to the bounce and positive values after.

In terms of the e-N-folds, the differential equation (1.61) governing the evolution of the tensor modes can be expressed as

$$\frac{d^2 h_k}{d\mathcal{N}^2} + \left(3\mathcal{N} + \frac{1}{H} \frac{dH}{d\mathcal{N}} - \frac{1}{\mathcal{N}} \right) \frac{dh_k}{d\mathcal{N}} + \left(\frac{k\mathcal{N}}{aH} \right)^2 h_k = 0, \quad (3.12)$$

where $H = a'/a^2$ is the Hubble parameter. Given the scale factor (3.1), the corresponding Hubble parameter can be easily evaluated in terms of the conformal time η . In order to express the Hubble parameter H in terms of the e-N-fold, we shall require η as a function of \mathcal{N} . Upon using the definition of the e-N-folds and the expression (3.1) for the scale factor, we obtain that

$$\eta(\mathcal{N}) = \pm k_0^{-1} \left(e^{\mathcal{N}^2/2} - 1 \right)^{1/2}. \quad (3.13)$$

Since the Hubble parameter is negative during the contracting phase and positive during the expanding regime, we have to choose the root of $\eta(\mathcal{N})$ accordingly during each phase. From the expression for the Hubble parameter, we evaluate the coefficients of the differential equation (3.12) in terms of \mathcal{N} . With the coefficients at hand, we numerically integrate the differential equation using a fifth order Runge-Kutta algorithm. We should

mention that we have also independently checked the numerical results using *Mathematica* [129]. Recall that, the initial conditions are imposed in a domain during the contracting phase wherein $k^2 \gg a''/a$. As is done in the context of inflation, we shall impose the initial conditions when $k = 10^2 \sqrt{(a''/a)}$ corresponding to, say, the e-N-fold \mathcal{N}_i . It should be pointed out that the initial conditions on the different modes are imposed at different times. In terms of the e-N-folds, the standard Bunch-Davies initial conditions can be expressed as

$$h_k \Big|_{\mathcal{N}_i} = \frac{1}{a(\mathcal{N}_i) \sqrt{2k}}, \quad (3.14a)$$

$$\frac{dh_k}{d\mathcal{N}} \Big|_{\mathcal{N}_i} = -\frac{i \mathcal{N}_i}{a^2(\mathcal{N}_i) H(\mathcal{N}_i)} \sqrt{\frac{k}{2}} - \frac{\mathcal{N}_i}{a(\mathcal{N}_i) \sqrt{2k}}. \quad (3.14b)$$

We impose these initial conditions well before the bounce and evolve the modes until a suitable time after the bounce. The tensor mode h_k evaluated in such a manner has been plotted for a given wavenumber (such that $k/k_0 \ll 1$) in Fig. 3.1. The figure also contains a plot of the analytical results (3.4) and (3.8) for the same wavenumber. As is evident from the figure, prior to the bounce and immediately after, the analytical results match the exact numerical results exceedingly well.

The tensor power spectrum after the bounce can be calculated using the solutions we have obtained. Recall that the tensor power spectrum is defined as in Eq. (1.65), with the spectrum to be evaluated at a suitable time. If we evaluate the tensor power spectrum at $\eta = \beta \eta_0$, we find that it can be expressed as

$$\mathcal{P}_T(k) = 4 \frac{k^3}{2\pi^2} |\mathcal{T}_{1k} + \mathcal{T}_{2k} g_1(\beta)|^2. \quad (3.15)$$

Note that, α is a quantity that we have artificially introduced and the actual problem does not contain α . For $k \ll k_0/\alpha$ and a sufficiently large α (as we had said, for $\alpha = 10^5$ or so), the above power spectrum reduces to a scale invariant form with a weak dependence on β , if β is reasonably larger than unity. If we further assume that β is large enough (say, 10^2), then the scale invariant amplitude is found to be: $\mathcal{P}_T(k) \simeq 9 k_0^2 / (2 M_{\text{Pl}}^2 a_0^2)$, as expected [47–49]. In Fig. 3.2, we have plotted the complete tensor power spectrum described by the expression (3.15) for a given set of parameters. We should stress that the power spectrum is actually valid only for modes which satisfy the condition $k \ll k_0/\alpha$. It is evident from the figure that the power spectrum is strictly scale invariant over this domain. Moreover, we find that the spectrum indeed reduces to the above-mentioned scale invariant amplitude for small values of the wavenumbers. We have also evaluated the tensor power spectrum numerically using the method described above. We have computed the spectrum at a given time soon after the bounce (corresponding to $\beta = 10^2$) for all the modes. We find that, for wavenumbers such that $k \ll k_0$, the numerical analysis also leads to a scale invariant spectrum whose amplitude matches the above analytical result to about 1%.

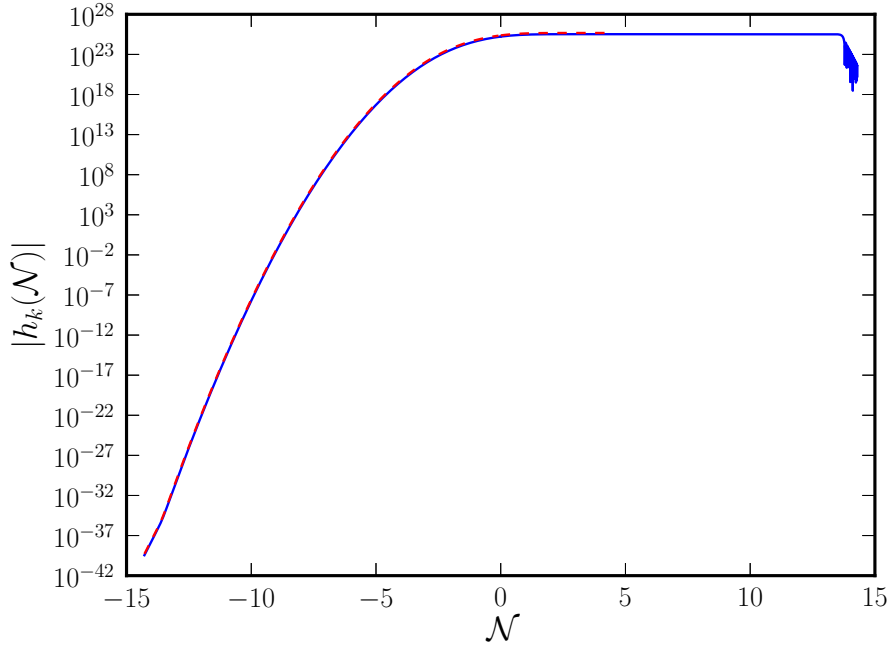


Figure 3.1: A comparison of the numerical results (in blue) with the analytical results (in red) for the amplitude of the tensor mode $|h_k|$ corresponding to the wavenumber $k/k_0 = 10^{-20}$. We have set $k_0/(a_0 M_{\text{Pl}}) = 10^{-5}$ and, for plotting the analytical results, we have chosen $\alpha = 10^5$. We have plotted the results from the initial e-N-fold \mathcal{N}_i [when $k = 10^2 \sqrt{(a''/a)}$] corresponding to the mode. While we have illustrated the exact numerical result till rather late times, we have plotted the analytical results until a time after the bounce when the power spectrum is evaluated. Evidently, the analytical and numerical results match extremely well, suggesting that the analytical approximation for the modes works to a very good accuracy.

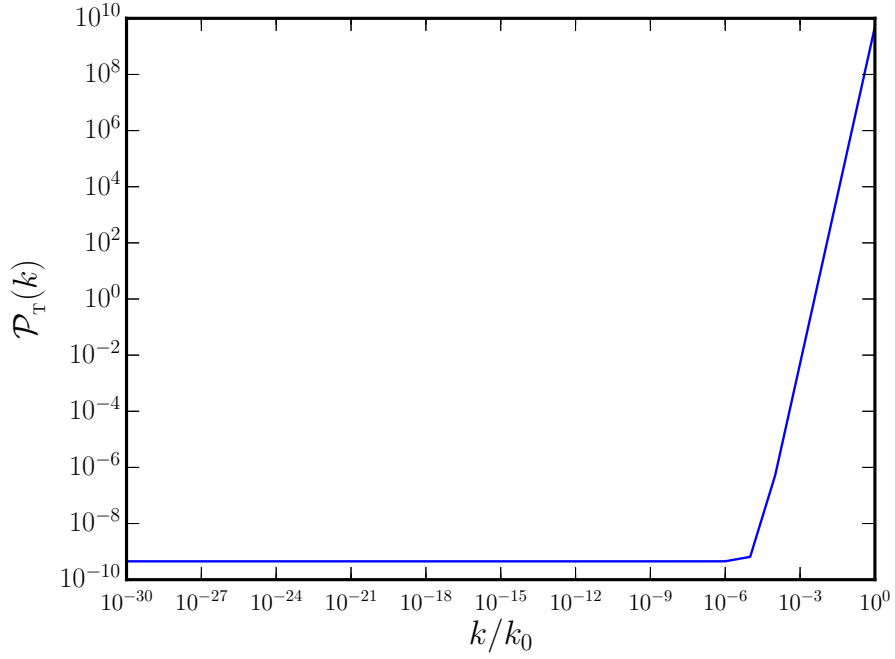


Figure 3.2: The behavior of the tensor power spectrum has been plotted as a function of k/k_0 for a wide range of wavenumbers. In plotting this figure, we have set $k_0/(a_0 M_{\text{Pl}}) = 10^{-5}$, $\alpha = 10^5$ and $\beta = 10^2$. We should emphasize that the approximations we have worked with are valid only over the domain wherein $k \ll k_0/\alpha$. Clearly, the power spectrum is scale invariant in this domain. We also find that, at small wavenumbers, the tensor power spectrum has the expected scale invariant amplitude of $\mathcal{P}_T(k) = 4.5 \times 10^{-10}$ corresponding to $k_0/(a_0 M_{\text{Pl}}) = 10^{-5}$.

3.3 Evaluating the tensor bispectrum

Our aim in this chapter is to evaluate the magnitude and shape of the tensor bispectrum and the corresponding non-Gaussianity parameter and compare with, say, the results in de Sitter inflation. Therefore, for simplicity, we shall set the polarization tensor to unity. In such a case, the expression (1.103) for the tensor bispectrum simplifies to

$$G_{\gamma\gamma\gamma}(\mathbf{k}_1, \mathbf{k}_2, \mathbf{k}_3) = M_{\text{Pl}}^2 [h_{k_1}(\eta_e) h_{k_2}(\eta_e) h_{k_3}(\eta_e) \bar{\mathcal{G}}_{\gamma\gamma\gamma}(\mathbf{k}_1, \mathbf{k}_2, \mathbf{k}_3) + \text{complex conjugate}], \quad (3.16)$$

where the quantity $\bar{\mathcal{G}}_{\gamma\gamma\gamma}(\mathbf{k}_1, \mathbf{k}_2, \mathbf{k}_3)$ is described by the integral

$$\bar{\mathcal{G}}_{\gamma\gamma\gamma}(\mathbf{k}_1, \mathbf{k}_2, \mathbf{k}_3) = -\frac{i}{4} (k_1^2 + k_2^2 + k_3^2) \int_{\eta_i}^{\eta_e} d\eta a^2 h_{k_1}^* h_{k_2}^* h_{k_3}^*. \quad (3.17)$$

We shall choose η_i to be an early time during the contracting phase when the initial conditions are imposed on the modes (*i.e.* when $k^2 \gg a''/a$), and η_e to be a suitably late time, say, some time after the bounce, when the bispectrum is evaluated. If we ignore the factors involving the polarization tensor, the expression for the non-Gaussianity parameter h_{NL} [cf. Eq. (1.106d)] reduces to

$$h_{\text{NL}}(\mathbf{k}_1, \mathbf{k}_2, \mathbf{k}_3) = -\left(\frac{4}{2\pi^2}\right)^2 [k_1^3 k_2^3 k_3^3 G_{\gamma\gamma\gamma}(\mathbf{k}_1, \mathbf{k}_2, \mathbf{k}_3)] \times \left[2 k_3^3 \mathcal{P}_{\text{T}}(k_1) \mathcal{P}_{\text{T}}(k_2) + \text{two permutations}\right]^{-1}. \quad (3.18)$$

With the forms of the scale factor and the mode functions [cf. Eqs. (3.4) and (3.8)] at hand, in order to arrive at the tensor bispectrum, it is now a matter of evaluating the integral (3.17) in the two domains.

Let us begin by considering the first domain. Upon using the behavior (3.3) of the scale factor and the mode (3.4) in the first domain, we find that the quantity $\bar{\mathcal{G}}_{\gamma\gamma\gamma}(\mathbf{k}_1, \mathbf{k}_2, \mathbf{k}_3)$ can be expressed as

$$\begin{aligned} \bar{\mathcal{G}}_{\gamma\gamma\gamma}^1(\mathbf{k}_1, \mathbf{k}_2, \mathbf{k}_3) &= \frac{-i (k_1^2 + k_2^2 + k_3^2)}{4 M_{\text{Pl}}^3 a_0 k_0^2 \sqrt{k_1 k_2 k_3}} \left[Q_2(k_{\text{T}}, k_0, \alpha) + i \left(\frac{1}{k_1} + \frac{1}{k_2} + \frac{1}{k_3} \right) Q_3(k_{\text{T}}, k_0, \alpha) \right. \\ &\quad \left. - \left(\frac{1}{k_1 k_2} + \frac{1}{k_2 k_3} + \frac{1}{k_1 k_3} \right) Q_4(k_{\text{T}}, k_0, \alpha) - \frac{i}{k_1 k_2 k_3} Q_5(k_{\text{T}}, k_0, \alpha) \right], \end{aligned} \quad (3.19)$$

where the quantities $Q_m(k_{\text{T}}, k_0, \alpha)$ are described by the integrals

$$Q_m(k_{\text{T}}, k_0, \alpha) = \int_{-\infty}^{-\alpha/k_0} \frac{d\eta}{\eta^m} e^{i k_{\text{T}} \eta}. \quad (3.20)$$

For $m > 1$, these integrals can be evaluated to yield

$$Q_{m+1}(k_T, k_0, \alpha) = -\frac{1}{m} \left(-\frac{k_0}{\alpha} \right)^m e^{-i\alpha k_T/k_0} + \frac{i k_T}{m} Q_m(k_T, k_0, \alpha), \quad (3.21)$$

while $Q_1(k_T, k_0, \alpha)$ is given by

$$Q_1(k_T, k_0, \alpha) = i\pi + \text{Ei}(-i\alpha k_T/k_0), \quad (3.22)$$

where $\text{Ei}(z)$ is the exponential integral function [58].

Let us now turn to evaluating $\bar{\mathcal{G}}_{\gamma\gamma\gamma}(\mathbf{k}_1, \mathbf{k}_2, \mathbf{k}_3)$ in the second domain. Upon using the behavior (3.1) of the scale factor and the mode (3.8), we find that the quantity can be expressed as

$$\begin{aligned} \bar{\mathcal{G}}_{\gamma\gamma\gamma}^2(\mathbf{k}_1, \mathbf{k}_2, \mathbf{k}_3) = & -\frac{i a_0^2 (k_1^2 + k_2^2 + k_3^2)}{4 k_0} \left[B_{1k_1}^* B_{1k_2}^* B_{1k_3}^* J_0(\alpha, \beta) \right. \\ & + (B_{1k_1}^* B_{1k_2}^* B_{2k_3}^* + B_{1k_1}^* B_{2k_2}^* B_{1k_3}^* + B_{2k_1}^* B_{1k_2}^* B_{1k_3}^*) J_1(\alpha, \beta) \\ & + (B_{1k_1}^* B_{2k_2}^* B_{2k_3}^* + B_{2k_1}^* B_{1k_2}^* B_{2k_3}^* + B_{2k_1}^* B_{2k_2}^* B_{1k_3}^*) J_2(\alpha, \beta) \\ & \left. + B_{2k_1}^* B_{2k_2}^* B_{2k_3}^* J_3(\alpha, \beta) \right], \end{aligned} \quad (3.23)$$

where $J_n(\alpha, \beta)$ are described by the integrals

$$J_n(\alpha, \beta) = \int_{-\alpha}^{\beta} dx (1+x^2)^2 g_1^n(x), \quad (3.24)$$

with the function $g_1(x)$ being given by Eq. (3.9). The integrals $J_0(\alpha, \beta)$ and $J_1(\alpha, \beta)$ can be readily evaluated to obtain that

$$J_0(\alpha, \beta) = \alpha + \frac{2\alpha^3}{3} + \frac{\alpha^5}{5} + \beta + \frac{2\beta^3}{3} + \frac{\beta^5}{5} \quad (3.25)$$

and

$$\begin{aligned} J_1(\alpha, \beta) = & -\frac{1}{5} \alpha^5 \tan^{-1} \alpha - \frac{\alpha^4}{5} - \frac{2}{3} \alpha^3 \tan^{-1} \alpha - \frac{4\alpha^2}{15} + \frac{4}{15} \ln(\alpha^2 + 1) - \alpha \tan^{-1} \alpha \\ & + \frac{1}{5} \beta^5 \tan^{-1} \beta + \frac{\beta^4}{5} + \frac{2}{3} \beta^3 \tan^{-1} \beta + \frac{4\beta^2}{15} - \frac{4}{15} \ln(\beta^2 + 1) + \beta \tan^{-1} \beta. \end{aligned} \quad (3.26)$$

In contrast, the integrals $J_2(\alpha, \beta)$ and $J_3(\alpha, \beta)$ are more involved. The integral $J_2(\alpha, \beta)$ can be divided into three parts and written as

$$J_2(\alpha, \beta) = J_{21}(\alpha, \beta) + J_{22}(\alpha, \beta) + J_{23}(\alpha, \beta), \quad (3.27)$$

where the integrals $J_{21}(\alpha, \beta)$ and $J_{22}(\alpha, \beta)$ can be easily evaluated to be

$$J_{21}(\alpha, \beta) = \int_{-\alpha}^{\beta} dx x^2 = \frac{\alpha^3}{3} + \frac{\beta^3}{3}, \quad (3.28)$$

$$\begin{aligned} J_{22}(\alpha, \beta) &= 2 \int_{-\alpha}^{\beta} dx x (1 + x^2) \tan^{-1} x \\ &= -\frac{\alpha^3}{6} + \frac{1}{2} (\alpha^2 + 1)^2 \tan^{-1} \alpha - \frac{\alpha}{2} - \frac{\beta^3}{6} + \frac{1}{2} (\beta^2 + 1)^2 \tan^{-1} \beta - \frac{\beta}{2}. \end{aligned} \quad (3.29)$$

The quantity $J_{23}(\alpha, \beta)$ is given by

$$J_{23}(\alpha, \beta) = \int_{-\alpha}^{\beta} dx (1 + x^2)^2 (\tan^{-1} x)^2, \quad (3.30)$$

and, upon setting $\tan^{-1} x = y$, it reduces to

$$J_{23}(\alpha, \beta) = \int_{-\tan^{-1} \alpha}^{\tan^{-1} \beta} dy y^2 \sec^6 y. \quad (3.31)$$

The integral involved can be evaluated to be (see, for instance, Ref. [58])

$$\begin{aligned} \int dy y^2 \sec^6 y &= \frac{-y (\cos y - 2 y \sin y)}{10 \cos^5 y} - \frac{4 y (\cos y - y \sin y)}{15 \cos^3 y} + \left(\frac{11}{30} + \frac{8 y^2}{15} \right) \tan y \\ &+ \frac{\tan^3 y}{30} + \frac{16}{15} \sum_{n=1}^{\infty} \frac{(-1)^n 2^{2n} (2^{2n} - 1) y^{2n+1}}{(2n+1) (2n)!} B_{2n}, \end{aligned} \quad (3.32)$$

where B_{2n} are the Bernoulli numbers. Needless to add, this result can be used to arrive at $J_{23}(\alpha, \beta)$. We should add that the infinite series in the above expression is convergent, and we find that it can be expressed as follows [129]:

$$\begin{aligned} \sum_{n=1}^{\infty} \frac{(-1)^n 2^{2n} (2^{2n} - 1) y^{2n+1}}{(2n+1) (2n)!} B_{2n} &= y \left\{ \ln \left[\Gamma \left(1 + \frac{y}{\pi} \right) \right] + \ln \left[\Gamma \left(1 - \frac{y}{\pi} \right) \right] \right. \\ &\quad \left. - \ln \left[\Gamma \left(1 - \frac{2y}{\pi} \right) \right] - \ln \left[\Gamma \left(1 + \frac{2y}{\pi} \right) \right] \right\} \\ &+ \pi \left\{ -\zeta' \left(-1, 1 + \frac{y}{\pi} \right) + \zeta' \left(-1, 1 - \frac{y}{\pi} \right) \right. \\ &\quad \left. + \frac{1}{2} \zeta' \left(-1, 1 + \frac{2y}{\pi} \right) - \frac{1}{2} \zeta' \left(-1, 1 - \frac{2y}{\pi} \right) \right\}, \end{aligned} \quad (3.33)$$

where $\zeta'(s, a)$ denotes the derivative of the Hurwitz zeta function $\zeta(s, a)$ with respect to the first argument and $\Gamma(n)$ is the Gamma function.

Let us now evaluate the last of the integrals, *viz.* $J_3(\alpha, \beta)$. It proves to be convenient to divide the integral into four parts as follows:

$$J_3(\alpha, \beta) = J_{31}(\alpha, \beta) + J_{32}(\alpha, \beta) + J_{33}(\alpha, \beta) + J_{34}(\alpha, \beta). \quad (3.34)$$

If we set $\tan^{-1} x = y$, we find that the integrals $J_{31}(\alpha, \beta)$, $J_{32}(\alpha, \beta)$ and $J_{33}(\alpha, \beta)$ can be easily evaluated to be

$$J_{31}(\alpha, \beta) = \int_{-\tan^{-1} \alpha}^{\tan^{-1} \beta} dy \tan^3 y = \frac{1}{2} [-\alpha^2 + \ln(\alpha^2 + 1) + \beta^2 - \ln(\beta^2 + 1)], \quad (3.35)$$

$$\begin{aligned} J_{32}(\alpha, \beta) &= 3 \int_{-\tan^{-1} \alpha}^{\tan^{-1} \beta} dy y^2 \tan y \sec^4 y \\ &= \frac{1}{4} \left[-\alpha^2 - 2 \ln(\alpha^2 + 1) + 2\alpha(\alpha^2 + 3) \tan^{-1} \alpha - 3(\alpha^2 + 1)^2 (\tan^{-1} \alpha)^2 \right. \\ &\quad \left. + \beta^2 + 2 \ln(\beta^2 + 1) + 3(\beta^2 + 1)^2 (\tan^{-1} \beta)^2 - 2\beta(\beta^2 + 3) \tan^{-1} \beta \right], \end{aligned} \quad (3.36)$$

$$\begin{aligned} J_{33}(\alpha, \beta) &= 3 \int_{-\tan^{-1} \alpha}^{\tan^{-1} \beta} dy y \tan^2 y \sec^2 y \\ &= \frac{1}{2} [-2\alpha^3 \tan^{-1} \alpha + \alpha^2 - \ln(\alpha^2 + 1) + 2\beta^3 \tan^{-1} \beta - \beta^2 + \ln(\beta^2 + 1)]. \end{aligned} \quad (3.37)$$

The integral $J_{34}(\alpha, \beta)$ is given by

$$J_{34}(\alpha, \beta) = \int_{-\tan^{-1} \alpha}^{\tan^{-1} \beta} dy y^3 \sec^6 y, \quad (3.38)$$

which can be evaluated using the result [58]

$$\begin{aligned} \int dy y^3 \sec^6 y &= -\frac{y^2 (3 \cos y - 4 y \sin y)}{20 \cos^5 y} - \frac{2 y^2 (3 \cos y - 2 y \sin y)}{15 \cos^3 y} \\ &\quad + \left(y + \frac{8 y^3}{15} \right) \tan y + \ln |\cos y| + \frac{y \sin y}{10 \cos^3 y} - \frac{1}{20 \cos^2 y} \\ &\quad + \frac{8}{5} \sum_{n=1}^{\infty} \frac{(-1)^n 2^{2n} (2^{2n} - 1) y^{2n+2}}{(2n+2)(2n)!} B_{2n}. \end{aligned} \quad (3.39)$$

The infinite series in the above expression is convergent, and it can be expressed as [129]

$$\begin{aligned}
 \sum_{n=1}^{\infty} \frac{(-1)^n 2^{2n} (2^{2n} - 1) y^{2n+2}}{(2n+2)(2n)!} B_{2n} = & y^2 \left\{ \ln \left[\Gamma \left(1 + \frac{y}{\pi} \right) \right] + \ln \left[\Gamma \left(1 - \frac{y}{\pi} \right) \right] \right. \\
 & \left. - \ln \left[\Gamma \left(1 - \frac{2y}{\pi} \right) \right] - \ln \left[\Gamma \left(1 + \frac{2y}{\pi} \right) \right] \right\} + \frac{3}{8} \zeta(3) \\
 & + \pi^2 \left[\zeta' \left(-2, 1 + \frac{y}{\pi} \right) + \zeta' \left(-2, 1 - \frac{y}{\pi} \right) \right. \\
 & \left. - \frac{1}{4} \zeta' \left(-2, 1 - \frac{2y}{\pi} \right) - \frac{1}{4} \zeta' \left(-2, 1 + \frac{2y}{\pi} \right) \right] \\
 & + \pi y \left[\zeta' \left(-1, 1 + \frac{2y}{\pi} \right) - \zeta' \left(-1, 1 - \frac{2y}{\pi} \right) \right. \\
 & \left. + 2 \zeta' \left(-1, 1 - \frac{y}{\pi} \right) - 2 \zeta' \left(-1, 1 + \frac{y}{\pi} \right) \right], \quad (3.40)
 \end{aligned}$$

where, as before, $\zeta(s)$ is the Riemann zeta function, $\zeta'(s, a)$ denotes the derivative of the Hurwitz zeta function $\zeta(s, a)$ with respect to the first argument, and $\Gamma(n)$ is the Gamma function.

3.4 Amplitude and shape of the non-Gaussianity parameter

We can now make use of the behavior of the mode h_k at $\eta_e = \beta \eta_0$ and substitute the results we have obtained above in the expressions (3.16) and (3.18) to arrive at the tensor bispectrum and the corresponding non-Gaussianity parameter h_{NL} for an arbitrary triangular configuration of the wavenumbers involved. The resulting expressions prove to be rather long and, for this reason, we shall illustrate the various results graphically for a set of suitable values of the parameters. Let us first compare the contributions from the two domains. Restricting ourselves to the equilateral limit, in Fig. 3.3, we have plotted the contributions to h_{NL} from the two domains that we have considered. It is evident from the figure that the contribution due to the second domain to the parameter h_{NL} turns out to be larger. We find that the second domain contributes more in the squeezed limit as well.

It is now a matter of adding the contributions from the two domains to arrive at the complete tensor bispectrum and the non-Gaussianity parameter h_{NL} . In Fig. 3.4, we have plotted the behavior of the non-Gaussianity parameter h_{NL} in the equilateral and the

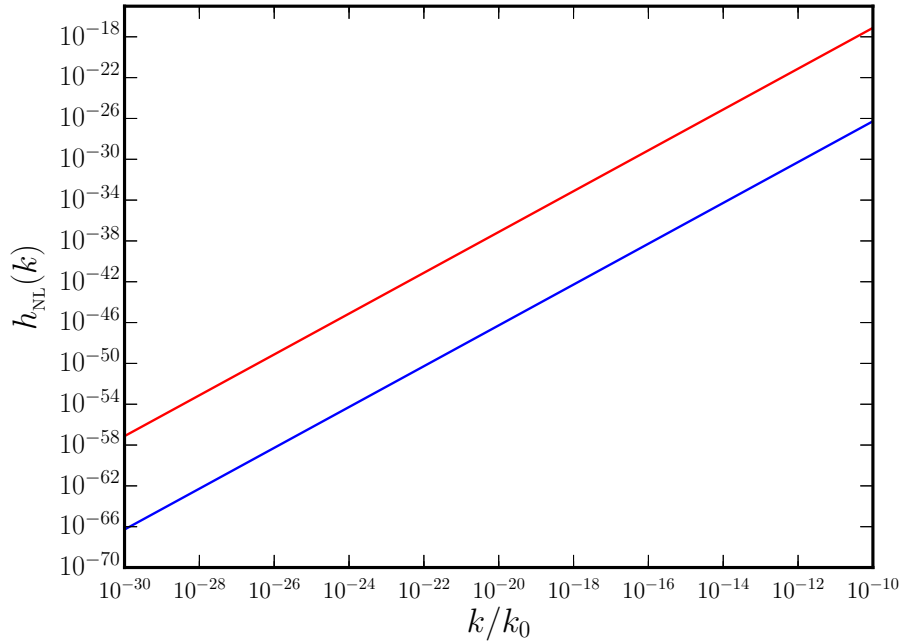


Figure 3.3: The contributions to the non-Gaussianity parameter h_{NL} in the equilateral limit from the first (in blue) and the second (in red) domains have been plotted as a function of k/k_0 for a wide range of wavenumbers such that $k \ll k_0/\alpha$. We have worked with the same set of values for the parameters as in the previous figure. Clearly, the second domain gives rise to a larger contribution to the non-Gaussianity parameter h_{NL} .

squeezed limits. Three points concerning the figure require emphasis. To begin with, we should mention that the non-Gaussianity parameter h_{NL} behaves as k^2 in both the equilateral and the squeezed limits, with virtually the same amplitude. Secondly, the value of the parameter h_{NL} is very small when compared to the values that occur in, say, de Sitter inflation wherein $3/8 \lesssim h_{\text{NL}} \lesssim 1/2$ (in this context, see Ref. [76]). Thirdly, since the tensor power spectrum is strictly scale invariant for wavenumbers such that $k \ll k_0/\alpha$, the amplitude of the non-Gaussianity parameter h_{NL} in the squeezed limit over such a domain should be equal to $3/8$, if the consistency relation holds true (see Eq. (1.118d), also see Ref. [79]). Whereas, we find that h_{NL} is considerably smaller than $3/8$ in the squeezed limit, which unambiguously implies that the consistency condition is violated [130]. Evidently, this behavior can be attributed to the fact that the amplitude of the tensor mode does not freeze to a constant value at late times. At this stage, we need to discuss the dependence of the tensor power and bispectra on the parameters α and β that we have introduced. We find that the tensor power spectrum and the bispectrum do not significantly depend on α over a wide range of values, say, $10^5 \lesssim \alpha \lesssim 10^{15}$. We had mentioned earlier that the tensor power spectrum has a rather weak dependence on β . Whereas, we find that the tensor bispectrum grows roughly as $\beta^{3/2}$. However, β cannot be allowed to be too large for two reasons. One may a priori expect that the analytical approxima-

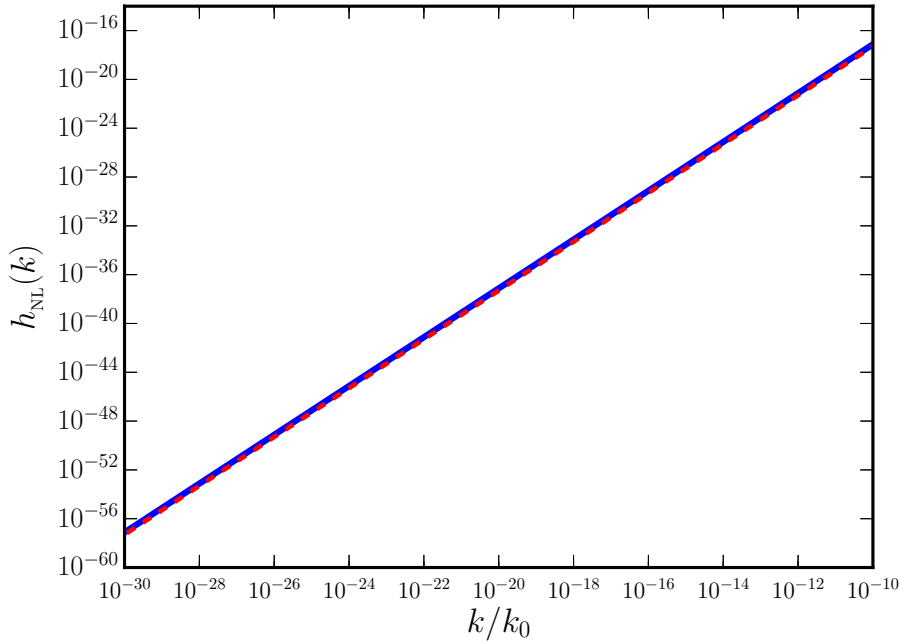


Figure 3.4: The behavior of the non-Gaussianity parameter h_{NL} in the equilateral (in blue) and the squeezed (in red) limits have been plotted as a function of k/k_0 for a wide range of wavenumbers such that $k \ll k_0/\alpha$. We have worked with the same set of values as in the earlier two figures. Clearly, the resulting h_{NL} is considerably small when compared to the values that arise in de Sitter inflation wherein $3/8 \lesssim h_{\text{NL}} \lesssim 1/2$. Moreover, we find that h_{NL} behaves as k^2 in the equilateral and the squeezed limits, with similar amplitudes. The fact that h_{NL} is much smaller than $3/8$ in the squeezed limit implies that the consistency condition is violated [130].

tion (3.8) will remain valid until the time $-\eta_k = \sqrt{2}/k$ after the bounce. We had pointed out that the evolution of the mode h_k is asymmetric in η . Actually, it can be shown that (using numerical analysis) the analytical approximation (3.8) breaks down much before $-\eta_k$. For this reason, we have chosen β to be smaller than α . Moreover, a transition to the radiation dominated phase is expected to take place sometime after the bounce. It seems reasonable to expect that such a transition will occur when the scale factor is $a \simeq 10^4 a_0$, which corresponds to $\beta = 10^2$. We find that our main conclusions, *viz.* that the value of h_{NL} is small over cosmological scales and that the consistency relation is violated in the squeezed limit, continue to remain valid even if we increase β by, say, a couple of orders of magnitude. In Fig. 3.5, we have plotted the non-Gaussianity parameter h_{NL} for an arbitrary triangular configuration of wavevectors. Clearly, the non-Gaussianity parameter exhibits a specific shape and the value of h_{NL} peaks in the equilateral limit.

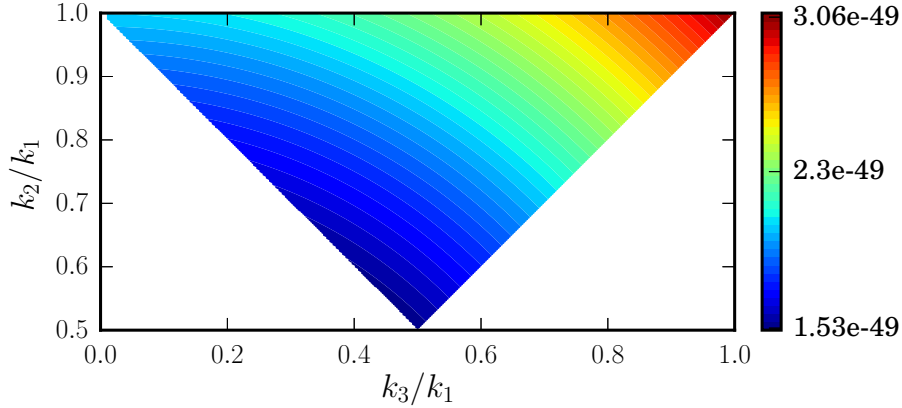


Figure 3.5: The behavior of the non-Gaussianity parameter h_{NL} has been plotted for an arbitrary triangular configuration of wavevectors. We have worked with the same set of values as in the previous figures. It is evident from the plot that the value of h_{NL} peaks in the equilateral limit.

3.5 Discussion

In this chapter, we have analytically calculated the tensor bispectrum in a matter bounce using the Maldacena formalism. While the matter bounce leads to a scale invariant tensor power spectrum for scales of cosmological interest as de Sitter inflation does, we have shown that the non-Gaussianity parameter h_{NL} that characterizes the amplitude of the tensor bispectrum is much smaller than the corresponding values in de Sitter inflation. We have also shown that, due to the growth in amplitude of the tensor modes as one approaches the bounce, the consistency condition is not satisfied by the tensor bispectrum in the squeezed limit. Recall that, in the absence of detailed modeling of the bounce, we had assumed that $k_0/(a_0 M_{\text{Pl}}) \simeq 10^{-5}$. We should however clarify that, since $k \ll k_0$ for cosmological scales, our essential conclusions, *viz.* that h_{NL} is small and that the consistency condition is violated over such scales, will remain unaffected even if we choose $k_0/(a_0 M_{\text{Pl}})$ to be a few orders of magnitude smaller than the value we have mentioned above. It will clearly be worthwhile to investigate these issues using a numerical approach in a wider class of bouncing models.

In the bouncing scenario that we have considered, at very early times, *i.e.* during the first domain of our interest, the contribution to the non-Gaussianity parameter h_{NL} can be said to be small because the amplitude of the tensor perturbations themselves are small. In the second domain, although the scale factor decreases gradually to reach its minimum at the bounce, the non-Gaussianities become larger as the perturbations grow. After the bounce, the scale factor increases steadily. Also, the amplitude of the perturbations do not freeze but grow slowly. Due to these reasons the contribution to the non-Gaussianity parameter is larger from this regime. However, essentially due to the form of the scale

factor, one finds that the parameter h_{NL} has an overall k^2 dependence. Since the scales of cosmological interest are about 25 to 30 orders below Planck scale, the non-Gaussianity parameter h_{NL} proves to be very small over such scales.

We believe that the results we have obtained have tremendous implications for the other three-point functions and, importantly, the scalar bispectrum. It seems clear that, due to the growth during the contracting phase near the bounce, the consistency conditions governing the other three-point functions will be violated as well [123]. This can possibly act as a powerful discriminator between the inflationary and bouncing scenarios. Within inflation, one requires peculiar situations to violate the consistency conditions [131]. In contrast, in a bouncing scenario, the consistency relations seem to be violated rather naturally. Notably, situations involving violations of the consistency conditions have been considered as possible sources of spherical asymmetry in the early universe [68, 69]. These aspects seem worth exploring in greater detail.

Chapter 4

Scale invariant magnetic fields in bouncing scenarios

4.1 Introduction

The observations of widely prevalent magnetic fields in the universe over an extensive range of scales, the origin of which cannot be satisfactorily accounted for by astrophysical processes alone, has been the principal motivation for looking into the generation of primordial magnetic fields. As is well known, inflation is currently considered the most promising paradigm to describe the origin of perturbations in the early universe. Hence, it seems natural to examine the generation of magnetic fields in the inflationary scenario. It has been established that the conformal invariance of the electromagnetic field has to be broken in order to generate magnetic fields of observable strengths in the early universe [96]. We have described the mechanism for generating such magnetic fields in the simple de Sitter inflationary scenario in Chap. 1. There exist many inflationary models which lead to nearly scale invariant magnetic fields of appropriate strength and correlation scales to match with the observations [97, 98, 102, 132–134]. However, most models of inflationary magnetogenesis typically suffer from the so-called backreaction and strong coupling problems (see, for instance, Refs. [102–104]).

Under such circumstances, it seems worthwhile to study the generation of magnetic fields in alternative scenarios of the early universe. A reasonably popular alternative are bouncing models wherein the universe undergoes a period of contraction until the scale factor attains a minimum value, after which it begins to expand (see, for instance, Refs. [27, 28, 30, 32, 38, 46, 49, 135], and the following reviews [51, 52]). As discussed previously in the introductory chapter, such bouncing scenarios provide an alternative to inflation to overcome the horizon problem. These models allow well motivated, Minkowski-like initial conditions to be imposed on the perturbations at early times during the con-

tracting phase. The generation of magnetic fields in such scenarios have been explored only to a limited extent [55, 132].

In a recent work [55], it was numerically shown that, for non-minimal couplings that are a simple power of the scale factor, scale invariant magnetic fields can be generated in certain bouncing scenarios. In this chapter, we shall investigate the problem analytically in a sub-class of these models wherein the non-minimal coupling is a positive power of the scale factor. We consider a specific form for the scale factor, leading to a non-singular bounce, which reduces to a power law form far from the bounce. We find that, in such situations, we can obtain analytical solutions for modes of the electromagnetic vector potential that are much smaller than the natural scale associated with the bounce. We divide the time period of our interest into two domains, one that corresponds to very early times and another closer to and across the bounce. We analytically evaluate the electromagnetic modes during these domains and arrive at the corresponding power spectra for the electric and magnetic fields. It can be easily shown that scale invariant magnetic fields can be generated before the bounce for specific values of the parameters involved. We evolve these modes across the bounce and calculate the power spectra in the early stages of the expanding phase *after* the bounce. We show that the shapes of the spectra are preserved for scales of cosmological interest as the modes evolve across the bounce.

The remainder of this chapter is organized as follows. In the following section, we shall introduce the forms of the scale factor and the coupling function that we consider. In Sec. 4.3, we shall divide the bounce into two domains and evaluate the modes analytically in each of these domains. We shall evaluate the power spectra prior to the bounce as well as soon after the bounce and illustrate that the shape of the power spectra are preserved across the bounce. In Sec. 4.4, we shall study the issue of backreaction using the analytical solutions for the modes. In Sec. 4.5, we shall illustrate that the power spectrum of the magnetic field is form invariant under a two parameter family of transformations of the coupling function. Finally, we shall conclude with a brief discussion in Sec. 4.6.

4.2 Non-minimal coupling in bounces

We shall model the non-singular bounce by assuming that the scale factor $a(\eta)$ behaves as follows [55, 130]:

$$a(\eta) = a_0 \left(1 + \frac{\eta^2}{\eta_0^2} \right)^q = a_0 (1 + k_0^2 \eta^2)^q, \quad (4.1)$$

where a_0 is the value of the scale factor at the bounce (*i.e.* when $\eta = 0$), $\eta_0 = 1/k_0$ denotes the time scale of the duration of the bounce, and $q > 0$. Note that, as discussed before, when $q = 1$, during very early times when $\eta \ll -\eta_0$, the scale factor behaves as in a matter dominated universe (*i.e.* $a \propto \eta^2$). Therefore, the $q = 1$ case is often referred to as the matter bounce scenario. We should mention here that, for certain values of the parameters

involved, the above scale factor leads to tensor power spectra that are consistent with the CMB observations (see, for instance, Refs. [130,136]). However, we should hasten to add that determining the corresponding scalar power spectra requires a detailed modeling of the bounce [56].

The scale factor (4.1) above can be achieved, for instance, if we consider that the universe is composed of two non-interacting fluids with constant equation of state parameters. Let the energy densities and pressure of the two fluids be denoted by ρ_i and p_i respectively, with $i = (1, 2)$. Also, let the equations of state for the two fluids be given by $p_i = w_i \rho_i$, where w_i is a constant. Since the two fluids are non-interacting, the equation governing the conservation of energy associated with the fluids can be integrated to yield that $\rho_i = M_i/a^{r_i}$, where M_i is a constant. As is well known, the index r_i is related to the equation of state parameter w_i by the relation: $r_i = 3(1 + w_i)$. It can be easily shown that the equation of state parameters w_1 and w_2 are related to the quantity q through the relations: $w_1 = (1 - q)/(3q)$ and $w_2 = (2 - q)/(3q)$. Further, one can show that $M_1 = 12 k_0^2 M_{\text{Pl}}^2 a_0^{1/q}$ and $M_2 = -M_1 a_0^{1/q}$. It is important to note that, while M_1 is positive, M_2 is negative. In other words, the energy density of the second fluid is always negative. This seems inevitable as the total energy density has to vanish at the bounce. For the specific case of $q = 1$, which is the matter bounce scenario, the first fluid corresponds to matter. The second fluid behaves in a manner similar to radiation as far as its time evolution is concerned, but it has a negative energy density. For our discussion, we shall assume that the evolution of the universe is achieved with the aid of suitable scalar field(s) which effectively mimic the behavior of the fluids (in this context, see, for example, Ref. [137]).

Given a scale factor, in order to arrive at the behavior of the electromagnetic modes in a FLRW universe, we shall also require the form of the non-minimal coupling function J . We shall assume that, as was done in the case of inflation, the coupling function can be conveniently expressed in terms of the scale factor as follows:

$$J(\eta) = J_0 a^{\bar{n}}(\eta), \quad (4.2)$$

where \bar{n} is a constant. It can be easily argued that the resulting power spectra are independent of the constant J_0 (in this context, see Ref. [55]). As we shall discuss in the following section, in this chapter, for the problem to be tractable completely analytically, we shall restrict ourselves to cases wherein \bar{n} is positive.

4.3 Analytical evaluation of the modes and the power spectra

Recall that in Chap. 3, we had divided the time period of interest in a bounce into two domains in order to facilitate analytical evaluation of the tensor modes. In a similar man-

ner, to arrive at analytical solutions for the electromagnetic modes, let us divide the time period of our interest into two domains, one far away from the bounce and another closer to and across the bounce. Let these two domains correspond to $-\infty < \eta < -\alpha \eta_0$ and $-\alpha \eta_0 < \eta < \beta \eta_0$, where α is a relatively large number, say, of the order of 10^5 or so, and $\beta = 10^2$.

During the first domain, the scale factor (4.1) reduces to the following power law form: $a(\eta) \propto \eta^{2q}$. In such a case, the non-minimal coupling function J also simplifies to a power law form and it behaves as $J(\eta) \propto \eta^{\bar{\gamma}}$, where we have set $\bar{\gamma} = 2\bar{n}q$. Under these conditions, we have $J''/J \simeq \bar{\gamma}(\bar{\gamma} - 1)/\eta^2$. This behavior is exactly what is encountered for a similar coupling function in power law inflation. Due to this reason, it is straightforward to show that the solutions to the modes of the electromagnetic vector potential \bar{A}_k in the first domain can be expressed in terms of the Bessel functions $J_\nu(x)$ [55,97,98,103,132]. One finds that the solutions to Eq. (1.129) can be expressed in terms of the quantity \mathcal{A}_k as follows:

$$\mathcal{A}_k(\eta) = \sqrt{-k\eta} \left[C_1(k) J_{\bar{\gamma}-1/2}(-k\eta) + C_2(k) J_{-\bar{\gamma}+1/2}(-k\eta) \right], \quad (4.3)$$

where the coefficients $C_1(k)$ and $C_2(k)$ are to be fixed by the initial conditions. On imposing the Bunch-Davies initial conditions at early times during the contracting phase, *i.e.* as $k\eta \rightarrow -\infty$, one obtains that

$$C_1(k) = \sqrt{\frac{\pi}{4k}} \frac{e^{-i\pi\bar{\gamma}/2}}{\cos(\pi\bar{\gamma})}, \quad C_2(k) = \sqrt{\frac{\pi}{4k}} \frac{e^{i\pi(\bar{\gamma}+1)/2}}{\cos(\pi\bar{\gamma})}. \quad (4.4)$$

At this stage, it is also useful to note that

$$\mathcal{A}'_k(\eta) - \frac{J'}{J} \mathcal{A}_k(\eta) = k \sqrt{-k\eta} \left[C_1(k) J_{\bar{\gamma}+1/2}(-k\eta) - C_2(k) J_{-\bar{\gamma}-1/2}(-k\eta) \right], \quad (4.5)$$

an expression we shall require to evaluate the power spectrum of the electric field.

Let us now evaluate the power spectra of the magnetic and electric fields as one approaches the bounce, *i.e.* in the limit $k|\eta| \ll 1$. It should be mentioned that, in order for the solutions we have obtained above to be applicable, we need to remain in the first domain (*i.e.* $-\infty < \eta < -\alpha \eta_0$) even as we consider this limit. This condition implies that we have to restrict ourselves to modes such that $k \ll k_0/\alpha$. The power spectra of the magnetic and electric fields can be arrived at from the above expressions for \mathcal{A}_k and $\mathcal{A}'_k - (J'/J) \mathcal{A}_k$ and the asymptotic forms of the Bessel functions. As is to be expected, the resulting spectra have the same form as one encounters in power law inflation. One finds that the spectrum of the magnetic field [cf. Eq. (1.130a)] can be written as [55,97,98,103]

$$\mathcal{P}_B(k) = \frac{\mathcal{F}(m)}{2\pi^2} \left(\frac{H}{2q} \right)^4 (-k\eta)^{4+2m}, \quad (4.6)$$

where $H \simeq (2q/a_0\eta)(\eta_0/\eta)^{2q}$, while $m = \bar{\gamma}$ for $\bar{\gamma} \leq 1/2$ and $m = 1 - \bar{\gamma}$ for $\bar{\gamma} \geq 1/2$. Moreover, the quantity $\mathcal{F}(m)$ is given by

$$\mathcal{F}(m) = \frac{\pi}{2^{2m+1} \Gamma^2(m + 1/2) \cos^2(\pi m)}. \quad (4.7)$$

Clearly, the case $m = -2$ leads to a scale invariant spectrum for the magnetic field, which corresponds to either $\bar{\gamma} = 3$ or $\bar{\gamma} = -2$. The associated spectrum for the electric field [cf. Eq. (1.130b)] can be evaluated to be

$$\mathcal{P}_E(k) = \frac{\mathcal{G}(m)}{2\pi^2} \left(\frac{H}{2q} \right)^4 (-k\eta)^{4+2m}, \quad (4.8)$$

where $m = 1 + \bar{\gamma}$ if $\bar{\gamma} \leq -1/2$ and $m = -\bar{\gamma}$ for $\bar{\gamma} \geq -1/2$, while $\mathcal{G}(m)$ is given by

$$\mathcal{G}(m) = \frac{\pi}{2^{2m+3} \Gamma^2(m + 3/2) \cos^2(\pi m)}. \quad (4.9)$$

It should be noted that, when $\bar{\gamma} = 3$ and $\bar{\gamma} = -2$, the power spectrum of the electric field behaves as k^{-2} and k^2 , respectively. These results imply that, in the bouncing scenario, one can expect these cases to lead to scale invariant spectra (corresponding to wavenumbers such that $k \ll k_0/\alpha$) for the magnetic field before the bounce. Using the analytical expressions (4.3) and (4.5), in Fig. 4.1, we have plotted the spectra of the magnetic and electric fields evaluated at $\eta = -\alpha \eta_0$ as a function of k/k_0 , for $\bar{\gamma} = 3$ and a set of values for the parameters q , $k_0/(a_0 M_{\text{Pl}})$, and α . In the domain $k \ll k_0/\alpha$ where our approximations are valid, it is evident from the figure that, while the spectrum of the magnetic field is scale invariant, the spectrum of the electric field behaves as k^{-2} . These are exactly the asymptotic forms (4.6) and (4.8) that we have arrived at above. The question that naturally arises is whether these spectra will retain their form as they traverse across the bounce.

Our analysis until now applies to both positive and negative values of \bar{n} . However, as we mentioned, we shall hereafter restrict our analysis to the cases wherein $\bar{n} > 0$. We shall illustrate that, in such cases, one can arrive at an analytical expression for the electromagnetic modes even during the bounce for wavenumbers such that $k \ll k_0$. When $\bar{n} > 0$, J grows away from the bounce and, hence, it seems natural to expect that J''/J will exhibit its maximum near the bounce. Actually, J''/J has a single maximum at the bounce for indices \bar{n} and q such that $\bar{\gamma} \leq 3$. One finds that, for other values of $\bar{\gamma}$, there arise two maxima and a minimum close to the bounce. The minimum occurs exactly at the bounce and its value proves to be $\bar{\gamma} k_0^2$. These behavior are clear from Fig. 4.2 wherein we have plotted the quantity J''/J for two different values of $\bar{\gamma}$. Therefore, when $\bar{n} > 0$, for scales of cosmological interest such that $k \ll k_0$, $k^2 \ll J''/J$ around the bounce. Hence, near the bounce, we can neglect the k^2 term in Eq. (1.127) [to be precise, we can ignore the k^2 term in Eq. (1.129)] so that we have

$$\bar{A}_k'' + 2 \frac{J'}{J} \bar{A}_k' \simeq 0. \quad (4.10)$$

This equation can be immediately integrated to yield

$$\bar{A}_k'(\eta) \simeq \bar{A}_k'(\eta_*) \frac{J^2(\eta_*)}{J^2(\eta)}, \quad (4.11)$$

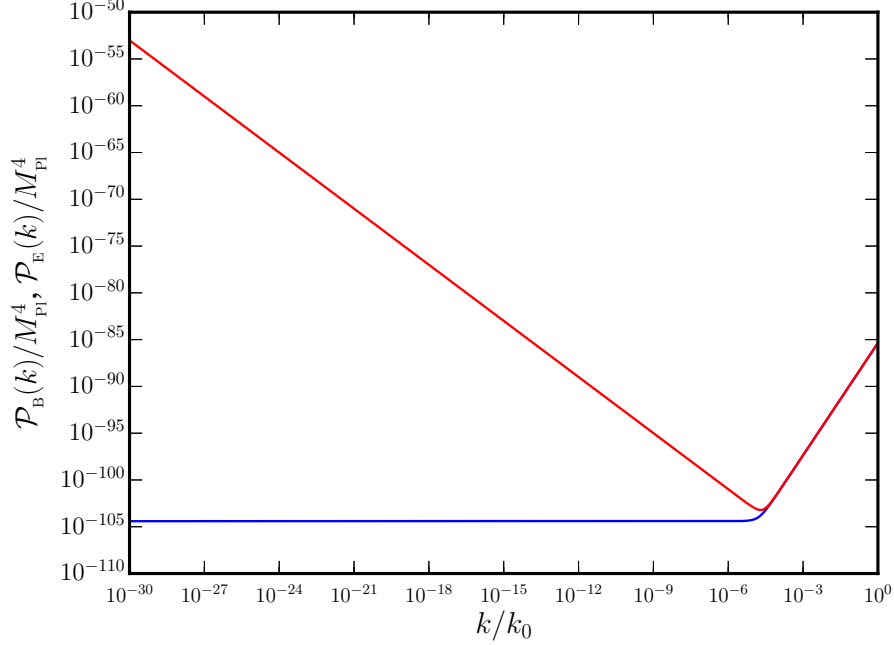


Figure 4.1: The power spectra of the magnetic (in blue) and electric (in red) fields, evaluated before the bounce at $\eta = -\alpha \eta_0$ using the analytical expressions (4.3) and (4.5), have been plotted as a function of k/k_0 for $\bar{\gamma} = 3$, $q = 1$, $k_0/(a_0 M_{\text{Pl}}) = 1.14 \times 10^{-11}$ and $\alpha = 10^5$. Also, we should mention that our analytical approximations are valid only for scales such that $k \ll k_0/\alpha$. Over this domain, while the spectrum of the magnetic field is strictly scale invariant, the spectrum of the electric field behaves as k^{-2} , as is suggested by the spectra (4.6) and (4.8) arrived at from the asymptotic forms of the Bessel functions. Needless to add, the question of interest is whether these power spectra will retain their shape after the bounce.

where η_* is a time when $k^2 \ll J''/J$ before the bounce. The above equation can be further integrated to arrive at

$$\bar{A}_k(\eta) \simeq \bar{A}_k(\eta_*) + \bar{A}'_k(\eta_*) \int_{\eta_*}^{\eta} d\tilde{\eta} \frac{J^2(\eta_*)}{J^2(\tilde{\eta})} = \bar{A}_k(\eta_*) + \bar{A}'_k(\eta_*) a^{2n}(\eta_*) \int_{\eta_*}^{\eta} \frac{d\tilde{\eta}}{a^{2n}(\tilde{\eta})}, \quad (4.12)$$

where we have set the constant of integration to be $\bar{A}_k(\eta_*)$. If we substitute the expression (4.1) for the scale factor, we find that the integral can be carried out for an arbitrary $\bar{\gamma}$ to obtain

$$\bar{A}_k(\eta) \simeq \bar{A}_k(\eta_*) + \bar{A}'_k(\eta_*) \frac{a^{2n}(\eta_*)}{a_0^{2n}} \left[\eta {}_2F_1 \left(\frac{1}{2}, \bar{\gamma}; \frac{3}{2}; -\frac{\eta^2}{\eta_0^2} \right) - \eta_* {}_2F_1 \left(\frac{1}{2}, \bar{\gamma}; \frac{3}{2}; -\frac{\eta_*^2}{\eta_0^2} \right) \right], \quad (4.13)$$

where ${}_2F_1(a, b; c; z)$ denotes the hypergeometric function [129]. We can now choose $\eta_* = -\alpha \eta_0$ to arrive at the behavior of $\bar{A}_k(\eta)$ and $\bar{A}'_k(\eta)$ in the second domain. In such a case,

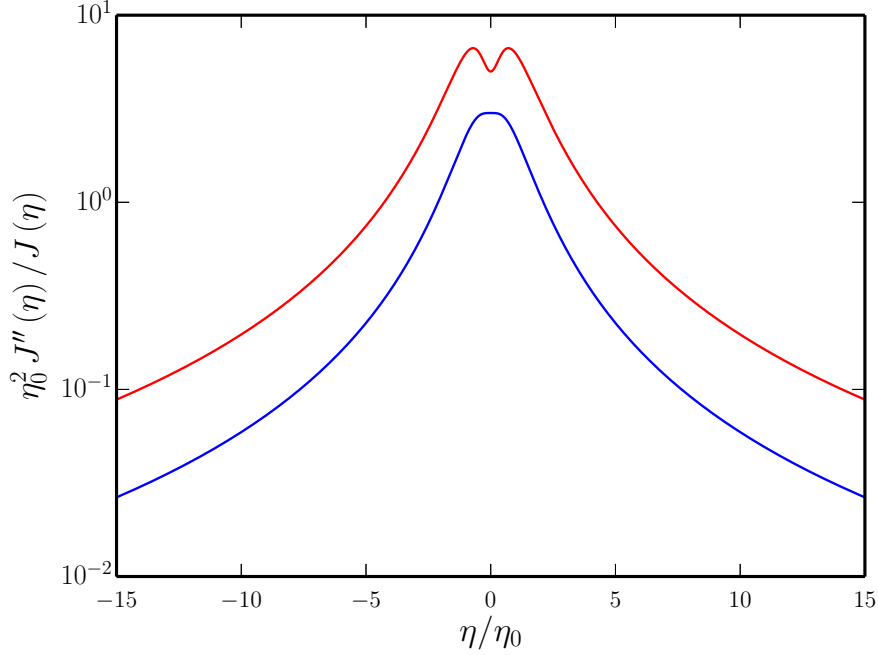


Figure 4.2: The behavior of $\eta_0^2 J''/J$, which depends only on η/η_0 , has been plotted for $\bar{\gamma} = 3$ (in blue) and $\bar{\gamma} = 5$ (in red). The figure has been plotted over a very narrow range of η/η_0 in order to illustrate the presence of a single maximum for $\bar{\gamma} = 3$ and two maxima and one minimum for $\bar{\gamma} = 5$.

we can make use of the solution (4.3) in the first domain to determine the values of $\bar{A}_k(\eta_*)$ and $\bar{A}'_k(\eta_*)$.

In fact, the solutions we have obtained above can be expected to be valid even after the bounce until the condition $k^2 \ll J''/J$ is violated. While the bounce is symmetric, the solution $\bar{A}_k(\eta_*)$ and its time derivative $\bar{A}'_k(\eta_*)$ are not symmetric [55]. Numerical analysis suggests that the analytical solutions will cease to be valid well before the condition $k^2 = J''/J$ is satisfied after the bounce. For this reason, as was done in the case of the tensor power spectrum in Chap. 3, we evaluate the electromagnetic spectra after the bounce at $\eta = \beta \eta_0$, with β chosen to be about 10^2 . This choice of β can be said to roughly correspond to the time of reheating after the more conventional inflationary scenario [55]. We can now evaluate the spectra *after* the bounce at $\eta = \beta \eta_0$ using the analytical expressions for \bar{A}_k and \bar{A}'_k we have obtained above [cf. Eqs. (4.12) and (4.11)]. In the scale invariant case corresponding to $\bar{\gamma} = 3$, the amplitude of the power spectrum for $k/(\alpha k_0) \ll 1$ can be determined to be

$$\mathcal{P}_B(k) \simeq \left(\frac{45}{16\beta} \right)^2 \left(\frac{k_0}{a_0} \right)^4. \quad (4.14)$$

For instance, if we choose, $k_0/(a_0 M_{\text{Pl}}) \simeq 10^{-7}$, we find that the above spectrum will lead to magnetic fields of femto Gauss strengths today. Recall that, while the power spectrum

of the electric field depends on \bar{A}'_k , the power spectrum of the magnetic field depends on \bar{A}_k . Since \bar{A}'_k after the bounce is related to the corresponding \bar{A}'_k at the end of the first domain only by a time dependent factor [cf. Eq. (4.11)], it is obvious that the shape of the electric field will not be affected by the bounce. In contrast, the quantity \bar{A}_k after the bounce depends on a combination of \bar{A}_k and \bar{A}'_k evaluated at the end of the first domain [cf. Eq. (4.12)]. So, it is not immediately evident that the shape of magnetic field will be preserved across the bounce. In Fig. 4.3, we have plotted these spectra after the bounce. Upon comparing Figs. 4.1 and 4.3, it is clear that, while the amplitudes of the spectra change, the shapes of the spectra before and after the bounce are identical [138].

4.4 The issue of backreaction

Note that, as discussed before, since the electromagnetic field is a test field, the energy density associated with it must always remain much smaller than the energy density that drives the background evolution. However, in certain cases, it is found that the energy density associated with the electromagnetic field can grow and dominate the background energy density [134]. This issue is regularly encountered in the context of inflation [97]. Such a situation is not viable and the energy density associated with the background must be dominant at all times. It is therefore imperative that we examine the issue of backreaction in bouncing models. In what follows, with the analytical results at hand, we shall evaluate the energy density in the generated electromagnetic field and investigate the issue of backreaction in the bouncing scenario of our interest.

Using the Friedmann equation, the background energy density, say, ρ_{bg} , can immediately be written as

$$\rho_{\text{bg}} = 3 M_{\text{Pl}}^2 H^2. \quad (4.15)$$

Upon using the expression (4.1) for the scale factor, we obtain that

$$\rho_{\text{bg}} = \frac{12 M_{\text{Pl}}^2 q^2 \eta^2}{a_0^2 \eta_0^4 (1 + k_0^2 \eta^2)^{2(q+1)}}. \quad (4.16)$$

The energy density in a particular mode k of the electromagnetic field is given by

$$\rho_{\text{EB}}^k = \mathcal{P}_{\text{B}}(k) + \mathcal{P}_{\text{E}}(k). \quad (4.17)$$

For the effects of backreaction to be negligible, the condition $\rho_{\text{bg}} > \rho_{\text{EB}}^k$ must be satisfied by all modes of cosmological interest at all times. However, we find that this condition is violated in this scenario, particularly around the bounce. To illustrate this issue, we have plotted the ratio of the background energy density and the electromagnetic energy density, *viz.* $r_{\text{br}} = \rho_{\text{bg}}/\rho_{\text{EB}}^k$. We should mention that we have evaluated the quantity ρ_{EB}^k from the analytical solutions we have obtained in the last section. In Fig. 4.4, we have

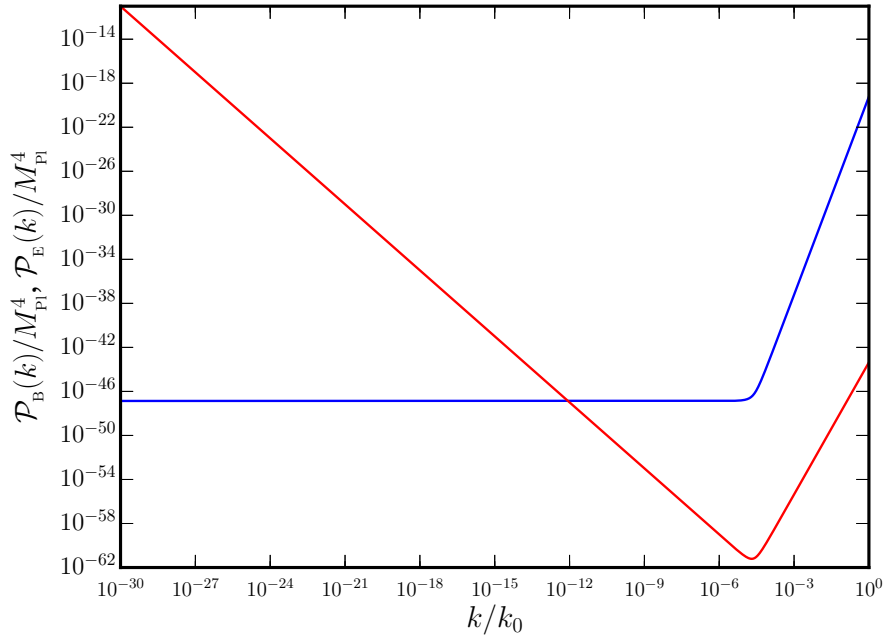


Figure 4.3: The power spectra of the electric (in red) and magnetic (in blue) fields, evaluated at $\eta = \beta \eta_0$, with $\beta = 10^2$, have been plotted for the same set of values of the parameters as in Fig. 4.1. Note that the shape of the spectra generated before the bounce is retained for scales such that $k \ll k_0/\alpha$ even after the bounce. We should mention that the values of the parameters we have worked with lead to magnetic fields of observed strengths today corresponding to a few femto Gauss. It should also be added that the electric field dominating the strength of the magnetic field is considered to be undesirable (see, for instance, Ref. [98]). This seems inevitable for positive \bar{n} that we are considering here, but it can be, for example, circumvented by choosing \bar{n} to be negative (in this context, see Ref. [55]).

plotted the quantity r_{br} as a function of e-N-folds. Since the Hubble parameter vanishes at the bounce, the background energy density also vanishes. Hence, any non-zero amount of electromagnetic energy density at the bounce would lead to a violation of the condition $r_{\text{br}} > 1$. We find that the condition is actually violated even as one approaches the bounce indicating that the problem is indeed a severe one.

We had mentioned earlier that no vector perturbations arise in the absence of vector sources. Note that the evolution of metric vector perturbations depends on the behavior of the scale factor [36]. In contrast, the evolution of the electromagnetic modes are determined by the form of the coupling function J . Evidently, we do not have any vector sources in the scenario of our interest here and, in fact, the electromagnetic modes we have considered have a quantum origin. For the form of the coupling function we have assumed here [J given by Eq. (4.2), with positive \bar{n}], the amplitude of the gener-

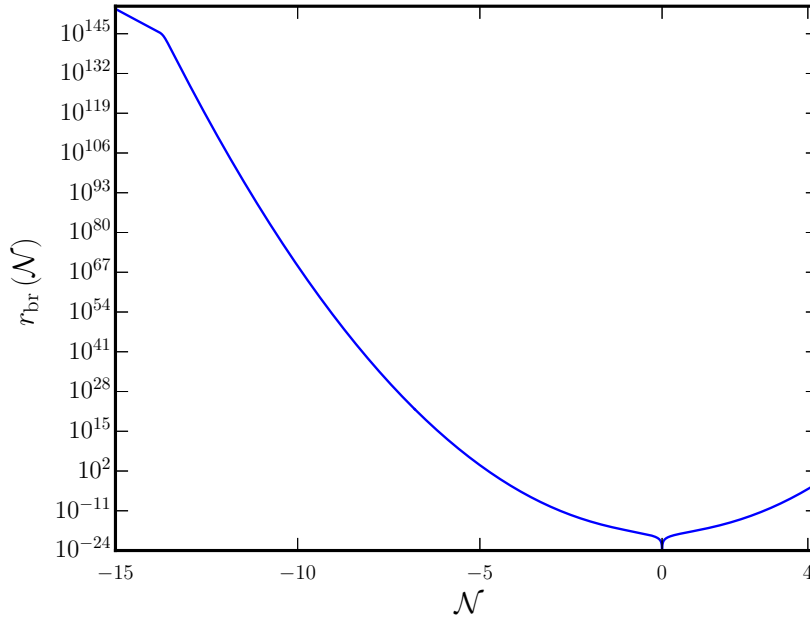


Figure 4.4: The evolution of the ratio of the background energy density to the sum of the energy densities in the electric and magnetic fields for a given mode ($k/k_0 = 10^{-20}$) has been plotted against e-N-folds. We should mention that we have assumed the same set of values for the various parameters as in Figs. 4.1 and 4.3. Evidently, the ratio has to remain large in order to avoid the backreaction problem. However, we find that the energy in the generated electromagnetic field rises sharply as one approaches the bounce, indicating that the problem of backreaction is the most severe at the bounce.

ated modes indeed grows rapidly during the contracting phase close to the bounce [55]. Therefore, in this case, the issue of backreaction can be considered to be a manifestation of the strong growth of the vector modes that is expected to occur as one approaches the bounce [36].

4.5 Duality invariance

Let us briefly remind ourselves about the property of duality invariance of the power spectra of the scalar and tensor perturbations that was discussed in Subsec. 1.4.4. The primordial scalar and tensor perturbations are governed by the so-called Mukhanov-Sasaki equations (see, for instance, Refs. [21, 22]). In these cases, it can be shown that the corresponding power spectra will remain invariant under a two parameter family of transformations of the homogeneous background quantity that determines the evolution of the perturbations (*viz.* the scale factor a in the case of tensor perturbations and a quantity

often denoted as z in the case of scalar perturbations) [48]. The new forms of the background quantities obtained as a transformation of the original quantities are called the dual functions. In this section, we shall extend these duality arguments to the generation of magnetic fields.

The argument is in fact relatively simple. The equation (1.129) that governs the dynamics of the quantity \mathcal{A}_k has the same form as the Mukhanov-Sasaki equations that describe the scalar and tensor perturbations [cf. Eqs. (1.55) and (1.62)]. Note that the quantity \mathcal{A}_k is determined by J''/J . Evidently, the solution to the differential equation (1.129) can be expected to behave in the same fashion and, hence, lead to the same power spectrum for the magnetic field if we can construct another coupling function that leads to the same J''/J . Given a coupling function J , its dual function, say, \tilde{J} , which leads to the same \tilde{J}''/\tilde{J} is found to be [138]

$$J(\eta) \rightarrow \tilde{J}(\eta) = C J(\eta) \int_{\eta_*}^{\eta} \frac{d\bar{\eta}}{J^2(\bar{\eta})}, \quad (4.18)$$

where C and η_* are constants. These constants can be suitably chosen to arrive at a physically reasonable form for \tilde{J} .

Let us now construct the dual form of the coupling function (4.2) that we had considered. The corresponding dual solution is described by the integral

$$\tilde{J}(\eta) = \frac{C}{J_0} a^n(\eta) \int_{\eta_*}^{\eta} \frac{d\bar{\eta}}{a^{2n}(\bar{\eta})}. \quad (4.19)$$

Let us first consider the behavior at very early times when the scale factor (4.1) reduces to the simple power law form. Recall that, in such a situation, the coupling function J behaves as $J(\eta) \propto \eta^{\bar{\gamma}}$. In such a case, the dual function \tilde{J} can be easily evaluated to be

$$\tilde{J}(\eta) = \frac{C \eta^{-\bar{\gamma}+1}}{-2\bar{\gamma}+1} \left(1 - \frac{\eta^{2\bar{\gamma}-1}}{\eta_*^{2\bar{\gamma}-1}} \right). \quad (4.20)$$

We are specifically interested in the cases where $\bar{\gamma} = 3$ and $\bar{\gamma} = -2$, as these lead to scale invariant spectra for the magnetic field. When $\bar{\gamma} = 3$, we have

$$\tilde{J}(\eta) = -\frac{C}{5\eta^2} \left(1 - \frac{\eta^5}{\eta_*^5} \right), \quad (4.21)$$

and, if we set $\eta_* \rightarrow -\infty$, we obtain that $\tilde{J}(\eta) \propto 1/\eta^2$. Also, when $\bar{\gamma} = -2$, we have

$$\tilde{J}(\eta) = \frac{C\eta^3}{5} \left(1 - \frac{\eta^5}{\eta_*^5} \right), \quad (4.22)$$

and, if we can choose η_* to be some large, but finite positive value, then at very early times, *i.e.* as $\eta \rightarrow -\infty$, we find that $\tilde{J}(\eta) \propto \eta^3$. Therefore, clearly, the coupling functions

corresponding to $\bar{\gamma} = 3$ and $\bar{\gamma} = -2$ are dual to each other. Given that one of these two cases leads to a scale invariant spectrum for the magnetic field before the bounce, their dual nature suggests that the other too will lead to the same spectrum, exactly as we have seen.

Let us now construct the dual form of the coupling function using the complete scale factor (4.1), which we had used to model the bounce. On substituting the expression for the scale factor in Eq. (4.18), we find that we can write the dual coupling function $\tilde{J}(\eta)$ in terms of the hypergeometric function as follows:

$$\tilde{J}(\eta) = \frac{C}{J_0 a_0^n} \left(1 + \frac{\eta^2}{\eta_0^2}\right)^{\bar{\gamma}/2} \left[\eta {}_2F_1\left(\frac{1}{2}, \bar{\gamma}; \frac{3}{2}; -\frac{\eta^2}{\eta_0^2}\right) - \eta_* {}_2F_1\left(\frac{1}{2}, \bar{\gamma}; \frac{3}{2}; -\frac{\eta_*^2}{\eta_0^2}\right) \right]. \quad (4.23)$$

This expression, though it is exact and is applicable to arbitrary $\bar{\gamma}$, does not reveal the behavior of the coupling function easily. However, we find that for the cases corresponding to $\bar{\gamma} = 3$ and $\bar{\gamma} = -2$, $\tilde{J}(\eta)$ can be written in terms of simple functions. When $\bar{\gamma} = 3$ (say, $n = 3/2$ and $q = 1$), the dual form of the coupling function can be expressed as

$$\begin{aligned} \tilde{J}(\eta) = & \frac{C \eta_0}{8 J_0 a_0^{3/2}} \left(1 + \frac{\eta^2}{\eta_0^2}\right)^{3/2} \left[\frac{5(\eta/\eta_0) + 3(\eta/\eta_0)^3}{(1 + \eta^2/\eta_0^2)^2} - \frac{5(\eta_*/\eta_0) + 3(\eta_*/\eta_0)^3}{(1 + \eta_*^2/\eta_0^2)^2} \right. \\ & \left. + 3 \tan^{-1}\left(\frac{\eta}{\eta_0}\right) - 3 \tan^{-1}\left(\frac{\eta_*}{\eta_0}\right) \right]. \end{aligned} \quad (4.24)$$

Note that the power spectrum for the electric field depends on the quantity J'/J [see Eq. (1.130b)]. Clearly, we shall require a well behaved \tilde{J}'/\tilde{J} to ensure that the electric field evolves smoothly. For this reason, it seems desirable to demand that the dual function \tilde{J} does not vanish over the domain of interest. We find that, if we set $\eta_* \rightarrow -\infty$, then with a suitable choice of the constant C , we can ensure that the above \tilde{J} remains positive at all times. We also find that at early times, *i.e.* as $\eta \rightarrow -\infty$, the above \tilde{J} reduces to $\tilde{J}(\eta) \propto 1/\eta^2$, as required. Let us now turn to the case $\bar{\gamma} = -2$ (say, $n = -1$ and $q = 1$). In this case, the dual form of this coupling function is given by

$$\tilde{J}(\eta) = \frac{C a_0 \eta_0}{J_0} \left(1 + \frac{\eta^2}{\eta_0^2}\right)^{-1} \left[\frac{\eta}{\eta_0} - \frac{\eta_*}{\eta_0} + \frac{2}{3} \left(\frac{\eta^3}{\eta_0^3} - \frac{\eta_*^3}{\eta_0^3} \right) + \frac{1}{5} \left(\frac{\eta^5}{\eta_0^5} - \frac{\eta_*^5}{\eta_0^5} \right) \right]. \quad (4.25)$$

We find that, in such a case, if we choose η_* to be a suitably large positive value (say, $\eta > \beta \eta_0$), then we can ensure that $\tilde{J}(\eta)$ remains positive over the domain that we are interested in. Also, we should point out that, at early times, *i.e.* as $\eta \rightarrow -\infty$, the $\tilde{J}(\eta)$ above reduces to $\tilde{J}(\eta) \propto \eta^3$, as required.

In Fig. 4.5, we have plotted the coupling function J and its dual \tilde{J} for the case $\bar{\gamma} = 3$, with a suitable choice of the parameters. Recall that our original choice for the coupling function J was symmetric about the bounce. While the dual function \tilde{J} behaves in a

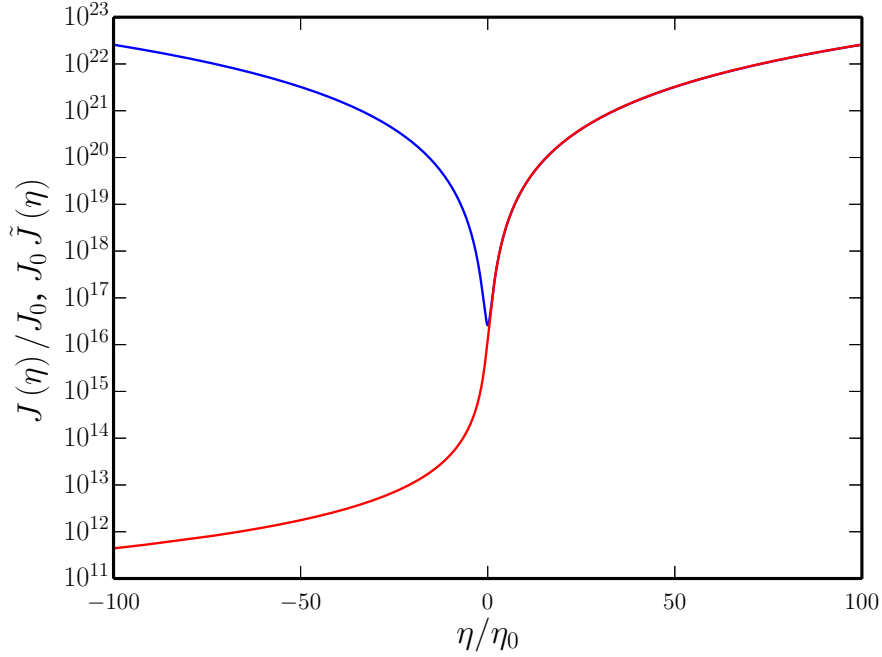


Figure 4.5: The coupling function J (in blue) and its dual \tilde{J} (in red) have been plotted as a function of η/η_0 for $\bar{\gamma} = 3$ and $\eta_* \rightarrow -\infty$ [cf. Eq. (4.24)]. Also, we have chosen the constant C to be $C/k_0 = 5.7 \times 10^{32}$ so that the dual function \tilde{J} matches the original coupling function J after the bounce.

similar fashion as J after the bounce (for a suitable choice of the constant C), we find that the dual function behaves very differently before the bounce. In fact, \tilde{J} is asymmetric about the bounce. For the case of $\bar{\gamma} = -2$, as we had discussed, η_* has to be chosen to be a large positive value in order to ensure that \tilde{J} does not vanish, which seems to pose difficulties for the evolution of the electric field.

4.6 Discussion

In this chapter, we have *analytically* studied the generation of primordial electromagnetic fields in a class of non-singular and symmetric bouncing scenarios. We have assumed that the electromagnetic field is coupled non-minimally to a background scalar field which is expected to drive the bounce. Considering specific forms of the scale factor and the coupling function, we have arrived at analytical expressions for the power spectra of the electric and magnetic fields. We find that a scale invariant spectrum for the magnetic field arises before the bounce for certain values of the parameters involved, while the corresponding electric field spectrum has a certain power law scale dependence. Interestingly, we have shown that, as the modes evolve across the bounce, these shapes of

the power spectra are preserved. However, a severe backreaction due to the generated electromagnetic fields seems unavoidable close to the bounce. This issue needs to be circumvented if the scenario has to be viable. We have further illustrated the existence of a two parameter family of transformations of the original coupling function under which the spectrum of the magnetic field remains invariant. The dual transformation leads to asymmetric forms for the coupling function and it seems to be a worthwhile exercise to explore these new forms. We are currently investigating the generation of magnetic fields in symmetric bounces with asymmetric coupling functions.

We need to emphasize a few points at this stage of our discussion. One may be concerned by the fact that the presence of radiation prior to the bounce can modify the equations of motion of the electromagnetic field which would, in turn, affect the process of magnetogenesis. We had described earlier as to how the class of bouncing models that we have considered can be driven with the aid of two fluids. We are envisaging a situation wherein such a behavior is actually achieved with the help of scalar fields. If, in addition to the scalar fields, radiation is also present before the bounce, its energy density can dominate close to the bounce, modifying the evolution of the background in the vicinity of the bounce and altering the form of the scale factor. Therefore, in our discussion, we have assumed that there is no radiation present before the bounce. We believe that, after the bounce, the scalar fields driving the bounce can decay into radiation via some mechanism (as it occurs immediately after inflation) and lead to the standard radiation dominated epoch. However, we should add that the phenomenon of reheating in bouncing scenarios and its effects on the process of magnetogenesis are not yet well understood.

Chapter 5

Cross-correlations between scalar perturbations and magnetic fields in bouncing universes

5.1 Introduction

In the previous chapter, we had analytically illustrated how scale invariant magnetic fields can be produced in a certain sub-class of symmetric bouncing scenarios. Using these analytical solutions, it would be interesting to examine the cross-correlations of these magnetic fields with scalar perturbations present in the bouncing scenarios. These correlations have been examined before in the context of inflation [99–101, 139, 140]. The magnitude of the non-Gaussianities generated through such correlations has been estimated to be quite large for inflation, and the shape of the non-Gaussianities peaks in the flattened limit, *i.e.* when the wavenumber of the scalar perturbation is twice the wavenumber associated with the two modes of the magnetic field. In this chapter, we shall study the cross-correlations of the magnetic fields produced in bouncing universes with the perturbations in an auxiliary scalar field. Ideally, it would be more appropriate to evaluate the cross-correlation between the primordial magnetic fields and the curvature perturbation. However, as is well known, examining the behavior of the curvature perturbations in bouncing models necessitates considerable modeling, often involving more than one field (see, for instance, Ref. [56]). Therefore, it would be instructive to first investigate the behavior of the cross-correlation of the magnetic fields with the perturbation in an auxiliary scalar field and explore its ramifications.

As we have already discussed before, one of the most important characteristics of three-point functions is their behavior in the squeezed limit of the wavenumbers involved, *i.e.* when one of the wavenumbers is assumed to be much smaller than the other

two. In inflation, typically, the amplitude of the mode with the longest wavelength and, therefore, the smallest wavenumber, freezes on super-Hubble scales. Therefore, in the squeezed limit, the three-point function can be completely expressed in terms of the two-point function through a relation referred to as the consistency condition (see Refs. [66,70,79,81–83,118,119] in the context of three-point functions involving scalar and tensor perturbations, and Refs. [100,101] for cross-correlations between the scalar perturbation and the magnetic fields). However, in the case of the bouncing models that we shall study, the amplitude of the scalar perturbations grows strongly as one approaches the bounce (in this context, see Ref. [56]). This suggests that the consistency relation may not hold in such scenarios (for a similar effect in the case of the tensor bispectrum, see Ref. [130]). Therefore, it is of utmost significance to examine whether the consistency relation, which holds true for inflationary magnetogenesis, would be valid in the bouncing model.

This chapter is organized as follows. In the following section, after briefly revisiting the calculation of the cross-correlations between the perturbation in the scalar field and the magnetic fields in the context of inflation, we shall evaluate the corresponding three-point function in the matter bounce scenario of our interest. In Sec. 5.3, we shall define a dimensionless non-Gaussianity parameter to characterize the three-point function and calculate the parameter in both the inflationary and bouncing models. In Sec. 5.4, we shall evaluate the cross-correlation in the squeezed limit and illustrate that, while the consistency relation holds true in the case of inflation, it is violated in the bouncing scenario. Finally, we shall conclude with a brief discussion in Sec. 5.5.

5.2 Evaluating the cross-correlations between scalar perturbations and magnetic fields

As is evident from the results of Subsec. 1.6.2 and Sec. 4.3, it is possible to obtain scale invariant magnetic fields of the requisite strength both in the case of inflation as well as in bouncing scenarios. Therefore, the behavior of the two-point function of the primordial magnetic fields alone is not adequate to distinguish between the inflationary and bouncing scenarios. It would hence be of utmost importance to study the cross-correlations of these fields with other fields that are expected to exist in the early universe, particularly the scalar fields. In this section, we shall arrive at the expression for the three-point function involving the magnetic field and the perturbation in the scalar field which leads to the non-minimal coupling. We shall first revisit the case of de Sitter inflation, wherein we shall consider the perturbation in an auxiliary scalar field and evaluate the three-point function. Thereafter, we shall calculate the three-point function in the bouncing model of our interest. We shall analyze the three-point function in these scenarios for two cases – one which leads to a scale invariant power spectrum for the magnetic field and another

which results in a blue-tilted power spectrum that scales as the square of the wavenumber involved. While the former is observationally relevant, the latter case involves simpler computations and we shall utilize it to illustrate certain points.

We shall consider the non-minimally coupled electromagnetic action (1.123). The action at the third order involving the perturbation $\delta\phi$ in the scalar field and the electromagnetic vector potential A_i can be easily obtained from the original action (1.123) to be

$$S_{\text{em}}^3[A_i, \phi] = \frac{1}{2\pi} \int d\eta \int d^3\mathbf{x} \left\{ J \frac{dJ}{d\phi} \delta\phi \left[\frac{1}{2} A_i'^2 - \frac{1}{4} (\partial_i A_j - \partial_j A_i)^2 \right] \right\}. \quad (5.1)$$

The corresponding interaction Hamiltonian can be determined to be [99]

$$H_{\text{int}} = \frac{1}{4\pi} \int d^3\mathbf{x} J \frac{dJ}{d\phi} \frac{\delta\phi}{M_{\text{Pl}}} \left[A_i'^2 + \frac{1}{2} (\partial_i A_j - \partial_j A_i)^2 \right], \quad (5.2)$$

where $\delta\phi$ denotes the perturbation in the scalar field. The cross-correlation between the perturbation in the scalar field and the magnetic field in real space is defined as

$$\begin{aligned} & \left\langle \frac{\hat{\delta}\phi(\eta, \mathbf{x})}{M_{\text{Pl}}} \hat{B}^i(\eta, \mathbf{x}) \hat{B}_i(\eta, \mathbf{x}) \right\rangle \\ &= \int \frac{d^3\mathbf{k}_1}{(2\pi)^{3/2}} \int \frac{d^3\mathbf{k}_2}{(2\pi)^{3/2}} \int \frac{d^3\mathbf{k}_3}{(2\pi)^{3/2}} \left\langle \frac{\hat{\delta}\phi_{\mathbf{k}_1}(\eta)}{M_{\text{Pl}}} \hat{B}_{\mathbf{k}_2}^i(\eta) \hat{B}_{i\mathbf{k}_3}(\eta) \right\rangle e^{i(\mathbf{k}_1 + \mathbf{k}_2 + \mathbf{k}_3) \cdot \mathbf{x}}, \end{aligned} \quad (5.3)$$

where the components B_i of the magnetic field are related to the vector potential A_i through the relation

$$B_i = \frac{1}{a} \epsilon_{ijl} \partial_j A_l, \quad (5.4)$$

while $\delta\phi_{\mathbf{k}}$ and $B_{\mathbf{k}}^i$ denote the Fourier modes associated with the perturbation in the scalar field and the i -th component of the magnetic field. According to the standard rules of perturbative quantum field theory, the cross-correlation between the perturbation in the scalar field and the magnetic field in Fourier space, evaluated at the end of inflation, is given by [99, 101]

$$\left\langle \frac{\hat{\delta}\phi_{\mathbf{k}_1}(\eta_e)}{M_{\text{Pl}}} \hat{B}_{\mathbf{k}_2}^i(\eta_e) \hat{B}_{i\mathbf{k}_3}(\eta_e) \right\rangle = -i \int_{\eta_i}^{\eta_e} d\eta \left\langle \left[\frac{\hat{\delta}\phi_{\mathbf{k}_1}(\eta)}{M_{\text{Pl}}} \hat{B}_{\mathbf{k}_2}^i(\eta) \hat{B}_{i\mathbf{k}_3}(\eta), \hat{H}_{\text{int}}(\eta) \right] \right\rangle, \quad (5.5)$$

where \hat{H}_{int} is the operator associated with the Hamiltonian (5.2) and the square brackets indicates the commutator.

We have already discussed the quantization of the electromagnetic modes in Subsec. 1.6.2. The perturbation in the scalar field can be quantized in terms of the corresponding Fourier modes, say, f_k , as

$$\hat{\delta}\phi(\eta, \mathbf{x}) = \int \frac{d^3\mathbf{k}}{(2\pi)^{3/2}} \left[\hat{a}_{\mathbf{k}} f_k(\eta) e^{i\mathbf{k} \cdot \mathbf{x}} + \hat{a}_{\mathbf{k}}^\dagger f_k^*(\eta) e^{-i\mathbf{k} \cdot \mathbf{x}} \right], \quad (5.6)$$

where the annihilation and creation operators $\hat{a}_{\mathbf{k}}$ and $\hat{a}_{\mathbf{k}}^\dagger$ satisfy the following standard commutation relations:

$$[\hat{a}_{\mathbf{k}}, \hat{a}_{\mathbf{k}'}] = [\hat{a}_{\mathbf{k}}^\dagger, \hat{a}_{\mathbf{k}'}^\dagger] = 0, \quad [\hat{a}_{\mathbf{k}}, \hat{a}_{\mathbf{k}'}^\dagger] = \delta^{(3)}(\mathbf{k} - \mathbf{k}'). \quad (5.7)$$

As we shall see, in order to achieve the coupling functions (1.131) and (4.2), we shall assume that the canonical scalar field is governed by a linear potential in the case of inflation and is free in the case of the bounce. In both these cases, the perturbation in the scalar field $\delta\phi$ is governed by the equation of motion

$$\delta\phi'' + 2\mathcal{H}\delta\phi' - \nabla^2\delta\phi = 0, \quad (5.8)$$

where $\mathcal{H} = a'/a$ is the conformal Hubble parameter. The Fourier modes $f_{\mathbf{k}}$ therefore satisfy the differential equation

$$f_{\mathbf{k}}'' + 2\mathcal{H}f_{\mathbf{k}}' + k^2 f_{\mathbf{k}} = 0. \quad (5.9)$$

Let us now define

$$\left\langle \frac{\delta\phi_{\mathbf{k}_1}(\eta_e)}{M_{\text{Pl}}} \hat{B}_{\mathbf{k}_2}^i(\eta_e) \hat{B}_{\mathbf{k}_3}^i(\eta_e) \right\rangle \equiv (2\pi)^{-3/2} G_{\delta\phi BB}(\mathbf{k}_1, \mathbf{k}_2, \mathbf{k}_3) \delta^{(3)}(\mathbf{k}_1 + \mathbf{k}_2 + \mathbf{k}_3). \quad (5.10)$$

Then, upon using the expression (5.5), along with the form of the interaction Hamiltonian (5.2) and Wick's theorem that applies to the products of the operators $\hat{A}_{\mathbf{k}}^i$ and $\delta\phi_{\mathbf{k}}$, one can show that the quantity $G_{\delta\phi BB}(\mathbf{k}_1, \mathbf{k}_2, \mathbf{k}_3)$ can be expressed as [141]

$$\begin{aligned} G_{\delta\phi BB}(\mathbf{k}_1, \mathbf{k}_2, \mathbf{k}_3) &= \frac{8\pi}{M_{\text{Pl}} a^2(\eta_e)} f_{k_1}(\eta_e) \bar{A}_{k_2}(\eta_e) \bar{A}_{k_3}(\eta_e) \left\{ 2(\mathbf{k}_2 \cdot \mathbf{k}_3) \mathcal{G}_{\delta\phi BB}^1(\mathbf{k}_1, \mathbf{k}_2, \mathbf{k}_3) \right. \\ &\quad \left. - \left[\frac{(\mathbf{k}_2 \cdot \mathbf{k}_3)^2}{k_2 k_3} + k_2 k_3 \right] \mathcal{G}_{\delta\phi BB}^2(\mathbf{k}_1, \mathbf{k}_2, \mathbf{k}_3) \right\} \\ &\quad + \text{complex conjugate}, \end{aligned} \quad (5.11)$$

where $\mathcal{G}_{\delta\phi BB}^1(\mathbf{k}_1, \mathbf{k}_2, \mathbf{k}_3)$ and $\mathcal{G}_{\delta\phi BB}^2(\mathbf{k}_1, \mathbf{k}_2, \mathbf{k}_3)$ are described by the integrals

$$\mathcal{G}_{\delta\phi BB}^1(\mathbf{k}_1, \mathbf{k}_2, \mathbf{k}_3) = i \int_{\eta_i}^{\eta_e} d\eta J \frac{dJ}{d\phi} f_{k_1}^*(\eta) \bar{A}_{k_2}'(\eta) \bar{A}_{k_3}'(\eta), \quad (5.12a)$$

$$\mathcal{G}_{\delta\phi BB}^2(\mathbf{k}_1, \mathbf{k}_2, \mathbf{k}_3) = i k_2 k_3 \int_{\eta_i}^{\eta_e} d\eta J \frac{dJ}{d\phi} f_{k_1}^*(\eta) \bar{A}_{k_2}^*(\eta) \bar{A}_{k_3}^*(\eta). \quad (5.12b)$$

Given the solutions for the electromagnetic modes $\bar{A}_{\mathbf{k}}$ and the scalar perturbations $f_{\mathbf{k}}$ [cf. Eqs. (1.127) and (5.9)], the above integrals can be evaluated in the inflationary and bouncing scenarios to arrive at the three-point function $G_{\delta\phi BB}(\mathbf{k}_1, \mathbf{k}_2, \mathbf{k}_3)$.

5.2.1 The three-point function in de Sitter inflation

Before we go on to evaluate the three-point function in the bouncing scenario, we shall first revisit its calculation in inflation in order to illustrate a few points. In Subsec. 1.6.2, when we had considered the evolution of the electromagnetic modes, for simplicity, we had assumed that the non-minimal coupling $J(\eta)$ is given by Eq. (1.131). In contrast, to evaluate the three-point function of interest, apart from J , we also need the behavior of $dJ/d\phi$ [cf. Eqs. (5.12)], which requires $J(\phi)$. This can be arrived at easily. Let the auxiliary scalar field ϕ that is evolving in de Sitter spacetime characterized by the scale factor (1.107a) be described by the potential $V(\phi)$. In de Sitter spacetime, the homogeneous scalar field ϕ satisfies the following equation of motion:

$$\phi'' - \frac{2}{\eta} \phi' + a^2 V_\phi = 0, \quad (5.13)$$

where $V_\phi = dV/d\phi$. If we now assume that $V(\phi) = -3n M_{\text{Pl}} H_1^2 \phi$, where n is a constant, then it is straightforward to show that, for a suitable choice of initial conditions, the solution to the above equation governing the scalar field can be written as [99]

$$\phi(\eta) = -n M_{\text{Pl}} \ln \eta. \quad (5.14)$$

Therefore, upon setting $J(\phi) = J_0 \exp(\phi/M_{\text{Pl}})$, we can arrive at the desired behavior of $J(\eta)$ [as given by Eq. (1.131)] that we had worked with. With $J(\phi)$ at hand, we can, evidently, obtain $dJ/d\phi$ to be

$$\frac{dJ}{d\phi} = \frac{J(\phi)}{M_{\text{Pl}}}, \quad (5.15)$$

thereby arriving at the required quantities related to the background.

We shall now evaluate the three-point function $G_{\delta\phi BB}(\mathbf{k}_1, \mathbf{k}_2, \mathbf{k}_3)$ for two specific values of n , as it proves to be difficult to evaluate the quantity for arbitrary n . Therefore, we shall consider the two cases wherein $n = 1$ and $n = 2$. The $n = 1$ case leads to a blue-tilted power spectrum for the magnetic field with the spectral index $n_B = 2$ [cf. Eq. (1.138)]. Whereas, the $n = 2$ case leads to the desired scale invariant spectrum. Note that the behavior of the mode f_k depends only on the scale factor [cf. Eq. (5.9)]. As is well known, in de Sitter spacetime, the mode f_k satisfying the standard Bunch-Davies initial condition is given by

$$f_k(\eta) = \frac{i H_1}{\sqrt{2} k^3} (1 + i k \eta) e^{-i k \eta}. \quad (5.16)$$

The case of $n = 1$

When $n = 1$, the electromagnetic mode \bar{A}_k and its derivative \bar{A}'_k can be written as [cf. Eq. (1.134)]

$$\bar{A}_k(\eta) = \sqrt{-\frac{\pi\eta}{4}} \left(\frac{\eta}{\eta_e}\right) e^{i\pi} H_{3/2}^{(1)}(-k\eta) = \frac{1}{\sqrt{2}k^3\eta_e} (-i + k\eta) e^{-ik\eta}, \quad (5.17a)$$

$$\bar{A}'_k(\eta) = -k \sqrt{-\frac{\pi\eta}{4}} \left(\frac{\eta}{\eta_e}\right) e^{i\pi} H_{1/2}^{(1)}(-k\eta) = -i \sqrt{\frac{k}{2}} \left(\frac{\eta}{\eta_e}\right) e^{-ik\eta}. \quad (5.17b)$$

Then, upon using the expressions (1.131) and (5.15) as well as the above modes in the integrals (5.12), we find that the integrals [*viz.* $\mathcal{G}_{\delta\phi BB}^1(\mathbf{k}_1, \mathbf{k}_2, \mathbf{k}_3)$ and $\mathcal{G}_{\delta\phi BB}^2(\mathbf{k}_1, \mathbf{k}_2, \mathbf{k}_3)$] can be evaluated easily to obtain

$$\mathcal{G}_{\delta\phi BB}^1(\mathbf{k}_1, \mathbf{k}_2, \mathbf{k}_3) = \frac{i H_1 \sqrt{k_2 k_3} e^{i k_T \eta_e}}{\sqrt{8} k_1^3 M_{\text{Pl}} k_T^2} (-i k_1 k_T \eta_e + 2 k_1 + k_2 + k_3), \quad (5.18a)$$

$$\begin{aligned} \mathcal{G}_{\delta\phi BB}^2(\mathbf{k}_1, \mathbf{k}_2, \mathbf{k}_3) = & \frac{H_1 k_2 k_3 e^{i k_T \eta_e}}{\sqrt{8} k_1^3 k_2^3 k_3^3 M_{\text{Pl}}} \left\{ \frac{1}{\eta_e} - \frac{k_1 k_2 k_3 \eta_e}{k_T} \right. \\ & \left. - \frac{i}{k_T^2} [k_1^2 (k_2 + k_3) + k_1 (k_2^2 + 4 k_2 k_3 + k_3^2) + k_2 k_3 (k_2 + k_3)] \right\}, \end{aligned} \quad (5.18b)$$

where, recall that, $k_T = k_1 + k_2 + k_3$. The two corresponding contributions to the three-point function can then be calculated to be

$$G_{\delta\phi BB(1)}(\mathbf{k}_1, \mathbf{k}_2, \mathbf{k}_3) = \frac{2\pi H_1^4}{M_{\text{Pl}}^2} \frac{(k_1 + k_T)(k_1^2 - k_2^2 - k_3^2)}{k_1^3 k_2 k_3 k_T^2}, \quad (5.19a)$$

$$\begin{aligned} G_{\delta\phi BB(2)}(\mathbf{k}_1, \mathbf{k}_2, \mathbf{k}_3) = & -\frac{\pi H_1^4}{2 M_{\text{Pl}}^2} \frac{1}{k_1^3 k_2^3 k_3^3 k_T^2} [k_1^4 - 2 k_1^2 (k_2^2 + k_3^2) + k_2^4 + 6 k_2^2 k_3^2 + k_3^4] \\ & \times \left[k_1^3 + k_2^3 + k_3^3 + 2 k_1^2 (k_2 + k_3) + 2 k_1 (k_2^2 + k_2 k_3 + k_3^2) \right. \\ & \left. + 2 k_2^2 k_3 + 2 k_2 k_3^2 \right]. \end{aligned} \quad (5.19b)$$

The complete three-point function $G_{\delta\phi BB}(\mathbf{k}_1, \mathbf{k}_2, \mathbf{k}_3)$ is evidently arrived at by adding the above two contributions.

The case of $n = 2$

Let us now consider the case of $n = 2$. Since the scalar modes depend only on the scale factor, they remain the same as in the case of $n = 1$ [*i.e.* as given by Eq. (5.16)]. Whereas,

the electromagnetic mode and its derivative are given by

$$\bar{A}_k(\eta) = \sqrt{-\frac{\pi \eta}{4}} \left(\frac{\eta}{\eta_e} \right)^2 e^{3i\pi/2} H_{5/2}^{(1)}(-k\eta) = \frac{-1}{\sqrt{2} k^5 \eta_e^2} (3 + 3i k \eta - k^2 \eta^2) e^{-ik\eta}, \quad (5.20a)$$

$$\bar{A}'_k(\eta) = -k \sqrt{-\frac{\pi \eta}{4}} \left(\frac{\eta}{\eta_e} \right)^2 e^{3i\pi/2} H_{3/2}^{(1)}(-k\eta) = \frac{-\eta}{\sqrt{2} k \eta_e^2} (1 + i k \eta) e^{-ik\eta}. \quad (5.20b)$$

The integrals (5.12) can be evaluated using the above modes to arrive at

$$\begin{aligned} \mathcal{G}_{\delta\phi BB}^1(\mathbf{k}_1, \mathbf{k}_2, \mathbf{k}_3) &= \frac{i H_1 e^{ik_T \eta_e}}{\sqrt{8 k_1^3 k_2 k_3} M_{\text{Pl}}} \left[\frac{i}{\eta_e} - \frac{i k_1 k_2 k_3 \eta_e}{k_T} \right. \\ &\quad \left. + \frac{k_1^2 (k_2 + k_3) + k_1 (k_2^2 + 4 k_2 k_3 + k_3^2) + k_2 k_3 (k_2 + k_3)}{k_T^2} \right], \end{aligned} \quad (5.21a)$$

$$\begin{aligned} \mathcal{G}_{\delta\phi BB}^2(\mathbf{k}_1, \mathbf{k}_2, \mathbf{k}_3) &= \frac{H_1 k_2 k_3}{\sqrt{8 k_1^3 k_2^5 k_3^5} M_{\text{Pl}}} \left\{ 3 i k_1^3 [\text{Ei}(i k_T \eta_e) + i \pi] + e^{ik_T \eta_e} \left[-\frac{3}{\eta_e^3} \right. \right. \\ &\quad \left. - \frac{i k_2 k_3 [3 k_1^2 (k_2 + k_3) + k_1 (3 k_2^2 + 8 k_2 k_3 + 3 k_3^2) + k_2 k_3 (k_2 + k_3)]}{k_T^2} \right. \\ &\quad \left. \left. + \frac{3 [-k_1^2 + k_1 (k_2 + k_3) + k_2 k_3]}{\eta_e} - \frac{k_1 k_2^2 k_3^2 \eta_e}{k_T} + \frac{3 i k_T}{\eta_e^2} \right] \right\}. \end{aligned} \quad (5.21b)$$

It should be mentioned that the integrals have been regulated (as is usually done in this context) in the $\eta \rightarrow -\infty$ limit to arrive at the above results.

Upon eventually taking the limit $\eta_e \rightarrow 0$, one can obtain that

$$\begin{aligned} G_{\delta\phi BB(1)}(\mathbf{k}_1, \mathbf{k}_2, \mathbf{k}_3) &= \frac{18 \pi H_1^6 a^2(\eta_e)}{M_{\text{Pl}}^2} \frac{(k_1^2 - k_2^2 - k_3^2)}{k_1^3 k_2^3 k_3^3 k_T^2} \left[k_1^3 + 2 k_1^2 (k_2 + k_3) \right. \\ &\quad \left. + 2 k_1 (k_2^2 + k_2 k_3 + k_3^2) + k_2^3 + 2 k_2^2 k_3 + 2 k_2 k_3^2 + k_3^3 \right], \end{aligned} \quad (5.22a)$$

$$\begin{aligned} G_{\delta\phi BB(2)}(\mathbf{k}_1, \mathbf{k}_2, \mathbf{k}_3) &= \frac{9 \pi H_1^6 a^2(\eta_e)}{2 M_{\text{Pl}}^2} \frac{1}{k_2^5 k_3^5} \left[k_1^4 - 2 k_1^2 (k_2^2 + k_3^2) + k_2^4 + 6 k_2^2 k_3^2 + k_3^4 \right] \\ &\quad \times \left\{ 3 \gamma_E + 3 \ln(-k_T \eta_e) - \frac{k_T^3}{k_1^3} - \frac{3 [k_1^2 - k_1 (k_2 + k_3) - k_2 k_3] k_T}{k_1^3} \right. \\ &\quad \left. - \frac{k_2 k_3 [3 k_1^2 (k_2 + k_3) + k_1 (3 k_2^2 + 8 k_2 k_3 + 3 k_3^2) + k_2 k_3 (k_2 + k_3)]}{k_1^3 k_T^2} \right\}, \end{aligned} \quad (5.22b)$$

where γ_E is the Euler-Mascheroni constant [58]. Clearly, the complete three-point function is a sum of the above two contributions.

A few clarifications need to be made regarding the expressions we have arrived at above in the $n = 2$ case. To begin with, note that the two contributions in this case explicitly depend on η_e [cf. Eqs. (5.22)]. The dependence arises through $a^2(\eta_e)$ as an overall factor and the term $\ln(-k_T \eta_e)$ that is encountered in the second contribution. While the first contribution is relatively straightforward to arrive at, the second requires some care (when considering the $\eta_e \rightarrow 0$ limit), specifically, in order to arrive at the logarithmic term. Later, in Sec. 5.3, we shall illustrate the amplitude and shape of the dimensionless non-Gaussianity parameter associated with the three-point function $G_{\delta\phi BB}(\mathbf{k}_1, \mathbf{k}_2, \mathbf{k}_3)$. The non-Gaussianity parameter will involve the ratio of the three-point function and the power spectra of the magnetic field as well as the perturbation in the scalar field. We shall see that the overall $a^2(\eta_e)$ term will be canceled by a similar term that arises in the power spectrum of the magnetic field. Also, we shall find that the logarithmic term considerably enhances the three-point function in the flattened limit (*i.e.* when $k_1 = 2 k_2 = 2 k_3$) leading to a characteristic shape for the non-Gaussianity parameter [101].

5.2.2 The three-point function in a matter bounce

Let us now turn to the evaluation of the three-point function in the bouncing models. In this case, we shall assume the canonical scalar field ϕ to be a free field. This choice is motivated by the fact that it will lead to a scale invariant spectrum for the perturbation in the scalar field in the matter bounce scenario (just as in de Sitter inflation) that we shall focus on [48, 130]. Such a scalar field is governed by the following equation of motion:

$$\phi'' + 2 \mathcal{H} \phi' = 0. \quad (5.23)$$

This equation can be immediately integrated to arrive at

$$\phi' = \frac{C_\phi}{a^2}, \quad (5.24)$$

where C_ϕ is a constant of integration. Recall that, apart from the form of the coupling function J [cf. Eq. (4.2)], we require its derivative $dJ/d\phi$ to calculate the three-point function. Upon using the quantity ϕ' we have obtained above, $dJ/d\phi$ can be expressed as

$$\frac{dJ}{d\phi} = \frac{dJ}{d\eta} \frac{d\eta}{d\phi} = \frac{2 J_0 \bar{n} q k_0^2 a_0^{1/q}}{C_\phi} \eta a^{\bar{n}+2-(1/q)}. \quad (5.25)$$

In what follows, we shall assume the background to be the matter bounce scenario wherein $q = 1$, and we shall consider the cases $\bar{n} = 1$ and $\bar{n} = 3/2$. Let us now understand the behavior of the modes. Since the Fourier modes f_k of the perturbation in the massless scalar field depend only on the scale factor [cf. Eq. (5.9)], it can be solved for independent of the value of \bar{n} . The modes f_k can be arrived at by dividing the period of interest into

two domains (over $-\infty < \eta < -\alpha \eta_0$ and $-\alpha \eta_0 < \eta < \beta \eta_0$, where $\alpha = 10^5$ and $\beta = 10^2$) just as we had done in the case of the electromagnetic modes in Chap. 4 as well as in the case of the tensors in Chap. 3. In the first domain, the mode is given by the following well known matter bounce form [48, 130]:

$$f_k(\eta) = \frac{1}{\sqrt{2k}} \frac{1}{a_0 k_0^2 \eta^2} \left(1 - \frac{i}{k \eta} \right) e^{-ik\eta}. \quad (5.26)$$

While in the second domain, it can be obtained to be (in this context, see Ref. [130])

$$f_k(\eta) = \mathcal{S}_{1k} + \mathcal{S}_{2k} g_1(k_0 \eta), \quad (5.27)$$

where

$$\mathcal{S}_{1k} = \frac{1}{\sqrt{2k}} \frac{1}{a_0 \alpha^2} \left(1 + \frac{i k_0}{\alpha k} \right) e^{i \alpha k / k_0} + \mathcal{S}_{2k} g_1(\alpha), \quad (5.28a)$$

$$\mathcal{S}_{2k} = \frac{1}{\sqrt{2k}} \frac{1}{2 a_0 \alpha^2} (1 + \alpha^2)^2 \left(\frac{3 i k_0}{\alpha^2 k} + \frac{3}{\alpha} - \frac{i k}{k_0} \right) e^{i \alpha k / k_0}, \quad (5.28b)$$

while the function $g_1(x)$ is given by Eq. (3.9). Note that the behavior of the modes f_k is similar to that of the tensor modes h_k [cf. Eq. (3.8)] discussed in Chap. 3, since they obey the same equation of motion. The behavior of the mode f_k is plotted in Fig. 5.1 (on page 112) as a function of so-called e-N-folds \mathcal{N} in terms of which the scale factor is given by $a(\mathcal{N}) = a_0 \exp(\mathcal{N}^2/2)$ [55], where a_0 is the value of the scale factor at the bounce. Note that the modes f_k and \bar{A}_k grow strongly as one approaches the bounce. Such a growth may lead to large non-Gaussianities in the bouncing scenarios.

The case of $\bar{n} = 1$

Let us first consider the case of $\bar{n} = 1$, as we had done in the context of inflation. In such a case, we have

$$\frac{dJ}{d\phi} = \frac{2 J_0 k_0^2 a_0^2}{C_\phi} \eta (1 + k_0^2 \eta^2)^2. \quad (5.29)$$

Since we now know the background quantities as well as the behavior of the modes, we have all the information required to evaluate the integrals characterizing the three-point function [cf. Eqs. (5.12)]. In order to calculate these integrals, evidently, we can divide the period of interest (*i.e.* $-\infty < \eta < \beta \eta_0$) into two domains ($-\infty < \eta < -\alpha \eta_0$ and $-\alpha \eta_0 < \eta < \beta \eta_0$) over which we have constructed solutions for the modes.

In the first domain, for the bouncing scenario of our interest, the scale factor can be approximately written as $a(\eta) \simeq a_0 k_0^2 \eta^2$. Therefore, we have [cf. Eqs. (4.2) and (5.25)]

$$J \frac{dJ}{d\phi} \simeq \frac{2 J_0^2 k_0^8 a_0^4}{C_\phi} \eta^7 = J_{00} \eta^7, \quad (5.30)$$

where we have set $J_{00} = 2 J_0^2 k_0^8 a_0^4 / C_\phi$. Also, when $\bar{n} = 1$, the electromagnetic modes (4.3) and their time derivative reduce to

$$\bar{A}_k(\eta) = \frac{-i}{\sqrt{2} k^3 a_0 J_0 k_0^2 \eta^3} (1 + i k \eta) e^{-i k \eta}, \quad (5.31a)$$

$$\bar{A}'_k(\eta) = \frac{1}{\sqrt{2} k^3 a_0 J_0 k_0^2 \eta^4} (3 i - 3 k \eta - i k^2 \eta^2) e^{-i k \eta}. \quad (5.31b)$$

Now, in order to arrive at the three-point function, we need to evaluate the integrals (5.12). After writing these equations in terms of the coupling function and the scalar and electromagnetic modes, we find that the integrals involved are mainly of the form described in Eq. (3.20). Therefore, in the first domain, using Eqs. (3.21) and (3.22), the integrals (5.12) can be written as follows:

$$\begin{aligned} \mathcal{G}_{\delta\phi BB}^1(\mathbf{k}_1, \mathbf{k}_2, \mathbf{k}_3) = & \frac{a_0 k_0 e^{-i \alpha k_T / k_0}}{\sqrt{2} \alpha^3 C_\phi (k_1 k_2 k_3)^{3/2} k_T^2} \left\{ 3 i \alpha^3 k_0 k_1^3 k_T^2 e^{i \alpha k_T / k_0} \text{Ei} \left(-\frac{i k_T \alpha}{k_0} \right) \right. \\ & + 3 k_0^4 k_T^2 + 3 i \alpha k_0^3 k_T^3 + 3 \alpha^2 k_0^2 k_T^2 [k_1^2 - k_1 (k_2 + k_3) - k_2 k_3] \\ & - \alpha^3 k_0 \left[3 \pi k_1^5 e^{i \alpha k_T / k_0} + 6 \pi k_1^4 (k_2 + k_3) e^{i \alpha k_T / k_0} + i k_2^2 k_3^2 (k_2 + k_3) \right. \\ & + 3 \pi k_1^3 (k_2 + k_3)^2 e^{i \alpha k_T / k_0} + 3 i k_1^2 k_2 k_3 (k_2 + k_3) \\ & \left. \left. + i k_1 k_2 k_3 (3 k_2^2 + 8 k_2 k_3 + 3 k_3^2) \right] + \alpha^4 k_1 k_2^2 k_3^2 k_T \right\}, \quad (5.32a) \end{aligned}$$

$$\begin{aligned} \mathcal{G}_{\delta\phi BB}^2(\mathbf{k}_1, \mathbf{k}_2, \mathbf{k}_3) = & \frac{a_0 k_0 k_2 k_3 e^{-i \alpha k_T / k_0}}{\sqrt{2} \alpha C_\phi (k_1 k_2 k_3)^{3/2} k_T^2} \left\{ k_0^2 k_T^2 + i \alpha k_0 \left[k_1^2 (k_2 + k_3) \right. \right. \\ & \left. \left. + k_1 (k_2^2 + 4 k_2 k_3 + k_3^2) + k_2 k_3 (k_2 + k_3) \right] - \alpha^2 k_1 k_2 k_3 k_T \right\}. \quad (5.32b) \end{aligned}$$

In the second domain, we have

$$J \frac{dJ}{d\phi} = J_{01} \eta (1 + k_0^2 \eta^2)^3, \quad (5.33)$$

where we have defined $J_{01} = 2 J_0^2 k_0^2 a_0^4 / C_\phi$. Also, the modes and their derivatives are given by the expressions [cf. Eq. (4.13)]

$$\bar{A}_k(\eta) = \mathcal{B}_{1k} + \mathcal{B}_{2k} g_1(k_0 \eta), \quad (5.34a)$$

$$\bar{A}'_k(\eta) = \frac{2 \mathcal{B}_{2k} k_0}{(1 + k_0^2 \eta^2)^2}, \quad (5.34b)$$

where

$$\mathcal{B}_{1k} = \bar{A}_k(-\alpha \eta_0) + \frac{1}{2 k_0} \bar{A}'_k(-\alpha \eta_0) (1 + \alpha^2)^2 g_1(\alpha), \quad (5.35a)$$

$$\mathcal{B}_{2k} = \frac{1}{2 k_0} \bar{A}'_k(-\alpha \eta_0) (1 + \alpha^2)^2, \quad (5.35b)$$

with $\bar{A}_k(-\alpha \eta_0)$ and $\bar{A}'_k(-\alpha \eta_0)$ being obtained from the corresponding values evaluated at the end of the first domain [cf. Eqs. (5.31)], while $g_1(x)$ is given by Eq. (3.9). On using the above expressions, we find that the integrals (5.12) in the second domain are of the following form:

$$\mathcal{G}_{\delta\phi BB}^1(\mathbf{k}_1, \mathbf{k}_2, \mathbf{k}_3) = 4i J_{01} \mathcal{B}_{2k_2}^* \mathcal{B}_{2k_3}^* k_0^2 \int_{-\alpha/k_0}^{\beta/k_0} d\eta \left(\frac{\eta}{1 + k_0^2 \eta^2} \right) [\mathcal{S}_{1k_1}^* + \mathcal{S}_{2k_1}^* g_1(k_0 \eta)], \quad (5.36a)$$

$$\begin{aligned} \mathcal{G}_{\delta\phi BB}^2(\mathbf{k}_1, \mathbf{k}_2, \mathbf{k}_3) &= i k_2 k_3 J_{01} \int_{-\alpha/k_0}^{\beta/k_0} d\eta \eta (1 + k_0^2 \eta^2)^3 [\mathcal{S}_{1k_1}^* + \mathcal{S}_{2k_1}^* g_1(k_0 \eta)] \\ &\times [\mathcal{B}_{1k_2}^* + \mathcal{B}_{2k_2}^* g_1(k_0 \eta)] [\mathcal{B}_{1k_3}^* + \mathcal{B}_{2k_3}^* g_1(k_0 \eta)]. \end{aligned} \quad (5.36b)$$

These integrals can be evaluated easily in terms of elementary functions. Thereafter, these two integrals can be combined to arrive at the total contribution to the three-point function from the second domain.

The case of $\bar{n} = 3/2$

For the case of $q = 1$ and $\bar{n} = 3/2$, which is when scale invariant magnetic fields are generated, we have

$$\frac{dJ}{d\phi} = \frac{3 J_0 k_0^2 a_0^{7/2}}{C_\phi} \eta (1 + k_0^2 \eta^2)^{5/2}. \quad (5.37)$$

In the first domain, for the matter bounce scenario, we therefore have

$$J \frac{dJ}{d\phi} \simeq \frac{3 J_0^2 k_0^{10} a_0^5}{C_\phi} \eta^9 = J_{10} \eta^9, \quad (5.38)$$

where we have set $J_{10} = 3 J_0^2 k_0^{10} a_0^5 / C_\phi$. In this case, the electromagnetic modes (4.3) in the first domain simplify to

$$\bar{A}_k(\eta) = \frac{1}{J_0 a_0^{3/2} k_0^3 \sqrt{2k}} \left(\frac{1}{\eta^3} - \frac{3i}{k\eta^4} - \frac{3}{k^2\eta^5} \right) e^{-ik\eta}, \quad (5.39a)$$

$$\bar{A}'_k(\eta) = \frac{1}{J_0 a_0^{3/2} k_0^3 \sqrt{2k}} \left(\frac{15}{k^2\eta^6} + \frac{15i}{k\eta^5} - \frac{6}{\eta^4} - \frac{ik}{\eta^3} \right) e^{-ik\eta}. \quad (5.39b)$$

Using these solutions, we can compute the contribution to the three-point function from the first domain. We find that the integrals (5.12) can be evaluated using Eqs. (3.21)

and (3.22) to obtain

$$\begin{aligned}
 \mathcal{G}_{\delta\phi BB}^1(\mathbf{k}_1, \mathbf{k}_2, \mathbf{k}_3) = & -\frac{3 a_0 k_0 e^{-i \alpha k_T/k_0}}{4 \sqrt{2} \alpha^5 C_\phi k_1^{3/2} k_2^{5/2} k_3^{5/2} k_T^2} \left\{ 90 k_0^6 k_T^2 + 90 i \alpha k_0^5 k_T^3 \right. \\
 & - 15 i \alpha^5 k_0 k_1^3 k_T^2 (k_1^2 - k_2^2 - k_3^2) e^{i \alpha k_T/k_0} \text{Ei} \left(-\frac{i k_T \alpha}{k_0} \right) \\
 & + 30 \alpha^2 k_0^4 k_T^2 [k_1^2 - 3 k_1 (k_2 + k_3) - k_2^2 - 3 k_2 k_3 - k_3^2] \\
 & - 15 i \alpha^3 k_0^3 k_T^2 \left[k_1^3 - 2 k_1^2 (k_2 + k_3) + 2 k_1 (k_2^2 + 3 k_2 k_3 + k_3^2) \right. \\
 & \left. + 2 k_2 k_3 (k_2 + k_3) \right] - 3 \alpha^4 k_0^2 k_T^2 \left[5 k_1^4 - 5 k_1^3 (k_2 + k_3) + 10 k_1^2 k_2 k_3 \right. \\
 & \left. - 10 k_1 k_2 k_3 (k_2 + k_3) - 4 k_2^2 k_3^2 \right] + \alpha^5 k_0 \left[15 \pi k_1^7 e^{i \alpha k_T/k_0} \right. \\
 & + 30 \pi k_1^6 (k_2 + k_3) e^{i \alpha k_T/k_0} + 30 \pi k_1^5 k_2 k_3 e^{i \alpha k_T/k_0} - 30 \pi k_1^4 \left(k_2^3 \right. \\
 & \left. + k_2^2 k_3 + k_2 k_3^2 + k_3^3 \right) e^{i \alpha k_T/k_0} + 12 i k_1^2 k_2^2 k_3^2 (k_2 + k_3) \\
 & + 4 i k_1 k_2^2 k_3^2 (3 k_2^2 + 7 k_2 k_3 + 3 k_3^2) + 2 i k_2^3 k_3^3 (k_2 + k_3) \\
 & \left. \left. - 15 \pi k_1^3 (k_2 + k_3)^2 (k_2^2 + k_3^2) e^{i \alpha k_T/k_0} \right] - 2 \alpha^6 k_1 k_2^3 k_3^3 k_T \right\}, \tag{5.40a}
 \end{aligned}$$

$$\begin{aligned}
 \mathcal{G}_{\delta\phi BB}^2(\mathbf{k}_1, \mathbf{k}_2, \mathbf{k}_3) = & -\frac{3 a_0 k_0 k_2 k_3 e^{-i \alpha k_T/k_0}}{2 \sqrt{2} \alpha^3 C_\phi k_1^{3/2} k_2^{5/2} k_3^{5/2} k_T^2} \left\{ 3 i \alpha^3 k_0 k_1^3 k_T^2 e^{i \alpha k_T/k_0} \text{Ei} \left(-\frac{i k_T \alpha}{k_0} \right) \right. \\
 & + 3 k_0^4 k_T^2 + 3 i \alpha k_0^3 k_T^2 + 3 \alpha^2 k_0^2 k_T^2 [k_1^2 - k_1 (k_2 + k_3) - k_2 k_3] \\
 & - \alpha^3 k_0 \left[3 \pi k_1^5 e^{i \alpha k_T/k_0} + 6 \pi k_1^4 (k_2 + k_3) e^{i \alpha k_T/k_0} \right. \\
 & + 3 \pi k_1^3 (k_2 + k_3)^2 e^{i \alpha k_T/k_0} + 3 i k_1^2 k_2 k_3 (k_2 + k_3) \\
 & \left. \left. + i k_1 k_2 k_3 (3 k_2^2 + 8 k_2 k_3 + 3 k_3^2) + i k_2^2 k_3^2 (k_2 + k_3) \right] + \alpha^4 k_1 k_2^2 k_3^2 k_T \right\}. \tag{5.40b}
 \end{aligned}$$

In the second domain, we have

$$J \frac{dJ}{d\phi} = J_{11} \eta (1 + k_0^2 \eta^2)^4, \tag{5.41}$$

where we have defined $J_{11} = 3 J_0^2 k_0^2 a_0^5 / C_\phi$. Also, the electromagnetic modes are given by

the following expressions:

$$\bar{A}_k(\eta) = \mathcal{C}_{1k} + \mathcal{C}_{2k} g_{\frac{3}{2}}(k_0 \eta), \quad (5.42a)$$

$$\bar{A}'_k(\eta) = \frac{8 \mathcal{C}_{2k} k_0}{(1 + k_0^2 \eta^2)^3}, \quad (5.42b)$$

where the quantities \mathcal{C}_{1k} and \mathcal{C}_{2k} can be written as

$$\mathcal{C}_{1k} = \bar{A}_k(-\alpha \eta_0) + \frac{1}{8 k_0} \bar{A}'_k(-\alpha \eta_0) (1 + \alpha^2)^3 g_{\frac{3}{2}}(\alpha), \quad (5.43a)$$

$$\mathcal{C}_{2k} = \frac{1}{8 k_0} \bar{A}'_k(-\alpha \eta_0) (1 + \alpha^2)^3, \quad (5.43b)$$

while the function $g_{\frac{3}{2}}(x)$ is given by

$$g_{\frac{3}{2}}(x) = \frac{(5 + 3x^2)x}{(1 + x^2)^2} + 3 \tan^{-1} x. \quad (5.44)$$

Upon using the above expressions for the modes, we find that the integrals (5.12) in the second domain are of the following form:

$$\mathcal{G}_{\delta\phi BB}^1(\mathbf{k}_1, \mathbf{k}_2, \mathbf{k}_3) = 64 i J_{11} \mathcal{C}_{2k_2}^* \mathcal{C}_{2k_3}^* k_0^2 \int_{-\alpha/k_0}^{\beta/k_0} \frac{d\eta \eta}{(1 + k_0^2 \eta^2)^2} [\mathcal{S}_{1k_1}^* + \mathcal{S}_{2k_1}^* g_1(k_0 \eta)], \quad (5.45a)$$

$$\begin{aligned} \mathcal{G}_{\delta\phi BB}^2(\mathbf{k}_1, \mathbf{k}_2, \mathbf{k}_3) &= i k_2 k_3 J_{11} \int_{-\alpha/k_0}^{\beta/k_0} d\eta \eta (1 + k_0^2 \eta^2)^4 [\mathcal{S}_{1k_1}^* + \mathcal{S}_{2k_1}^* g_1(k_0 \eta)] \\ &\times [\mathcal{C}_{1k_2}^* + \mathcal{C}_{2k_2}^* g_{\frac{3}{2}}(k_0 \eta)] [\mathcal{C}_{1k_3}^* + \mathcal{C}_{2k_3}^* g_{\frac{3}{2}}(k_0 \eta)]. \end{aligned} \quad (5.45b)$$

These integrals can again be evaluated easily and expressed in terms of elementary functions and they can then be combined to arrive at the complete three-point function.

It is useful to note here that, on comparing the amplitude of the contributions to the three-point function from the first and second domains, we find that the second domain leads to a much larger contribution than that from the first domain in both the cases of $\bar{n} = 1$ and $\bar{n} = 3/2$. The final expressions describing the three-point functions prove to be quite lengthy and cumbersome. Due to this reason, rather than write them down explicitly, we shall instead illustrate the behavior of the corresponding non-Gaussianity parameter as density plots in the next section.

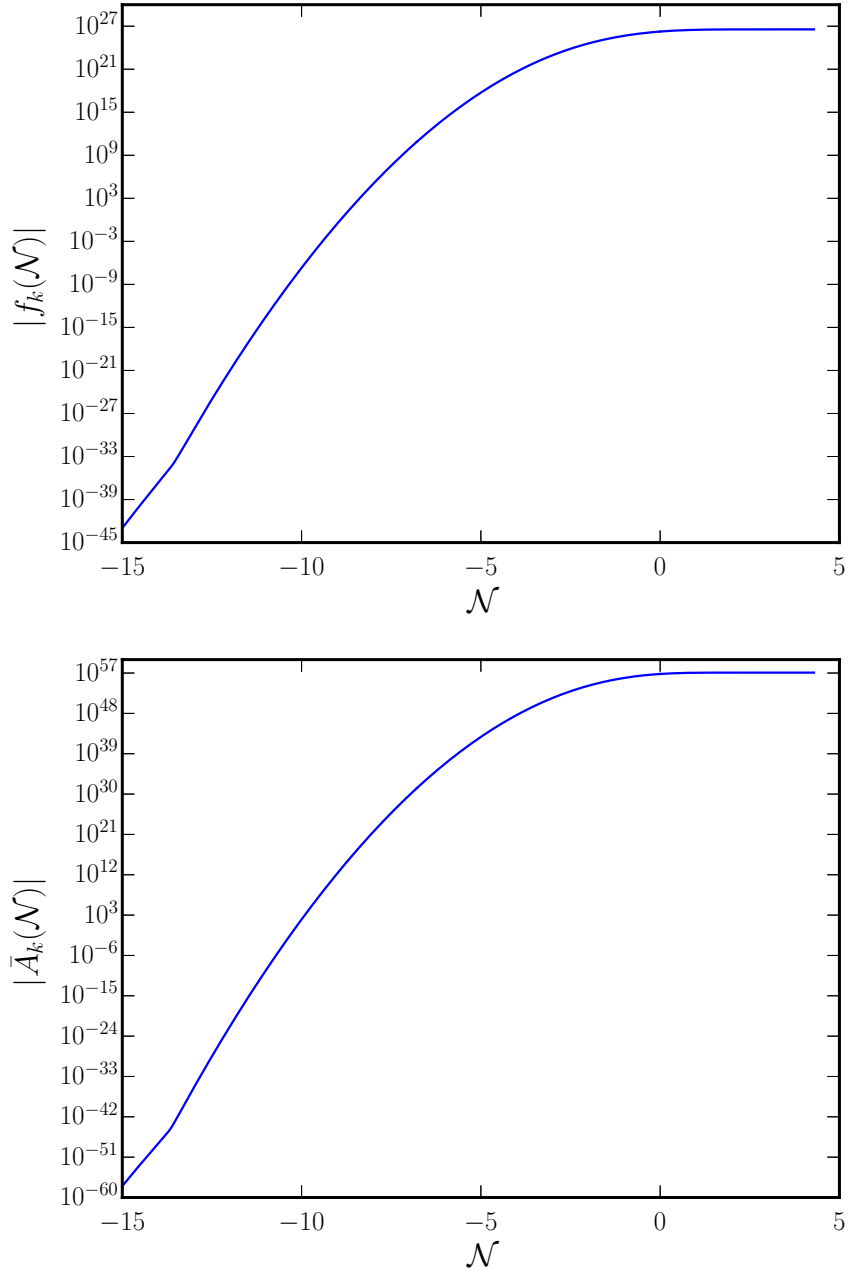


Figure 5.1: The behavior of the scalar mode f_k (on the top) and the electromagnetic mode \bar{A}_k (at the bottom, for the case $\bar{n} = 3/2$) in the matter bounce scenario (*i.e.* when $q = 1$) has been plotted as a function of time. We have chosen to work with a time variable called e-N-folds that is convenient to describe symmetric bounces [55]. Note that both the modes grow as one approaches the bounce. This property can lead to large non-Gaussianities. These plots correspond to a typical cosmological scale with wavenumber $k/k_0 = 10^{-20}$ and we should add that modes corresponding to all the scales of cosmological interest behave in a similar fashion. We should also point out that numerical analyses suggest that these analytical approximations match the exact numerical solutions very well [55, 130, 138].

5.3 Amplitude and shape of the non-Gaussianity parameter

Motivated by definitions of the non-Gaussianity parameters describing the three-point auto and cross-correlations of the scalar and tensor perturbations [76, 80], we shall now define a non-Gaussianity parameter b_{NL} to characterize the cross-correlation between the magnetic field and the perturbation in the scalar field. As we shall see, the parameter will prove to be a dimensionless quantity involving the ratio of the cross-correlation and the power spectra of the scalar perturbation and the magnetic field. The parameter captures the amplitude and shape of the three-point function, and we should clarify that it has a form very similar to the parameters defined earlier in this context [99–101]. In this section, we shall arrive at the expression for the non-Gaussianity parameter by following the same procedure as was used to arrive at similar parameters for the three-point functions involving the scalar and tensor perturbations [76]. With the definition at hand, we shall evaluate the parameter for the inflationary and bouncing scenarios of our interest.

The amplitude of the non-Gaussianity in the local model for the scalar three-point function is usually parameterized in terms of a parameter f_{NL} which, in this model, coincides with the bispectrum scaled by products of the power spectra. Here, we generalize that analogously to a non-Gaussianity parameter b_{NL} which we define through the following relation:

$$\hat{B}_{i\mathbf{q}}(\eta) = \hat{B}_{i\mathbf{q}}^{(\text{G})}(\eta) + \frac{b_{\text{NL}}}{2 M_{\text{Pl}}} \int \frac{d^3\mathbf{p}}{(2\pi)^{3/2}} \hat{\phi}_{\mathbf{q}-\mathbf{p}}(\eta) \hat{B}_{i\mathbf{p}}^{(\text{G})}(\eta), \quad (5.46)$$

where $\hat{B}_{i\mathbf{q}}$ is the Fourier mode of the actual magnetic field and $\hat{B}_{i\mathbf{q}}^{(\text{G})}$ indicates the Fourier mode of its Gaussian part, while, as usual, $\hat{\phi}_{\mathbf{q}-\mathbf{p}}$ refers to Fourier mode of the perturbation in the scalar field which has already been assumed to be Gaussian. We can evaluate the three-point function of our interest, *viz.* $\langle \hat{\phi}_{\mathbf{k}_1} \hat{B}_{i\mathbf{k}_2} \hat{B}_{i\mathbf{k}_3} \rangle$, upon using the above definition of $\hat{B}_{i\mathbf{q}}$ and Wick's theorem which applies to Gaussian operators. On making use of the definition (5.10) of $G_{\delta\phi BB}(\mathbf{k}_1, \mathbf{k}_2, \mathbf{k}_3)$ and inverting the resulting expression, we obtain the following expression for b_{NL} [141]:

$$b_{\text{NL}}(\mathbf{k}_1, \mathbf{k}_2, \mathbf{k}_3) = \frac{1}{16\pi^5} \frac{J^2(\eta_e)}{a^2(\eta_e)} \left[k_1^3 k_2^3 k_3^3 G_{\delta\phi BB}(\mathbf{k}_1, \mathbf{k}_2, \mathbf{k}_3) \right] \times \left\{ \mathcal{P}_{\delta\phi}(k_1) \left[k_3^3 \mathcal{P}_B(k_2) + k_2^3 \mathcal{P}_B(k_3) \right] \right\}^{-1}. \quad (5.47)$$

In this expression, $\mathcal{P}_B(k)$ is the power spectrum of the magnetic field we have discussed earlier, while $\mathcal{P}_{\delta\phi}(k)$ is the power spectrum of the scalar field, given by

$$\mathcal{P}_{\delta\phi}(k) = \frac{k^3}{2\pi^2 M_{\text{Pl}}^2} |f_k|^2, \quad (5.48)$$

with the right hand side to be evaluated as $\eta_e \rightarrow 0$ in the context of inflation and at $\eta = \beta \eta_0$ in the context of the bouncing models. Due to their dual nature [48], both de Sitter inflation and matter bounce are expected to lead to scale invariant spectra for the perturbation in the scalar field. In de Sitter inflation, the spectrum is given by the well known scale invariant form

$$\mathcal{P}_{\delta\phi}(k) = \frac{H_1^2}{4\pi^2 M_{\text{Pl}}^2}. \quad (5.49)$$

In the matter bounce, using the modes (5.27), it can be determined to be [130]

$$\mathcal{P}_{\delta\phi}(k) = \frac{9k_0^2}{16a_0^2 M_{\text{Pl}}^2}. \quad (5.50)$$

Let us first consider the amplitude and shape of the non-Gaussianity parameter b_{NL} for an arbitrary triangular configuration of the wavevectors $\mathbf{k}_1, \mathbf{k}_2$ and \mathbf{k}_3 in the context of inflation. In de Sitter inflation, for the case of $n = 1$, from the two contributions (5.19) to the three-point function and the power spectra (1.135) and (5.49), the parameter b_{NL} can be obtained to be

$$\begin{aligned} b_{\text{NL}}(\mathbf{k}_1, \mathbf{k}_2, \mathbf{k}_3) = & -\frac{1}{2k_2^2 k_3^2 (k_2 + k_3) k_{\text{T}}^2} \left\{ 4k_2^2 k_3^2 (k_1 + k_{\text{T}}) (-k_1^2 + k_2^2 + k_3^2) \right. \\ & + \left[k_1^4 - 2k_1^2 (k_2^2 + k_3^2) + k_2^4 + 6k_2^2 k_3^2 + k_3^4 \right] \left[k_1^3 + 2k_1^2 (k_2 + k_3) \right. \\ & \left. \left. + 2k_1 (k_2^2 + k_2 k_3 + k_3^2) + k_2^3 + 2k_2^2 k_3 + 2k_2 k_3^2 + k_3^3 \right] \right\}. \quad (5.51) \end{aligned}$$

Note that, in the squeezed limit, wherein $k_1 \rightarrow 0$ and $k_2 = k_3$, we have $b_{\text{NL}} = -4$. For the case of $n = 2$, the non-Gaussianity parameter can be obtained [from Eqs. (5.22), (1.135) and (5.49)] to be

$$\begin{aligned} b_{\text{NL}}(\mathbf{k}_1, \mathbf{k}_2, \mathbf{k}_3) = & \frac{1}{2k_2^2 k_3^2 (k_2^3 + k_3^3) k_{\text{T}}^2} \left\{ 4k_2^2 k_3^2 (k_1^2 - k_2^2 - k_3^2) \left[k_1^3 + 2k_1^2 (k_2 + k_3) \right. \right. \\ & + 2k_1 (k_2^2 + k_2 k_3 + k_3^2) + k_2^3 + 2k_2^2 k_3 + 2k_2 k_3^2 + k_3^3 \left. \right] - \left[k_1^4 + k_2^4 + k_3^4 \right. \\ & - 2k_1^2 (k_2^2 + k_3^2) + 6k_2^2 k_3^2 \left. \right] \left[-3\gamma_{\text{E}} k_1^3 k_{\text{T}}^2 - 3k_1^3 k_{\text{T}}^2 \ln(-k_{\text{T}} \eta_e) \right. \\ & + k_2 k_3 \left(3k_1^2 (k_2 + k_3) + k_1 (3k_2^2 + 8k_2 k_3 + 3k_3^2) + k_2 k_3 (k_2 + k_3) \right) \\ & \left. \left. + 3 \left(k_1^2 - k_1 (k_2 + k_3) - k_2 k_3 \right) k_{\text{T}}^3 + k_{\text{T}}^5 \right] \right\}. \quad (5.52) \end{aligned}$$

In the squeezed limit, we have $b_{\text{NL}} = -8$. In the next section, we shall discuss the properties of b_{NL} in the squeezed limit in more detail.

For the matter bounce scenario and the two cases of $\bar{n} = 1$ and $\bar{n} = 3/2$ that we had considered, we can arrive at the non-Gaussianity parameter b_{NL} from the various expressions we had obtained earlier and the corresponding power spectra. However, as the resulting expressions are too lengthy and cumbersome, we do not explicitly write them down here. We shall plot them below and compare them with the results in inflation.

In Figs. 5.2 and 5.3, we have illustrated the non-Gaussianity parameter b_{NL} as a density plot for an arbitrary triangular configuration of the wavevectors \mathbf{k}_1 , \mathbf{k}_2 , and \mathbf{k}_3 , as is often done for the scalar non-Gaussianity parameter f_{NL} (see, for instance, Ref. [80]). In these plots, the x -axis corresponds to the ratio of the amplitudes of \mathbf{k}_1 and \mathbf{k}_2 , while the y -axis corresponds to the ratio of the amplitudes of \mathbf{k}_3 and \mathbf{k}_2 . We have plotted the b_{NL} parameter over the ranges $0.0 < k_1/k_2 < 2.0$ and $0.0 < k_3/k_2 < 1.0$. These values of the ratios of wavenumbers can satisfactorily represent the entire range of triangular configuration of wavevectors of our interest (as we have discussed in Chap. 2).

A few points need to be stressed regarding the results that have been illustrated in Figs. 5.2 and 5.3. Let us first discuss the case of de Sitter inflation. To begin, note that, in this case, the amplitude as well as the shape of the non-Gaussianity parameter b_{NL} is considerably different depending on whether $n = 1$ or $n = 2$. Also, the amplitude in the $n = 2$ case is substantially larger due to the appearance of the $\ln(-k_{\text{T}} \eta_e)$ term, with the maximum values of the parameter arising in the flattened limit wherein $k_1 = 2k_2 = 2k_3$. Moreover, as we have already mentioned, in the squeezed limit wherein $k_1 \rightarrow 0$ and $k_2 = k_3$, we have $b_{\text{NL}} = -4$ when $n = 1$ and $b_{\text{NL}} = -8$ when $n = 2$. This is essentially the consistency relation which we shall establish in the next section for an arbitrary n in the case of inflation. In contrast, the non-Gaussianity parameter seems to have primarily the same shape for $\bar{n} = 1$ and $\bar{n} = 3/2$ in the matter bounce case. This can be attributed to the fact that, as the wavenumbers of cosmological interest are much smaller than the bounce scale, the matter bounce scenario is unable to strongly discriminate between these modes. However, the amplitude of b_{NL} in the matter bounce is considerably larger than in de Sitter inflation, which is possibly because of the form of the coupling function that we have considered [141]. While, for $\bar{n} = 1$, b_{NL} is nearly scale invariant, say, in the equilateral limit, we find that the parameter has a strong red tilt when $\bar{n} = 3/2$ (with b_{NL} behaving as k^{-2}), leading to rather large values for the small wavenumbers (say, for $10^{-20} < k/k_0 < 10^{-15}$) corresponding to cosmological scales. We shall discuss the implications of this result in the concluding section.

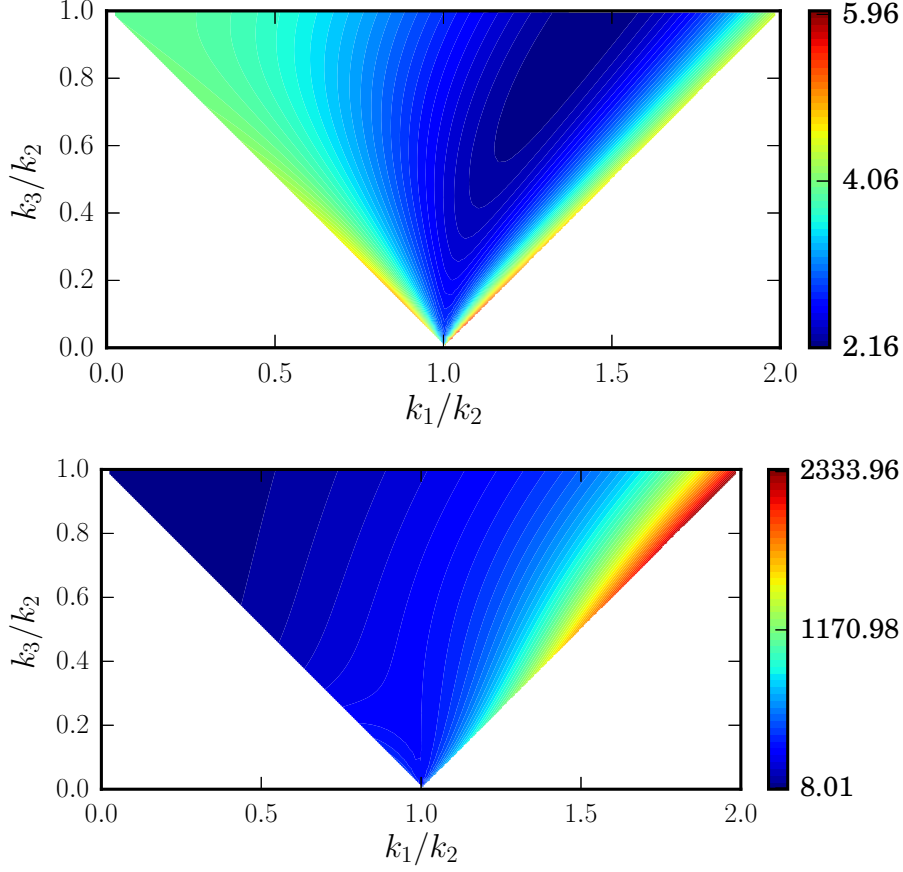


Figure 5.2: The dimensionless non-Gaussianity parameter b_{NL} arising in de Sitter inflation has been illustrated as a density plot for an arbitrary triangular configuration of wavevectors for the two cases of n that we had considered (with $n = 1$ on the top and $n = 2$ at the bottom). Recall that the $n = 2$ case leads to a scale invariant spectrum for the magnetic field. The amplitude as well as the shape of the parameter is considerably different in the two cases. Moreover, in the case of $n = 2$, the parameter is considerably enhanced in the flattened limit (due to the logarithmic term depending on η_e that arises in the three-point function), *i.e.* when $k_1 = 2k_2 = 2k_3$ [100, 101]. Further, b_{NL} tends to -4 and -8 when $n = 1$ and $n = 2$ in the squeezed limit (*i.e.* as $k_1 \rightarrow 0$), respectively, indicating that the cross-correlation satisfies the consistency relation, a point which we shall discuss in some generality in the next section. We have chosen η_e such that the pivot scale of $k_* = 0.002 \text{ Mpc}^{-1}$ leaves the Hubble radius 50 e-folds before the end of inflation. In this case, note that, we can write $\ln(-k_T \eta_e) = \ln(k_T/k_*) - 50$.

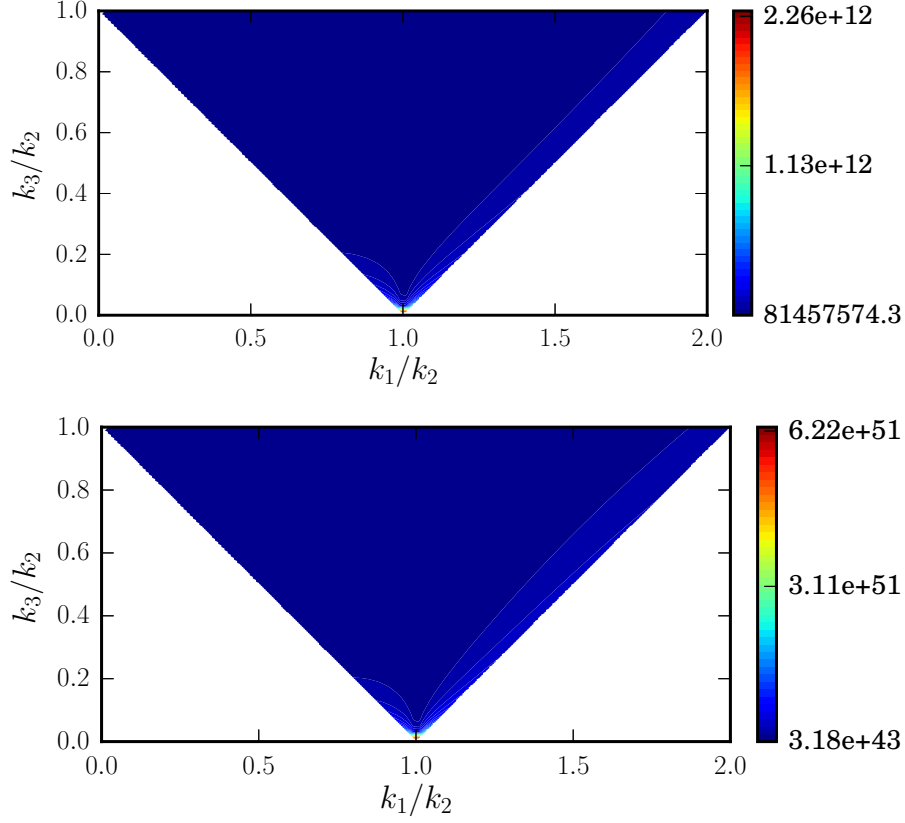


Figure 5.3: The dimensionless non-Gaussianity parameter b_{NL} arising in the matter bounce scenario has been illustrated in the form of density plots as in the previous figure for the two cases of \bar{n} we had discussed ($\bar{n} = 1$ on the top and $\bar{n} = 3/2$ at the bottom). When compared with the results in the inflationary case, two points are evident. Firstly, the shape of the parameter proves to be considerably more homogeneous. This is primarily because of the fact that all the scales of cosmological interest are much smaller than the bounce scale k_0 , and hence the simple bouncing scenario we are considering here does not strongly discriminate between the wavenumbers of interest. Secondly, the amplitude of b_{NL} is considerably larger. This can be completely attributed to the forms of the coupling functions that we have considered. Moreover, in the $\bar{n} = 3/2$ case, there arises a strong red tilt with, say, b_{NL} behaving as k^{-2} in the equilateral limit, which leads to even larger values (compared to the $\bar{n} = 1$ case, where it is nearly scale invariant) over cosmological scales. In contrast, in de Sitter inflation, b_{NL} is nearly scale invariant in all the limits for both the values of n that we have considered.

5.4 The three-point function in the squeezed limit and the consistency relation

In this section, we shall obtain the consistency relation for the three-point function involving the magnetic field and the scalar perturbation in the case of de Sitter inflation. We shall also discuss its validity in the bouncing scenario.

Let us first consider the case of de Sitter inflation. In the squeezed limit, *i.e.* when $k_1 \rightarrow 0$ and, say, $\mathbf{k}_2 = -\mathbf{k}_3 = \mathbf{k}$, the scalar mode with wavenumber k_1 can be considered to have exited the Hubble radius and hence its amplitude can be treated as a constant, as we have discussed in Subsec. 1.5.5. Therefore, the mode f_k can be extracted out of the integrals (5.12). For the coupling function $J(\phi)$ that we had considered, given the modes (1.134), we obtain that, for arbitrary n [58],

$$\begin{aligned} \mathcal{G}_{\delta\phi BB}^1(\mathbf{k}_1, \mathbf{k}, -\mathbf{k}) &= \frac{i}{M_{\text{Pl}}} \int_{-\infty}^{\eta_e} d\eta J^2(\eta) f_{k_1}^*(\eta) \bar{A}_k'^{*2}(\eta) \\ &\simeq \frac{i}{M_{\text{Pl}}} f_{k_1}^*(\eta_e) \int_{-\infty}^{\eta_e} d\eta J^2(\eta) \bar{A}_k'^{*2}(\eta) \\ &= \frac{i \pi k^2 \eta_e^2 e^{-i n \pi}}{8 M_{\text{Pl}}} f_{k_1}^*(\eta_e) \\ &\quad \times \left\{ \left[H_{n-1/2}^{(2)}(-k \eta_e) \right]^2 - H_{n-3/2}^{(2)}(-k \eta_e) H_{n+1/2}^{(2)}(-k \eta_e) \right\}, \end{aligned} \quad (5.53a)$$

$$\begin{aligned} \mathcal{G}_{\delta\phi BB}^2(\mathbf{k}_1, \mathbf{k}, -\mathbf{k}) &= \frac{i}{M_{\text{Pl}}} k^2 \int_{-\infty}^{\eta_e} d\eta J^2(\eta) f_{k_1}^*(\eta) \bar{A}_k'^{*2}(\eta) \\ &\simeq \frac{i k^2}{M_{\text{Pl}}} f_{k_1}^*(\eta_e) \int_{-\infty}^{\eta_e} d\eta J^2(\eta) \bar{A}_k'^{*2}(\eta) \\ &= \frac{i \pi k^2 \eta_e^2 e^{-i n \pi}}{8 M_{\text{Pl}}} f_{k_1}^*(\eta_e) \\ &\quad \times \left\{ \left[H_{n+1/2}^{(2)}(-k \eta_e) \right]^2 - H_{n-1/2}^{(2)}(-k \eta_e) H_{n+3/2}^{(2)}(-k \eta_e) \right\}. \end{aligned} \quad (5.53b)$$

Adding the contributions due to these two integrals, the three-point function in the

squeezed limit can be written as

$$\begin{aligned}
 G_{\delta\phi BB}(\mathbf{k}_1, \mathbf{k}, -\mathbf{k}) &= \frac{-i \pi^3 H_1^2 \eta_e^5 k^4}{2 M_{\text{Pl}}^2} |f_{k_1}^*(\eta_e)|^2 \\
 &\times \left(\left[H_{n+1/2}^{(1)}(-k \eta_e) \right]^2 \left\{ \left[H_{n-1/2}^{(2)}(-k \eta_e) \right]^2 + \left[H_{n+1/2}^{(2)}(-k \eta_e) \right]^2 \right. \right. \\
 &\quad \left. \left. - H_{n-3/2}^{(2)}(-k \eta_e) H_{n+1/2}^{(2)}(-k \eta_e) - H_{n-1/2}^{(2)}(-k \eta_e) H_{n+3/2}^{(2)}(-k \eta_e) \right\} \right. \\
 &\quad \left. - \left[H_{n+1/2}^{(2)}(-k \eta_e) \right]^2 \left\{ \left[H_{n-1/2}^{(1)}(-k \eta_e) \right]^2 + \left[H_{n+1/2}^{(1)}(-k \eta_e) \right]^2 \right. \right. \\
 &\quad \left. \left. - H_{n-3/2}^{(1)}(-k \eta_e) H_{n+1/2}^{(1)}(-k \eta_e) - H_{n-1/2}^{(1)}(-k \eta_e) H_{n+3/2}^{(1)}(-k \eta_e) \right\} \right).
 \end{aligned} \tag{5.54}$$

Using this result, the expressions for the power spectra of the scalar field and the magnetic field as well as the behavior of Hankel functions $H_\nu(x)$ for small values of x , we can obtain the non-Gaussianity parameter in the squeezed limit to be [58]

$$\lim_{k_1 \rightarrow 0} b_{\text{NL}}(\mathbf{k}_1, \mathbf{k}, -\mathbf{k}) = 2 n_{\text{B}} - 8, \tag{5.55}$$

where, recall that, $n_{\text{B}} = (4 - 2n)$ is the spectral index of the power spectrum of the magnetic field [cf. Eq. (1.138)]. This implies that, in the squeezed limit, $b_{\text{NL}} = -4$ for $n = 1$ and $b_{\text{NL}} = -8$ for $n = 2$, results that we had already arrived at in the previous section.

In the bouncing scenario under consideration, we find that the scalar mode strongly grows as one approaches the bounce and, in fact, also exhibits a slow growth even after the bounce [in this context, see Fig. 5.1 (on page 112)]. Specifically, in contrast to its behavior in de Sitter inflation, the scalar mode f_k does not become a constant at late times. Therefore, it can be expected that, contrary to the reduced integrals (5.53) that we had obtained in the squeezed limit in the inflationary context, the corresponding integrals in bounces would involve all the three modes. Consequently, the consistency relation (5.55) that is valid in the case of de Sitter inflation may not hold true in the bouncing model. On evaluating the three-point function and the non-Gaussianity parameter in the bounce, we find that the consistency relation is indeed violated [141]. The violation of the consistency relation corresponding to the tensor bispectrum in a matter bounce was observed in Chap. 3, and it is interesting to note that a similar behavior is exhibited by the three-point function involving one scalar and two electromagnetic modes as well. This difference in the behavior of the non-Gaussianity parameter between de Sitter inflation and matter bounce scenarios, despite the similarities in the two-point functions obtained in these two models, can potentially serve as a discriminator between the inflationary paradigm and the bouncing scenarios.

5.5 Discussion

The magnetic fields existing on various scales in the universe are considered to have originated from a primordial seed field. Although the generation of such fields via the inflationary mechanism has been well studied, there have been far fewer endeavors to investigate the origin of the primordial magnetic fields in bouncing models. One of the most important signatures of such fields would be the extent of non-Gaussianity associated with the cross-correlations between these fields and the scalar perturbations. These three-point functions have been evaluated in certain inflationary scenarios and it has been found that the corresponding non-Gaussianity parameter can be expected to be quite large.

In the matter bounce scenario of our interest, the modes grow as one approaches the bounce, and grow very slowly thereafter. Due to the enhancement in the amplitude of the modes, it can be expected that the non-Gaussianities associated with the three-point functions would be very large. In Chap. 3, it was shown that despite the growth of the tensor modes in a matter bounce, the corresponding tensor non-Gaussianity is rather small and the consistency relation for the tensor bispectrum is violated [130]. In contrast, in this chapter, we find that the non-Gaussianity parameter associated with the cross-correlations involving the primordial magnetic fields and the scalar perturbations is very large and, in fact, is much larger than what is expected in the de Sitter inflationary scenario. Further, the corresponding consistency relation is violated in the bouncing model. It should be noted that the bouncing scenario that we have considered here suffers from considerable backreaction in the vicinity of the bounce [55, 138], which can possibly be responsible for the large non-Gaussianity that we encounter. The issue of circumventing the backreaction in the proximity of the bounce is non-trivial and needs to be investigated in more detail.

Recall that we have restricted ourselves to the matter bounce scenario. Evidently, other combinations of the parameters \bar{n} and q can also lead to scale invariant magnetic power spectra of relevant amplitude. It would be interesting to examine whether other scenarios that result in similar amplitude for the scale invariant power spectrum also lead to similar results for the non-Gaussianity parameter. Note that the extent of non-Gaussianity depends on $J(\phi)$ as well as $dJ/d\phi$, with the latter depending on ϕ' [cf. Eq. (5.25)]. Therefore, it is important to explore a wide variety of coupling functions $J(\phi)$, some of which may lead to considerably different levels of non-Gaussianity. We are currently exploring some of these issues.

Chapter 6

Enhancing the cross-correlations between magnetic fields and scalar perturbations through parity violation

6.1 Introduction

In the context of primordial magnetogenesis, another interesting aspect is to study the magnetic fields generated due to the addition of a parity violating term to the standard electromagnetic action. Such a term would lead to the generation of the so-called helical magnetic fields [142–145]. In this situation, two modes with positive and negative helicity are generated, which evolve differently and, as a consequence, can conceivably lead to distinct imprints, such as correlations between B-mode and E-mode polarizations or the temperature and B-mode polarizations in the CMB [143, 146]. They can also lead to the production of helical gravitational waves with possible observational imprints (in this context, see, for example, Refs. [143, 146, 147]). Further, it has been shown that, the helical fields evolve strongly in the cosmic magnetohydrodynamic plasma through an inverse cascade mechanism, resulting in an augmentation of the power on large scales [148].

An additional way to constrain these magnetic fields would be to study their cross-correlations at the level of the three-point functions with the scalar perturbations and their possible observational imprints. While such three-point functions have already been studied for the case of non-helical magnetic fields [99–101, 139], we believe it is of utmost interest to study the non-Gaussianities produced due to the helical fields as well. Analytically, the evaluation of these three-point functions seems to be a formidable task, due to the non-trivial form of the helical modes involving the Coulomb functions [143–145]. In this chapter, we shall *numerically* evaluate the three-point function involving the helical magnetic fields and the perturbations in an auxiliary scalar field and examine its

implications.

This chapter is structured as follows. In the next section, we shall discuss the action governing non-minimally coupled helical electromagnetic fields, their quantization and the power spectrum associated with the magnetic field. In Sec. 6.3, working with a specific form of the non-minimal coupling, we shall revisit the evaluation of the power spectrum of helical magnetic fields arising in de Sitter inflation. In Sec. 6.4, by suitably perturbing the action, we shall arrive at the Hamiltonian describing the interaction between the perturbed scalar field and the electromagnetic field. Using the interaction Hamiltonian, we shall arrive at the formal structure of the three-point function describing the cross-correlation between the perturbation in the scalar field and the electromagnetic field. In Sec. 6.5, we shall outline the numerical procedure that we shall adopt to compute the cross-correlation. In Sec. 6.6, we shall first compare our numerical results with the analytical results available in the non-helical case for two different situations (one leading to a power spectrum with a tilt and another which leads to a scale invariant spectrum) and present the corresponding results in the helical case. We shall conclude in Sec. 6.7 with a brief summary of the results we have obtained.

6.2 Non-minimally coupled, helical electromagnetic fields, quantization and power spectrum

We consider the action [145]

$$S_{\text{em}}[A^\mu, \phi] = -\frac{1}{16\pi} \int d^4x \sqrt{-g} \left[J^2(\phi) F_{\mu\nu} F^{\mu\nu} - \frac{\gamma}{2} I^2(\phi) F_{\mu\nu} \tilde{F}^{\mu\nu} \right], \quad (6.1)$$

where, as before, the electromagnetic field tensor $F_{\mu\nu}$ is given by

$$F_{\mu\nu} = \partial_\mu A_\nu - \partial_\nu A_\mu. \quad (6.2)$$

The dual of the electromagnetic tensor $\tilde{F}^{\mu\nu}$ is defined as

$$\tilde{F}^{\mu\nu} = \epsilon^{\mu\nu\alpha\beta} F_{\alpha\beta}, \quad (6.3)$$

with $\epsilon^{\mu\nu\alpha\beta} = (1/\sqrt{-g}) \mathcal{A}^{\mu\nu\alpha\beta}$, where $\mathcal{A}^{\mu\nu\alpha\beta}$ is the totally antisymmetric Levi-Civita tensor and $\mathcal{A}^{0123} = 1$. Clearly, the function $J(\phi)$ describes the non-minimal coupling, while the function $I(\phi)$ (along with the parameter γ) leads to parity violation.

We shall assume that there is no homogeneous component to the electromagnetic field. We shall choose to work in the Coulomb gauge wherein $A_0 = 0$ and $\partial_i A^i = 0$. In such a gauge, at the quadratic order in the inhomogeneous modes, the action describing the electromagnetic field is found to be

$$S[A_i] = \frac{1}{4\pi} \int d\eta \int d^3x \left\{ J^2(\phi) \left[\frac{1}{2} A_i'^2 - \frac{1}{4} (\partial_i A_j - \partial_j A_i)^2 \right] + \gamma I^2(\phi) \epsilon^{ijk} A_i' \partial_j A_k \right\}, \quad (6.4)$$

where ϵ^{ijk} is the three-dimensional completely anti-symmetric tensor. We can vary this action to arrive at the following equation of motion for the electromagnetic vector potential:

$$A_i'' + 2 \frac{J'}{J} A_i' - \nabla^2 A_i = -\frac{\gamma}{J^2} \frac{dI^2}{d\eta} \delta_{il} \epsilon^{lnm} \partial_n A_m. \quad (6.5)$$

For each comoving wave vector \mathbf{k} , we can define the right-handed orthonormal basis $(\epsilon_1^{\mathbf{k}}, \epsilon_2^{\mathbf{k}}, \hat{\mathbf{k}})$, where

$$|\epsilon_i^{\mathbf{k}}|^2 = 1, \quad \epsilon_1^{\mathbf{k}} \times \epsilon_2^{\mathbf{k}} = \hat{\mathbf{k}}, \quad \text{and} \quad \epsilon_1^{\mathbf{k}} \cdot \epsilon_2^{\mathbf{k}} = \hat{\mathbf{k}} \cdot \epsilon_1^{\mathbf{k}} = \hat{\mathbf{k}} \cdot \epsilon_2^{\mathbf{k}} = 0. \quad (6.6)$$

While this is a suitable basis for expressing the non-helical modes, it is not ideally suited for the helical case as the two helical modes would be coupled in this basis. In such a situation, it is convenient to identify two transverse directions to form the helicity basis, wherein the modes decouple, as follows [143, 144]:

$$\epsilon_{\pm}^{\mathbf{k}} = \frac{1}{\sqrt{2}} (\epsilon_1^{\mathbf{k}} \pm i \epsilon_2^{\mathbf{k}}). \quad (6.7)$$

In such a basis, on quantization, the vector potential \hat{A}_i can be Fourier decomposed as [145]:

$$\hat{A}_i(\eta, \mathbf{x}) = \sqrt{4\pi} \int \frac{d^3 \mathbf{k}}{(2\pi)^{3/2}} \sum_{\sigma=\pm} \left[\epsilon_{\sigma i}^{\mathbf{k}} \hat{b}_{\mathbf{k}}^{\sigma} \bar{A}_k^{\sigma}(\eta) e^{i\mathbf{k} \cdot \mathbf{x}} + \epsilon_{\sigma i}^{\mathbf{k}*} \hat{b}_{\mathbf{k}}^{\sigma\dagger} \bar{A}_k^{\sigma}(\eta) e^{-i\mathbf{k} \cdot \mathbf{x}} \right], \quad (6.8)$$

where the Fourier modes \bar{A}_k^{σ} satisfy the differential equation

$$\bar{A}_k^{\sigma''} + 2 \frac{J'}{J} \bar{A}_k^{\sigma'} + \left(k^2 + \frac{\sigma \gamma k}{J^2} \frac{dI^2}{d\eta} \right) \bar{A}_k^{\sigma} = 0. \quad (6.9)$$

Note that $\sigma = \pm 1$, and this causes considerable difference in the evolution of the modes. As we shall see, one of the modes will be strongly amplified on super-Hubble scales and the extent of amplification will depend on the quantity γ . The operators $\hat{b}_{\mathbf{k}}^{\sigma}$ and $\hat{b}_{\mathbf{k}}^{\sigma\dagger}$ are the annihilation and creation operators satisfying the following standard commutation relations:

$$[\hat{b}_{\mathbf{k}}^{\sigma}, \hat{b}_{\mathbf{k}'}^{\sigma'}] = [\hat{b}_{\mathbf{k}}^{\sigma\dagger}, \hat{b}_{\mathbf{k}'}^{\sigma'\dagger}] = 0 \quad \text{and} \quad [\hat{b}_{\mathbf{k}}^{\sigma}, \hat{b}_{\mathbf{k}'}^{\sigma'\dagger}] = \delta^{(3)}(\mathbf{k} - \mathbf{k}') \delta_{\sigma\sigma'}. \quad (6.10)$$

Let us define $\mathcal{A}_k^{\sigma} = J \bar{A}_k^{\sigma}$. In terms of the new variable \mathcal{A}_k^{σ} , Eq. (6.9) can be rewritten as

$$\mathcal{A}_k^{\sigma''} + \left(k^2 - \frac{J''}{J} + \frac{\sigma \gamma k}{J^2} \frac{dI^2}{d\eta} \right) \mathcal{A}_k^{\sigma} = 0. \quad (6.11)$$

In this chapter, we shall restrict ourselves to the simplest scenarios wherein $I = J$. In such a case, the above equation simplifies to

$$\mathcal{A}_k^{\sigma''} + \left(k^2 - \frac{J''}{J} + \frac{2\sigma\gamma k J'}{J} \right) \mathcal{A}_k^{\sigma} = 0. \quad (6.12)$$

Since we shall be only interested in the behavior of the helical magnetic fields, we shall not discuss the electric field in this chapter. Let $\hat{\rho}_B$ denote the operator corresponding to the energy density associated with the magnetic field. Upon using the decomposition (6.8) of the vector potential, the expectation value of the energy density $\hat{\rho}_B$ can be evaluated in the vacuum state, say, $|0\rangle$, that is annihilated by the operator \hat{b}_k^σ for all k and σ . It can be shown that the spectral energy density of the magnetic field can be expressed in terms of the modes \bar{A}_k^σ and the coupling function J as follows [143,145,149]:

$$\mathcal{P}_B(k) = \frac{d\langle 0|\hat{\rho}_B|0\rangle}{d \ln k} = \frac{J^2(\eta)}{4\pi^2} \frac{k^5}{a^4(\eta)} [|\bar{A}_k^+(\eta)|^2 + |\bar{A}_k^-(\eta)|^2]. \quad (6.13)$$

The spectral energy density $\mathcal{P}_B(k)$ is referred to as the power spectrum for the magnetic field. A flat or scale invariant magnetic field spectrum corresponds to a constant, *i.e.* k -independent, $\mathcal{P}_B(k)$.

6.3 Power spectra of the helical magnetic fields generated in de Sitter inflation

Let us consider the simple case of de Sitter inflation, wherein the scale factor is given by Eq. (1.107a), where H_I is the value of the Hubble parameter during inflation. In order to solve for the electromagnetic modes, we need to choose a form of the coupling function. We shall work with a coupling function of the form given by Eq. (1.131), which ensures that J reduces to unity at η_e .

For the form of the coupling function given by Eq. (1.131), the solutions to the electromagnetic modes satisfying Eq. (6.12) can be written as follows [58,145,150]:

$$\mathcal{A}_k^\sigma(\eta) = \frac{1}{\sqrt{2k}} [G_n(\sigma\xi, -k\eta) + i F_n(\sigma\xi, -k\eta)], \quad (6.14)$$

where $G_n(\sigma\xi, -k\eta)$ and $F_n(\sigma\xi, -k\eta)$ represent the irregular and regular Coulomb functions respectively and $\xi = -n\gamma$. For $-k\eta \ll \sigma\xi$, which corresponds to modes of interest, the contribution of $F_n(\sigma\xi, -k\eta)$ to the mode is negligible. We also find that the mode with negative helicity (*i.e.* with $\sigma = -1$) is amplified in comparison to the positive helicity mode. In this regime, the irregular Coulomb function can be written in terms of the modified Bessel function $K_\nu(z)$ as follows [150]:

$$G_L(y, z) = \frac{2(2y)^L}{(2L+1)! C_L(y)} (2yz)^{1/2} K_{2L+1}(\sqrt{8yz}), \quad (6.15)$$

where $C_L(y)$ is given by

$$C_L(y) = \frac{2^L e^{-\pi y/2} |\Gamma(L+1+iy)|}{\Gamma(2L+2)}. \quad (6.16)$$

Hence the modes (6.14) reduce to

$$\mathcal{A}_k^-(\eta) \simeq \sqrt{-\frac{2\eta}{\pi}} e^{-\pi\xi} K_{2n+1} \left(\sqrt{8\xi k \eta} \right). \quad (6.17)$$

Also, for $-k\eta \ll 1/\xi$, which corresponds to late times during inflation, using the properties of the modified Bessel function for small arguments, we obtain that [151]

$$\mathcal{A}_k^-(\eta) \simeq \sqrt{-\frac{\eta}{2\pi}} e^{-\pi\xi} \Gamma(|2n+1|) |2\xi k \eta|^{-|n+\frac{1}{2}|}. \quad (6.18)$$

Therefore, using Eq. (6.13), the power spectrum for the magnetic field evaluated as $\eta_e \rightarrow 0$ can be expressed as [145]

$$\mathcal{P}_B(k) \simeq \frac{H_1^4}{8\pi^3} e^{-2\pi\xi} [\Gamma(|2n+1|)]^2 |2\xi|^{-2|n+\frac{1}{2}|} (k\eta_e)^{5-2|n+\frac{1}{2}|}. \quad (6.19)$$

Evidently, the spectral index n_B [cf. Eq. (1.138)] of the power spectrum of the magnetic field is given by

$$n_B = 5 - 2 \left| n + \frac{1}{2} \right|. \quad (6.20)$$

This implies that we obtain a scale invariant power spectrum for the magnetic field when $n = -3$ or $n = 2$, just as in the non-helical case. Note that the power spectrum is completely independent of time in these situations. However, when $n < 0$, it is found that the energy in the electromagnetic field grows rapidly at late times. As we have discussed earlier, such a growth leads to severe backreaction and can result in the termination of inflation within a few e-folds [99–101]. Because of this reason, in this chapter, we shall focus only on the cases wherein $n > 0$.

6.4 Formal structure of the three-point function

In the preceding section, when we had considered the evolution of the electromagnetic modes, for simplicity, we had assumed the non-minimal coupling $J(\eta)$ to be given by Eq. (1.131). However, as discussed in Subsec. 5.2.1, in order to evaluate the cross-correlation between the perturbation in the scalar field and the magnetic field, other than J , we shall also require the function $J_\phi = dJ/d\phi$. Since $J_\phi = J'/\phi'$ and, as $J(\eta)$ has been chosen already [cf. Eq. (1.131)], clearly, we can arrive at $dJ/d\phi$ if we know ϕ' . This can be achieved by choosing a potential $V(\phi)$ to drive the scalar field. Then, a suitable $J(\phi)$ can lead to the desired $J(\eta)$.

Note that, we have assumed the electromagnetic field to be inhomogeneous. In order to calculate the three-point function involving perturbations in the scalar field and the

electromagnetic vector potential, we need the interaction Hamiltonian at the third order in the perturbations. This can be arrived at by perturbing the electromagnetic action (6.1) with respect to the scalar field. It is straightforward to show that the third order action for the case $I = J$ is given by

$$S[A_i] = \frac{1}{2\pi} \int d\eta \int d^3\mathbf{x} J J_\phi \delta\phi \left\{ \left[\frac{1}{2} A_i'^2 - \frac{1}{4} (\partial_i A_j - \partial_j A_i)^2 \right] + \gamma \epsilon^{ijk} A_i' \partial_j A_k \right\}. \quad (6.21)$$

The interaction Hamiltonian can be obtained from this third order action. It is found to be

$$H_{\text{int}} = \frac{1}{4\pi} \int d^3\mathbf{x} J J_\phi \delta\phi \left\{ A_i'^2 + \frac{1}{2} (\partial_i A_j - \partial_j A_i)^2 \right\}. \quad (6.22)$$

Two points need to be stressed regarding this interaction Hamiltonian [152]. Firstly, the parity violating term does not contribute to the Hamiltonian. This implies that the formal structure of the resulting three-point function will be largely similar to the non-helical case that has been considered earlier in the last chapter [99–101, 139, 141]. Secondly, as we shall see below, the effects of non-zero helicity will be essentially encoded in the way it affects the evolution of the modes.

The cross-correlation between the perturbation in the scalar field and the magnetic field in real space is defined as

$$\begin{aligned} & \left\langle \frac{\hat{\delta}\phi(\eta, \mathbf{x})}{M_{\text{Pl}}} \hat{B}^i(\eta, \mathbf{x}) \hat{B}_i(\eta, \mathbf{x}) \right\rangle \\ &= \int \frac{d^3\mathbf{k}_1}{(2\pi)^{3/2}} \int \frac{d^3\mathbf{k}_2}{(2\pi)^{3/2}} \int \frac{d^3\mathbf{k}_3}{(2\pi)^{3/2}} \left\langle \frac{\hat{\delta}\phi_{\mathbf{k}_1}(\eta)}{M_{\text{Pl}}} \hat{B}_{\mathbf{k}_2}^i(\eta) \hat{B}_{\mathbf{k}_3}(\eta) \right\rangle e^{i(\mathbf{k}_1 + \mathbf{k}_2 + \mathbf{k}_3) \cdot \mathbf{x}}, \end{aligned} \quad (6.23)$$

where the components B_i of the magnetic field are related to the vector potential A_i through the relation

$$B_i = \frac{1}{a} \epsilon_{ijl} \partial_j A_l, \quad (6.24)$$

while $\hat{\delta}\phi_{\mathbf{k}}$ and $\hat{B}_{\mathbf{k}}^i$ denote the Fourier modes associated with the perturbation in the scalar field and the i -th component of the magnetic field. As per the standard rules of perturbative quantum field theory, the cross-correlation between the perturbation in the scalar field and the magnetic field in Fourier space, evaluated at the end of inflation, is given by [99, 101]

$$\left\langle \frac{\hat{\delta}\phi_{\mathbf{k}_1}(\eta_e)}{M_{\text{Pl}}} \hat{B}_{\mathbf{k}_2}^i(\eta_e) \hat{B}_{\mathbf{k}_3}(\eta_e) \right\rangle = -i \int_{\eta_i}^{\eta_e} d\eta \left\langle \left[\frac{\hat{\delta}\phi_{\mathbf{k}_1}(\eta)}{M_{\text{Pl}}} \hat{B}_{\mathbf{k}_2}^i(\eta) \hat{B}_{\mathbf{k}_3}(\eta), \hat{H}_{\text{int}}(\eta) \right] \right\rangle, \quad (6.25)$$

where \hat{H}_{int} is the operator associated with the Hamiltonian (6.22) and the square brackets indicates the commutator.

We had discussed the quantization of the helical electromagnetic field in the previous section. The quantization of the perturbation in the scalar field $\delta\phi$ was discussed in Sec. 5.2 [cf. Eq. (5.6)]. We can now determine the three-point function using the expression (6.25), along with the form of the interaction Hamiltonian (6.22) and Wick's theorem that applies to the products of Gaussian operators. We find that the cross-correlation $G_{\delta\phi BB}(\mathbf{k}_1, \mathbf{k}_2, \mathbf{k}_3)$ [cf. Eq. (5.10)] can be expressed as [153]

$$\begin{aligned}
 G_{\delta\phi BB}(\mathbf{k}_1, \mathbf{k}_2, \mathbf{k}_3) = & \frac{8\pi}{M_{\text{Pl}} a^2(\eta_e)} [(\mathbf{k}_2 \cdot \mathbf{k}_3) \delta_{qn} - k_{2n} k_{3q}] \sum_{\sigma \sigma'} f_{k_1}(\eta_e) \bar{A}_{k_2}^\sigma(\eta_e) \bar{A}_{k_3}^{\sigma'}(\eta_e) \\
 & \times \left\{ \varepsilon_{\sigma q}(\mathbf{k}_2) \varepsilon_{\sigma l}^*(\mathbf{k}_2) \varepsilon_{\sigma' n}(\mathbf{k}_3) \varepsilon_{\sigma' l}^*(\mathbf{k}_3) \mathcal{G}_1^{\sigma\sigma'}(\mathbf{k}_1, \mathbf{k}_2, \mathbf{k}_3) \right. \\
 & - \left[\frac{(\mathbf{k}_2 \cdot \mathbf{k}_3)}{k_2 k_3} \varepsilon_{\sigma q}(\mathbf{k}_2) \varepsilon_{\sigma r}^*(\mathbf{k}_2) \varepsilon_{\sigma' n}(\mathbf{k}_3) \varepsilon_{\sigma' r}^*(\mathbf{k}_3) \right. \\
 & \left. \left. - \frac{(k_{2l} k_{3r})}{k_2 k_3} \varepsilon_{\sigma q}(\mathbf{k}_2) \varepsilon_{\sigma r}^*(\mathbf{k}_2) \varepsilon_{\sigma' n}(\mathbf{k}_3) \varepsilon_{\sigma' l}^*(\mathbf{k}_3) \right] \mathcal{G}_2^{\sigma\sigma'}(\mathbf{k}_1, \mathbf{k}_2, \mathbf{k}_3) \right\} \\
 & + \text{complex conjugate}, \tag{6.26}
 \end{aligned}$$

where the quantities $\mathcal{G}_1^{\sigma\sigma'}(\mathbf{k}_1, \mathbf{k}_2, \mathbf{k}_3)$ and $\mathcal{G}_2^{\sigma\sigma'}(\mathbf{k}_1, \mathbf{k}_2, \mathbf{k}_3)$ are described by the integrals

$$\mathcal{G}_1^{\sigma\sigma'}(\mathbf{k}_1, \mathbf{k}_2, \mathbf{k}_3) = i \int_{\eta_i}^{\eta_e} d\eta J \frac{dJ}{d\phi} f_{k_1}^*(\eta) \bar{A}_{k_2}^{*\sigma}(\eta) \bar{A}_{k_3}^{\prime\sigma'}(\eta), \tag{6.27a}$$

$$\mathcal{G}_2^{\sigma\sigma'}(\mathbf{k}_1, \mathbf{k}_2, \mathbf{k}_3) = i k_2 k_3 \int_{\eta_i}^{\eta_e} d\eta \left(J \frac{dJ}{d\phi} \right) f_{k_1}^*(\eta) \bar{A}_{k_2}^{*\sigma}(\eta) \bar{A}_{k_3}^{\prime\sigma'}(\eta). \tag{6.27b}$$

6.5 Numerical evaluation of the three-point function

It is evident that evaluating the cross-correlation of our interest involves integrals over products of the electromagnetic modes and the modes corresponding to the perturbation in the scalar field. Earlier, we had solved for the electromagnetic modes analytically in order to arrive at the power spectrum. The analytical solutions entail writing the modes in terms of Coulomb functions [cf. Eq. (6.14)], which seem non-trivial to integrate. Therefore, in order to evaluate the three-point function, we shall resort to numerical computations. In order to obtain the three-point function, we need to solve for the electromagnetic modes as well as for the modes of the scalar perturbations numerically. Thereafter, we need to integrate these modes in order to arrive at the complete three-point function.

6.5.1 Evolution of the modes

Let us first discuss the method we shall adopt to numerically solve for the electromagnetic and scalar modes \bar{A}_k^σ and f_k . The most efficient time variable to perform numerical

analyses in inflationary scenarios is the e-fold N . In terms of e-folds, for the $I = J$ case, Eq. (6.9) can be written as

$$\frac{d^2 \bar{A}_k^\sigma}{dN^2} + \left(\frac{\mathcal{H}_N}{\mathcal{H}} + 2 \frac{J_N}{J} \right) \frac{d \bar{A}_k^\sigma}{dN} + \left(\frac{k^2}{\mathcal{H}^2} + \frac{2 \sigma \gamma k}{\mathcal{H}} \frac{J_N}{J} \right) \bar{A}_k^\sigma = 0, \quad (6.28)$$

where the subscript N refers to a derivative with respect to the e-fold. For the case of de Sitter inflation and the form of the coupling function under consideration, we obtain that $\mathcal{H}_N/\mathcal{H} = 1$ and $J_N/J = n$. Under these conditions, the above differential equation simplifies to

$$\frac{d^2 \bar{A}_k^\sigma}{dN^2} + (2n + 1) \frac{d \bar{A}_k^\sigma}{dN} + \left(\frac{k^2}{\mathcal{H}^2} + \frac{2 \sigma \gamma k n}{\mathcal{H}} \right) \bar{A}_k^\sigma = 0. \quad (6.29)$$

Similarly, Eq. (5.9) governing the evolution of the scalar modes can be rewritten as

$$\frac{d^2 f_k}{dN^2} + \left(2 + \frac{\mathcal{H}_N}{\mathcal{H}} \right) \frac{d f_k}{dN} + \frac{k^2}{\mathcal{H}^2} f_k = 0, \quad (6.30)$$

which, for the case of de Sitter inflation, simplifies to

$$\frac{d^2 f_k}{dN^2} + 3 \frac{d f_k}{dN} + \frac{k^2}{\mathcal{H}^2} f_k = 0. \quad (6.31)$$

Recall that, during inflation, in the case of the scalar and tensor modes, the standard Bunch-Davies initial conditions are imposed on the modes when they are well inside the Hubble radius. It is clear from Eq. (6.12) governing the dynamics of the electromagnetic modes that, at very early times, it is the term involving k^2 that dominates the other two terms within the parentheses. In fact, we find that, for the coupling function of our choice [cf. Eq. (1.131)], it is the second term that dominates the third during the early stages. These properties permit us to impose Bunch-Davies like initial conditions on the modes, and evolve them thereafter. Numerically, we shall impose the initial conditions when $k = 300 \sqrt{J''/J}$, corresponding to the e-fold, say, N_i (this specific choice will be justified in the next subsection). In terms of e-folds, the standard initial conditions on the modes can be expressed as follows:

$$\bar{A}_k^\sigma \Big|_{N_i} = \frac{1}{J(N_i) \sqrt{2k}}, \quad (6.32a)$$

$$\frac{d \bar{A}_k^\sigma}{dN} \Big|_{N_i} = -\frac{n}{J(N_i) \sqrt{2k}} - \frac{i k}{\mathcal{H}(N_i) J(N_i) \sqrt{2k}}. \quad (6.32b)$$

We then solve Eq. (6.29) with these initial conditions using a fifth order Runge-Kutta routine to obtain the behavior of \bar{A}_k^σ . The differential equation (6.31) governing the scalar modes can be solved for in a similar manner. The initial conditions on the scalar modes

are given by

$$f_k \Big|_{N_i} = \frac{1}{a(N_i) \sqrt{2k}}, \quad (6.33a)$$

$$\frac{df_k}{dN} \Big|_{N_i} = \frac{1}{\mathcal{H}(N_i) a(N_i) \sqrt{2k}} [-ik - \mathcal{H}(N_i)]. \quad (6.33b)$$

After imposing these initial conditions on the modes, we shall evolve them till about 42 e-folds for $n = 1$ and up to 30 e-folds for the $n = 2$ case (the reason for these choices will be explained later).

In Fig. 6.1, we have plotted the numerical solutions for the helical as well as the non-helical electromagnetic modes for the cases of $n = 1$ and $n = 2$. It is evident from the plots that the modes with negative helicity (*i.e.* with $\sigma = -1$) are amplified when compared to the non-helical case, around the time they leave the Hubble radius [153]. Also, one finds that the amplitude of the modes with positive helicity (*i.e.* with $\sigma = 1$) are suppressed when compared with the non-helical modes around Hubble exit. Moreover, the amplification and suppression is more in the case of $n = 2$ than $n = 1$. This is to be expected because of the reason that, larger the n , larger is the amplitude of the parity violating term [cf. Eq. (6.29)].

6.5.2 Evaluation of the three-point function

Before we go on to consider the cross-correlation of our interest, let us make a few clarifying remarks concerning the numerical evaluation of the inflationary two-point and three-point functions involving the scalar and the tensor perturbations. The inflationary correlation functions are formally expected to be evaluated at the end of inflation. However, it is well known that, during inflation, the amplitude of the scalar and the tensor perturbations freeze on super-Hubble scales (apart from some peculiar situations). This behavior makes it convenient for the numerical evaluation of the power spectra, since they can be evaluated soon after the modes leave the Hubble radius. Typically, the initial conditions are imposed when the modes are sufficiently inside the Hubble radius [say, when $k/(aH) \simeq 10^2$] and the power spectra are evaluated when the modes are sufficiently outside [say, when $k/(aH) \simeq 10^{-5}$]. As far as the three-point functions are concerned, apart from arriving at the modes, we also need to integrate over them from very early to late times. One can show that, due to the abovementioned freezing of the amplitude of the perturbations, the super-Hubble contributions to the three-point functions are insignificant (in this context, see, for instance, Refs. [76, 78, 83]). Since the three-point function involves an arbitrary triangular configuration of wavevectors, to arrive at them, the initial conditions are imposed when the mode with the smallest of the wavenumbers is sufficiently inside the Hubble radius (say, at the e-fold N_i) and the integrals involved

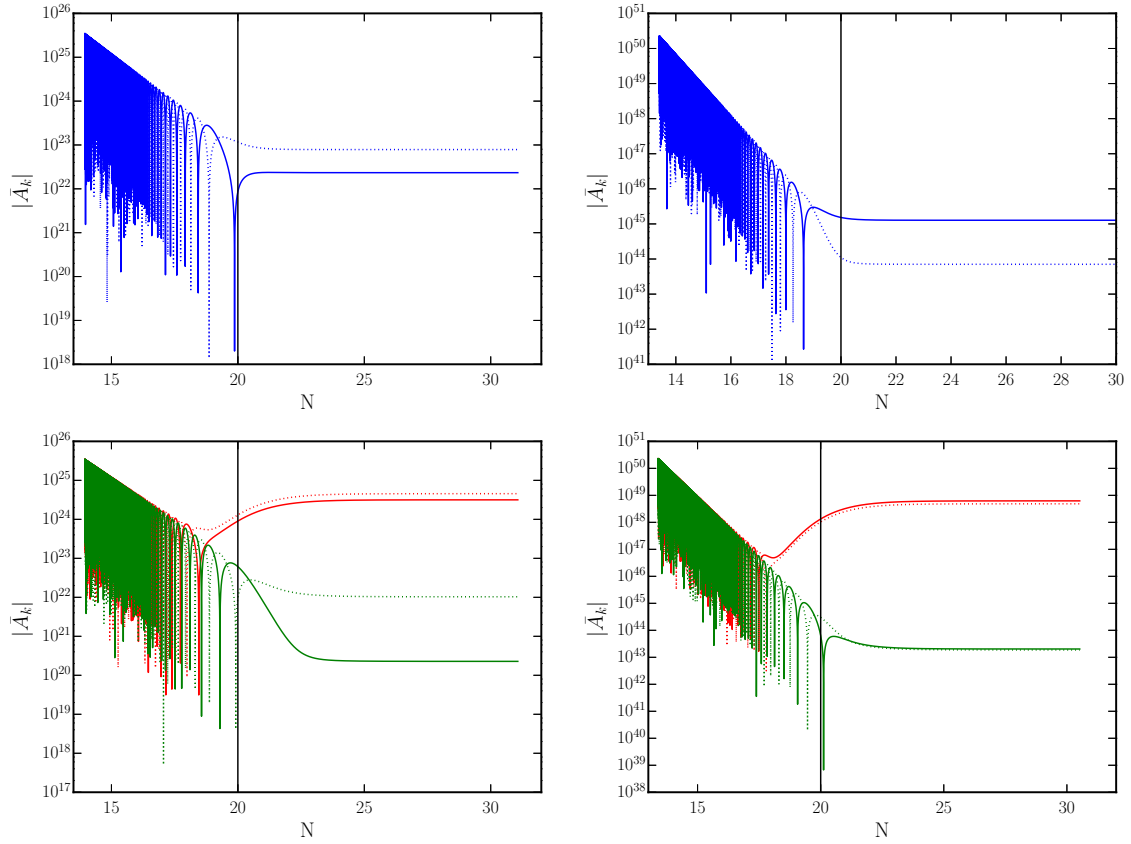


Figure 6.1: The evolution of the mode \bar{A}_k^σ has been plotted as a function of e-folds N for $n = 1$ (on the left) and $n = 2$ (on the right) for the wavenumber $k = 0.002 \text{ Mpc}^{-1}$ for the cases $\gamma = 0$ (on top, in blue) and $\gamma = 2$ (at the bottom, in red and green). We have plotted the absolute values of the real (solid lines) and imaginary (dashed lines) parts separately so that the oscillations are visible. The vertical black line in each plot indicates the e-fold at which the modes leave the Hubble radius. Note that, around the time when the modes leave the Hubble radius, the $\sigma = -1$ mode (in red) is amplified when compared to the non-helical case, whereas the $\sigma = 1$ mode (in green) is suppressed. Also, as expected, the amplification and suppression are more in the $n = 2$ case than in the $n = 1$ case.

are evaluated until the mode with the largest of the wavenumbers is adequately outside (say, at N_s) [76, 78, 83, 154].

There is yet another point to be attended to when evaluating the three-point functions numerically. All the modes will oscillate strongly in the sub-Hubble domain. Therefore, in order to evaluate the integrals involved, analytically, a small parameter, say, κ , is introduced to achieve an exponential cut-off and thereby regulate these oscillations (see our discussion in Chap. 1). Actually, as we had also mentioned earlier, such a regulation is essential to ensure the correct choice of the perturbative quantum vacuum [66, 72]. One eventually considers the vanishing limit of the parameter κ to arrive at the final forms of

the three-point functions. The regulator proves to be very convenient in the numerical efforts, as it can ensure the convergence of the integrals. But, a couple of exercises need to be carried out to identify an apt value for the cut-off parameter such that the resulting three-point function is ideally independent of the choice of κ , N_i and N_s . We find that the above arguments for the scalar and the tensor perturbations can be applied to the cross-correlation of our interest for the $n = 1$ case. However, the $n = 2$ case poses a peculiar difficulty not often encountered in the three-point functions involving the scalars and the tensors, and needs to be handled with care. We shall make use of the analytical expressions available in the non-helical case to check the accuracy of our numerical computations.

In order to identify suitable values of κ , N_i and N_s , we shall evaluate the two contributions to the three-point function of our interest [described by the integrals (6.27)] in the equilateral limit for different combinations of these variables. Earlier, we had mentioned that we solve the differential equations involved [*viz.* Eqs. (6.29) and (6.31)] using the fifth order Runge-Kutta routine. We shall carry out the integrals (6.27) using the Boole's rule [155]. We should add that, in our discussion hereafter, for convenience, we shall simply set the polarization tensor $\varepsilon_{\sigma i}^k$ to unity. However, we shall include all the contributions due to the positive and negative helicity modes as well as the cross terms that arise. We shall first keep N_s fixed and calculate the quantities for three different values of N_i and varied κ . This helps us identify a suitable combination of N_i and κ for which the three-point function is insensitive to the choice of these variables. We shall then choose these values of N_i and κ and attempt to identify a suitable choice for N_s . The results of these exercises are plotted in Figs. 6.2 and 6.3 for both the non-helical and helical cases for $n = 1$ as well as $n = 2$. In Fig. 6.2, we have illustrated the dependence of the two contributions to the three-point function on the sub-Hubble cut-off parameter κ for different choices of N_i . It is clear from the figure that, for instance, for N_i corresponding to $k = 300 \sqrt{J''/J}$, the two contributions to the three-point function are largely independent of κ around $\kappa = 0.1$. Therefore, we shall work with these values.

Let us now turn to determining a suitable N_s . With κ and N_i fixed at the aforementioned values, in Fig. 6.3 (on page 134), we have plotted the two contributions as a function of N_s . Note that, in the $n = 1$ case, the results are independent of the choice N_s , provided we choose it corresponding to a time reasonably after Hubble exit. In contrast, when $n = 2$, it is clear from the figure that there is a slow growth as a function of N_s . Such a behavior is peculiar to the model and the choices of the parameter involved. This growth is well known from the analytical calculations and, in the non-helical case, it can be shown to behave as $\ln(-k \eta_e)$ (in the equilateral limit we are focusing on) [101, 141], which is exactly the behavior we observe numerically. It is also clear from Fig. 6.3 (on page 134) that the introduction of helicity considerably enhances the amplitude of the three-point function in both the $n = 1$ and $n = 2$ cases. Moreover, it is evident that the enhancement occurs as the modes leave the Hubble radius, which is further accentuated

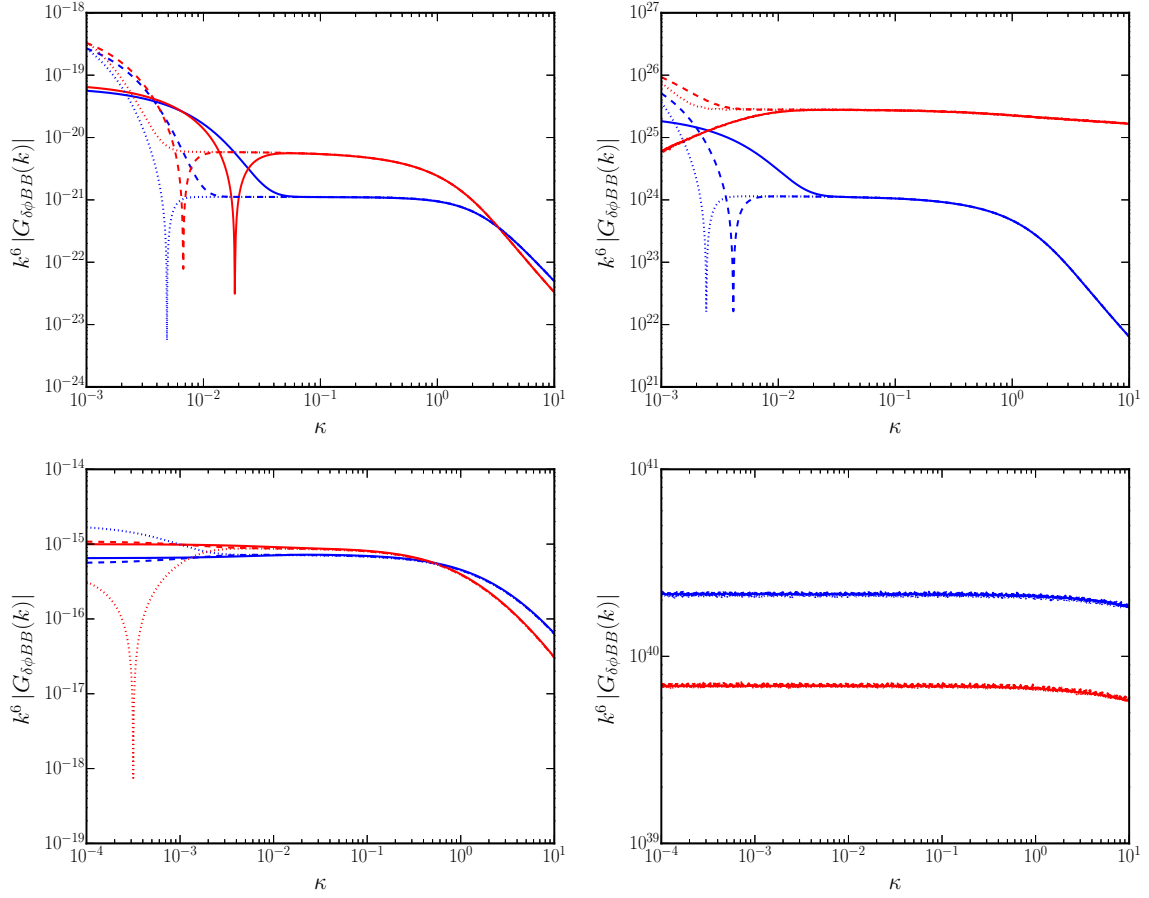


Figure 6.2: The amplitudes of the contributions to the three-point function arising from the first (in blue) and second (in red) integrals [cf. Eqs. (6.27)] have been plotted for the $n = 1$ case (on the left) and the $n = 2$ case (on the right) as functions of the cut-off parameter κ . We have plotted the results for three different choices of N_i corresponding to $k = 100 \sqrt{J''/J}$ (as solid lines), $k = 500 \sqrt{J''/J}$ (as dashed lines) and $k = 1000 \sqrt{J''/J}$ (as dotted lines). Also, we have plotted them for the non-helical case (on top) as well as the helical case with $\gamma = 2$ (at the bottom). Note that the two contributions to the three-point function have been multiplied with suitable powers of k . It should be clear from the above plots that, for the choice of $k = 300 \sqrt{J''/J}$, the resulting contributions are largely insensitive to κ around $\kappa = 0.1$. Because of this reason, we shall choose to evaluate the three-point function and the corresponding non-Gaussianity parameter (see the next section) for this choice of values. It is also useful to note from the final plot that the three-point function corresponding to $n = 2$ in the helical case is largely unaffected by the value of the sub-Hubble cut-off parameter. As we shall see in the next figure, this occurs due to the fact that the dominant contribution to this three-point function arises from the super-Hubble domain.

in the $n = 2$ case due to the super-Hubble contributions that arise. While the results will be independent of N_s in the $n = 1$ case, they will strongly depend on the parameter when $n = 2$. Ideally, it would have been desirable to evaluate the three-point function when inflation ends at 60 e-folds or so since the earliest time when, say, the largest scale was sufficiently inside the Hubble radius. However, evolving the modes for this duration and evaluating the integrals introduce inaccuracies after about 30 e-folds or so. Therefore, we shall evaluate the three-point function in the $n = 2$ case for $N_s \simeq 30$.

6.6 Amplitude and shape of the non-Gaussianity parameter

In this section, we shall numerically evaluate the dimensionless non-Gaussianity parameter b_{NL} which characterizes the amplitude and shape of the three-point function involving the helical magnetic field and the perturbations in the scalar field. This parameter was introduced in Sec. 5.3. Here we shall present the numerical results for b_{NL} for the different cases we had discussed. In order to illustrate the accuracy of our numerical methods, we shall also compare our numerical results with the analytical results that are available in the non-helical case.

In Fig. 6.4, we have plotted the numerical results for the non-Gaussianity parameter b_{NL} (for an arbitrary triangular configuration of wavevectors, in this context, see Ref. [141]) for the cases of $n = 1$ and $n = 2$ when $\gamma = 0$ and $\gamma = 2$. We have also plotted the analytical results available for $n = 1$ and $n = 2$ in the non-helical case, to illustrate the extent of accuracy of our numerical methods. On comparing the results in the non-helical case for $n = 1$ and $n = 2$, we find that the analytical and numerical results match up to about 5–10%. Recall that we have been working with $\gamma = 2$. Even for such a relatively small value of γ , we find that the introduction of helicity considerably amplifies non-Gaussianities [153].

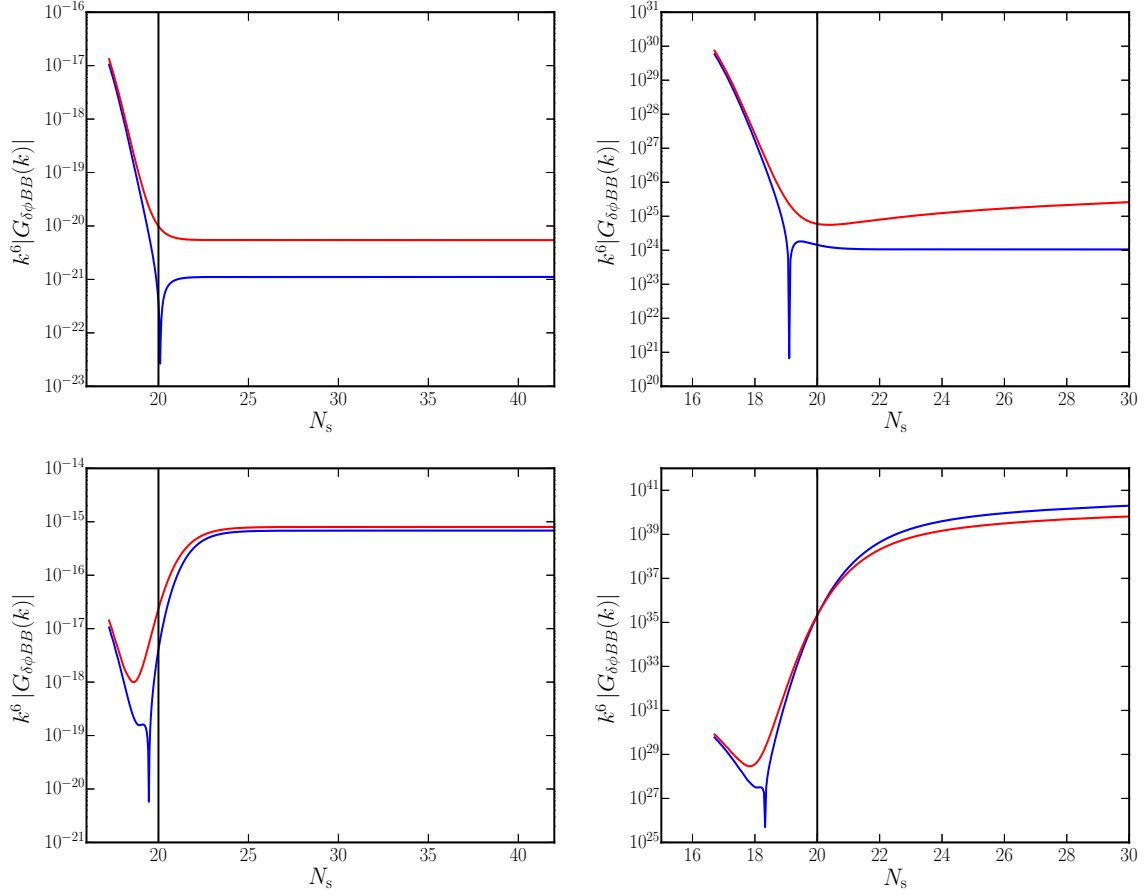


Figure 6.3: The amplitudes of the contributions to the three-point function arising from the first and the second integrals have been plotted for the $n = 1$ and the $n = 2$ cases as functions of N_s , with the same choice of colors as in the previous figure. Also, we have plotted the non-helical and the helical cases just as in the last figure. We have imposed the initial condition at an N_i corresponding to $k = 300 \sqrt{J''/J}$, and we have set $\kappa = 0.1$ in arriving at the above plots. We have plotted the results for a mode with the wavenumber $k = 0.002 \text{ Mpc}^{-1}$, which is often chosen as the pivot scale when comparing with the observations. The vertical black lines in the plots indicate the e-fold at which the mode leaves the Hubble radius. Note that, in the $n = 1$ case, the amplitude of the two terms freeze soon after Hubble exit, which implies that the super-Hubble contributions to the three-point function are negligible. This is true in the corresponding helical case as well. When $n = 2$, for the non-helical case, even though the first integral flattens out in the super-Hubble limit, the contribution due to the second integral continues to grow. This behavior has been encountered in analytical calculations and it can be attributed to the $\ln(-k\eta_e)$ term that arises in this case. It is also clear from the plots that the introduction of helicity considerably enhances the amplitude of the three-point functions. Moreover, the enhancement occurs around the time the mode leaves the Hubble radius. This is further accentuated by the super-Hubble contributions that are encountered in the $n = 2$ case.

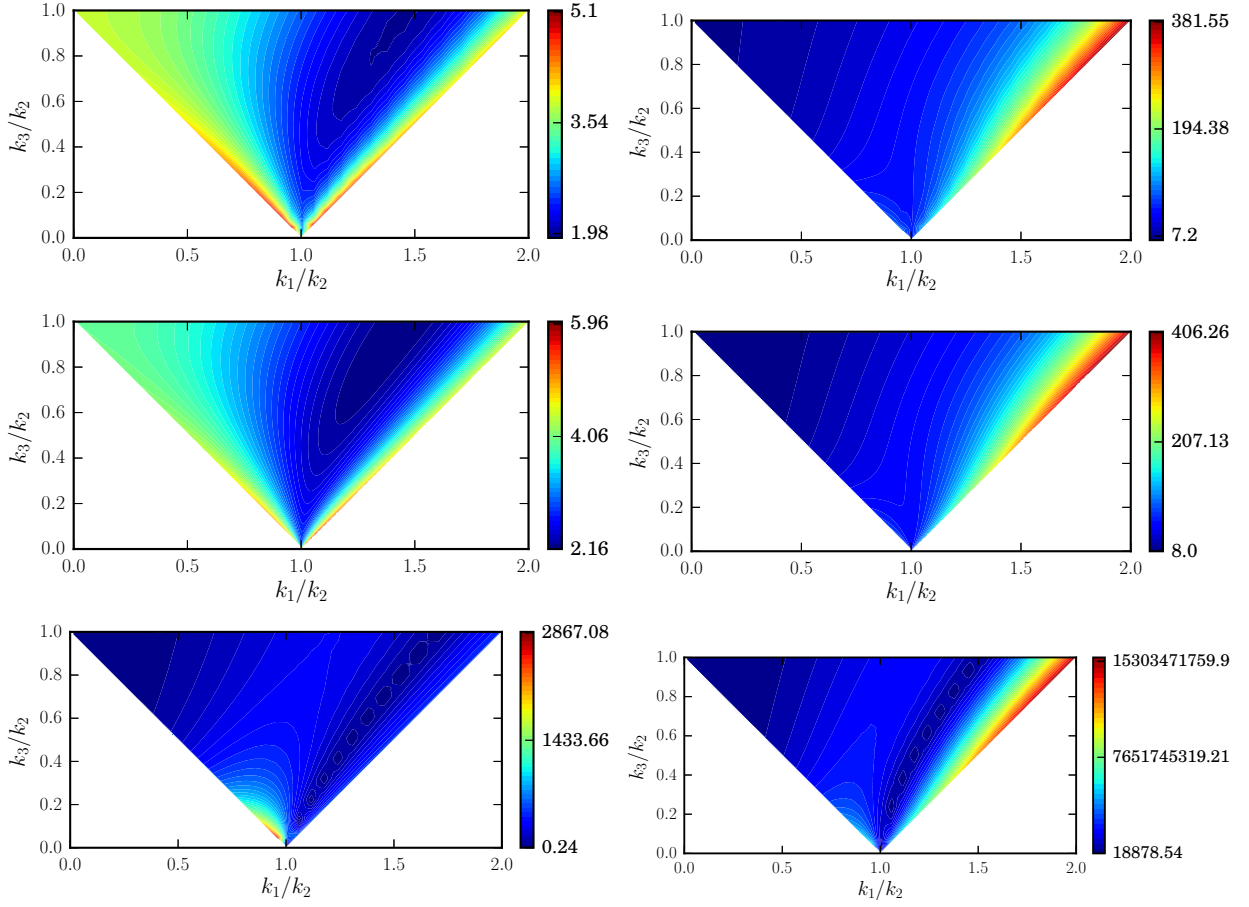


Figure 6.4: The non-Gaussianity parameter b_{NL} has been plotted for the non-helical case obtained numerically (top row), analytically (middle row), and the helical case arrived at numerically (third row of plots) for the cases of $n = 1$ (on the left) and $n = 2$ (on the right). For reasons we have discussed, in the $n = 2$ case, we have evaluated the non-Gaussianity parameter corresponding to $N_s \sim 30$. From the first and second rows, we find that the analytical and numerical results match up to 5–10%. It is evident from the third row of plots that the helical term substantially boosts the value of b_{NL} for both the $n = 1$ and $n = 2$ cases, with the amplification being larger for $n = 2$.

6.7 Discussion

The generation and evolution of primordial magnetic fields has been studied extensively in the context of inflation. By introducing a non-minimal coupling term in the standard electromagnetic action, it has been possible to obtain scale invariant magnetic fields of the requisite amplitude to be in conformity with the observations. It has also been realized that adding a parity violating term to the electromagnetic action results in the production of helical magnetic fields, which can have significant observational imprints [143, 146,

147]. Specifically, helicity considerably boosts the amplitude of the power spectrum of the magnetic field.

The non-Gaussian signatures generated via cross-correlations between the primordial magnetic fields and the perturbations in a scalar field can provide additional constraints to characterize the magnetic fields. These non-Gaussianities, at the level of three-point functions, have been examined earlier in the non-helical case [99–101, 139]. In this chapter, we have numerically evaluated the three-point functions involving primordial helical magnetic fields and the perturbations in a scalar field. Since the introduction of the helical term in the action amplifies the strength of the magnetic field, it can also be expected to lead to larger non-Gaussianities. We have found that even with a small value of the parameter quantifying the extent of helicity, there is a substantial enhancement in the non-Gaussianity parameter b_{NL} . It would be interesting to explore related observational consequences, and possibly arrive at constraints on the mechanisms that could lead to the generation of the helical magnetic fields (in this context, see Ref. [140]). Another important aspect would be to investigate into the behavior of the three-point functions involving the helical magnetic fields and the curvature perturbation [101, 139]. Importantly, in such a case, one may encounter additional terms arising in the action describing the interaction term. Also, while the magnitude of b_{NL} in, say, slow roll inflation, may not differ substantially from the case we have examined, considering the curvature perturbation can provide us with additional parameters (*viz.* the slow roll parameters) to more effectively constrain the non-Gaussianities generated. We are presently working on these issues.

Chapter 7

Conclusions

7.1 Summary of work done

In light of the unprecedented advancement in obtaining accurate cosmological data, it has been possible to compare theoretical models of the early universe with observations at extraordinary levels of precision. The inflationary paradigm has emerged as the most widely accepted theoretical framework to describe the early universe [20–22]. The relative efficacy of constructing inflationary models has led to the advent of a surfeit of models, most of which are in conformity with observations at the level of two-point functions [61], especially in the absence of a direct detection of primordial tensor modes on cosmological scales. This has compelled us to look for additional observables that can constrain the class of inflationary models more effectively. In this context, non-Gaussian signatures, primarily at the level of three-point functions, have amassed a lot of attention [73,74,106]. It is expected that bounds on non-Gaussianities would be instrumental in restricting the available set of inflationary models into a smaller viable class. Moreover, features in the inflationary potential are known to lead to non-trivial characteristics in the power spectra and the three-point functions, the observational signatures of which can conceivably rule out a large class of models [108,109]. Further, propositions of alternative scenarios, such as bouncing models, have been put forward [27,52]. These models, albeit onerous to construct, seem to be feasible and often lead to similar predictions as inflation, especially at the level of two-point functions. It seems imperative to arrive at observables that can possibly distinguish between inflation and bouncing scenarios. Comparing and contrasting between three-point functions generated in these alternative frameworks seems to hold much promise in this regard. Additionally, the effects due to the presence of gauge fields, such as electromagnetic fields present in the early universe, are also interesting to examine [14,87]. In particular, the imprints of these fields on the primordial scalar and tensor perturbations can lead to potentially observable signatures on the CMB and LSS. With this objective in mind, in this thesis, we have studied the three-point functions gen-

erated in the presence of features in an inflationary model. We have also considered a specific bouncing scenario and, after analytically evaluating the tensor non-Gaussianity in the model, we have compared its characteristics with a standard de Sitter inflationary scenario. We have also investigated the origin and characteristics of primordial magnetic fields in the bouncing model of our interest, and have evaluated the cross-correlations of these magnetic fields with scalar perturbations. Additionally, we have studied the imprints of parity violation on the generation of non-Gaussianities involving primordial magnetic fields and scalar perturbations in de Sitter inflation.

In Chap. 2, we have discussed the evaluation of the scalar-scalar-tensor three-point function in the axion monodromy model of inflation [114–116]. This model is characterized by a potential with persistent oscillations, leading to features in the scalar and tensor power spectra. It has been established that the presence of such features leads to an improvement in the fit to the CMB data, when juxtaposed with the conventional nearly scale invariant spectra [110, 111, 115]. This has been an incentive for the comparison of this model with observations at the level of the three-point functions. There exist standard templates for the primordial scalar and tensor power spectra which are made use of while matching with data. In a similar manner, in order to enable efficient comparison, it behooves one to have analytical templates for the various three-point functions as well. Prompted by the comparisons of the scalar bispectrum with the CMB data with the aid of templates [113, 114, 117], in this thesis, we have arrived at a similar template for the scalar-scalar-tensor three-point function. In contrast to the analytical evaluation of the scalar bispectrum wherein it was sufficient to take into account the changes in the slow roll parameters due to the presence of modulations in the potential, the calculation of the scalar-scalar-tensor three-point function involves considering the effects of the departure from slow roll on the scalar and tensor modes as well. We have also analytically evaluated the non-Gaussianity parameter corresponding to the scalar-scalar-tensor three-point function and established that the consistency relation for this three-point function is valid even in the presence of features [121].

In Chap. 3, we have considered a particular matter bounce scenario. We have analytically evaluated the tensor modes and the tensor power spectrum in this scenario. We have observed that the power spectrum is scale invariant over the domain of our interest, a behavior which mirrors that of the tensor power spectrum in de Sitter inflation [130]. This implies that the characteristics of the tensor power spectrum alone are not adequate to differentiate between the inflationary and bouncing scenarios. Evidently, the next cogent attempt would be to compare the amplitude and shape of the three-point function involving the tensor perturbations generated in de Sitter and bouncing scenarios. With this motivation, we have also analytically evaluated the tensor bispectrum. We find that at the level of the three-point function, there arises a crucial difference between the two alternative scenarios, namely, the consistency relation corresponding to the tensor bispectrum is violated in the matter bounce [130]. We believe this has strong implications with

regard to arriving at discriminating observables between the inflationary and bouncing scenarios.

In Chap. 4, we have examined the generation of primordial magnetic fields in a bouncing model. The magnetic fields observed today over extensive scales in the universe are conjectured to have originated from primordial seed fields. This issue, referred to as primordial magnetogenesis, has been investigated in detail in the context of inflationary scenarios [97, 98, 102, 133, 134]. With the introduction of a non-minimal coupling function in the standard electromagnetic action, thereby breaking the conformal invariance, it has been possible to obtain magnetic fields compatible with observations [96]. In this thesis, we have examined the generation of primordial magnetic fields in bouncing scenarios. We find that for a convenient choice of the coupling function, it is possible to obtain scale invariant magnetic fields of relevant strengths over the scales of cosmological interest [138]. Further, we also illustrate the property of duality invariance of the magnetic power spectrum, wherein the shape of the power spectrum remains invariant under a two parameter family of transformations of the non-minimal coupling function. This is an interesting property since we show that even two widely disparate coupling functions can lead to similar magnetic power spectra.

In Chap. 5, we have evaluated the cross-correlations between perturbations in an auxiliary scalar field and the primordial magnetic fields generated in bouncing universes. The magnitude of such cross-correlations has been estimated before in the case of inflation [99–101, 139, 140], and it has been realized that the associated non-Gaussianities can be large. With the aim to compare the non-Gaussian signatures generated in bouncing scenarios with those produced in de Sitter inflation, we have analytically calculated the three-point function involving the scalar perturbations and the primordial magnetic fields in a matter bounce. We find that the corresponding non-Gaussianity parameter is significantly larger than that obtained in de Sitter inflation [141]. Moreover, the consistency relation associated with the three-point function of our interest, which remains valid in the de Sitter inflationary scenario, is violated in the bouncing model. This behavior again highlights a pivotal distinction between the attributes of non-Gaussianities generated in bouncing and inflationary frameworks.

In Chap. 6, we have numerically evaluated the cross-correlations between perturbations in an auxiliary scalar field and primordial helical magnetic fields generated in de Sitter inflation. The addition of a non-minimally coupled parity violating term to the electromagnetic action results in the production of magnetic fields with two helicities that evolve independently and, consequently, can possibly lead to distinct observable effects on the CMB [143, 146, 147]. Further, the helical modes can also augment the amplitude of the magnetic power spectrum. In order to arrive at stronger constraints on primordial helical magnetic fields, it would be useful to understand the characteristics of their cross-correlations with scalar perturbations. On numerical evaluation of these three-point functions, we find that even with the introduction of a relatively small amount of helicity,

the resultant non-Gaussianity parameter is inordinately large [153].

7.2 Outlook

As we have discussed, there are broadly three topics that we have investigated in this thesis. Firstly, we have evaluated the cross-correlations involving tensors in the presence of oscillatory features in the inflationary potential. Secondly, we have examined the evolution of tensor perturbations in a specific bouncing scenario and the non-Gaussianities generated therein. The third category of problem we have studied entails the issue of primordial magnetogenesis and the cross-correlations of these magnetic fields with scalar perturbations, as well as the effects of parity violation at the level of three-point functions in the case of inflationary magnetogenesis. There are several avenues to explore in relation to the topics discussed in this thesis.

Firstly, analytical investigations into the non-trivial effects due to presence of features in an inflationary potential can be extended to include other such models that are in accordance with observations. It would be of tremendous interest to study the other non-Gaussian signatures apart from the scalar-scalar-tensor three-point function as well. Importantly, investigating the imprints of these non-Gaussianities on the CMB would allow us to arrive at constraints on the three-point functions. Such analyses could turn out to be of considerable importance, in particular, if tensors are observed at the level of the power spectrum.

The examination of non-Gaussianities in the case of bouncing scenarios has been restricted to the tensor bispectrum in this thesis. It would be of paramount importance to study the other three-point functions, especially the scalar bispectrum, which leads to the most significant imprints on the non-Gaussianities, for the bouncing models of our interest. We believe that this point has not been addressed satisfactorily as yet. The evaluation of non-Gaussianities is substantially more challenging in the case of bounces. Many of the super-Hubble contributions that can be ignored during inflation may not be ignorable in bouncing scenarios. Therefore, we believe that the usual approaches for the evaluation of three-point functions in inflationary scenarios may not be applicable in bouncing universes. This issue needs to be studied carefully in greater detail.

Investigating the effects of primordial magnetic fields on the scalar and tensor perturbations, both in the inflationary and bouncing scenarios, also seems particularly important. It would be interesting to probe into the cross-correlations involving the scalar perturbations and magnetic fields in the presence of features in the inflationary potential. We could also examine the effects on the three-point functions due to the epoch of reheating, and thereby arrive at stringent constraints on these quantities. We have already obtained the consistency relation associated with the three-point function involving the perturbations in a scalar field and the primordial magnetic fields in the inflationary scenario. It

would be worthwhile to investigate how the consistency relation gets modified in the presence of a parity violating term, leading to helical magnetic fields. We are presently studying some of these issues.

Bibliography

- [1] E. W. Kolb and M. S. Turner, *The Early Universe* (Addison-Wesley, Redwood City, California, 1990); S. Dodelson, *Modern Cosmology* (Academic Press, San Diego, U.S.A., 2003); V. F. Mukhanov, *Physical Foundations of Cosmology* (Cambridge University Press, Cambridge, England, 2005); S. Weinberg, *Cosmology* (Oxford University Press, Oxford, England, 2008); R. Durrer, *The Cosmic Microwave Background* (Cambridge University Press, Cambridge, England, 2008); D. H. Lyth and A. R. Liddle, *The Primordial Density Perturbation* (Cambridge University Press, Cambridge, England, 2009); P. Peter and J-P. Uzan, *Primordial Cosmology* (Oxford University Press, Oxford, England, 2009); H. Mo, F. v. d. Bosch and S. White, *Galaxy Formation and Evolution* (Cambridge University Press, Cambridge, England, 2010); D. Baumann and L. McAllister, *Inflation and String Theory* (Cambridge University Press, Cambridge, England, 2015).
- [2] E. Hubble, PNAS **15**, 3 (1929).
- [3] C. L. Bennet *et al.*, Astrophys. J. Suppl. **436**, 423 (1994); E. L. Wright *et al.*, Astrophys. J. Suppl. **436**, 443 (1994); K. M. Gorski, Astrophys. J. Suppl. **430**, L85 (1994); K. M. Gorski *et al.*, Astrophys. J. Suppl. **430**, L89 (1994).
- [4] J. Dunkley *et al.*, Astrophys. J. Suppl. **180**, 306 (2009); E. Komatsu *et al.*, Astrophys. J. Suppl. **180**, 330 (2009); D. Larson *et al.*, Astrophys. J. Suppl. **192**, 16 (2011); E. Komatsu *et al.*, Astrophys. J. Suppl. **192**, 18 (2011); C. L. Bennett *et al.*, Astrophys. J. Suppl. **208**, 20 (2013); G. Hinshaw *et al.*, Astrophys. J. Suppl. **208**, 19 (2013).
- [5] N. Aghanim *et al.*, Astron. Astrophys. **594**, A11 (2016).
- [6] P. A. R. Ade *et al.*, Astron. Astrophys. **594**, A13 (2016).
- [7] P. A. R. Ade *et al.*, Astron. Astrophys. **594**, A20 (2016).
- [8] N. Aghanim *et al.*, arXiv:1807.06209 [astro-ph.CO].
- [9] Y. Akrami *et al.*, arXiv:1807.06211 [astro-ph.CO].
- [10] J. Yang, M. S. Turner, G. Steigman, D. N. Schramm and K. A. Olive, Astrophys. J. **281**, 493 (1984); S. Burles, K. M. Nollett, M. S. Turner, Astrophys. J. **552**, L1 (2001); S. Burles, K. M. Nollett, M. S. Turner, Phys. Rev. D **63**, 063512 (2001); K. A. Olive, G. Steigman and T. P. Walker, Phys. Rep. **333**, 389 (2000).

- [11] M. Colless *et al.*, Mon. Not. Roy. Astron. Soc. **328**, 1039 (2001).
- [12] K. Abazajian *et al.*, Astrophys. J. Suppl. **182**, 543 (2009).
- [13] J. Yadav, S. Bharadwaj, B. Pandey, and T. R. Seshadri, Mon. Not. Roy. Astron. Soc. **364**, 601 (2005); P. Sarkar, J. Yadav, B. Pandey and S. Bharadwaj, Mon. Not. Roy. Astron. Soc. **399**, L128 (2009).
- [14] A. Kandus, K. E. Kunze, and C. G. Tsagas, Phys. Rep. **505**, 1 (2011); L. M. Widrow, D. Ryu, D. R. G. Schleicher, K. Subramanian, C. G. Tsagas, and R. A. Treumann, Space Sci. Rev. **166**, 37 (2012); R. Durrer and A. Neronov, Astron. Astrophys. Rev. **21**, 62 (2013);
- [15] D. H. Perkins, *Introduction to high energy physics* (Cambridge University Press, Cambridge, England, 1982); F. Halzen and A. D. Martin, *Quarks & Leptons: An Introductory Course in Modern Particle Physics* (Wiley, New York, USA, 1984); D. Griffiths, *Introduction to Elementary Particles* (Wiley-VCH, Weinheim, Germany, 2008).
- [16] D. Scott, A. S. P. Conference Series **201**, 403 (2000).
- [17] S. Perlmutter *et al.*, Astrophys. J. **517**, 565 (1999);
- [18] J. Guy *et al.*, Astron. Astrophys. **523**, A7 (2010); M. Sullivan *et al.*, Astrophys. J. **737**, 102 (2011).
- [19] P. A. R. Ade *et al.*, Astron. Astrophys. **594**, A14 (2016).
- [20] H. Kodama and M. Sasaki, Prog. Theor. Phys. Suppl. **78**, 1 (1984); V. F. Mukhanov, H. A. Feldman and R. H. Brandenberger, Phys. Rep. **215**, 203 (1992); J. E. Lidsey, A. Liddle, E. W. Kolb, E. J. Copeland, T. Barreiro and M. Abney, Rev. Mod. Phys. **69**, 373 (1997); A. Riotto, arXiv:hep-ph/0210162; W. H. Kinney, astro-ph/0301448; J. Martin, Lect. Notes Phys. **738**, 193 (2008); J. Martin, Lect. Notes Phys. **669**, 199 (2005); J. Martin, Braz. J. Phys. **34**, 1307 (2004); B. Bassett, S. Tsujikawa and D. Wands, Rev. Mod. Phys. **78**, 537 (2006); W. H. Kinney, arXiv:0902.1529 [astro-ph.CO]; D. Baumann, arXiv:0907.5424v1 [hep-th].
- [21] L. Sriramkumar, Curr. Sci. **97**, 868 (2009); L. Sriramkumar, in *Vignettes in Gravitation and Cosmology*, Eds. L. Sriramkumar and T. R. Seshadri (World Scientific, Singapore, 2012), pp. 207-249.
- [22] J. Martin, Astrophys. Space Sci. Proc. **45**, 41 (2016).
- [23] A. R. Liddle and S. M. Leach, Phys. Rev. D **68**, 103503 (2003).
- [24] D. J. Schwarz, C. A. Terrero-Escalante and A. A. Garcia, Phys. Lett. B **517**, 243 (2001); S. M. Leach, A. R. Liddle, J. Martin and D. J. Schwarz, Phys. Rev. D **66**, 023515 (2002).
- [25] G. Gubitosi, M. Lagos, J. Magueijo, and R. Allison, JCAP **1606**, 002 (2016).
- [26] A. Ijjas, P. J. Steinhardt, and A. Loeb, Scientific American **316**, 32 (2017).
- [27] J. Martin, P. Peter, N. Pinto-Neto, and D. J. Schwarz, Phys. Rev. D **65**, 123513 (2002); S. Tsujikawa, R. Brandenberger, and F. Finelli, Phys. Rev. D **66**, 083513 (2002);

- V. Bozza and G. Veneziano, *Phys. Lett. B* **625**, 177 (2005); D. Wands, *Adv. Sci. Lett.* **2**, 194 (2009); Y. -F. Cai, R. H. Brandenberger, and P. Peter, *Class. Quantum Grav.* **30**, 075019 (2013); S. D. Odintsov and V. K. Oikonomou, *Phys. Rev. D* **90**, 124083 (2014); J. Quintin, Z. Sherkatghanad, Y. -F. Cai, and R. H. Brandenberger, *Phys. Rev. D* **92**, 063532 (2015); S. Nojiri, S. D. Odintsov, and V. K. Oikonomou, *Phys. Rev. D* **93**, 084050 (2016); J. Quintin and R. H. Brandenberger, *JCAP* **1611**, 029 (2016).
- [28] Y. -F. Cai, J. Quintin, E. N. Saridakis, and E. Wilson-Ewing, *JCAP* **1407**, 033 (2014); Y. -F. Cai, T. Qiu, R. Brandenberger, and X. Zhang, *Phys. Rev. D* **80**, 023511 (2009); Y. -F. Cai, D. A. Easson, and R. Brandenberger, *JCAP* **1208**, 020 (2012); Y. -F. Cai, E. McDonough, F. Duplessis, and R. H. Brandenberger, *JCAP* **1310**, 024 (2013).
- [29] J. Khoury, B. A. Ovrut, P. J. Steinhardt, and N. Turok, *Phys. Rev. D* **64**, 123522 (2001); J. Khoury, B. A. Ovrut, P. J. Steinhardt, and N. Turok, *Phys. Rev. D* **66**, 046005 (2002).
- [30] P. Peter and N. Pinto-Neto, *Phys. Rev. D* **66**, 063509 (2002); P. Peter, N. Pinto-Neto, and D. A. Gonzalez, *JCAP* **0312**, 003 (2003); J. Martin and P. Peter, *Phys. Rev. D* **68**, 103517 (2003); F. Finelli, P. Peter, and N. Pinto-Neto, *Phys. Rev. D* **77**, 103508 (2008).
- [31] A. M. Levy, *Phys. Rev. D* **95**, 023522 (2017).
- [32] L. E. Allen and D. Wands, *Phys. Rev. D* **70**, 063515 (2004);
- [33] Y. -F. Cai, T. Qiu, Y. -S. Piao, M. Li, and X. Zhang, *JHEP* **0710**, 071 (2007).
- [34] Y. -F. Cai, T. Qiu, R. Brandenberger, Y. -S. Piao, and X. Zhang, *JCAP* **0803**, 013 (2008).
- [35] J. -L. Lehnert, *Phys. Rep.* **465**, 223 (2008).
- [36] T. J. Battefeld and R. Brandenberger, *Phys. Rev. D* **70**, 121302 (2004); N. Pinto-Neto and S. D. P. Vitenti, *Phys. Rev. D* **89**, 028301 (2014).
- [37] A. M. Levy, A. Ijjas, and P. J. Steinhardt, *Phys. Rev. D* **92**, 063524 (2015).
- [38] F. T. Falciiano, M. Lilley, and P. Peter, *Phys. Rev. D* **77**, 083513 (2008).
- [39] C. Lin, R. H. Brandenberger, and L. Perreault Levasseur, *JCAP* **1104**, 019 (2011).
- [40] A. Fertig, J. -L. Lehnert, E. Mallwitz, and E. Wilson-Ewing, *JCAP* **1610**, 005 (2016).
- [41] Y. -F. Cai, R. Brandenberger, and X. Zhang, *JCAP* **1103**, 003 (2011).
- [42] T. Qiu, J. Evslin, Y. -F. Cai, M. Li, and X. Zhang, *JCAP* **1110**, 036 (2011).
- [43] A. Ijjas and P. J. Steinhardt, *Phys. Rev. Lett.* **117**, 121304 (2016).
- [44] D. A. Easson, I. Sawicki, and A. Vikman, *JCAP* **1111**, 021 (2011).
- [45] X. Gao, M. Lilley, and P. Peter, *Phys. Rev. D* **91**, 023516 (2015).
- [46] J. Martin and P. Peter, *Phys. Rev. Lett.* **92**, 061301 (2004); J. Martin and P. Peter, *Phys. Rev. D* **69**, 107301 (2004); P. Creminelli, A. Nicolis, and M. Zaldarriaga, *Phys. Rev. D* **71**, 063505 (2005); L. R. Abramo and P. Peter, *JCAP* **0709**, 001 (2007); Y. -F. Cai, S. -H. Chen, J. B. Dent, S. Dutta, and E. N. Saridakis, *Class. Quantum Grav.* **28**, 215011 (2011).
- [47] A. A. Starobinsky, *JETP Lett.* **30**, 682 (1979).

- [48] D. Wands, Phys. Rev. D **60**, 023507 (1999).
- [49] F. Finelli and R. Brandenberger, Phys. Rev. D **65**, 103522 (2002).
- [50] P. Creminelli, and L. Senatore, JCAP **0711**, 010 (2007).
- [51] M. Novello and S. E. P. Bergliaffa, Phys. Rep. **463**, 127 (2008); R. H. Brandenberger, arXiv:1206.4196 [astro-ph.CO]; Y. -F. Cai, Sci. China Phys. Mech. Astron. **57**, 1414 (2014).
- [52] D. Battefeld and P. Peter, Phys. Rep. **571**, 1 (2015); R. Brandenberger and P. Peter, Found. Phys. **47**, 797 (2017).
- [53] S. D. P. Viteni and N. Pinto-Neto, Phys. Rev. D **85**, 023524 (2012); D. A. Easson and A. Vikman, arXiv:1607.00996 [gr-qc].
- [54] V. A. Belinsky, I. M. Khalatnikov, and E. M. Lifshitz, Adv. Phys. **19**, 525 (1970).
- [55] L. Sriramkumar, K. Atmjeet, and R. K. Jain, JCAP **1509**, 010 (2015).
- [56] R. N. Raveendran, D. Chowdhury, and L. Sriramkumar, JCAP **1801**, 030 (2018).
- [57] E. D. Stewart and D. H. Lyth, Phys. Lett. B **302**, 171 (1993); J. Martin and D. J. Schwarz, Phys. Rev. D, **62**, 103520 (2000).
- [58] I. S. Gradshteyn and I. M. Ryzhik, *Table of Integrals, Series and Products*, Seventh Edition (Academic Press, New York, 2007).
- [59] E. F. Bunn, A. R. Liddle and M. J. White, Phys. Rev. D **54**, R5917 (1996).
- [60] J. Martin, C. Ringeval, and R. Trotta, Phys. Rev. D **83**, 063524 (2011).
- [61] J. Martin, C. Ringeval, and V. Vennin, Phys. Dark Univ. **5-6**, 75 (2014); J. Martin, C. Ringeval, R. Trotta, and V. Vennin, JCAP **1403**, 039 (2014).
- [62] J. Martin, Astrophys. Space Sci. Proc. **45**, 41 (2016).
- [63] J. Martin, C. Ringeval, and V. Vennin, JCAP **1410**, 038 (2014).
- [64] P. A. R. Ade *et al.*, Astron. Astrophys. **594**, A17 (2016).
- [65] R. Arnowitt, S. Deser and C. W. Misner, Phys. Rev. **117**, 1595 (1960).
- [66] J. Maldacena, JHEP **0305**, 013 (2003).
- [67] X. Gao, T. Kobayashi, M. Shiraishi, M. Yamaguchi, J. Yokoyama and S. Yokoyama, PTEP **2013**, 053E03 (2013).
- [68] L. Dai, D. Jeong, and M. Kamionkowski, Phys. Rev. D **87**, 103006 (2013).
- [69] D. Jeong and M. Kamionkowski, Phys. Rev. Lett. **108**, 251301 (2012); L. Dai, D. Jeong, and M. Kamionkowski, Phys. Rev. D **88**, 043507 (2013).
- [70] S. Kundu, JCAP **1404**, 016 (2014).
- [71] J. Maldacena and G. L. Pimentel, JHEP **1109**, 045 (2011); X. Gao, T. Kobayashi, M. Yamaguchi and J. Yokoyama, Phys. Rev. Lett. **107**, 211301 (2011).
- [72] D. Seery and J. E. Lidsey, JCAP **0506**, 003 (2005).

-
- [73] X. Chen, Phys. Rev. D **72**, 123518 (2005); X. Chen, M.-x. Huang, S. Kachru and G. Shiu, JCAP **0701**, 002 (2007); D. Langlois, S. Renaux-Petel, D. A. Steer and T. Tanaka, Phys. Rev. Lett. **101**, 061301 (2008); Phys. Rev. D **78**, 063523 (2008).
 - [74] X. Chen, Adv. Astron. **2010**, 638979 (2010); Y. Wang, Commun. Theor. Phys. **62**, 109 (2014);
 - [75] J. Martin and L. Sriramkumar, JCAP **1201**, 008 (2012).
 - [76] V. Sreenath, R. Tibrewala, and L. Sriramkumar, JCAP **1312**, 037 (2013).
 - [77] D. K. Hazra, J. Martin and L. Sriramkumar, Phys. Rev. D **86**, 063523 (2012).
 - [78] D. K. Hazra, L. Sriramkumar and J. Martin, JCAP **1305**, 026 (2013).
 - [79] V. Sreenath and L. Sriramkumar, JCAP **1410**, 021 (2014).
 - [80] E. Komatsu, Class. Quantum Grav. **27**, 124010 (2010).
 - [81] P. Creminelli and M. Zaldarriaga, JCAP **0410**, 006 (2004); C. Cheung, A. L. Fitzpatrick, J. Kaplan and L. Senatore, JCAP **0802**, 021 (2008); S. Renaux-Petel, JCAP **1010**, 020 (2010); J. Ganc and E. Komatsu, JCAP **1012**, 009 (2010); P. Creminelli, G. D'Amico, M. Musso and J. Norena, JCAP **1111**, 038 (2011).
 - [82] J. Martin, H. Motohashi and T. Suyama, Phys. Rev. D **87**, 023514 (2013).
 - [83] V. Sreenath, D. K. Hazra, and L. Sriramkumar, JCAP **1502**, 029 (2015).
 - [84] N. Kundu, A. Shukla, and S. P. Trivedi, JHEP **04**, 061 (2015); N. Kundu, A. Shukla, and S. P. Trivedi, JHEP **01**, 046 (2016).
 - [85] C. T. Byrnes and K. -Y. Choi, Adv. Astron. **2010**, 724525 (2010).
 - [86] L. Senatore, K. M. Smith, and M. Zaldarriaga, JCAP **1001**, 028 (2001); C. Burrage, C. de Rham, D. Seery, and A. J. Tolley, JCAP **1101**, 014 (2011); N. Bartolo, M. Fasiello, S. Matarrese, and A. Riotto, JCAP **1008**, 008 (2010); N. Arkani-Hamed, P. Creminelli, S. Mukohyama, and M. Zaldarriaga, JCAP **0404**, 001 (2004); C. Cheung, P. Creminelli, A. L. Fitzpatrick, J. Kaplan, and L. Senatore, JHEP **03**, 014 (2008).
 - [87] K. Subramanian, Rep. Prog. Phys. **79**, 076901 (2016).
 - [88] D. Grasso and H. R. Rubinstein, Phys. Rep. **348**, 163 (2001); L. M. Widrow, Rev. Mod. Phys. **74**, 775 (2002).
 - [89] A. Neronov and I. Vovk, Science **328**, 73 (2010); F. Tavecchio, G. Ghisellini, L. Foschini, G. Bonnoli, G. Ghirlanda, and P. Coppi, Mon. Not. Roy. Astron. Soc. **406**, L70 (2010).
 - [90] C. D. Dermer, M. Cavadini, S. Razzaque, J. D. Finke, B. Lott, Astrophys. J. **733**, L21 (2011); I. Vovk, A. M. Taylor, D. Semikoz, and A. Neronov, Astrophys. J. **747**, L14 (2012); F. Tavecchio, G. Ghisellini, G. Bonnoli, and L. Foschini, Mon. Not. Roy. Astron. Soc. **414**, 3566 (2011). K. Dolag, M. Kachelriess, S. Ostapchenko, and R. Tomas, Astrophys. J. **727**, L4 (2011); A. M. Taylor, I. Vovk, and A. Neronov, Astron. Astrophys. **529**, A144 (2011); K. Takahashi, M. Mori, K. Ichiki, and S. Inoue, Astrophys. J. **744**, L7 (2012). H. Huan, T. Weisgarber, T. Arlen, and S. P. Wakely, Astrophys. J. **735**,

- L28 (2011); J. D. Finke, L. C. Reyes, M. Georganopoulos, K. Reynolds, M. Ajello, S. J. Fegan, and K. McCann, *Astrophys. J.* **814**, 20 (2015).
- [91] P. A. R. Ade *et al.*, *Astron. Astrophys.* **594**, A19 (2016).
- [92] P. A. R. Ade *et al.*, *Phys. Rev. D* **92**, 123509 (2015).
- [93] M. S. Pshirkov, P. G. Tinyakov, and F. R. Urban, *Phys. Rev. Lett.* **116**, 191302 (2016).
- [94] D. G. Yamazaki, K. Ichiki, T. Kajino, and G. J. Mathews, *Phys. Rev. D* **81**, 023008 (2010); T. Kahniashvili, A. G. Tevzadze, S. K. Sethi, K. Pandey, and B. Ratra, *Phys. Rev. D* **82**, 083005 (2010); C. Caprini, *PoS TEXAS2010*, 222 (2010).
- [95] J. R. Shaw and A. Lewis, *Phys. Rev. D* **86**, 043510 (2012); D. R. G. Schleicher and F. Miniati, *Mon. Not. Roy. Astron. Soc.* **418**, 143 (2011); C. Fedeli and L. Moscardini, *JCAP* **1211**, 055 (2012); T. Kahniashvili, Y. Maravin, A. Natarajan, N. Battaglia, and A. G. Tevzadze, *Astrophys. J.* **770**, 47 (2013); K. L. Pandey, T. R. Choudhury, S. K. Sethi, and A. Ferrara, *Mon. Not. Roy. Astron. Soc.* **451**, 1692 (2015).
- [96] M. S. Turner and L. M. Widrow, *Phys. Rev. D* **37**, 2743 (1988); B. Ratra, *Astrophys. J.* **391**, L1 (1992).
- [97] J. Martin and J. Yokoyama, *JCAP* **0801**, 025 (2008).
- [98] K. Subramanian, *Astron. Nachr.* **331**, 110 (2010).
- [99] R. R. Caldwell, L. Motta, and M. Kamionkowski, *Phys. Rev. D* **84**, 123525 (2011).
- [100] R. K. Jain and M. S. Sloth, *Phys. Rev. D* **86**, 123528 (2012).
- [101] R. K. Jain and M. S. Sloth, *JCAP* **1302**, 003 (2013).
- [102] V. Demozzi, V. Mukhanov, and H. Rubinstein, *JCAP* **0908**, 025 (2009).
- [103] R. J. Z. Ferreira, R. K. Jain, and M. S. Sloth, *JCAP* **1310**, 004 (2013).
- [104] R. J. Z. Ferreira, R. K. Jain, and M. S. Sloth, *JCAP* **1406**, 053 (2014).
- [105] M. J. Mortonson, H. V. Peiris, and R. Easther, *Phys. Rev. D* **83**, 043505 (2011); R. Easther and H. V. Peiris, *Phys. Rev. D* **85**, 103533 (2012); J. Norena, C. Wagner, L. Verde, H. V. Peiris, and R. Easther, *Phys. Rev. D* **86**, 023505 (2012); J. Martin, C. Ringeval, R. Trotta, and V. Vennin, *Phys. Rev. D* **90**, 063501 (2014).
- [106] A. Gangui, F. Lucchin, S. Matarrese and S. Mollerach, *Astrophys. J.* **430**, 447 (1994); A. Gangui, *Phys. Rev. D* **50**, 3684 (1994); A. Gangui and J. Martin, *Mon. Not. Roy. Astron. Soc.* **313**, 323 (2000); L. Wang and M. Kamionkowski, *Phys. Rev. D* **61**, 063504 (2000).
- [107] E. Komatsu and D. N. Spergel, *Phys. Rev. D* **63**, 063002 (2001); E. Komatsu, D. N. Spergel and B. D. Wandelt, *Astrophys. J.* **634**, 14 (2005); D. Babich and M. Zaldarriaga, *Phys. Rev. D* **70**, 083005 (2004); M. Liguori, F. K. Hansen, E. Komatsu, S. Matarrese and A. Riotto, *Phys. Rev. D* **73**, 043505 (2006); C. Hikage, E. Komatsu and T. Matsubara, *Astrophys. J.* **653** (2006) 11 (2006); J. R. Fergusson and E. P. S. Shellard, *Phys. Rev. D* **76**, 083523 (2007); A. P. S. Yadav, E. Komatsu and B. D. Wandelt, *Astrophys. J.* **664**, 680 (2007); P. Creminelli, L. Senatore and M. Zaldarriaga,

- JCAP **0703**, 019 (2007); A. P. S. Yadav and B. D. Wandelt, Phys. Rev. Lett. **100**, 181301 (2008); C. Hikage, T. Matsubara, P. Coles, M. Liguori, F. K. Hansen and S. Matarrese, Mon. Not. Roy. Astron. Soc. **389**, 1439 (2008); O. Rudjord, F. K. Hansen, X. Lan, M. Liguori, D. Marinucci and S. Matarrese, Astrophys. J. **701**, 369 (2009); K. M. Smith, L. Senatore and M. Zaldarriaga, JCAP **0909**, 006 (2009); J. Smidt, A. Amblard, C. T. Byrnes, A. Cooray, A. Heavens and D. Munshi, Phys. Rev. D **81**, 123007 (2010); J. R. Fergusson, M. Liguori and E. P. S. Shellard, JCAP **1212**, 032 (2012). M. Liguori, E. Sefusatti, J. R. Fergusson and E. P. S. Shellard, Adv. Astron. **2010**, 980523 (2010); A. P. S. Yadav and B. D. Wandelt, Adv. Astron. **2010**, 565248 (2010).
- [108] R. K. Jain, P. Chingangbam, J.-O. Gong, L. Sriramkumar and T. Souradeep, JCAP **0901**, 009 (2009).
- [109] R. K. Jain, P. Chingangbam, L. Sriramkumar and T. Souradeep, Phys. Rev. D **82**, 023509 (2010); D. K. Hazra, M. Aich, R. K. Jain, L. Sriramkumar and T. Souradeep, JCAP **1010**, 008 (2010); D. K. Hazra, A. Shafieloo and T. Souradeep, JCAP **1307**, 031 (2013); D. K. Hazra, A. Shafieloo and T. Souradeep, JCAP **1411**, 011 (2014); P. Hunt and S. Sarkar, JCAP **1401**, 025 (2014); P. Hunt and S. Sarkar, JCAP **1512**, 052 (2015); D. K. Hazra, A. Shafieloo, G. F. Smoot and A. A. Starobinsky, Phys. Rev. Lett. **113**, 071301 (2014); D. K. Hazra, A. Shafieloo, G. F. Smoot and A. A. Starobinsky, JCAP **1408**, 048 (2014).
- [110] P. D. Meerburg, D. N. Spergel and B. D. Wandelt, Phys. Rev. D **89**, 063536 (2014).
- [111] P. D. Meerburg and D. N. Spergel, Phys. Rev. D **89**, 063537 (2014).
- [112] J. Martin and C. Ringeval, Phys. Rev. D **69**, 083515 (2004); Phys. Rev. D **69**, 127303 (2004); JCAP **0501**, 007 (2005); M. Zarei, Phys. Rev. D **78**, 123502 (2008); C. Pahud, M. Kamionkowski and A. R. Liddle, Phys. Rev. D **79**, 083503 (2009); T. Kobayashi and F. Takahashi, JCAP **1101**, 026 (2011).
- [113] J. R. Fergusson, H. F. Gruetjen, E. P. S. Shellard, and M. Liguori, Phys. Rev. D **91**, 023502 (2015); J. R. Fergusson, H. F. Gruetjen, E. P. S. Shellard, and B. Wallisch, Phys. Rev. D **91**, 123506 (2015).
- [114] R. Flauger, L. McAllister, E. Pajer, A. Westphal and G. Xu, JCAP **1006**, 009 (2010).
- [115] M. Aich, D. K. Hazra, L. Sriramkumar and T. Souradeep, Phys. Rev. D **87**, 083526 (2013); H. Peiris, R. Easther, and R. Flauger, JCAP **1309**, 018 (2013); R. Easther and R. Flauger, JCAP **1402**, 037 (2014).
- [116] P. D. Meerburg, Phys. Rev. D **90**, 063529 (2014).
- [117] R. Flauger and E. Pajer, JCAP **1101**, 017 (2011).
- [118] E. Dimastrogiovanni, M. Fasiello, D. Jeong, and M. Kamionkowski, JCAP **1412**, 050 (2014).
- [119] E. Dimastrogiovanni, M. Fasiello, and M. Kamionkowski, JCAP **1602**, 017 (2016).

- [120] D. Chialva, JCAP **1201**, 037 (2012); K. Schalm, G. Shiu, and T. van der Aalst, JCAP **1303**, 005 (2013); E. Pajer, F. Schmidt, and M. Zaldarriaga, Phys. Rev. D **88**, 083502 (2013); Z. Kenton and D. J. Mulryne, JCAP **1510**, 018 (2015); Z. Kenton and D. J. Mulryne, JCAP **1610**, 035 (2016).
- [121] D. Chowdhury, V. Sreenath, and L. Sriramkumar, JCAP **1611**, 041 (2016).
- [122] P. D. Meerburg, J. Meyers, A. van Engelen, and Y. Ali-Haïmoud, Phys. Rev. D **93**, 123511 (2016).
- [123] Y. -F. Cai, W. Xue, R. Brandenberger, and X. Zhang, JCAP **0905**, 011 (2009).
- [124] X. Gao, M. Lilley, and P. Peter, JCAP **1407**, 010 (2014).
- [125] P. Creminelli, C. Pitrou, and F. Vernizzi, JCAP **1111**, 025 (2011); A. Lewis, JCAP **1206**, 023 (2012); M. Shiraishi, E. Komatsu, M. Peloso, and N. Barnaby, JCAP **1305**, 002 (2013).
- [126] A. Kehagias, A. Moradinezhad-Dizgah, J. Noreña, H. Perrier, and A. Riotto, JCAP **1410**, 011 (2014).
- [127] M. Liguori, E. Sefusatti, J. R. Fergusson, and E. P. S. Shellard, Adv. Astron. **2010**, 980523 (2010); C. -T. Chiang, C. Wagner, F. Schmidt, and E. Komatsu, JCAP **1405**, 048 (2014); M. Mirbabayi, M. Simonović, and M. Zaldarriaga, arXiv:1412.3796 [astro-ph.CO].
- [128] D. S. Salopek, J. R. Bond and J. M. Bardeen, Phys. Rev. D **40**, 1753 (1989); C. Ringeval, Lect. Notes Phys. **738**, 243 (2008).
- [129] Wolfram Research, Inc., *Mathematica11.0* (Champaign, IL, 2016).
- [130] D. Chowdhury, V. Sreenath, and L. Sriramkumar, JCAP **1511**, 002 (2015).
- [131] M. H. Namjoo, H. Firouzjahi and M. Sasaki, Europhys. Lett. **101**, 39001 (2013); X. Chen, H. Firouzjahi, M. Namjoo and M. Sasaki, Europhys. Lett. **102**, 59001 (2013).
- [132] J. M. Salim, N. Souza, S. E. Perez Bergliaffa, and T. Prokopec, JCAP **0704**, 011 (2007); F. A. Membiela, Nucl. Phys. B **885**, 196 (2014).
- [133] K. Bamba and J. Yokoyama, Phys. Rev. D **69**, 043507 (2004); K. Bamba and M. Sasaki, JCAP **0702**, 030 (2007); L. Campanelli, Int. J. Mod. Phys. D **18**, 1395 (2009); R. Durrer, L. Hollenstein, and R. K. Jain, JCAP **1103**, 037 (2011); C. T. Byrnes, L. Hollenstein, R. K. Jain, and F. R. Urban, JCAP **1203**, 009 (2012); R. K. Jain, R. Durrer, and L. Hollenstein, J. Phys. Conf. Ser. **484**, 012062 (2014); T. Kahniashvili, A. Brandenburg, L. Campanelli, B. Ratra, and A. G. Tevzadze, Phys. Rev. D **86**, 103005 (2012); K. -W. Ng, S. -L. Cheng, and W. Lee, Chin. J. Phys. **53**, 110105 (2015); K. Bamba, Phys. Rev. D **91**, 043509 (2015); T. Fujita, R. Namba, Y. Tada, N. Takeda, and H. Tashiro, JCAP **1505**, 054 (2015); L. Campanelli, Eur. Phys. J. **C75**, 278 (2015); T. Fujita and R. Namba, Phys. Rev. D **94**, 043523 (2016); C. G. Tsagas, Phys. Rev. D **93**, 103529 (2016).
- [134] S. Kanno, J. Soda, and M. Watanabe, JCAP **0912**, 009 (2009); F. R. Urban, JCAP **1112**, 012 (2011).

- [135] T. J. Battefeld, S. P. Patil, and R. Brandenberger, Phys. Rev. D **70**, 066006 (2004); G. Geshnizjani and T. J. Battefeld, Phys. Rev. D **73**, 048501 (2006); P. Peter and N. Pinto-Neto, Phys. Rev. D **78**, 063506 (2008); A. Cardoso and D. Wands, Phys. Rev. D **77**, 123538 (2008).
- [136] D. J. Stargen and V. Sreenath, arXiv:1605.07311 [gr-qc].
- [137] S. Unnikrishnan and L. Sriramkumar, Phys. Rev. D **81**, 103511 (2010).
- [138] D. Chowdhury, L. Sriramkumar, and R. K. Jain, Phys. Rev. D **94**, 083512 (2016).
- [139] L. Motta and R. R. Caldwell, Phys. Rev. D **85**, 103532 (2012).
- [140] K. E. Kunze, Phys. Rev. D **87**, 103005 (2013).
- [141] D. Chowdhury, L. Sriramkumar, and M. Kamionkowski, arXiv:1807.05530 [astro-ph.CO].
- [142] L. Campanelli, Int. J. Mod. Phys. D **18**, 1395 (2009); R. Sharma, K. Subramanian, and T. R. Seshadri, Phys. Rev. D **97**, 083503 (2018).
- [143] R. Durrer, L. Hollenstein, and R. K. Jain, JCAP **1103**, 037 (2011).
- [144] R. K. Jain, R. Durrer, and L. Hollenstein, J. Phys. Conf. Ser. **484**, 012062 (2014).
- [145] C. Caprini and L. Sorbo, JCAP **1410**, 056 (2014).
- [146] C. Caprini, R. Durrer, and T. Kahniashvili, Phys. Rev. D **69**, 063006 (2004); M. Ballardini, F. Finelli, and D. Paoletti, JCAP **1510**, 031 (2015).
- [147] N. Seto and A. Taruya, Phys. Rev. D **77**, 103001 (2008).
- [148] A. Brandenburg and K. Subramanian, Phys. Rep. **417**, 1 (2005); R. Banerjee and K. Jedamzik, Phys. Rev. D **70**, 123003 (2004); L. Campanelli, Phys. Rev. Lett. **98**, 251302 (2007).
- [149] M. M. Anber and L. Sorbo, JCAP **0610**, 018 (2006).
- [150] F. W. J. Olver, A. B. Olde Daalhuis, D. W. Lozier, B. I. Schneider, R. F. Boisvert, C. W. Clark, B. R. Miller, and B. V. Saunders, eds., *NIST Digital Library of Mathematical Functions* (<http://dlmf.nist.gov/>, Release 1.0.19 of 2018-06-22).
- [151] M. Abramowitz and I. A. Stegun, *Handbook of Mathematical Functions* (Dover, New York, U.S.A., 2001).
- [152] N. Bartolo, S. Matarrese, M. Peloso, and M. Shiraishi, JCAP **1507**, 039 (2015); N. Bartolo, S. Matarrese, M. Peloso, and M. Shiraishi, JCAP **1501**, 027 (2015).
- [153] D. Chowdhury, L. Sriramkumar, and M. Kamionkowski, arXiv:1807.07477 [astro-ph.CO].
- [154] X. Chen, R. Easther, and E. A. Lim, JCAP **0706**, 023 (2007); X. Chen, R. Easther, and E. A. Lim, JCAP **0804**, 010 (2008).
- [155] W. H. Press, S. A. Teukolsky, W. T. Vetterling, and B. P. Flannery, *Numerical Recipes 3rd Edition: The Art of Scientific Computing* (Cambridge University Press, New York, NY, USA, 2007).

List of papers on which this thesis is based

Papers in Refereed Journals

1. **D. Chowdhury**, V. Sreenath and L. Sriramkumar, *The tensor bi-spectrum in a matter bounce*, JCAP **1511**, 002 (2015) [arXiv:1506.06475 [astro-ph.CO]].
2. **D. Chowdhury**, L. Sriramkumar and R. K. Jain, *Duality and scale invariant magnetic fields from bouncing universes*, Phys. Rev. D **94**, 083512 (2016) [arXiv:1604.02143 [gr-qc]].
3. **D. Chowdhury**, V. Sreenath and L. Sriramkumar, *The scalar-scalar-tensor inflationary three-point function in the axion monodromy model*, JCAP **1611**, 041 (2016) [arXiv:1605.05292 [astro-ph.CO]].
4. **D. Chowdhury**, L. Sriramkumar and M. Kamionkowski, *Cross-correlations between scalar perturbations and magnetic fields in bouncing universes*, arXiv:1807.05530 [astro-ph.CO], submitted for publication.
5. **D. Chowdhury**, L. Sriramkumar and M. Kamionkowski, *Enhancing the cross-correlations between magnetic fields and scalar perturbations through parity violation*, arXiv:1807.07477 [astro-ph.CO], submitted for publication.

Papers in refereed journals that are not part of the thesis

1. R. N. Raveendran, **D. Chowdhury**, and L. Sriramkumar, *Viable tensor-to-scalar ratio in a symmetric matter bounce*, JCAP **1801**, 030 (2018) [arXiv:1703.10061 [gr-qc]].

Presentations in Conferences

1. *Analytical templates for the inflationary three-point functions in the axion monodromy model*, contributed talk in *The XXVIII Meeting of the Indian Association*

- of General Relativity and Gravitation*, Raman Research Institute, Bengaluru, India, March 18–20, 2015.
2. *The tensor bi-spectrum in a matter bounce*, contributed talk in *The VIII International Conference on Gravitation and Cosmology*, Indian Institute of Science Education and Research Mohali, Mohali, India, December 14–18, 2015.
 3. *Three-point functions in the early universe*, poster in *Summer School on Cosmology*, International Centre for Theoretical Physics, Trieste, Italy, June 6–17, 2016.
 4. *Duality and the generation of scale invariant primordial magnetic fields in bouncing scenarios*, contributed talk in *Hot topics in Modern Cosmology (Spontaneous Workshop XI)*, Institut d'Études Scientifiques de Cargèse, Cargèse, France, May 1–6, 2017.
 5. *Primordial magnetic fields in bouncing universes*, poster in *YKIS2018a symposium (Gravity and Cosmology 2018)*, Yukawa Institute for Theoretical Physics, Kyoto University, Kyoto, Japan, February 19–23, 2018.

CURRICULUM VITAE

Personal Details:

Name: Debika Chowdhury
Date of Birth: May 15, 1990
Gender: Female
Permanent Address: 486, Jaigir Ghat Road,
Thakurpukur, Kolkata 700063.

Academic History:

2013–Present Ph.D. Physics
Department of Physics,
Indian Institute of Technology Madras, Chennai.
Date of registration: July 15, 2013.

2011-2013 M.Sc. Physics
Department of Physics,
Indian Institute of Technology Madras, Chennai.

2008-2011 B.Sc. Physics
St. Xavier's College, Kolkata.

DOCTORAL COMMITTEE

Guide: Prof. L. Sriramkumar,
Professor,
Department of Physics, Indian Institute of Technology Madras, Chennai.

Co-Guide: Dr. Dawood Kothawala,
Assistant Professor,
Department of Physics, Indian Institute of Technology Madras, Chennai.

Members: Dr. Prasanta Kumar Tripathy,
Associate Professor,
Department of Physics, Indian Institute of Technology Madras, Chennai.

Prof. Suresh Govindarajan,
Professor,
Department of Physics, Indian Institute of Technology Madras, Chennai.

Prof. T. R. Govindarajan,
Professor,
Chennai Mathematical Institute, Chennai.